



THE UNIVERSITY  

---

of ADELAIDE

**Identifying the pathological changes caused by familial  
Alzheimer's disease-like mutations in zebrafish *psen2***

**Haowei Jiang**

School of Biological Sciences

A thesis submitted for the degree of Doctor of Philosophy

The University of Adelaide

May 2018

## Table of Contents

<b>Abstract</b> .....	<b>1</b>
<b>Thesis Declaration Statement</b> .....	<b>2</b>
<b>Acknowledgement</b> .....	<b>3</b>
<b>Chapter 1 Literature Review</b> .....	<b>4</b>
1.1 Introduction.....	4
1.2 A review of <i>PRESENILIN2</i> and its roles in Alzheimer’s disease pathogenesis.....	4
1.3 References.....	28
<b>Chapter 2 Identifying the transcriptomic changes caused by a premature termination codon mutation in <i>psen2</i>, using the zebrafish model</b> .....	<b>36</b>
2.1 Introduction, Significance and Commentary.....	36
2.2 Transcriptome analysis indicates significant effects on mitochondrial function of heterozygosity for a premature termination codon mutation in the zebrafish gene <i>psen2</i> .....	37
2.3 Supplementary Information.....	87
<b>Chapter 3 Generation of familial Alzheimer’s disease-like mutations in zebrafish <i>psen2</i> using the CRISPR/Cas9 system</b> .....	<b>95</b>
3.1 Introduction, Significance and Commentary.....	95
3.2 The zebrafish orthologue of familial Alzheimer’s disease gene <i>PRESENILIN 2</i> is required for normal adult melanotic skin pigmentation.....	96
3.3 Supplementary Information.....	135
<b>Chapter 4 Ratiometric assays of autophagic flux in zebrafish for analysis of familial Alzheimer’s disease-like mutations</b> .....	<b>155</b>
4.1 Introduction, Significance and Commentary.....	155
4.2 Ratiometric assays of autophagic flux in zebrafish for analysis of familial Alzheimer’s disease-like mutations.....	156
4.3 Supplementary Information.....	194

<b>Chapter 5 locomotion tests on <i>psen2</i> mutants.....</b>	<b>209</b>
<b>5.1 Abstract.....</b>	<b>209</b>
<b>5.2 Introduction.....</b>	<b>210</b>
<b>5.3 Methods and materials.....</b>	<b>211</b>
<b>5.4 Results.....</b>	<b>213</b>
<b>5.5 Discussion.....</b>	<b>213</b>
<b>5.6 References.....</b>	<b>219</b>
<b>Chapter 6 Conclusion and Perspective.....</b>	<b>221</b>
<b>6.1 Conclusion.....</b>	<b>221</b>
<b>6.2 Perspective.....</b>	<b>223</b>
<b>6.3 References.....</b>	<b>230</b>
<b>Appendix.....</b>	<b>231</b>

## Abstract

This project aimed to investigate the pathological changes caused by familial Alzheimer's disease-related (fAD-related) mutations in the gene *PSEN2* based on a zebrafish model system. The CRISPR/Cas9 system was used to generate fAD-like mutations in the zebrafish genome. Although this mutagenesis system failed to generate mutations directly equivalent to the fAD mutations N141I and V148I, (N140I and V147I in zebrafish *psen2*), a fAD-like mutation *psen2*<sup>T141\_L142delinsMISLISV</sup>, a truncation mutation *psen2*<sup>N140fs</sup>, and a putative null mutation *psen2*<sup>S4Ter</sup>, were generated. Allele-specific expression tests using digital quantitative PCR were applied to all three mutations, and nonsense mediated decay was found to occur for the *psen2*<sup>N140fs</sup> transcript. RNA-seq-based transcriptomic analysis was performed on brains from *psen2*<sup>S4Ter</sup> heterozygous and wild type siblings from a single family and revealed a likely relationship between *psen2* and mitochondrial formation and function, which are thought to be associated with AD pathology. A GFP-Lc3a-GFP construct was designed to assay changes in autophagic flux in zebrafish larvae. By applying this assay to *psen2*<sup>S4Ter</sup>-carrying mutant larvae, as well as larvae possessing mutations in *psen1*, the Psen2 protein was seen to play a role in autophagy, which is also thought to be a process important in the development of AD pathology. Thus, the results of this project may contribute to a better understanding of the pathological mechanisms underlying AD.

### **Thesis Declaration Statement by Author**

I certify that this work contains no material which has been accepted for the award of any other degree or diploma in my name, in any university or other tertiary institution and, to the best of my knowledge and belief, contains no material previously published or written by another person, except where due reference has been made in the text. In addition, I certify that no part of this work will, in the future, be used in a submission in my name, for any other degree or diploma in any university or other tertiary institution without the prior approval of the University of Adelaide and where applicable, any partner institution responsible for the joint-award of this degree.

I acknowledge that copyright of published works contained within this thesis resides with the copyright holder(s) of those works.

I also give permission for the digital version of my thesis to be made available on the web, via the University's digital research repository, the Library Search and also through web search engines, unless permission has been granted by the University to restrict access for a period of time.

Name of Candidate: Haowei Jiang

Signature:

Date: 2/5/2018

## **Acknowledgement**

I would like to express my most sincere gratitude to my principle supervisor Dr Michael Lardelli and co-supervisor Dr Morgan Newman, for their invaluable help with my research projects and my thesis writing. Without their help, it would be impossible for me to finish my PhD research.

I also want to thank the previous and present members in Lardelli lab for their support in my research, including Dr Seyyed Hani Moussavi Nik, Tanya Jayne, Karissa Barthelson and Yang Dong.

I would like to thank Dr Stephen Martin Pederson and Dr Dhanushika Ratnayake for their valuable comments and help for preparing my research manuscripts.

Last but not least, I want to thank my parents and grandparents for their firm support and encouragements during the last three and a half years of my PhD. It would be impossible for me to adhere to my dream of being a scientist without their support.

## Chapter 1 Literature Review

### 1.1 Introduction

In this project, different mutations were generated in the zebrafish gene *presenilin 2*, (*psen2*), which is orthologous to human *PRESENILIN 2*, (*PSEN2*), to improve our understanding of the role(s) of *PSEN2* in Alzheimer's disease (AD). Therefore, this chapter reviews the roles of *PSEN2* in AD pathogenesis through previous studies on how *PSEN2* function contributes to  $\gamma$ -secretase activity, innate immunity, neurodevelopment, calcium homeostasis, autophagy, mitochondrial function, and ischemic oxidative stress. These are all cellular functions that have been found to be associated with the progression of AD pathology.

### 1.2 A review of *PRESENILIN2* and its roles in Alzheimer's disease pathogenesis

#### Abstract

*PRESENILIN2* (*PSEN2*) is one of the causative genes associated with autosomal dominant familial Alzheimer's disease (fAD). However, the function of this gene and how it contributes to fAD pathogenesis has not been fully determined. In this brief review we give an overview of recent research on *PSEN2* to generate an outline of its role in AD progression. As a core component of the  $\gamma$ -secretase complex, the *PSEN2* protein is involved in many  $\gamma$ -secretase-related physiological activities, including innate

immunity, Notch signaling, autophagy, mitochondrial function etc. These physiological activities have all been associated with AD progression, which indicates that *PSEN2* plays a particular role in AD pathogenesis.

### **The *PSEN2* gene**

PRESENILINs are essential components of the  $\gamma$ -secretase complex, and both *PRESENILIN 1 (PSEN1)* and *PRESENILIN 2 (PSEN2)* are loci for mutations causing familial Alzheimer disease (fAD) (Hutton 1997). Interestingly, there have been nearly 200 potentially pathogenic mutations identified in *PSEN1*, but only about 20 mutations have been reported in *PSEN2* to date (Jayadev, Leverenz et al. 2010). It seems that, although these two PRESENILINs are highly homologous (they share 62% identity at the amino acid residue sequence level (Newman, Musgrave et al. 2007)), they can contribute to different biological processes (Lee, Slunt et al. 1996; Lai, Chen et al. 2003). However, the complete function of the two *PRESENILIN* genes and how they contribute to fAD pathogenesis has not yet been determined. In this review, we focus specifically on the multiple roles of *PSEN2* and how it contributes to fAD pathogenesis.

### **PSEN2 protein and $\gamma$ -secretase**

*PSEN2* was first identified as *STM2*, a candidate gene for the chromosome 1 AD locus, when a point mutation resulting in the substitution of an isoleucine for an asparagine



(N141I) was found in a Volga German AD family in 1995 (Levy-Lahad, Wasco et al. 1995). PSEN2 is identified as a 50 to 55kDa protein that consists of nine transmembrane domains (TMDs), a cytosolic N-terminus, a luminal C-terminus and a “cytosolic loop” between the sixth and seventh TMD (Figure 4) (Jayadev, Leverenz et al. 2010). The active site of the  $\gamma$ -secretase complex is thought to be formed by two aspartyl residues in adjacent TMDs, residues D263 and D366 of PSEN2 (residues D257 and D385 in PSEN1). PSEN2 can be cleaved by  $\gamma$ -secretase itself, within the cytosolic loop, to generate a longer N-terminal fragment (NTF) and a shorter C-terminal fragment (CTF) (Thinakaran, Borchelt et al. 1996; Tomita, Maruyama et al. 1997). Other type I membrane proteins, such as APP and Notch, are also identified as substrates of  $\gamma$ -secretase. A cytosolic CTF is normally generated by the cleavage of these transmembrane proteins by  $\gamma$ -secretase. For Notch, this fragment is identified as Notch intracellular domain (NICD) (De Strooper, Annaert et al. 1999). The CTF produced by  $\gamma$ -secretase is then translocated to the nucleus to modulate gene expression (Cao and Sudhof 2001).

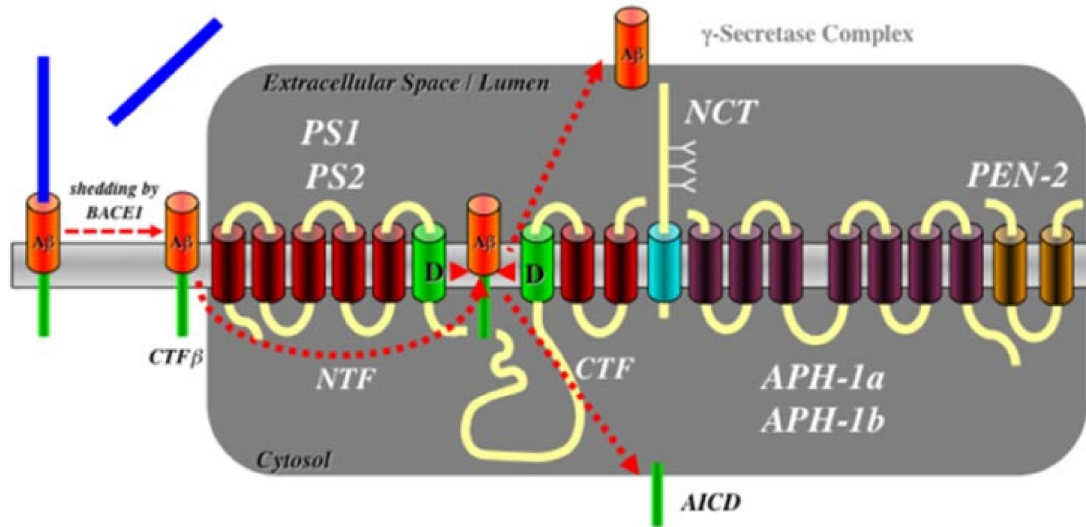


**Figure 1.2.1.**  $\gamma$ -secretase complex (Steiner, Fluhner et al. 2008).

PRESENILINS are the catalytic core of the  $\gamma$ -secretase complex that can cleave the A $\beta$  peptide from APP (following cleavage by  $\alpha$ - or  $\beta$ -secretase). The other three structural subunits of the  $\gamma$ -secretase complex are nicastrin (NCT), PSEN enhancer 2 (PSENEN or PEN-2), and either anterior pharynx 1 (APH-1) a or b (Steiner, Fluhner et al. 2008). NCT functions as a  $\gamma$ -secretase substrate receptor (Shah, Lee et al. 2005). PSENEN is required for the stabilization of the heterodimer of PRESENILIN N- and C-terminal fragments within the  $\gamma$ -secretase complex (Prokop, Shirotani et al. 2004). APH-1 stabilizes newly synthesized PRESENILIN holoprotein, and is possibly able to downregulate the activity of uncleaved PRESENILIN holoprotein (Cooper, Deng et al.).

As a type I transmembrane protein, APP is one of the substrates of  $\gamma$ -secretase. After synthesis, APP can be cleaved through either the non-amyloidogenic or amyloidogenic pathways (Figure 1.2.2). The non-amyloidogenic pathway is more prevalent in most cell types. In this pathway, APP is first cleaved by  $\alpha$ -secretase into a soluble N-terminal

fragment (sAPP $\alpha$ ) and an 83 amino acid C-terminal fragment (named as  $\alpha$ -CTF or C83). The C83 fragment is then cleaved by  $\gamma$ -secretase into an APP intracellular domain (AICD) and a p3 peptide. The amyloidogenic pathway is an important processing pathway for neurons. In this pathway, APP is first cleaved by  $\beta$ -secretase into sAPP $\beta$  and  $\beta$ -CTF (also named C99). The C99 fragment is then cleaved by  $\gamma$ -secretase into AICD and A $\beta$  (Thinakaran and Koo 2008). Cleavage at three major sites in APP is mediated by  $\gamma$ -secretase (Figure 1.2.3), namely  $\epsilon$ -site cleavage (A $\beta$  49),  $\zeta$ -site cleavage (A $\beta$  46) and  $\gamma$ -site cleavage (A $\beta$  42/40) (Xu 2009; Zhang, Thompson et al. 2011).

A $\beta$ 40 (the 40aa form of A $\beta$ ) is the predominant A $\beta$  species, while A $\beta$ 42 is a minor product of APP cleavage. A $\beta$ 40 and A $\beta$ 42 are produced from two different “production lines” of sequential cleavage by the  $\gamma$ -secretase enzyme, A $\beta$ 49 $\rightarrow$ A $\beta$ 46 $\rightarrow$ A $\beta$ 43 $\rightarrow$ A $\beta$ 40 and A $\beta$ 48 $\rightarrow$ A $\beta$ 45 $\rightarrow$ A $\beta$ 42 $\rightarrow$ A $\beta$ 38 (Figure 1.2.4). In these production lines, long A $\beta$ s are shortened by consecutive carboxypeptidase-like  $\gamma$ -cleavages, and the hydrophobicity of A $\beta$ s can be decreased during this process, so that these A $\beta$ s are more easily moved into the extracellular environment (Chavez-Gutierrez, Bammens et al. 2012). A $\beta$ 42 has a much stronger tendency to aggregate than A $\beta$ 40, as the biophysical and biochemical properties of A $\beta$  vary strongly with its length. Normally, A $\beta$ 42 only contributes about 10% of the total secreted A $\beta$  (Suzuki, Cheung et al. 1994). However, since longer A $\beta$  peptides promote aggregation and neurotoxicity, an increase of the relative amount of A $\beta$ 42 versus A $\beta$ 40, which may be caused by either an increase in A $\beta$ 42 production or a decrease in A $\beta$ 40 levels, has been proposed to be involved in the

pathogenesis of AD (Kuperstein, Broersen et al. 2010). Some of the fAD mutations in *PSEN1* and *PSEN2* have been reported to cause increased ratios of A $\beta$ 42/40 (Xu 2009).

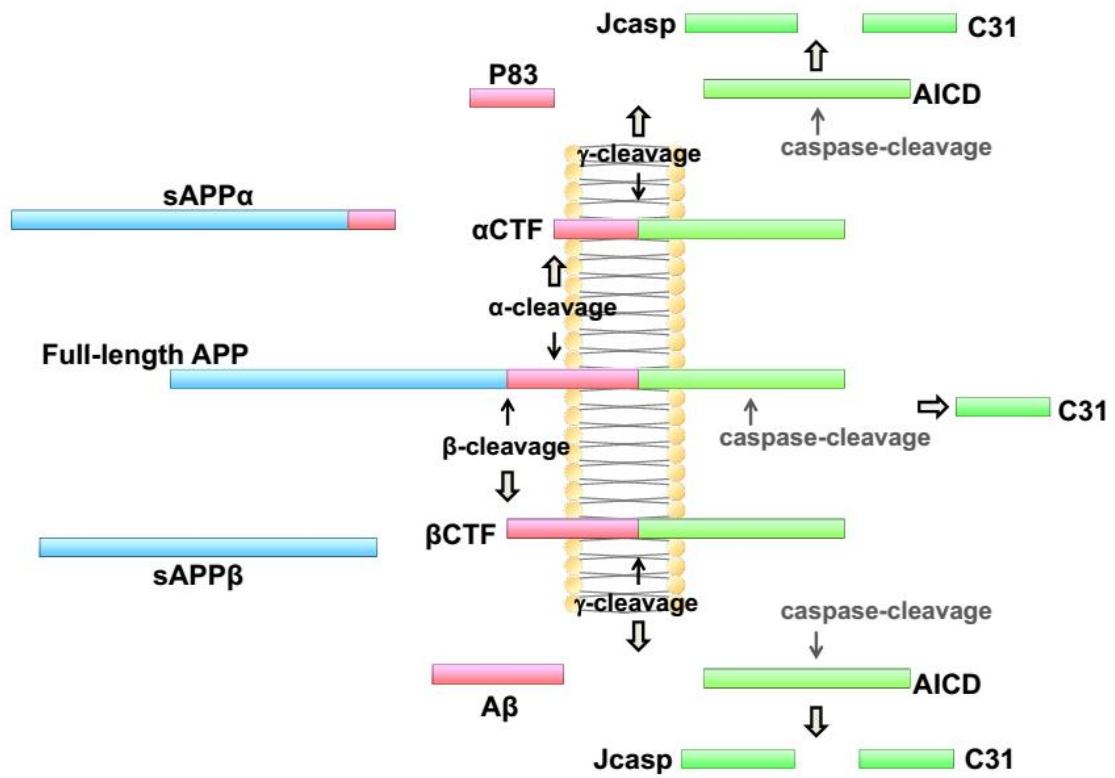


**Figure 1.2.2.** APP processing (Zhang, Thompson et al. 2011).

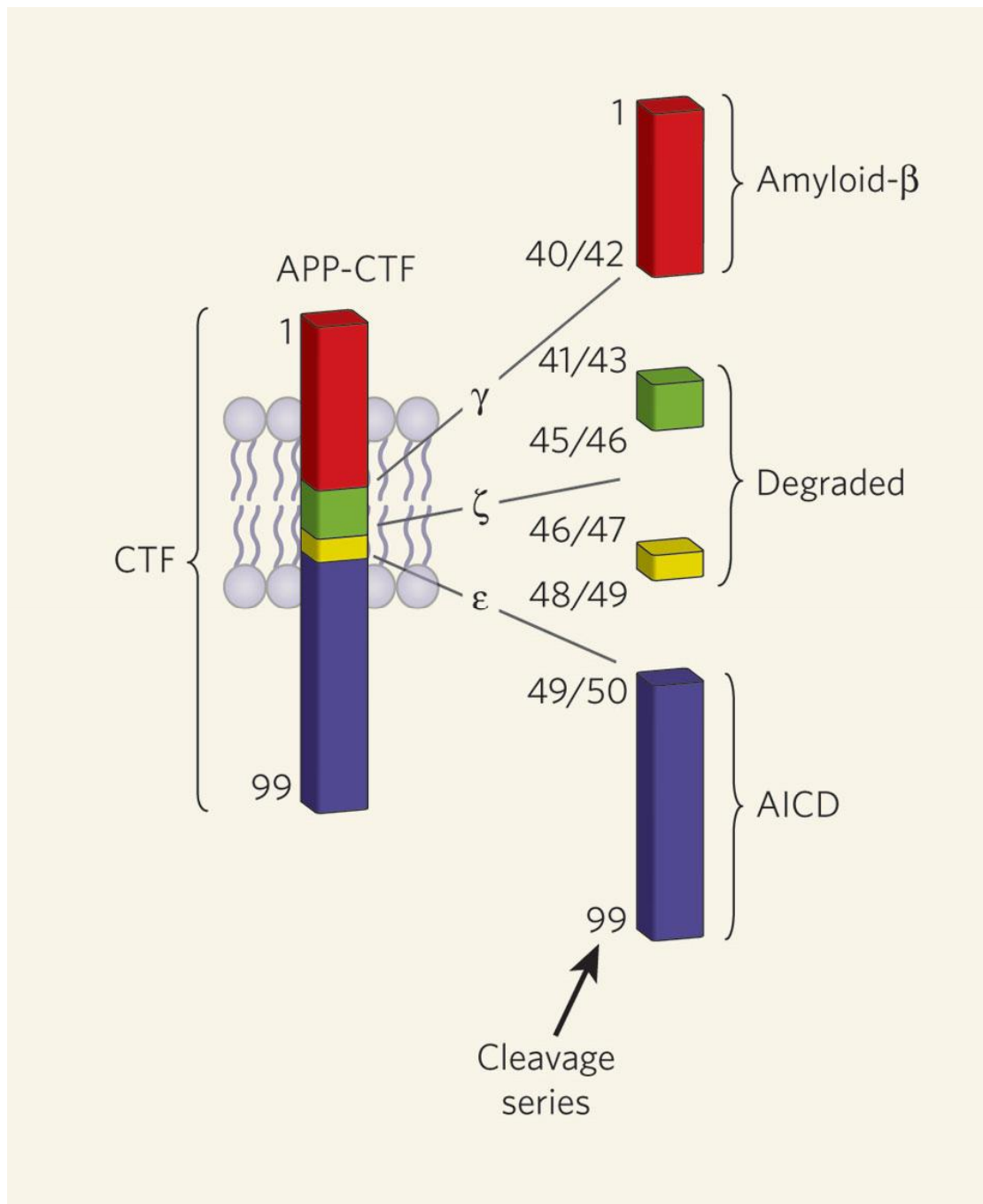


**Figure 1.2.3.** Complexities of PRESENILIN-dependent cleavage (St George-Hyslop and Schmitt-Ulms 2010)

The CTF of APP can be cleaved by  $\gamma$ -secretase at three main sites,  $\epsilon$ ,  $\zeta$  and  $\gamma$ , generating various cleavage products.

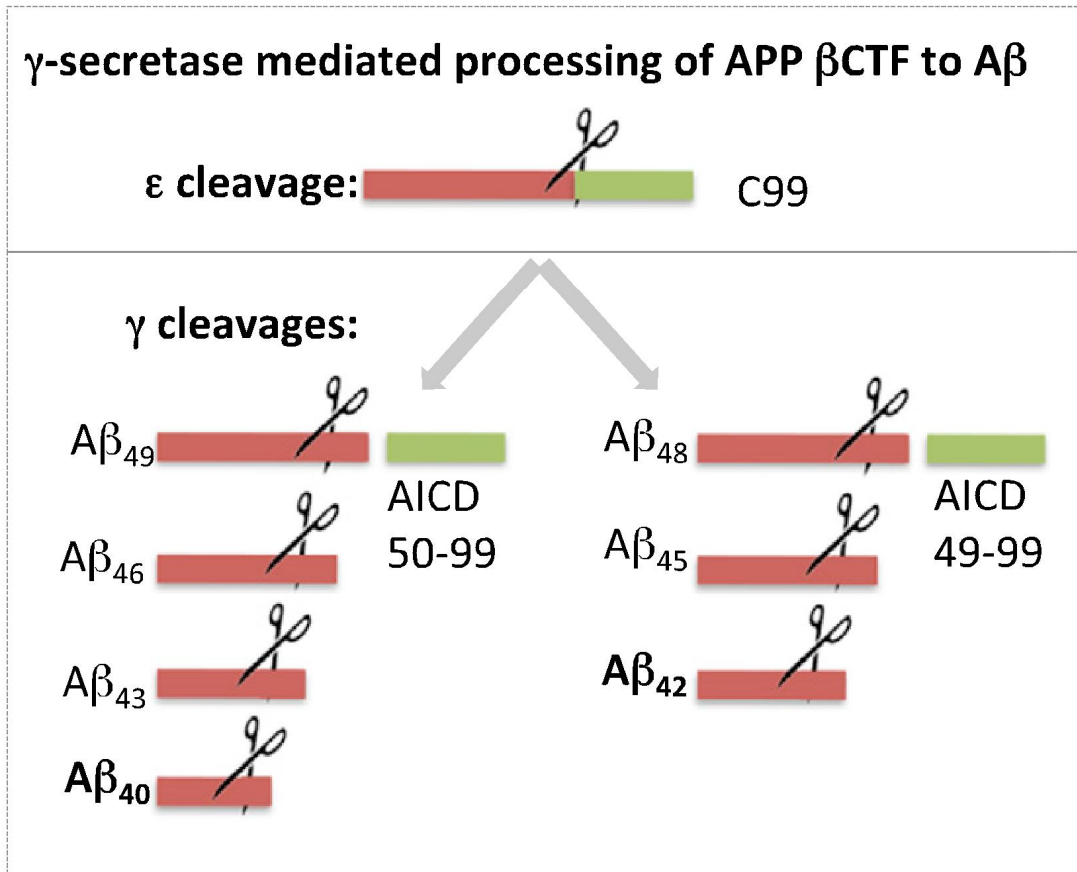


**Figure 1.2.4.**  $\gamma$ -secretase-mediated processing of APP  $\beta$ CTF to A $\beta$  (Siegel, Gerber et al. 2017).

The absence of PSEN1 is thought to reduce the activity of  $\gamma$ -secretase complexes (De Strooper, Saftig et al. 1998; Naruse, Thinakaran et al. 1998), and the absence of both PSEN1 and PSEN2 is thought to eliminate the function of  $\gamma$ -secretase complexes completely (Herreman, Serneels et al. 2000; Zhang, Nadeau et al. 2000). Although these two PRESENILINs are thought to complement each other, their functions may not be completely the same. In mouse blastocyst-derived (BD) cells that were transiently transfected with the C100 fragment of APP, the relative cellular activity (measured by secreted A $\beta$  per total Psen1 or Psen2) of Psen1-associated- $\gamma$ -secretase complexes (in

Psen1<sup>+/+</sup>Psen2<sup>-/-</sup> BD cells) was found to be ~38-fold greater than that of Psen2-associated- $\gamma$ -secretase complexes (in Psen1<sup>-/-</sup>Psen2<sup>+/+</sup> BD cells), indicating that Psen1 is more active than Psen2 toward the APP's C100 fragment (Lai, Chen et al. 2003). In a yeast reconstitution system, it has been found that PSEN1-associated- $\gamma$ -secretase complexes can generate ~ 24-fold more total A $\beta$  than PSEN2-associated- $\gamma$ -secretase complexes (measured by secreted A $\beta$  per  $\gamma$ -secretase complex), but since the amount of PSEN1 in the  $\gamma$ -secretase complexes was ~28 times higher than that of PSEN2, PSEN1 seemed to not have significantly higher activity than PSEN2 when calculating  $\gamma$ -secretase activity per one  $\gamma$ -secretase complex (Yonemura, Futai et al. 2011). Another study in a *Psen1<sup>-/-</sup>Psen2<sup>-/-</sup>* mouse fibroblast line showed that human PSEN1 generated more A $\beta$  (resulting from  $\gamma$ -site cleavage) than PSEN2, while the levels of the physiologically active APP intracellular domain (AICD) product (resulting from  $\epsilon$ -site cleavage) provided by these two PRESENILINs were the same (Pintchovski, Schenk et al. 2013).

Interestingly, a hypothesis suggested that since PSEN2 provides less A $\beta$  than PSEN1, mutations in *PSEN2* that cause AD must result in a more severe impact on  $\gamma$ -secretase than those in *PSEN1*, so that the effect on A $\beta$  levels can be strong enough to produce the disease with the presence of normal *PSEN1* alleles (Walker, Martinez et al. 2005). Functional analyses of putative *PSEN2* fAD mutations also supported this hypothesis, as these mutations cause dramatic changes in the A $\beta$  42/40 ratio (Walker, Martinez et al. 2005) and this ratio is proposed to be related to development of AD (Graff-Radford,

Crook et al. 2007; Barucker, Harmeier et al. 2014). Furthermore, these analyses revealed that most of the *PSEN2* mutations also show parallel decreases in the generation of CTF $\gamma$ , a CTF generated from the cleavage of APP by  $\gamma$ -secretase, as well as in Notch intracellular domain (NICD) production. Some very early-onset age *PSEN1* fAD mutations also show similar effects on CTF $\gamma$  and NICD production (Walker, Martinez et al. 2005).

### **PSEN2 and innate immunity associated with $\gamma$ -secretase activity**

Dysfunction of the immune system has been considered a possible major factor in AD (Jevtic, Sengar et al. 2017). As one of the important immune cell types, microglia are essential for surveillance in, and rapidly respond to changes in, the central nervous system (CNS) (Salter and Beggs 2014). However, in some neurodegenerative diseases, microglia may also cause neuronal injury through upregulating the production of inflammatory cytokines, neurotoxins, excitotoxins and other reactive oxygen species (Jayadev, Case et al. 2010; Heneka, Kummer et al. 2014). In AD, microglia are able to bind to A $\beta$  through cell-surface receptors and drive A $\beta$  fibrils into the endolysosomal pathway (Heneka, Carson et al. 2015).

In previous studies, *Psen1* was thought to contribute more to  $\gamma$ -secretase-associated APP and Notch cleavage than *Psen2* since knockout of *Psen1* in mice resulted in an embryonic lethal phenotype and a significant decrease in A $\beta$  levels (Shen, Bronson et



al. 1997; Palacino, Berechid et al. 2000), while knockout of Psen2 resulted in no overt embryonic phenotype or change of A $\beta$  levels (Herreman, Hartmann et al. 1999). Another study showed that, in mouse BD cells, the activities of Psen1-associated  $\gamma$ -secretase complexes and Psen2-associated  $\gamma$ -secretase complexes could be discriminated based on their susceptibility to potent  $\gamma$ -secretase inhibitors, indicating that these two classes of  $\gamma$ -secretase complexes may have different active sites with different substrate preferences (Lai, Chen et al. 2003). This study also revealed that only ~14% of the Psen1 in wild-type BD cells was engaged in active  $\gamma$ -secretase complexes, suggesting that the remaining Psen1 serves other biological functions rather than forming  $\gamma$ -secretase complexes (Lai, Chen et al. 2003). Additionally, there is supporting evidence that Psen2 is the predominant  $\gamma$ -secretase in microglia (from where inflammatory cytokines, neurotoxins and excitotoxins are released) (Jayadev, Case et al. 2010). In mouse microglia, although Psen1 and Psen2 show compensatory regulation (i.e. knockdown of one leads to upregulation of the other), only Psen2 knockdown leads to markedly decreased  $\gamma$ -secretase activity that leads to an exaggerated proinflammatory cytokine release from microglia (Jayadev, Case et al. 2010).

A negative regulator of monocyte pro-inflammatory response, miR146, has been reported to be constitutively downregulated in the microglia of Psen2 knockout mice, showing that the absence of Psen2 activity may impact neurodegeneration by disturbing the pro-inflammatory behavior of microglia (Jayadev, Case et al. 2013). Reduced

responsiveness to lipopolysaccharide (LPS), decreased nuclear factor kappa-light-chain-enhancer of activated B cells (NF- $\kappa$ B), mitogen-activated protein kinase (MAPK) activity and pro-inflammatory cytokine production have also been reported in *Psen2*- (but not *Psen1*-) knockout mice (Agrawal, Sawhney et al. 2016). All these studies indicate that *Psen2* may play a specific role in central nervous system (CNS) innate immunity not performed by *Psen1*.

### **PSEN2 and neurodevelopment (Notch signaling)**

In mice, the absence of both *Presenilin* genes results in embryonic lethality, indicating that *Presenilins* are essential for embryonic development (Donoviel, Hadjantonakis et al. 1999; Palacino, Berechid et al. 2000). In embryos of *Presenilin* double knockout mice (mice lacking both *Psen1* and *Psen2* activity), there is a loss of neural progenitor cells (NPCs) and disrupted neuronal migration at embryonic day 11 (Kim and Shen 2008). The Notch signaling pathway, which controls cellular fate choices throughout neurodevelopment (Louvi and Artavanis-Tsakonas 2006), was also found to be blocked in *Presenilin* double knockout mice embryos, indicating that *Presenilins* are essential for neurodevelopment (Kim and Shen 2008; Shen 2014). Premature differentiation of NPCs and inhibition of the Notch signaling pathway (as well as skeletal defects (Shen, Bronson et al. 1997)) were also found in *Psen1* knockout mice and resulted in perinatal lethality (Handler, Yang et al. 2000; Palacino, Berechid et al. 2000). However, the absence of **Psen2** in mice did not show any effect on the physiologically important

process of apoptosis during embryonic development (Brill, Torchinsky et al. 1999). This indicated that, in mice, *Psen1* is essential for neurodevelopment, in contrast to *Psen2* (Herreman, Hartmann et al. 1999).

### **PSEN2 and tumorigenesis**

An inverse association between cancer and AD has been observed in a population-based cohort study, which revealed that patients with prevalent cancer had a 43% lower risk of developing AD, while those with AD had a 69% lower risk of having cancer (Driver, Beiser et al. 2012). Presenilins are thought to have an anti-oncogenic function since the overexpression of both *Presenilins* promotes cellular apoptosis (Kovacs, Mancini et al. 1999; Yun, Park et al. 2016), and the knockout of either *Presenilin* results in higher rates of tumorigenesis (Xia, Qian et al. 2001; Serrano, Fernandez et al. 2010; Yun, Park et al. 2014).

The AICD produced through  $\gamma$ -secretase cleavage of APP was found to be able to regulate *epidermal growth factor receptor (EGFR)* transcription (which is upregulated in a wide variety of tumors) via binding to the *EGFR* promoter to provide a tumor suppressive effect (Zhang, Wang et al. 2007). The anti-apoptotic oncogene *bcl-2* was found to be downregulated during *PSEN2*-mediated apoptosis in primary cultured neurons (Suh and Checler 2002). The expression of PEROXIREDOXIN 6 (PRDX6), a tumor-promoting protein, was also found decreased in AD patients through elevated  $\gamma$ -

secretase activity induced by mutation of *PSEN2* (Park, Yun et al. 2017). A mouse model also verified that an fAD mutation of *PSEN2* (*NI41I*) could reduce PRDX6 activity via increased  $\gamma$ -secretase activity, leading to a reduced incidence of spontaneous and carcinogen-induced lung tumor development (Park, Yun et al. 2017).

### **PSEN2 and autophagy**

Autophagic/lysosomal dysfunction is thought to be extensively involved in the neurodegenerative process in AD since the endosomal-lysosomal system is a prominent site of APP processing, A $\beta$  uptake, and A $\beta$  production (Orr and Oddo 2013). The transport of autophagic vacuoles (AVs) and their maturation to lysosomes may be impaired in AD brains (Yu, Cuervo et al. 2005), and significant accumulations of AVs have also been detected in AD brains (Nixon, Wegiel et al. 2005).

Deletion of the *Psen1* gene in murine blastocysts was found to cause complete loss of macroautophagy without affecting non-lysosomal forms of proteolysis. This was due to the failure of the V0a1 subunit of v-ATPase to become N-glycosylated in the endoplasmic reticulum (ER), resulting in a selective impairment of autolysosome acidification and cathepsin activation (Lee, Yu et al. 2010). In human fibroblasts, fAD mutations in *PSEN1* resulted in even more severe impairment of lysosomal/autophagic functions compared to the affects seen in *PSEN1* knockout cells (Lee, Yu et al. 2010). However, the roles of PRESENILINs in lysosomal/autophagic functions are still

controversial. Another study in mouse cells revealed that, although the deletion of either *Psen1* or *Psen2* in mouse embryonic fibroblasts caused impaired autophagic function, no deficits in lysosomal acidification were found (Neely, Green et al. 2011). In that study, it was also found that deletion of both *Presenilins* in mouse fibroblasts (which resulted in loss of  $\gamma$ -secretase activity) led to impaired autophagic function, while  $\gamma$ -secretase inhibitors (which also led to loss of  $\gamma$ -secretase activity) did not adversely impact autophagy, indicating that *Presenilins* are involved in the autophagic function in a  $\gamma$ -secretase-independent manner (Neely, Green et al. 2011). It was also revealed that, although both *Presenilins* are involved in regulating autophagy, one cannot compensate for the loss of the other (Neely, Green et al. 2011). Additionally, in *PSEN1*<sup>-/-</sup> hippocampal neurons, a greatly decreased lysosomal calcium release that altered ion channels in the endoplasmic reticulum has been reported (Coen, Flannagan et al. 2012). Similar alterations in calcium homeostasis and reduced autophagic function were also observed in *Presenilin*-double knockout mouse embryonic fibroblasts, which seemed to indicate that *Presenilins* are necessary for calcium homeostasis (Neely Kayala, Dickinson et al. 2012)

### **PSEN2 and mitochondrial function**

Evidence suggests that *PRESENILINs* play roles in mitochondrial function (Behbahani, Shabalina et al. 2006) which is essential for energy supply in cells and for other cellular processes such as apoptosis, reactive oxygen species (ROS) production, and calcium

homeostasis (Hroudova, Singh et al. 2014). For neuronal survival, due to the limited glycolytic capacity of neurons, their energy supply is highly dependent on aerobic oxidative phosphorylation (OXPHOS) that occurs in mitochondria (Moreira, Carvalho et al. 2010). Moreover, the “mitochondrial cascade hypothesis” postulates that mitochondrial dysfunction is a primary event in both sporadic and autosomal dominant forms of AD (Swerdlow and Khan 2004; Swerdlow and Khan 2009). Although mutations in both *PSEN1* and *PSEN2* have been shown to sensitize cells to apoptosis through impaired mitochondrial function, there is evidence suggesting that PSEN2 (PSEN2-associated  $\gamma$ -secretase activity) may play a specific role required for proper mitochondrial function (Yun, Park et al. 2016). Some early studies in cell lines showed that the apoptotic cell death induced by overexpression of a fAD mutant form of *PSEN2* (*NI411*) was sensitive to inhibition by pertussis toxin, indicating that heterotrimeric GTP-binding proteins were involved in this process (Wolozin, Iwasaki et al. 1996). Furthermore, the overexpression of this fAD mutation in mice caused up-regulated  $\gamma$ -secretase activity specifically in mitochondrial fractions. This induced the production of A $\beta$ -42 peptides and contributed to mitochondrial dysfunction and AD pathology (Yun, Park et al. 2016). In mouse embryonic fibroblasts, it has been found that knockout of *Psen2* caused a significantly lower basal respiratory rate compared to knockout of *Psen1* or compared to wild type cells, and the percentage of fully functional mitochondria in *Psen2* knockout cells (and *Presenilin* double knockout cells) was much lower than that in wild type cells or cells lacking only *Psen1*. (Behbahani, Shabalina et al. 2006). Another study in mouse embryonic fibroblasts indicated that deficiency of

Psen2 led to a reduction in subunits responsible for mitochondrial OXPHOS with an altered morphology of the mitochondrial cristae, as well as an increase in glycolytic flux. This indicated that absence of Psen2 causes an impairment in respiratory capacity but also an increase in glycolytic flux to support energy needs (Contino, Porporato et al. 2017).

### **PSEN2 and calcium homeostasis**

Calcium homeostasis has been found to play an important role in AD progression, and calcium dysregulation may contribute to increased A $\beta$  production (Querfurth, Jiang et al. 1997), enhanced vulnerability to neuronal apoptosis (Mattson, Guo et al. 1998), and numerous processes underlying aging-related changes in the brain (Disterhoft, Moyer et al. 1994). Moreover, the changes in the concentration of calcium ions not only affect membrane channels but also diverse intracellular calcium-regulating structures and systems, such as mitochondria, and enzymes like calcium-dependent ATPases (Korol', Korol' et al. 2008).

Independent of their role in  $\gamma$ -secretase activity, PRESENILINs also appear to function as passive ER Ca<sup>2+</sup> leak channels (Tu, Nelson et al. 2006). Mutations in both *PSEN1* and *PSEN2* were found able to affect intracellular calcium homeostasis (Leisring, Parker et al. 1999; Mattson, Chan et al. 2001). Overexpression of fAD *PSEN1* mutations in cultured neural cells resulted in increased cytoplasmic calcium and

induced calcium release from the ER when stimulated by agonists (such as carbachol and bradykinin) (Guo, Furukawa et al. 1996). It was reported that such elevations of calcium can induce oxidative stress (Lafon-Cazal, Pietri et al. 1993; Mattson, Lovell et al. 1995), which mediates staurosporine-induced mitochondrial dysfunction and apoptosis (Kruman, Guo et al. 1998). *M146L* and *M146V* are both human fAD mutations in *PSEN1*. Mice with a knock-in of M146V show elevation of cytoplasmic calcium levels in synaptosomes, but this was not seen in M146L knock-in mice expressing lower (closer to physiologic) levels of mutant *PSEN1* (Begley, Duan et al. 1999). Mitochondrial dysfunction and caspase activation were also observed in synaptosomes of *PSEN1* mutant (*M146V*) knockin mice (Begley, Duan et al. 1999; Pak, Chan et al. 2003).

The level of calcium in the ER is also dependent on plasma membrane store-operated calcium channels (SOCCs) during capacitative calcium entry (CCE) (also known as store-operated calcium entry, which is triggered by depletion of intracellular calcium stores) (Putney 1986). In fAD *PSEN1* mutation (*M146V*) knockin mouse fibroblasts, elevated ER calcium levels and deficits in CCE (but functional SOCCs) were detected (Leissring, Akbari et al. 2000). Additionally, in CHO cells that stably overexpress wild type APP, both overexpression of the *PSEN1* mutation, *D257A*, and co-expression of *D257A* and the *PSEN2* mutation, *D366A*, (mutations decreasing  $\gamma$ -secretase activity) resulted in reduced intracellular calcium stores and enhanced CCE compared to overexpression of wild type *PSEN1*. However, expression of another dominant negative



isoform of *PSENI*,  $\Delta$ TM1-2 (which also abrogates  $\gamma$ -secretase activity), led to reduced intracellular calcium stores and a deficit of CCE (Akbari, Hitt et al. 2004). Thus, modulation of CCE appears to be independent of the function of PRESENILINs in  $\gamma$ -secretase activity (Akbari, Hitt et al. 2004).

The knockdown of the gene *PRESENILIN ENHANCER 2*, *C. ELEGANS*, *HOMOLOG OF (PSENE)* in HeLa cells, results in inhibition of proteolytic processing of PRESENILINs (Bandara, Malmersjo et al. 2013), thus, increasing the holoprotein form of these proteins. The holoprotein form of Psen1 in *Aph-1abc<sup>-/-</sup>* mouse embryonic fibroblasts (where  $\gamma$ -secretase activity is completely absent and Psen1 is present as a holoprotein) was found to greatly increase the calcium leak rate, strongly suggesting that the holoprotein forms of the Presenilins are the functional forms in calcium leakage (Tu, Nelson et al. 2006).

Knockdown of *PSEN2* activity in HeLa cells was found to reduce dramatically the ER calcium leak rate and to produce a large increase in ER calcium load (Bandara, Malmersjo et al. 2013). The *PSEN2* mutation, *NI411*, was found to induce ER calcium leak and reduce the ER calcium pool (Tu, Nelson et al. 2006; Kipanyula, Contreras et al. 2012). However, in SH-SY5Y neuroblastoma cell lines, it has been reported that *PSEN2*, but not *PSEN1*, modulates the shuttling of  $\text{Ca}^{2+}$  between the ER and mitochondria since mitochondrial  $\text{Ca}^{2+}$  dynamics were reduced by *PSEN2* down-regulation and enhanced by the expression of the *PSEN2* mutant forms, *NI411*, *D366A*

and *T122R* (Zampese, Fasolato et al. 2011).

Over-expression of both wild type and mutant *PSEN2* (*N141I*) in cultured neural cells (PC12 cells) was found to induce apoptosis in the absence of an apoptotic insult (Deng, Pike et al. 1996; Wolozin, Iwasaki et al. 1996), while no spontaneous apoptosis was observed in PC12 cells with overexpression of either wild type or mutant PSEN1 (either the L286V or M146V mutations) (Guo, Christakos et al. 1998).

### **PSEN2 and ischemic oxidative stress**

Brain ischemia has long been considered one of the possible causes of AD (Pluta, Jablonski et al. 2013). Dysregulated APP, the PRESENILINs,  $\beta$ -secretase and APOLIPOPROTEINs (the APOE4 allele is considered to be the major genetic risk factor for late onset, sporadic AD (Kim, Basak et al. 2009)) have been observed in experimental models of incomplete brain ischemia (Pluta, Furmaga-Jablonska et al. 2013). In rats, after 10 min of global brain ischemia, the expression of *Psen1* showed a modest trend of downregulation from days 2 to 7 post-ischemia, with an opposite trend at day 30. The expression of *Psen2* showed significant overexpression on day 2 post-ischemia and was only modestly elevated on day 7 followed by a slight down-regulation on day 30, indicating that the two *Presenilins* may have different roles during brain ischemia (Pluta, Kocki et al. 2016). This brain ischemia model supported that PSEN2 plays a role in the modulation of apoptosis (Suh and Checler 2002), since neurons in

ischemic injured areas of the brain began to die from days 2 to 7 post-ischemia (Pluta, Kocki et al. 2016). Although the PRESENILINs appear to complement each other's functions, PSEN1 seems to provide a basic constitutive function, while PSEN2 appears to operate as an emergency helper under ischemic oxidative stress (Kocki, Ulamek-Koziol et al. 2015).

Interestingly, PS2V, a truncated isoform of PSEN2 protein produced by alternative *PSEN2* gene transcript splicing that excludes exon 5 sequence from *PSEN2* (Figure 1.2.5), is preferentially expressed in AD brains (Sato, Hori et al. 1999). In human neuroblastoma SK-N-SH cells, the expression of PS2V is induced by hypoxia, but not by many other stresses (Sato, Imaizumi et al. 2001). This finding is also supported by observations in animal models, i.e. in a guinea pig model (Sharman, Moussavi Nik et al. 2013) and in a zebrafish model (Moussavi Nik, Newman et al. 2015). However, in zebrafish, hypoxia induces alternative splicing of transcripts of the *psen1* gene rather than *psen2* to produce a PS2V-equivalent isoform named PS1IV. Although PS1IV is far smaller than PS2V, it is still able to stimulate  $\gamma$ -secretase activity (Moussavi Nik, Newman et al. 2015). Further study of PS1IV revealed that the absence of PS1IV under hypoxia-like conditions changes the expression of genes involved in inflammation (i.e. gene IL1B which is recognised as an AD risk locus (Sciacca, Ferri et al. 2003)) (Ebrahimie, Moussavi Nik et al. 2016)

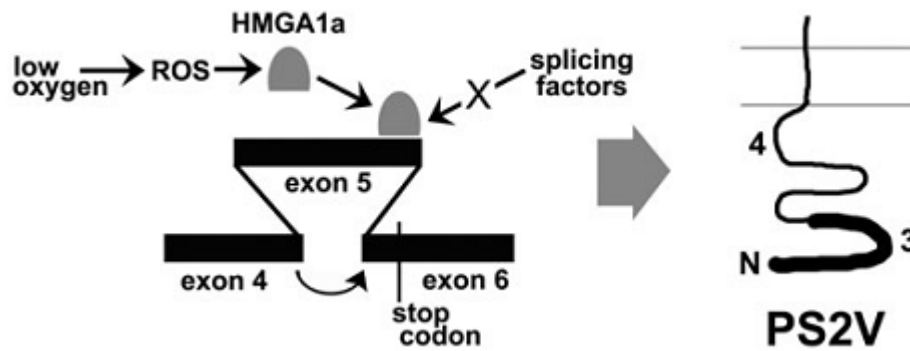


**Figure 1.2.5.** The generation of PS2V (Moussavi Nik, Newman et al. 2015).

Under hypoxia, reactive oxygen species are released from mitochondria and induce the expression of HMGA1a that binds to *PSEN2* transcripts at the 3' end of exon 5. This excludes splicing factors causing exon 4 to be ligated to exon 6. This causes a frameshift that results in early termination of the coding sequence, translation of which produces PS2V (Moussavi Nik, Newman et al. 2015).

### **PSEN2 and gonadal steroids**

AD has been found to be more prevalent in women than in men (Vina and Lloret 2010). AD histopathology (Barnes, Wilson et al. 2005) and AD-related cognitive decline (Sinforiani, Citterio et al. 2010) have been reported to be greater in women than in men. Although the mechanism of this gender difference in the development of AD is still unclear, sex steroid hormones are thought to be one possible cause since it is known that sex steroid hormones are involved in neural development (Bowers, Waddell et al. 2010).

The expression of PRESENILINS has been found to change with age and sex. In mice, it was found that, in old mice, *Psen1* is down-regulated and *Psen2* is upregulated in both sexes, while the expression of *Psen1* is relatively higher and that of *Psen2* is lower in female compared to male mice (Thakur and Ghosh 2007). This research group found that the expression of *Psen1* is down-regulated by gonadal hormones (17 $\beta$ -estradiol and testosterone in the cerebral cortex) in all females and adult male mice, while in old male mice, it is up-regulated (Ghosh and Thakur 2008). The expression of *Psen2* is down-regulated after gonadectomy, while supplementation of gonadal steroids is able to up-regulate the expression of *Psen2* in both mouse sexes (Ghosh and Thakur 2008). Another research group found that there is no difference between female hypogonadal mice and their littermate controls in expression of Alzheimer's disease-related proteins, while male hypogonadal mice show altered expression of these proteins (Drummond, Martins et al. 2012). It appears that the expression of gonadal steroids (perhaps mainly related to the concentration of androgen) may affect the expression of the Presenilins and subsequently affect Presenilin-related pathways.

### **Zebrafish as a model for investigation of AD**

For modelling of Alzheimer's disease pathology, both mammalian and non-mammalian animals have been used. *Danio rerio*, also known as the zebrafish, presents many advantages as a model organism for the study of AD.

Both the organization of zebrafish and human genome structures and the genetic pathways (controlling signal transduction and development) in zebrafish and humans are highly conserved (Postlethwait, Woods et al. 2000). The genome and anatomy of zebrafish are the result of ~420 million years of divergent evolution from the human lineage (Ravi and Venkatesh 2008), and most human genes have clearly identifiable orthologues in zebrafish. The size of the zebrafish genome is only half that of the human genome, but there are more genes in the zebrafish genome because of a whole genome duplication that occurred early in the history of the teleost lineage (Wittbrodt, Meyer et al. 1998). As gene regulatory regions may diverge after a duplication event, these duplicates may, together, fulfill the function of their single mammalian orthologues. Thus, a single gene may be represented by one or more “co-orthologues” in the zebrafish, allowing a more detailed dissection of gene function (Force, Lynch et al. 1999).

The small size of zebrafish eggs and larvae is another property that makes zebrafish an excellent model system for studies on human diseases. Due to this small size, the eggs or larvae can be incubated in 96 well plates, which allows for high throughput *in vivo* screening of responses to chemicals in their support medium. The high fecundity of the zebrafish also guarantees plentiful supplies of eggs or larvae for *in vivo* analysis (Best and Alderton 2008). This also allows us to raise a large number of siblings from pair matings in the same environment (the same tank) to reduce environmental and genetic variability in transcriptomic and other “omics” analyses. Moreover, the zebrafish model

is an excellent system for study of AD-relevant genes and pathways. The genes *apoec* and *apoeb* in zebrafish are co-orthologues of human *APOE* (Babin, Thisse et al. 1997; Woods, Wilson et al. 2005), genes *appa* and *appb* are co-orthologues of human APP, and genes *psen1* (Leimer, Lun et al. 1999) and *psen2* (Groth, Nornes et al. 2002) are orthologues of human *PSEN1* and *PSEN2*, respectively.

## **Conclusion**

*PSEN2* is one of the genes implicated in fAD pathogenesis, but our understanding of how it contributes to AD progression is still limited. As one of the essential components of the  $\gamma$ -secretase complex, PSEN2 protein has been found to be involved in  $\gamma$ -secretase-related physiological activities that are associated with AD progression such as innate immunity, Notch signaling, tumorigenesis and autophagy. It has also been found that PSEN2 plays a specific role(s) in mitochondrial function since it is involved in regulating calcium homeostasis. Research using animal models has also found that expression of Psen2 changes with age and sex, and, significantly, is altered under ischemic oxidative stress which is probably a major contributor to AD pathogenesis. However, this may be only the tip of the iceberg of PSEN2's functions, and more research must be done to fully identify and understand PSEN2's roles in normal cell biology and AD.

## **1.3 References**

- Agrawal, V., N. Sawhney, et al. (2016). "Loss of Presenilin 2 Function Is Associated with Defective LPS-Mediated Innate Immune Responsiveness." *Molecular Neurobiology* **53**(5): 3428-3438.
- Akbari, Y., B. D. Hitt, et al. (2004). "Presenilin regulates capacitative calcium entry dependently and independently of gamma-secretase activity." *Biochem Biophys Res Commun* **322**(4): 1145-1152.
- Babin, P. J., C. Thisse, et al. (1997). "Both apolipoprotein E and A-I genes are present in a nonmammalian vertebrate and are highly expressed during embryonic development." *Proc Natl Acad Sci U S A* **94**(16): 8622-8627.
- Bandara, S., S. Malmersjo, et al. (2013). "Regulators of calcium homeostasis identified by inference of kinetic model parameters from live single cells perturbed by siRNA." *Sci Signal* **6**(283): 2003649.
- Barnes, L. L., R. S. Wilson, et al. (2005). "Sex differences in the clinical manifestations of Alzheimer disease pathology." *Arch Gen Psychiatry* **62**(6): 685-691.
- Barucker, C., A. Harmeier, et al. (2014). "Nuclear translocation uncovers the amyloid peptide Abeta42 as a regulator of gene transcription." *J Biol Chem* **289**(29): 20182-20191.
- Begley, J. G., W. Duan, et al. (1999). "Altered Calcium Homeostasis and Mitochondrial Dysfunction in Cortical Synaptic Compartments of Presenilin-1 Mutant Mice." *Journal of Neurochemistry* **72**(3): 1030-1039.
- Behbahani, H., I. G. Shabalina, et al. (2006). "Differential role of Presenilin-1 and -2 on mitochondrial membrane potential and oxygen consumption in mouse embryonic fibroblasts." *J Neurosci Res* **84**(4): 891-902.
- Best, J. D. and W. K. Alderton (2008). "Zebrafish: An in vivo model for the study of neurological diseases." *Neuropsychiatr Dis Treat* **4**(3): 567-576.
- Bowers, J. M., J. Waddell, et al. (2010). "A developmental sex difference in hippocampal neurogenesis is mediated by endogenous oestradiol." *Biol Sex Differ* **1**(1): 2042-6410.
- Brill, A., A. Torchinsky, et al. (1999). "The role of apoptosis in normal and abnormal embryonic development." *J Assist Reprod Genet* **16**(10): 512-519.
- Cao, X. and T. C. Sudhof (2001). "A transcriptionally [correction of transcriptively] active complex of APP with Fe65 and histone acetyltransferase Tip60." *Science* **293**(5527): 115-120.
- Chavez-Gutierrez, L., L. Bammens, et al. (2012). "The mechanism of gamma-Secretase dysfunction in familial Alzheimer disease." *Embo J* **31**(10): 2261-2274.
- Coen, K., R. S. Flannagan, et al. (2012). "Lysosomal calcium homeostasis defects, not proton pump defects, cause endo-lysosomal dysfunction in PSEN-deficient cells." *J Cell Biol* **198**(1): 23-35.
- Contino, S., P. E. Porporato, et al. (2017). "Presenilin 2-Dependent Maintenance of Mitochondrial Oxidative Capacity and Morphology." *Front Physiol* **8**(796).
- Cooper, E., W. M. Deng, et al. [Aph-1 is required to regulate Presenilin-mediated gamma-secretase activity and cell survival in Drosophila wing development](#), *Genesis*. 2009 Mar;47(3):169-74. doi: 10.1002/dvg.20478.
- De Strooper, B., W. Annaert, et al. (1999). "A presenilin-1-dependent [gamma]-secretase-like protease mediates release of Notch intracellular domain." *Nature* **398**(6727): 518-522.
- De Strooper, B., P. Saftig, et al. (1998). "Deficiency of presenilin-1 inhibits the normal cleavage of amyloid precursor protein." *Nature* **391**(6665): 387-390.
- Deng, G., C. J. Pike, et al. (1996). "Alzheimer-associated presenilin-2 confers increased sensitivity to apoptosis in PC12 cells." *FEBS Letters* **397**(1): 50-54.



Disterhoft, J. F., J. R. Moyer, Jr., et al. (1994). "The calcium rationale in aging and Alzheimer's disease. Evidence from an animal model of normal aging." Ann N Y Acad Sci **747**: 382-406.

Donoviel, D. B., A. K. Hadjantonakis, et al. (1999). "Mice lacking both presenilin genes exhibit early embryonic patterning defects." Genes Dev **13**(21): 2801-2810.

Driver, J. A., A. Beiser, et al. (2012). "Inverse association between cancer and Alzheimer's disease: results from the Framingham Heart Study." Bmj **12**(344).

Drummond, E. S., R. N. Martins, et al. (2012). "Altered expression of Alzheimer's disease-related proteins in male hypogonadal mice." Endocrinology **153**(6): 2789-2799.

Ebrahimie, E., S. H. Moussavi Nik, et al. (2016). "The Zebrafish Equivalent of Alzheimer's Disease-Associated PRESENILIN Isoform PS2V Regulates Inflammatory and Other Responses to Hypoxic Stress." J Alzheimers Dis **52**(2): 581-608.

Force, A., M. Lynch, et al. (1999). "Preservation of duplicate genes by complementary, degenerative mutations." Genetics **151**(4): 1531-1545.

Ghosh, S. and M. K. Thakur (2008). "PS1 expression is downregulated by gonadal steroids in adult mouse brain." Neurochem Res **33**(3): 365-369.

Ghosh, S. and M. K. Thakur (2008). "PS2 protein expression is upregulated by sex steroids in the cerebral cortex of aging mice." Neurochem Int **52**(3): 363-367.

Graff-Radford, N. R., J. E. Crook, et al. (2007). "Association of low plasma A $\beta$ 42/A $\beta$  40 ratios with increased imminent risk for mild cognitive impairment and Alzheimer disease." Archives of Neurology **64**(3): 354-362.

Groth, C., S. Nornes, et al. (2002). "Identification of a second presenilin gene in zebrafish with similarity to the human Alzheimer's disease gene presenilin2." Development Genes and Evolution **212**(10): 486-490.

Guo, Q., S. Christakos, et al. (1998). "Calbindin D28k blocks the proapoptotic actions of mutant presenilin 1: reduced oxidative stress and preserved mitochondrial function." Proc Natl Acad Sci U S A **95**(6): 3227-3232.

Guo, Q., K. Furukawa, et al. (1996). "Alzheimer's PS-1 mutation perturbs calcium homeostasis and sensitizes PC12 cells to death induced by amyloid beta-peptide." Neuroreport **8**(1): 379-383.

Handler, M., X. Yang, et al. (2000). "Presenilin-1 regulates neuronal differentiation during neurogenesis." Development **127**(12): 2593-2606.

Heneka, M. T., M. J. Carson, et al. (2015). "Neuroinflammation in Alzheimer's disease." The Lancet Neurology **14**(4): 388-405.

Heneka, M. T., M. P. Kummer, et al. (2014). "Innate immune activation in neurodegenerative disease." Nat Rev Immunol **14**(7): 463-477.

Herreman, A., D. Hartmann, et al. (1999). "Presenilin 2 deficiency causes a mild pulmonary phenotype and no changes in amyloid precursor protein processing but enhances the embryonic lethal phenotype of presenilin 1 deficiency." Proc Natl Acad Sci U S A **96**(21): 11872-11877.

Herreman, A., L. Serneels, et al. (2000). "Total inactivation of gamma-secretase activity in presenilin-deficient embryonic stem cells." Nat Cell Biol **2**(7): 461-462.

Hroudova, J., N. Singh, et al. (2014). "Mitochondrial dysfunctions in neurodegenerative diseases: relevance to Alzheimer's disease." Biomed Res Int **175062**(10): 12.

Hutton, M. (1997). "The Presenilins and Alzheimer's Disease." Human Molecular Genetics **6**(10): 1639-1646.

Jayadev, S., A. Case, et al. (2013). "Presenilin 2 influences miR146 level and activity in microglia." Journal

- of *Neurochemistry* **127**(5): 592-599.
- Jayadev, S., A. Case, et al. (2010). "Presenilin 2 is the predominant gamma-secretase in microglia and modulates cytokine release." *PLoS ONE* **5**(12): 0015743.
- Jayadev, S., J. B. Leverenz, et al. (2010). "Alzheimer's disease phenotypes and genotypes associated with mutations in presenilin 2." *Brain* **133**(Pt 4): 1143-1154.
- Jevtic, S., A. S. Sengar, et al. (2017). "The role of the immune system in Alzheimer disease: Etiology and treatment." *Ageing Res Rev* **40**: 84-94.
- Kim, J., J. M. Basak, et al. (2009). "The role of apolipoprotein E in Alzheimer's disease." *Neuron* **63**(3): 287-303.
- Kim, W. Y. and J. Shen (2008). "Presenilins are required for maintenance of neural stem cells in the developing brain." *Mol Neurodegener* **3**(2): 1750-1326.
- Kipanyula, M. J., L. Contreras, et al. (2012). "Ca<sup>2+</sup> dysregulation in neurons from transgenic mice expressing mutant presenilin 2." *Aging Cell* **11**(5): 885-893.
- Kocki, J., M. Ulamek-Kozioł, et al. (2015). "Dysregulation of Amyloid-beta Protein Precursor, beta-Secretase, Presenilin 1 and 2 Genes in the Rat Selectively Vulnerable CA1 Subfield of Hippocampus Following Transient Global Brain Ischemia." *J Alzheimers Dis* **47**(4): 1047-1056.
- Korol', T. Y., S. V. Korol', et al. (2008). "Disruption of Calcium Homeostasis in Alzheimer's Disease." *Neurophysiology* **40**(5): 385-392.
- Kovacs, D. M., R. Mancini, et al. (1999). "Staurosporine-induced activation of caspase-3 is potentiated by presenilin 1 familial Alzheimer's disease mutations in human neuroglioma cells." *J Neurochem* **73**(6): 2278-2285.
- Kruman, I., Q. Guo, et al. (1998). "Calcium and reactive oxygen species mediate staurosporine-induced mitochondrial dysfunction and apoptosis in PC12 cells." *J Neurosci Res* **51**(3): 293-308.
- Kuperstein, I., K. Broersen, et al. (2010). "Neurotoxicity of Alzheimer's disease Aβ peptides is induced by small changes in the Aβ<sub>42</sub> to Aβ<sub>40</sub> ratio." *EMBO J* **29**(19): 3408-3420.
- Lafon-Cazal, M., S. Pietri, et al. (1993). "NMDA-dependent superoxide production and neurotoxicity." *Nature* **364**(6437): 535-537.
- Lai, M.-T., E. Chen, et al. (2003). "Presenilin-1 and Presenilin-2 Exhibit Distinct yet Overlapping γ-Secretase Activities." *Journal of Biological Chemistry* **278**(25): 22475-22481.
- Lee, J. H., W. H. Yu, et al. (2010). "Lysosomal proteolysis and autophagy require presenilin 1 and are disrupted by Alzheimer-related PS1 mutations." *Cell* **141**(7): 1146-1158.
- Lee, M. K., H. H. Slunt, et al. (1996). "Expression of presenilin 1 and 2 (PS1 and PS2) in human and murine tissues." *J Neurosci* **16**(23): 7513-7525.
- Leimer, U., K. Lun, et al. (1999). "Zebrafish (Danio rerio) Presenilin Promotes Aberrant Amyloid β-Peptide Production and Requires a Critical Aspartate Residue for Its Function in Amyloidogenesis†." *Biochemistry* **38**(41): 13602-13609.
- Leissring, M. A., Y. Akbari, et al. (2000). "Capacitative calcium entry deficits and elevated luminal calcium content in mutant presenilin-1 knockin mice." *J Cell Biol* **149**(4): 793-798.
- Leissring, M. A., I. Parker, et al. (1999). "Presenilin-2 Mutations Modulate Amplitude and Kinetics of Inositol 1,4,5-Trisphosphate-mediated Calcium Signals." *Journal of Biological Chemistry* **274**(46): 32535-32538.
- Levy-Lahad, E., W. Wasco, et al. (1995). "Candidate gene for the chromosome 1 familial Alzheimer's disease locus." *Science* **269**(5226): 973-977.
- Louvi, A. and S. Artavanis-Tsakonas (2006). "Notch signalling in vertebrate neural development." *Nature*

Reviews Neuroscience **7**(2): 93+.

- Mattson, M. P., S. L. Chan, et al. (2001). "Presenilin mutations and calcium signaling defects in the nervous and immune systems." BioEssays **23**(8): 733-744.
- Mattson, M. P., Q. Guo, et al. (1998). "Presenilins, the endoplasmic reticulum, and neuronal apoptosis in Alzheimer's disease." J Neurochem **70**(1): 1-14.
- Mattson, M. P., M. A. Lovell, et al. (1995). "Neurotrophic factors attenuate glutamate-induced accumulation of peroxides, elevation of intracellular Ca<sup>2+</sup> concentration, and neurotoxicity and increase antioxidant enzyme activities in hippocampal neurons." J Neurochem **65**(4): 1740-1751.
- Moreira, P. I., C. Carvalho, et al. (2010). "Mitochondrial dysfunction is a trigger of Alzheimer's disease pathophysiology." Biochimica et Biophysica Acta (BBA) - Molecular Basis of Disease **1802**(1): 2-10.
- Moussavi Nik, S. H., M. Newman, et al. (2015). "Alzheimer's disease-related peptide PS2V plays ancient, conserved roles in suppression of the unfolded protein response under hypoxia and stimulation of gamma-secretase activity." Human Molecular Genetics **26**.
- Naruse, S., G. Thinakaran, et al. (1998). "Effects of PS1 deficiency on membrane protein trafficking in neurons." Neuron **21**(5): 1213-1221.
- Neely Kayala, K. M., G. D. Dickinson, et al. (2012). "Presenilin-null cells have altered two-pore calcium channel expression and lysosomal calcium: implications for lysosomal function." Brain Res **13**: 8-16.
- Neely, K. M., K. N. Green, et al. (2011). "Presenilin is necessary for efficient proteolysis through the autophagy-lysosome system in a gamma-secretase-independent manner." J Neurosci **31**(8): 2781-2791.
- Newman, M., I. F. Musgrave, et al. (2007). "Alzheimer disease: amyloidogenesis, the presenilins and animal models." Biochim Biophys Acta **3**: 285-297.
- Nixon, R. A., J. Wegiel, et al. (2005). "Extensive Involvement of Autophagy in Alzheimer Disease: An Immuno-Electron Microscopy Study." Journal of Neuropathology & Experimental Neurology **64**(2): 113-122.
- Orr, M. E. and S. Oddo (2013). "Autophagic/lysosomal dysfunction in Alzheimer's disease." Alzheimers Res Ther **5**(5).
- Pak, K., S. L. Chan, et al. (2003). "Presenilin-1 mutation sensitizes oligodendrocytes to glutamate and amyloid toxicities, and exacerbates white matter damage and memory impairment in mice." NeuroMolecular Medicine **3**(1): 53-64.
- Palacino, J. J., B. E. Berechid, et al. (2000). "Regulation of amyloid precursor protein processing by presenilin 1 (PS1) and PS2 in PS1 knockout cells." J Biol Chem **275**(1): 215-222.
- Park, M. H., H. M. Yun, et al. (2017). "Presenilin Mutation Suppresses Lung Tumorigenesis via Inhibition of Peroxiredoxin 6 Activity and Expression." Theranostics **7**(15): 3624-3637.
- Pintchovski, S. A., D. B. Schenk, et al. (2013). "Evidence that enzyme processivity mediates differential Aβeta production by PS1 and PS2." Curr Alzheimer Res **10**(1): 4-10.
- Pluta, R., W. Furmaga-Jablonska, et al. (2013). "Brain ischemia activates beta- and gamma-secretase cleavage of amyloid precursor protein: significance in sporadic Alzheimer's disease." Mol Neurobiol **47**(1): 425-434.
- Pluta, R., M. Jablonski, et al. (2013). "Sporadic Alzheimer's disease begins as episodes of brain ischemia and ischemically dysregulated Alzheimer's disease genes." Mol Neurobiol **48**(3): 500-515.

- Pluta, R., J. Kocki, et al. (2016). "Alzheimer-associated presenilin 2 gene is dysregulated in rat medial temporal lobe cortex after complete brain ischemia due to cardiac arrest." Pharmacological Reports **68**(1): 155-161.
- Postlethwait, J. H., I. G. Woods, et al. (2000). "Zebrafish Comparative Genomics and the Origins of Vertebrate Chromosomes." Genome Research **10**(12): 1890-1902.
- Prokop, S., K. Shirotani, et al. (2004). "Requirement of PEN-2 for Stabilization of the Presenilin N-/C-terminal Fragment Heterodimer within the  $\gamma$ -Secretase Complex." Journal of Biological Chemistry **279**(22): 23255-23261.
- Putney, J. W., Jr. (1986). "A model for receptor-regulated calcium entry." Cell Calcium **7**(1): 1-12.
- Querfurth, H. W., J. Jiang, et al. (1997). "Caffeine stimulates amyloid beta-peptide release from beta-amyloid precursor protein-transfected HEK293 cells." J Neurochem **69**(4): 1580-1591.
- Ravi, V. and B. Venkatesh (2008). "Rapidly evolving fish genomes and teleost diversity." Current Opinion in Genetics & Development **18**(6): 544-550.
- Salter, M. W. and S. Beggs (2014). "Sublime microglia: expanding roles for the guardians of the CNS." Cell **158**(1): 15-24.
- Sato, N., O. Hori, et al. (1999). "A novel presenilin-2 splice variant in human Alzheimer's disease brain tissue." J Neurochem **72**(6): 2498-2505.
- Sato, N., K. Imaizumi, et al. (2001). "Increased production of beta-amyloid and vulnerability to endoplasmic reticulum stress by an aberrant spliced form of presenilin 2." J Biol Chem **276**(3): 2108-2114.
- Sciacca, F. L., C. Ferri, et al. (2003). "Interleukin-1B polymorphism is associated with age at onset of Alzheimer's disease." Neurobiol Aging **24**(7): 927-931.
- Serrano, J., A. P. Fernandez, et al. (2010). "High sensitivity to carcinogens in the brain of a mouse model of Alzheimer's disease." Oncogene **29**(15): 2165-2171.
- Shah, S., S. F. Lee, et al. (2005). "Nicastrin functions as a gamma-secretase-substrate receptor." Cell **122**(3): 435-447.
- Sharman, M. J., S. H. Moussavi Nik, et al. (2013). "The Guinea Pig as a Model for Sporadic Alzheimer's Disease (AD): The Impact of Cholesterol Intake on Expression of AD-Related Genes." PLoS ONE **8**(6): e66235.
- Shen, J. (2014). "Function and dysfunction of presenilin." Neurodegener Dis **13**(2-3): 61-63.
- Shen, J., R. T. Bronson, et al. (1997). "Skeletal and CNS defects in Presenilin-1-deficient mice." Cell **89**(4): 629-639.
- Siegel, G., H. Gerber, et al. (2017). "The Alzheimer's Disease  $\gamma$ -Secretase Generates Higher 42:40 Ratios for  $\beta$ -Amyloid Than for p3 Peptides." Cell Reports **19**(10): 1967-1976.
- Sinforiani, E., A. Citterio, et al. (2010). "Impact of gender differences on the outcome of Alzheimer's disease." Dement Geriatr Cogn Disord **30**(2): 147-154.
- St George-Hyslop, P. and G. Schmitt-Ulms (2010). "Alzheimer's disease: Selectively tuning [gamma]-secretase." Nature **467**(7311): 36-37.
- Steiner, H., R. Fluhner, et al. (2008). "Intramembrane proteolysis by gamma-secretase." J Biol Chem **283**(44): 29627-29631.
- Suh, Y. H. and F. Checler (2002). "Amyloid precursor protein, presenilins, and alpha-synuclein: molecular pathogenesis and pharmacological applications in Alzheimer's disease." Pharmacol Rev **54**(3): 469-525.
- Suzuki, N., T. T. Cheung, et al. (1994). "An increased percentage of long amyloid beta protein secreted

- by familial amyloid beta protein precursor (beta APP717) mutants." Science **264**(5163): 1336-1340.
- Swerdlow, R. H. and S. M. Khan (2004). "A "mitochondrial cascade hypothesis" for sporadic Alzheimer's disease." Medical Hypotheses **63**(1): 8-20.
- Swerdlow, R. H. and S. M. Khan (2009). "The Alzheimer's disease mitochondrial cascade hypothesis: An update." Experimental Neurology **218**(2): 308-315.
- Thakur, M. K. and S. Ghosh (2007). "Age and sex dependent alteration in presenilin expression in mouse cerebral cortex." Cell Mol Neurobiol **27**(8): 1059-1067.
- Thinakaran, G., D. R. Borchelt, et al. (1996). "Endoproteolysis of presenilin 1 and accumulation of processed derivatives in vivo." Neuron **17**(1): 181-190.
- Thinakaran, G. and E. H. Koo (2008). "Amyloid precursor protein trafficking, processing, and function." J Biol Chem **283**(44): 29615-29619.
- Tomita, T., K. Maruyama, et al. (1997). "The presenilin 2 mutation (N141I) linked to familial Alzheimer disease (Volga German families) increases the secretion of amyloid  $\beta$  protein ending at the 42nd (or 43rd) residue." Proceedings of the National Academy of Sciences **94**(5): 2025-2030.
- Tu, H., O. Nelson, et al. (2006). "Presenilins form ER Ca<sup>2+</sup> leak channels, a function disrupted by familial Alzheimer's disease-linked mutations." Cell **126**(5): 981-993.
- Vina, J. and A. Lloret (2010). "Why women have more Alzheimer's disease than men: gender and mitochondrial toxicity of amyloid-beta peptide." J Alzheimers Dis **20**(2): 2010-100501.
- Walker, E. S., M. Martinez, et al. (2005). "Presenilin 2 familial Alzheimer's disease mutations result in partial loss of function and dramatic changes in A $\beta$  42/40 ratios." Journal of Neurochemistry **92**(2): 294-301.
- Wittbrodt, J., A. Meyer, et al. (1998). "More genes in fish?" BioEssays **20**(6): 511-515.
- Wolozin, B., K. Iwasaki, et al. (1996). "Participation of Presenilin 2 in Apoptosis: Enhanced Basal Activity Conferred by an Alzheimer Mutation." Science **274**(5293): 1710-1713.
- Woods, I. G., C. Wilson, et al. (2005). "The zebrafish gene map defines ancestral vertebrate chromosomes." Genome Res **15**(9): 1307-1314.
- Xia, X., S. Qian, et al. (2001). "Loss of presenilin 1 is associated with enhanced beta-catenin signaling and skin tumorigenesis." Proc Natl Acad Sci U S A **98**(19): 10863-10868.
- Xu, X. (2009). "Gamma-secretase catalyzes sequential cleavages of the A $\beta$ PP transmembrane domain." J Alzheimers Dis **16**(2): 211-224.
- Yonemura, Y., E. Futai, et al. (2011). "Comparison of presenilin 1 and presenilin 2 gamma-secretase activities using a yeast reconstitution system." J Biol Chem **286**(52): 44569-44575.
- Yu, W. H., A. M. Cuervo, et al. (2005). "Macroautophagy--a novel Beta-amyloid peptide-generating pathway activated in Alzheimer's disease." J Cell Biol **171**(1): 87-98.
- Yun, H. M., M. H. Park, et al. (2014). "Loss of presenilin 2 is associated with increased iPLA2 activity and lung tumor development." Oncogene **33**(44): 5193-5200.
- Yun, W. B., J. J. Park, et al. (2016). "Overexpression of N141I PS2 increases gamma-secretase activity through up-regulation of Presenilin and Pen-2 in brain mitochondria of NSE/hPS2m transgenic mice." Lab Anim Res **32**(4): 249-256.
- Zampese, E., C. Fasolato, et al. (2011). "Presenilin 2 modulates endoplasmic reticulum (ER)-mitochondria interactions and Ca<sup>2+</sup> cross-talk." Proc Natl Acad Sci U S A **108**(7): 2777-2782.
- Zhang, Y.-w., R. Thompson, et al. (2011). "APP processing in Alzheimer's disease." Molecular Brain **4**(1): 3.

- Zhang, Y. W., R. Wang, et al. (2007). "Presenilin/gamma-secretase-dependent processing of beta-amyloid precursor protein regulates EGF receptor expression." Proc Natl Acad Sci U S A **104**(25): 10613-10618.
- Zhang, Z., P. Nadeau, et al. (2000). "Presenilins are required for gamma-secretase cleavage of beta-APP and transmembrane cleavage of Notch-1." Nat Cell Biol **2**(7): 463-465.

## **Chapter 2 Identifying the transcriptomic changes caused by a premature termination codon mutation in *psen2*, using the zebrafish model**

### **2.1 Introduction, Significance and Commentary**

Although hundreds of different fAD mutations in *PSEN1* and *PSEN2* have been identified, none of them are null mutations. Thus, we need to examine the specific cellular changes caused by null mutation of *psen2*, so that when we identify the changes caused by fAD-like mutations in the same gene, the null mutation effects can be identified as less likely to be critical to the fAD pathology.

In this chapter, a premature termination codon mutation in *psen2*, *psen2*<sup>S4Ter</sup>, which refers to a deletion of 8 nucleotides resulting in a translation termination codon at the 4<sup>th</sup> codon, was generated in the zebrafish genome using the CRISPR/Cas9 system. Transcriptomic changes caused by this mutation in adult fish brains were predicted to affect brain mitochondrial activity, glucocorticoid signalling activity and intracellular iron trafficking. A severe haploinsufficiency phenotype due to this mutation was identified since no significant differences were observed between the heterozygous and homozygous brain states.

The significances of this work includes:

1. This is the first generation of a premature termination codon mutation in *psen2* in the zebrafish model. This can be used for future studies on *PSEN2* functions and fAD-like mutations.

2. The transcriptomic analysis that indicated *psen2* is likely involved in brain mitochondrial activity, glucocorticoid signalling activity and intracellular iron trafficking strongly supporting that *PSEN2* plays an important role in the development of AD pathology.

**2.2** Transcriptome analysis indicates significant effects on mitochondrial function of heterozygosity for a premature termination codon mutation in the zebrafish gene *psen2*.

This chapter is included in the thesis in the form of a research paper manuscript authored by H. Jiang, S. M. Pederson, M. Newman, and M. Lardelli, and which is ready for submission for peer review by a scientific journal.



## Statement of Authorship

### Statement of Authorship

Title of Paper	Transcriptome analysis indicates significant effects on mitochondrial function of heterozygosity for a premature termination codon mutation in the zebrafish gene <i>psen2</i>
Publication Status	<input type="checkbox"/> Published <input type="checkbox"/> Accepted for Publication <input type="checkbox"/> Submitted for Publication <input checked="" type="checkbox"/> Unpublished and Unsubmitted work written in manuscript style
Publication Details	Has been prepared for submission.

#### Principal Author

Name of Principal Author (Candidate)	Haowei Jiang		
Contribution to the Paper	Research plan, most of the experiments, data analysis, manuscript drafting.		
Overall percentage (%)	70%		
Certification:	This paper reports on original research I conducted during the period of my Higher Degree by Research candidature and is not subject to any obligations or contractual agreements with a third party that would constrain its inclusion in this thesis. I am the primary author of this paper.		
Signature		Date	1/5/18

#### Co-Author Contributions

By signing the Statement of Authorship, each author certifies that:

- i. the candidate's stated contribution to the publication is accurate (as detailed above);
- ii. permission is granted for the candidate to include the publication in the thesis; and
- iii. the sum of all co-author contributions is equal to 100% less the candidate's stated contribution.

Name of Co-Author	Stephen Martin Pederson		
Contribution to the Paper	RNA-seq data analysis, manuscript drafting.		
Signature		Date	1/5/18

Name of Co-Author	Morgan Newman		
Contribution to the Paper	Supervision and help with the experiments.		
Signature		Date	1/5/2018

Name of Co-Author	Michael Lardelli	
Contribution to the Paper	Supervision, help with data analysis, manuscript drafting.	
Signature		
	Date	11/5/2018

**Title: Transcriptome analysis indicates significant effects on mitochondrial function of heterozygosity for a premature termination codon mutation in the zebrafish gene *psen2***

**Authors:** Haowei Jiang<sup>1,\*</sup>, Stephen Martin Pederson<sup>2</sup>, Morgan Newman<sup>1</sup>, Michael Lardelli<sup>1</sup>

**Affiliations:** <sup>1</sup>University of Adelaide, School of Biological Sciences, Alzheimer's Disease Genetics Laboratory, North Terrace, Adelaide, SA 5005, AUSTRALIA

<sup>2</sup> University of Adelaide, School of Biological Sciences, Bioinformatics Hub, North Terrace, Adelaide, SA 5005, AUSTRALIA

**\*Corresponding Author:** Haowei Jiang, University of Adelaide, School of Biological Sciences, Alzheimer's Disease Genetics Laboratory, North Terrace, Adelaide, SA 5005, AUSTRALIA. Email: [haowei.jiang@adelaide.edu.au](mailto:haowei.jiang@adelaide.edu.au)

**Key words:** CRISPR/Cas9 system, familial Alzheimer's disease, PRESENILIN 2, RNA-seq, zebrafish

**Abbreviations:** Alzheimer's Disease; CNS, central nervous system; dqPCR, digital quantitative PCR; DE, differentially expressed; ER, endoplasmic reticulum; GO, Gene Ontology; NHEJ, non-homologous end joining; NMD, nonsense-mediated mRNA

decay; NPC, neural progenitor cells; OXPHOS, oxidative phosphorylation; PSEN, presenilin; ROS, reactive oxygen species

**Financial Disclosure Statement:** This research was supported by grants from the National Health and Medical Research Council of Australia, GNT1061006 and GNT1126422, and by funds from the School of Biological Sciences of the University of Adelaide. HJ is supported by an Adelaide Scholarship International from the University of Adelaide.

**Conflict of Interest Statement:** The authors declare no conflict of interest.

## Abstract

*PRESENILIN 2 (PSEN2)* is one of the genes mutated in early onset familial Alzheimer's disease (EOfAD). *PSEN2* shares significant amino acid sequence identity with another EOfAD-related gene *PRESENILIN 1 (PSEN1)*, and partial functional overlap is seen between these two genes. However, the complete range of functions of *PSEN1* and *PSEN2* is not yet understood. In this study, we performed targeted mutagenesis using the CRISPR Cas9 system to generate a premature termination codon close to the translation start of the *psen2* coding sequence, *psen2*<sup>S4Ter</sup>. Homozygotes for this mutation are viable and fertile, and adults do not show any gross pigmentation defects. Transcripts containing the mutation do not appear affected by nonsense-mediated decay. Transcriptome analysis of brains from a family of wild type, heterozygous and homozygous mutant female siblings predicts very significant effects on mitochondrial function and, potentially, glucocorticoid signaling and iron homeostasis. No significant gene expression differences were observed between heterozygous and homozygous mutant brains indicating either widespread haploinsufficiency or a neomorphic, dominant phenotype of the *S4Ter* mutation. Assessment of the numbers of Dorsal Longitudinal Ascending (DoLA) interneurons that are responsive to *psen2* but not *psen1* activity during embryogenesis did not support that *S4Ter* decreases *psen2* function.

## Introduction

*PRESENILIN 2 (PSEN2)* was first identified as a candidate locus for mutations causing familial Alzheimer's disease (fAD) with early onset (EOfAD) when a point mutation resulting in the substitution of an isoleucine residue for an asparagine residue (N141I) was found in a Volga German AD family in 1995 (Levy-Lahad, Wasco et al. 1995). *PSEN2* is similar in structure to the major fAD gene *PRESENILIN 1 (PSEN1)*. The two genes encode proteins sharing 62% amino acid sequence identity (Newman, Musgrave et al. 2007). The age of onset of Alzheimer's disease (AD) caused by mutations in *PSEN2* ranges from 39 to 75 years, which overlaps both with *PSEN1* EOfAD-associated mutation disease onset ages and with late onset, sporadic AD (Ryman, Acosta-Baena et al. 2014). The later mean onset age of AD caused by *PSEN2* mutations compared to mutations in *PSEN1* is still unexplained, but some studies suggest that it may be caused by the partial replacement of *PSEN2* function by *PSEN1* (Jayadev, Leverenz et al. 2010). However, the functions of *PSEN1* and *PSEN2* have not yet been comprehensively determined. Moreover, despite the partial functional overlap between *PSEN1* and *PSEN2*, *in vitro* studies have shown that the protein products of the two genes also play divergent roles in cellular physiology (Lee, Slunt et al. 1996; Kang, Yoon et al. 2005).

Both PSEN1 and PSEN2 proteins are components of  $\gamma$ -secretase complexes. The absence of PSEN1 is thought to reduce  $\gamma$ -secretase activity in mammalian cells (De

Strooper, Saftig et al. 1998; Naruse, Thinakaran et al. 1998), while the absence of both PSEN1 and PSEN2 is thought to eliminate it completely (Herreman, Serneels et al. 2000; Zhang, Nadeau et al. 2000) although some data does not agree with this (reviewed in Jayne et al. (Jayne, Newman et al. 2016)). In mice, the loss of *Psen1* causes premature differentiation of neural progenitor cells (NPC) and inhibition of Notch signaling leading to skeletal defects (Shen, Bronson et al. 1997), and, ultimately, perinatal lethality (Handler, Yang et al. 2000). Mouse embryos lacking both *Psen1* and *Psen2* activity are more severely affected with earlier lethality and a developmental phenotype similar to loss of *Notch1* activity (Donoviel, Hadjantonakis et al. 1999; Ferjentsik, Hayashi et al. 2009). However, by itself, the absence of *Psen2* activity in mice does not appear to affect development significantly (Herreman, Hartmann et al. 1999). In zebrafish, the inhibition of either *Psen1* or *Psen2* translation caused decreased melanocyte numbers in trunk and tail and other effects of decreased Notch signaling indicating a possibly greater role in Notch signaling for *Psen2* protein in zebrafish compared to in mammals (Nornes, Newman et al. 2008). Inhibition of *Psen2* translation also led to increased Dorsal Longitudinal Ascending (DoLA) interneuron number, while inhibition of *Psen1* translation showed no effect on this neuronal cell type (Nornes, Newman et al. 2008). Thus, in zebrafish, *Psen2* apparently plays greater roles in Notch signalling and embryo development than in mammals.

Although *Psen1* and *Psen2* show compensatory regulation with forced down-regulation of one causing up-regulation of the other (Wang, Pereira et al. 2003; Jayadev, Case et

al. 2010), only *Psen2* down-regulation causes markedly decreased  $\gamma$ -secretase activity in the microglial cells of mice. The inhibition of  $\gamma$ -secretase activity caused by forced down-regulation of *Psen2* led to exaggerated proinflammatory cytokine release from microglia, indicating that *Psen2* plays an important role in central nervous system (CNS) innate immunity (Jayadev, Case et al. 2010). Furthermore, a negative regulator of monocyte pro-inflammatory response, miR146, was found to be constitutively down-regulated in the microglia of a *Psen2* knockout mouse strain, supporting that *Psen2* dysfunction may be involved in neurodegeneration through its impacts on the pro-inflammatory behavior of microglia (Jayadev, Case et al. 2013). Also, *Psen2* (but not *Psen1*) knockout mice show reduced responsiveness to lipopolysaccharide (LPS) as well as decreased expression of nuclear factor kappa-light-chain-enhancer of activated B cells (NF-kappaB), reduced mitogen-activated protein kinase (MAPK) activity and reduced pro-inflammatory cytokine production. This indicates that *Psen2* has a specific function(s) in innate immunity independent of *Psen1* (Agrawal, Sawhney et al. 2016).

The particular role of mammalian PSEN2 protein in inflammation is consistent with its restricted localisation to the mitochondrial associated membranes (MAM) of the endoplasmic reticulum (ER) (Area-Gomez, de Groof et al. 2009). MAM formation has been shown to influence inflammatory responses, is the site of autophagosome initiation, and plays a major role in regulating mitochondrial activity (reviewed in Marchi et al (Marchi, Patergnani et al. 2014)).



Considerable evidence supports roles for PRESENILIN proteins in the function of mitochondria (Behbahani, Shabalina et al. 2006), which are central to energy production in cells and to other cellular processes affected in AD such as apoptosis, reactive oxygen species (ROS) production, and calcium homeostasis (Hroudova, Singh et al. 2014). In human cell lines, it has been reported that PSEN2, but not PSEN1, modulates the  $\text{Ca}^{2+}$  shuttling between the ER and mitochondria since mitochondrial  $\text{Ca}^{2+}$  dynamics are reduced by PSEN2 down-regulation and enhanced by the expression of mutant forms of PSEN2 (Zampese, Fasolato et al. 2011). In mouse cell lines, deficiency of *Psen2* led to reduced expression of subunits responsible for mitochondrial oxidative phosphorylation (OXPHOS) with altered morphology of the mitochondrial cristae, as well as an increase in glycolytic flux. This indicated that the absence of *Psen2* protein causes an impairment in respiratory capacity with a corresponding increase in glycolytic flux to support cells' energy needs (Contino, Porporato et al. 2017).

Despite the identification of hundreds of different fAD mutations in human *PSEN1* and *PSEN2*, none of these appear to remove all gene function (i.e. none are null mutations). As part of an effort using zebrafish to identify the specific cellular changes caused by fAD-like mutations in these genes, we wished to examine null mutations so that their effects could be excluded from consideration. In this paper we describe attempted generation of a null mutation of the zebrafish orthologue of the human *PSEN2* gene, *psen2*, by introduction of a premature termination codon downstream of the assumed

translation start codon. We then examined the transcriptome of young adult brains either heterozygous or homozygous for this mutation. Gene ontology analysis supports very significant changes in brain mitochondrial activity with significant changes also predicted in glucocorticoid signalling activity and intracellular iron trafficking. Surprisingly we see evidence of either widespread haploinsufficiency or a dominant, neomorphic effect since no significant differences are noted between the heterozygous and homozygous brain states.

## **Method and Materials**

### **Animal ethics**

All experiments using zebrafish were conducted under the auspices of the Animal Ethics Committee of the University of Adelaide. Permits S-2014-108 and S-2017-073.

### **sgRNA design and synthesis**

The target sequence of Ps2Ex3 sgRNA is 5'-CAGACAGTGAAGAGGAC TCC-3'. This target sequence was cloned into the plasmid pDR274 (Addgene plasmid # 42250) (Hwang, Fu et al. 2013). The Ps2Ex3 pDR274 plasmid was linearised with *HindIII*-HF<sup>®</sup> (NEB, Ipswich, Massachusetts, USA, R3104S), and then used as a template for synthesis of Ps2Ex3 sgRNA with the MAXIscript<sup>™</sup> T7 Transcription Kit (Ambion,

Inc, Foster City, California, USA, AM1312).

### **Injection of zebrafish embryos**

Tübingen (wild type) embryos were generated by mass mating. Ps2Ex3 sgRNA (90 ng/ $\mu$ L final concentration) was first mixed with Cas9 nuclease (Invitrogen, Carlsbad, California, USA, B25640), and then incubated at 37°C for 15 min to maximise cleavage efficiency. 5-10 nL of the mixture was injected into zebrafish embryos at the one-cell stage. The injected embryos were subsequently raised up for mutation screening.

### **Mutation detection in G0 injected embryos T7 endonuclease I**

Mutation detection was based on the T7 endonuclease I assay (Babon, McKenzie et al. 2003). Since mismatches, small insertions or deletions generated through non-homologous end joining (NHEJ) result in failure of base-pairing in heteroduplexes at mutation sites, T7 endonuclease I is able to recognise and cleave at the sites of these mutations.

To test whether the CRISPR/Cas9 system had functioned in the injected G0 embryos, 10 embryos were randomly selected from each injected batch and pooled together for genomic DNA extraction at ~24 hours post fertilisation (hpf). To extract the genomic

DNA, these 10 embryos were placed in 100  $\mu$ L of 50 mM NaOH and then heated to 95°C for 15 min, and then 1/10th volume of 1 M Tris-HCl, pH 8.0 was added to each sample to neutralise the basic solution after cooling to 4°C (Meeker, Hutchinson et al. 2007). A pair of primers (5'- AGGCCACATCACGATACAC -3' and 5'- TGACCCGTTTGCTGTCTG-3') binding to the flanking regions of the intended cleavage site was designed to amplify the test region (~472 bp) through PCR. The PCR conditions for this amplification reaction were 95°C, 2 min; 31 cycles of [95°C, 30 s; 58°C, 30 s; 72°C, 30 s]; then 72°C, 5 min. The PCR products were purified using the Wizard® SV Gel and PCR Clean-Up System (Promega, Wisconsin, USA, A9281) and annealed (denaturation at 95°C for 5 min and then slow cooling of the samples at the rate of -2°C/sec from 95°C to 85°C and then -0.1°C/sec from 85°C to 25°C for annealing of heteroduplexes) before addition of T7 endonuclease I (NEB, Ipswich, Massachusetts, USA, M0302S). Heteroduplexes containing small mutations at the intended site should be cleaved into two fragments, ~313 bp (upstream) and ~159 bp (downstream).

When the T7 endonuclease I assay on injected G0 embryos showed the presence of mutation at the target site, the remaining embryos from the same injection batch were raised for further mutation screening and breeding.

### **Mutation detection in adult G0 and F1 fish using T7 endonuclease I and Sanger sequencing**

When a G0 injected fish had grown to sufficient size (>2 cm in length, 2 to 3 months old), the tip of its tail (~2 mm in length) was biopsied (clipped) under Tricaine (1.68µg/mL) anaesthesia for genomic DNA extraction. The clipped tail was placed in 100 µL of 50 mM NaOH and then heated to 95°C for 15 min to extract genomic DNA. The sample was then cooled to 4°C, and a 1/10th volume of 1 M Tris-HCl, pH 8.0 was then added to each sample to neutralise the basic solution (Meeker, Hutchinson et al. 2007). The same T7 endonuclease I assay used previously for mutation detection in G0 embryos was then applied to the genomic DNA extracted from the G0 adult fish biopsy (S1A and S1B Figures). However, since each G0 mutation-carrying fish was probably mosaic for several different mutations at the target site, each G0 fish was outbred to a wild type Tübingen fish, to produce the F1 progeny, some of which could be heterozygous for single mutations. The F1 fish were biopsied and screened using the T7 endonuclease I assay when large enough (S1C and S1D Figures). For F1 fish found to carry mutations, the PCR-amplified fragments were sent to the Australian Genome Research Facility (AGRF, North Melbourne, VIC, Australia) for Sanger sequencing to identify the mutations.

An 8-bp deletion resulting in a frameshift downstream of the start codon of *psen2*, *psen2*<sup>S4Ter</sup> (Figure 1), was identified. PCR primers specifically detecting this mutation were designed (*psen2*<sup>S4Ter</sup> forward primer: 5'-TTCATGAATACCTGAAGAGG-3', wild type forward primer: 5'- TTCATGAATACCTCAGACAGTG-3', and reverse

primer: 5'-GAACAGAGAATGTACTGGCAGC-3') for further screening. The PCR conditions for *psen2*<sup>S4Ter</sup> mutant detection are 95°C, 2 min; 31 cycles of [95°C, 30 s; 55°C, 30 s; and then 72°C, 30 s]; 72°C, 5 min. The length of PCR products is ~230 bp. The PCR conditions for wild type-specific detection are 95°C, 2 min; 31 cycles of [95°C, 30 s; 60°C, 30 s; and 72°C 30 s]; 72°C, 5 min and the anticipated length of the PCR products is ~230 bp (S1E and S1F Figures).

<i>psen2</i> wildtype	cDNA	ATGAAATACCTCAGACAGTGAAGAGGACTCCTACAAAGAGAGGTCCGCTCTGGTCCAGTCCGA
	Protein	M N T S D S E E D S Y N E R S A L V Q S E
<i>psen2</i> <sup>S4Ter</sup>	cDNA	ATGAAATACCT-----GAAGAGGACTCCTACAAAGAGAGGTCCGCTCTGGTCCAGTCCGA
	Protein	M N T ■-----* R G L L Q R E V R S G P V R
	Start Codon	

**Figure 1. Predicted protein sequence of *psen2*<sup>S4Ter</sup>.** An 8-bp deletion resulted in a frameshift downstream of the nominal translation start codon of *psen2* creating a stop codon as the 4<sup>th</sup> codon.

### Breeding of *psen2*<sup>S4Ter</sup> mutant fish

The initial F1 fish carrying the *psen2*<sup>S4Ter</sup> mutation was outbred to a wild type fish to generate a population of F2 progeny that was 50% heterozygous mutants and 50% wild type fish. Two F2 heterozygous mutant fish were then inbred to generate a family of F3 fish consisting of (theoretically) 50% heterozygous mutants, 25% homozygous mutants and 25% wild type fish. This F3 family was then allowed to age for six months before brain removal and total brain RNA extraction for RNA-seq and other analyses.

## **Total RNA extraction from 6-month-old zebrafish brains**

Individual fish were genotyped using PCR and then brains from desired genotypes were removed for extraction of total RNA for either digital quantitative PCR (dqPCR) on cDNA or RNA-seq (below).

For dqPCR tests, six wild type, six heterozygous and six homozygous fish from the F3 family were selected. Three of each genotype were then exposed to hypoxia (dissolved oxygen content of the water was ~1.0 mg/L) for ~2.5 h, while the remaining three of each genotype were exposed to normoxia. The brains of these fish were subsequently removed after humane killing, and total RNA was extracted using the RNeasy Mini Kit (QIAGEN, Venlo, Netherlands, 74104). cDNA was synthesised from brain RNAs using the SuperScript™ III First-Strand Synthesis System (Invitrogen, Carlsbad, California, USA, 18080051) with Random Primers (Promega, Madison, Wisconsin, USA, C1181).

For RNA-seq, four wild type, four *psen2*<sup>S4Ter</sup> heterozygous and four *psen2*<sup>S4Ter</sup> homozygous mutant brains (all from female fish) were extracted from the same family. Total RNA from these brains was extracted using the *mirVana*™ miRNA Isolation Kit (Ambion, Inc, Foster City, California, USA, AM1560). RNA samples were sent to the Australian Cancer Research Foundation (ACRF) Cancer Genomics Facility, Adelaide SA, Australia for sequencing.

## **Allele specific expression analysis by dqPCR**

Primers for dqPCR, including a reverse primer specifically detecting the wild type allele (5'-TCGTTGTAGGAGTCCTCTTCACTG-3'), a reverse primer specifically detecting the *psen2*<sup>S4Ter</sup> allele (5'-TCGTTGTAGGAGTCCTCTTCAGG-3') and a common forward primer (5'-TTCCTCACTGAATTGGCGATG-3'), were designed for allele specific expression analysis of the F3 family using the QuantStudio™ 3D Digital PCR System (Life Sciences, Waltham, MA, USA) with the QuantStudio™ 3D Digital PCR 20K Chip Kit v2 and Master Mix (Life Sciences, Waltham, MA, USA, A26317) and SYBR™ Green I Nucleic Acid Gel Stain (Life Sciences, Waltham, MA, USA, S7563). The dqPCR conditions for assays of mutant allele or wild type allele expression were 96°C, 10 min; 49 cycles of [62°C, 2 min; 98°C, 30 s]; 62°C, 2 min. The lengths of the anticipated PCR products are ~130 bp. 25 ng of total cDNA\* from a sample was loaded into one chip for the dqPCR. The chips were read using QuantStudio™ 3D AnalysisSuite Cloud Software (Life Sciences, Waltham, MA, USA).

\*Stated cDNA concentrations are based on measured concentrations of RNA under the assumption that subsequent reverse transcription is completely efficient.

## **RNA-seq data processing**

Paired-end (2x150bp) RNA-seq libraries were generated for  $n = 4$  samples from each



of the genotypes: wild type (WT, *psen2*<sup>+/+</sup>), heterozygous (Het, *psen2*<sup>S4Ter/+</sup>) and homozygous (Hom, *psen2*<sup>S4Ter/psen2</sup><sup>S4Ter</sup>), ranging in size from 27,979,654 to 37,144,975 reads. Libraries were trimmed to remove Illumina Adapter sequences, bases with a PHRED score < 20 were removed, and reads shorter than 35bp after trimming were discarded. Libraries were aligned to known rRNA sequences obtained from the SILVA project (Quast, Pruesse et al. 2013) on 2017/05/24 before alignment to build GRCz10 of zebrafish genome, using the default settings of the splice-aware aligner HISAT2 (Kim, Langmead et al. 2015). Alignments were deduplicated after identification of duplicate alignments using MarkDuplicates from the Picard suite of tools (<http://broadinstitute.github.io/picard/>).

### **RNA-seq Analysis**

Unique alignments corresponding to gene models in Ensembl release 88 were counted using featureCounts from the Subread package (Liao, Smyth et al. 2013), giving total counts per sample which ranged between 8,844,634 and 10,850,749. Genes with counts per million (CPM) > 0.9 in at least four samples were retained, with genes corresponding to rRNAs additionally removed from the dataset, giving 19,211 genes for differential expression analysis. Voom precision weights (Law, Chen et al. 2014) were calculated incorporating sample-level weights using the function `voomWithQualityWeights`, and pair-wise comparisons were performed between all three genotypes. P-values from moderated t-tests were adjusted using the Benjamini-

Hochberg procedure. Genes with an FDR-adjusted p-value  $< 0.05$  and estimates of  $\log_2$  fold-change (logFC) beyond the range  $\pm 1$  were considered as differentially-expressed (DE) between sample groups. When defining DE genes common to both comparisons of mutant and wild type fish, genes were considered as commonly DE if both FDR-adjusted p-values were  $< 0.05$ , and logFC was beyond the range  $\pm 1$  in at least one of the two comparisons.

### **GO enrichment analysis**

Each set of differentially expressed (DE) genes was tested for enrichment of Gene Ontology (GO) terms in comparison to the set of genes not considered as DE in any comparison. Only GO terms represented amongst each set of DE genes were tested, and terms with fewer than three steps back to the ontology root terms were also excluded from testing. Enrichment was assessed using Fisher's Exact Test and p-values were adjusted using the False Discovery Rate of Benjamini-Hochberg (Benjamini and Hochberg 1995).

### ***In situ* transcript hybridisation analysis of DoLA neuron number**

This was performed as previously described (Nornes, Newman et al. 2009) on embryos from a pair mating of two *S4Ter* heterozygous mutants. After counting of DoLA neurons in an embryo by direct observation, the embryo was subjected to DNA extraction as for

the tail biopsies (above) and then its *psen2* genotype was determined by allele-specific PCRs.

## Results

### Generation of a putatively null mutation in zebrafish *psen2*

As part of a program analysing the function of genes involved in familial Alzheimer's disease, we wished to identify changes in the expression of genes in adult brains due to simple loss of *PSEN2* activity. We previously identified the *psen2* gene in zebrafish (Groth, Nornes et al. 2002) and the ENSEMBL database (<http://asia.ensembl.org>) reports one *psen2* transcript (ENSDART00000006381.7) with 11 exons and the translation start codon residing in exon 2. Therefore, we used the CRISPR Cas9 system to generate a frameshift mutation just downstream of this transcript's nominal translation start codon (to allow ribosomes to initiate translation but not translate Psen2 protein). A frameshift mutation (a deletion of 8 nucleotides) starting in the 4<sup>th</sup> codon and resulting in the creation of a translation termination codon was isolated (Figure 1). The mutant allele is designated *psen2*<sup>S4Ter</sup>.

### Large zebrafish families facilitate reduction of genetic and environmental noise

An advantage of genetic analysis in zebrafish is the ability to reduce genetic and

environmental variation in statistical analyses through breeding of large families of siblings that are then raised under near identical environmental conditions (i.e. in the same fish tank or recirculated water aquarium system). The initial heterozygous individual fish identified as carrying *psen2*<sup>S4Ter</sup> was outbred to a wild type fish of the same strain (Tübingen) and then two heterozygous individuals were mated to produce a large family of siblings with wild type (+/+), heterozygous (*psen2*<sup>S4Ter/+</sup>), or homozygous (*psen2*<sup>S4Ter/psen2</sup><sup>S4Ter</sup>) genotypes. (We have subsequently established a line of fish homozygous for the *psen2*<sup>S4Ter</sup> mutant allele, demonstrating that these fish are both viable and fertile.)

Laboratory zebrafish become sexually mature at between 3 and 5 months of age. Therefore, to examine the transcriptome of young adult zebrafish brains we identified individuals of the desired genotype using PCRs specific for the mutant and wild type alleles on DNA from tail biopsies (“tail clips”) and then removed brains from fish of the desired genotypes at 6 months of age. Total RNA was then purified from these and subjected to either RNA-Seq analysis or digital quantitative PCR (dqPCR).

### **No decreased stability of mutant allele transcripts under normoxia or hypoxia**

Premature termination codons in transcripts frequently cause nonsense-mediated decay when more than 50-55 nucleotides upstream of an exon-exon boundary (Brognia and

Wen 2009). Also, hypoxia appears to be an important element in AD (Zetterberg, Mortberg et al. 2011; Gao, Tian et al. 2013) and increases expression of *PSEN* gene transcripts in both human and zebrafish cells (Mohuczy, Qian et al. 2002; Ebrahimie, Moussavi Nik et al. 2016). Therefore, we sought to determine whether *psen2*<sup>S4Ter</sup> allele transcripts are less stable than wild type transcripts and to observe the expression of mutant allele transcripts under acute hypoxia. We used dqPCR with allele-specific primer pairs to quantify relative transcript numbers in cDNA synthesised from wild type, heterozygous and homozygous mutant fish brains under normoxia or acute hypoxia (see Materials and Methods). The results of this analysis are shown in Figure 2. In heterozygous fish under normoxia, both wild type and mutant allele transcripts are expressed at similar levels in 6-month-old brains, with the wild type allele expressed at approximately half the level seen in wild type fish (i.e. that possess two wild type alleles). As expected, acute hypoxia increases the expression of the wild type transcript and this is also observed for the mutant transcript that shows no evidence of destabilisation (Figure 2).

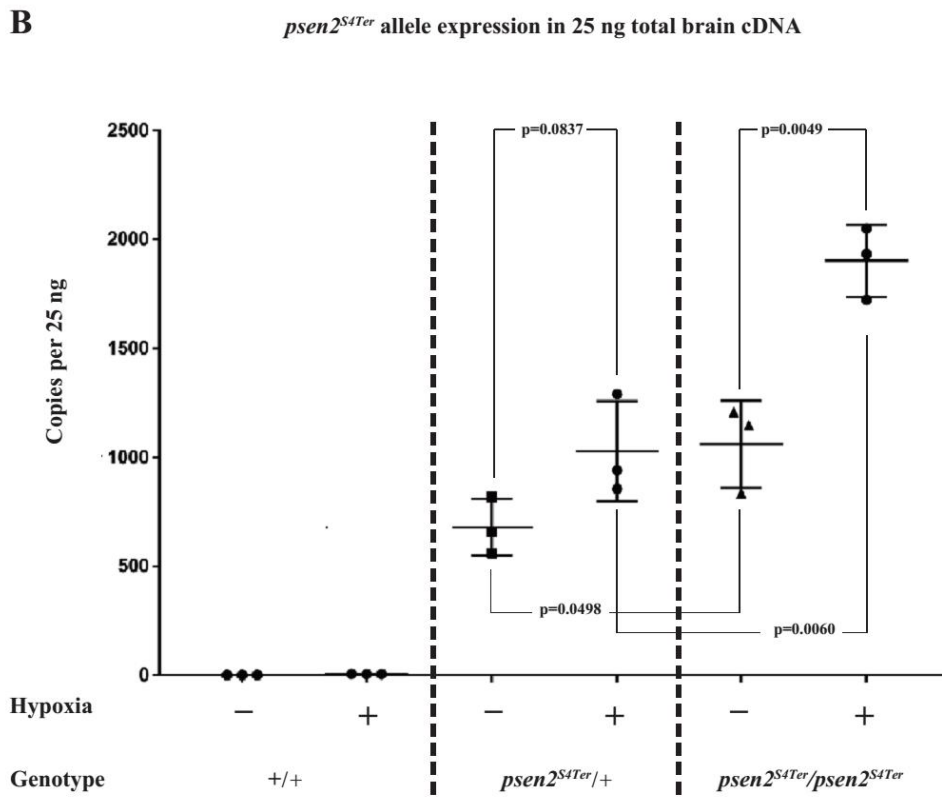
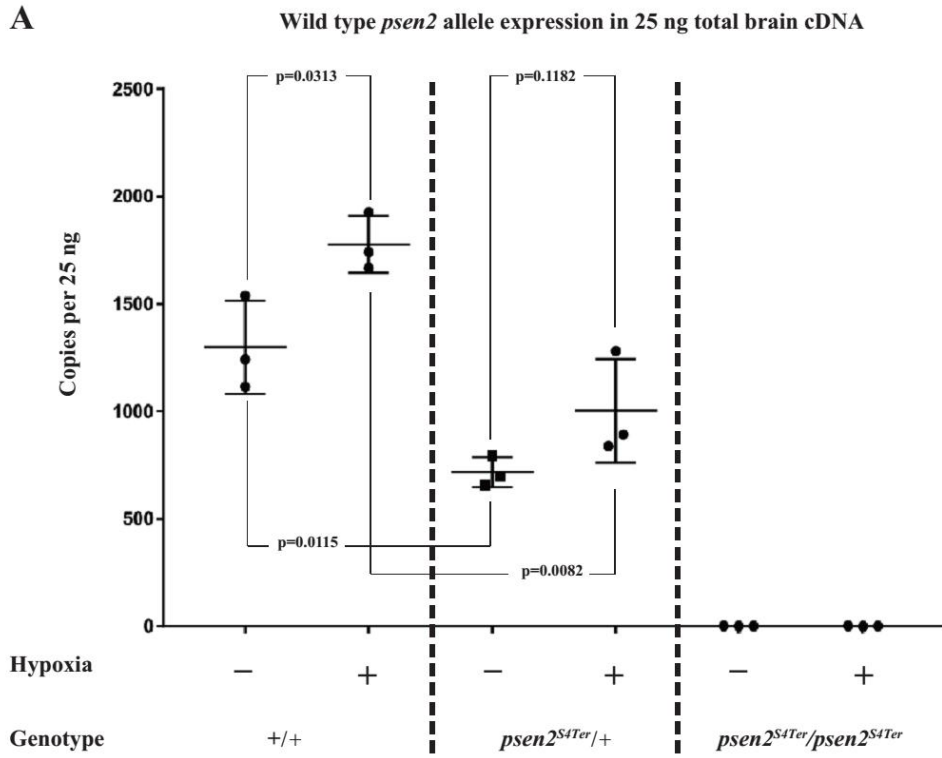


Figure 2. Allele-specific mRNA expression in the brains of 6-month-old fish of

**different genotypes under normoxia or acute hypoxia. (as copies per 25 ng of brain cDNA in each digital qPCR)** (A) The levels of wild type *psen2* allele mRNA in the *psen2<sup>S4Ter/+</sup>* fish (~700 copies) were significantly ( $p=0.0115$ ) lower than in their wild type siblings (~1,300 copies) under normoxia. Under hypoxia, the levels of wild type *psen2* allele mRNA in both the *psen2<sup>S4Ter/+</sup>* fish (~1,000 copies) and their wild type siblings (~1,800 copies) were up-regulated, but only the higher levels in the wild type fish showed a statistically significant increase ( $p=0.0313$ ) compared to the normoxic controls. (B) The levels of *psen2<sup>S4Ter</sup>* allele mRNA in the *psen2<sup>S4Ter/+</sup>* fish (~700 copies) were significantly ( $p=0.0498$ ) lower than in the *psen2<sup>S4Ter/psen2<sup>S4Ter</sup></sup>* fish (~1,000 copies) under normoxia. Under hypoxia, the levels of *psen2<sup>S4Ter</sup>* allele mRNA in both the *psen2<sup>S4Ter/+</sup>* fish (~1,000 copies) and the *psen2<sup>S4Ter/psen2<sup>S4Ter</sup></sup>* fish (~1,900 copies) were upregulated. This up-regulation (Figure 2B) in the *psen2<sup>S4Ter/psen2<sup>S4Ter</sup></sup>* fish was clearly significant ( $p=0.0049$ ), while that in the *psen2<sup>S4Ter/+</sup>* fish was apparent, but not statistically significant ( $p=0.0837$ ).

### **No increase in DoLA neuron number in embryos homozygous for *S4Ter***

Currently, we do not have an antibody against zebrafish Psen2 protein that would allow us to demonstrate loss of Psen2 in homozygous mutants. Also concerning is that a frameshift allele of *psen2* that we have isolated, *NI40fs*, shows a surface pigmentation phenotype when homozygous suggestive of loss of  $\gamma$ -secretase activity (Jiang, unpublished results) whereas homozygous *S4Ter* mutants do not. Therefore, we sought

an alternative method to demonstrate loss of *psen2* function due to the *S4Ter* mutation.

Inhibition of *psen2* mRNA translation has been shown to increase the number of a particular spinal cord interneuron – the Dorsal Longitudinal Ascending (DoLA) neuron in zebrafish embryos at 24 hpf (Nornes, Newman et al. 2009). Therefore, if *S4Ter* decreases *psen2* function, it might be expected to increase DoLA number (although, as an endogenous mutation rather than blockage of gene expression using a morpholino, *S4Ter* might induce genetic compensation to suppress this phenotype (Rossi, Kontarakis et al. 2015)). To examine the effect of *S4Ter* on DoLA number, we collected embryos from a pair-mating of two *psen2*<sup>*S4Ter*/+</sup> fish to generate a family of embryos comprised, theoretically, of 50% heterozygous mutants, 25% homozygous mutants and 25% wild type genotypes. The embryos were allowed to develop to the 24 hpf stage before *in situ* transcript hybridisation against transcripts of the gene *tbx16* that labels DoLA neurons (Tamme, Wells et al. 2002). After the number of DoLA neurons in each embryo had been recorded, each embryo was genotyped using PCRs specific for the mutant and wild type alleles. Two-tailed t-tests found no significant differences in DoLA number between any two genotypes which does not support that *S4Ter* reduces *psen2* activity (Figure 3). Nevertheless, transcriptome analysis (below) shows distinct differences between the brain transcriptomes of *S4Ter* mutant and wild type siblings.



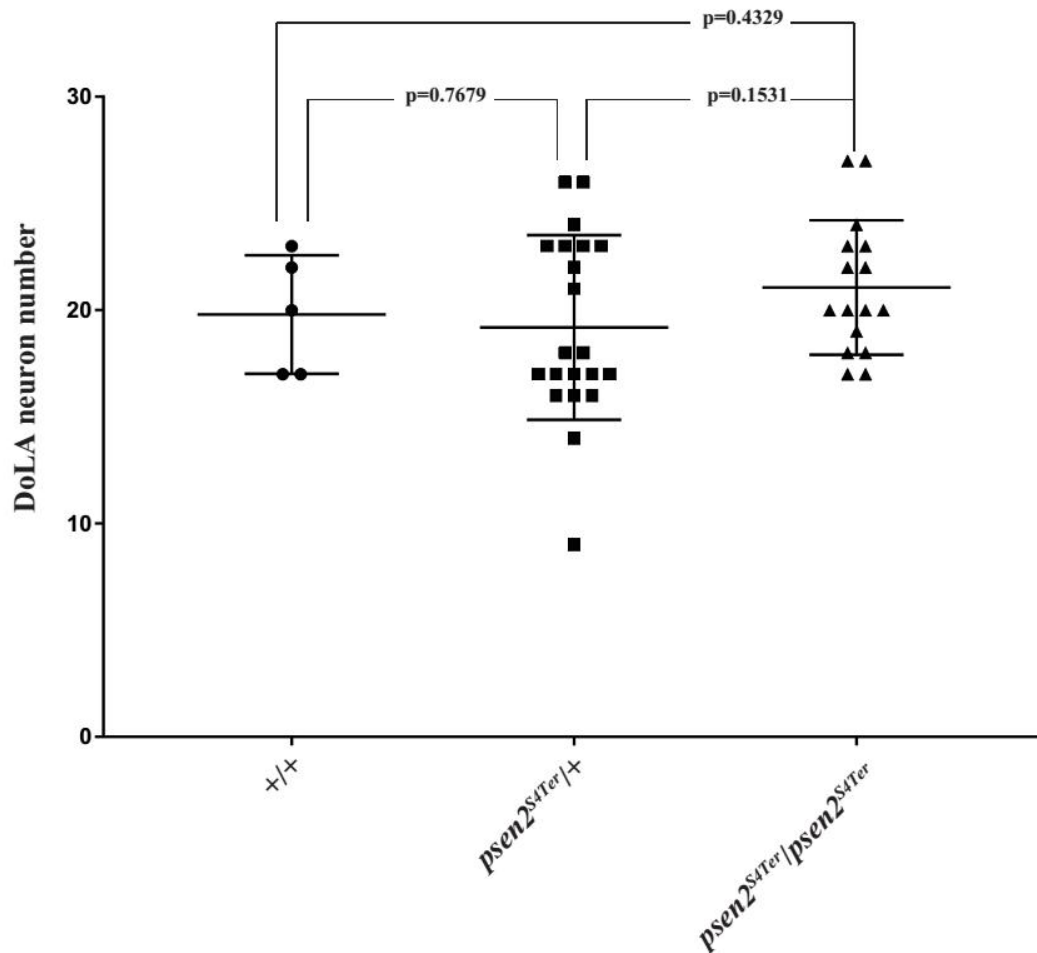


**Figure 3. DoLA neuron number assessment of *psen2* activity.** 42 embryos at 24 hpf from a pair-mating of a *psen2*<sup>S4Ter/+</sup> female and a *psen2*<sup>S4Ter/+</sup> male were subjected to *in situ* hybridisation to detect DoLA neurons that were then counted. Subsequent genotyping of individual embryos revealed 21 heterozygous mutants, 16 homozygous mutants and 5 wild type embryos. Values of p were determined in two-tailed t-tests.

### RNA-seq data and analysis

To analyse and compare the brain transcriptomes of 6-month-old wild type, heterozygous and homozygous mutant siblings, four female fish of each genotype were

examined. An exploratory principal component analysis (PCA) of gene expression across all samples was generated using gene-level,  $\log_2$ -transformed counts per million (Figure 4), indicating that the difference between wild type (+/+) samples and mutant samples was the dominant source of variability, with PC1 (23.7% of variance) clearly separating both mutant types from the wild type fish. The separation between homozygous ( $psen2^{S4Ter}/psen2^{S4Ter}$ ) and heterozygous ( $psen2^{S4Ter}/+$ ) mutants was much less pronounced along PC2 (14.3% of variance), and after calculation of sample-weights the center of mass for each mutant sample group was clearly located near each other, leaving within group variability as the dominant characteristic for PC2.

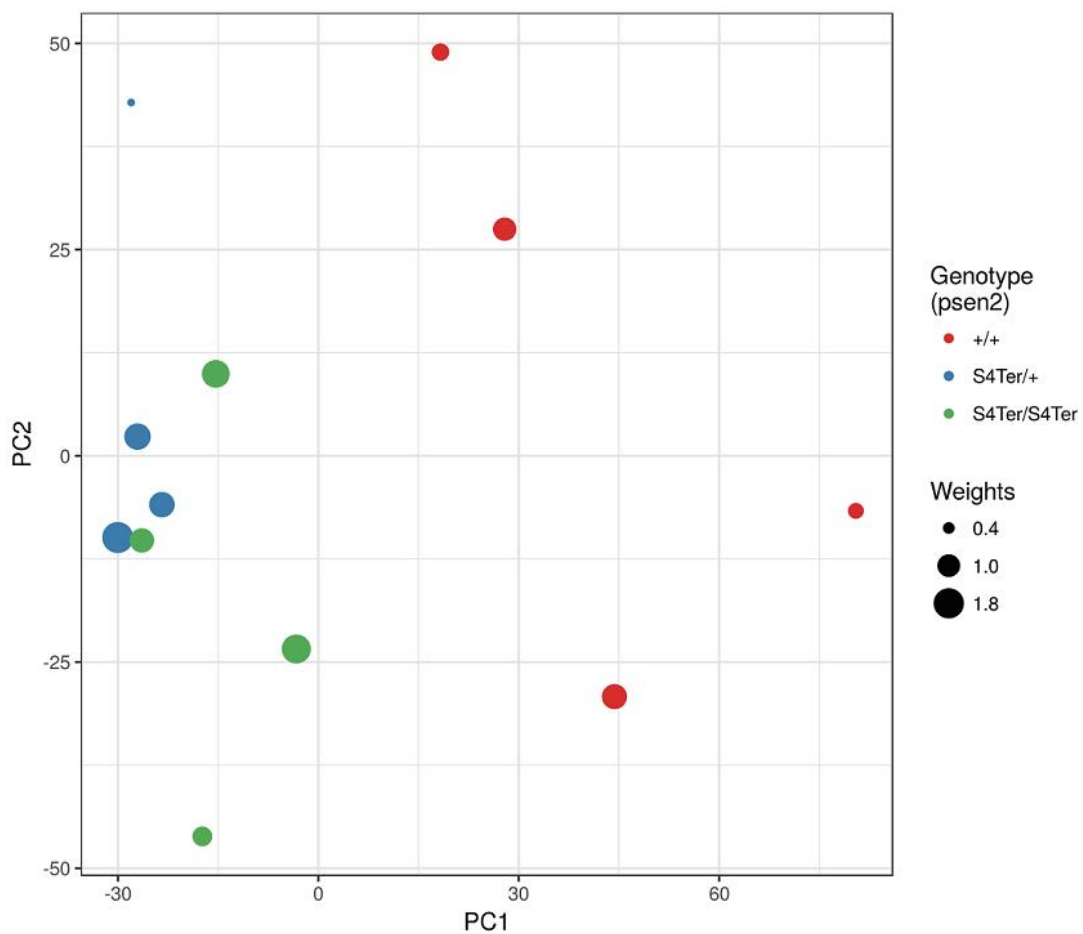


**Figure 4. PCA analysis showing PC1 and PC2 for TMM normalised counts.** Point sizes indicate sample weights as calculated by `voomWithQualityWeights` from the R package `limma`. Lower weights indicate samples which were downweighted during differential expression analysis. The largest source of variability within this dataset was clearly the difference between wild type samples and those containing one or two copies of the *psen2*<sup>S4Ter</sup> allele.

Three pairwise comparisons were performed between the sample groups and a ranked list of genes was obtained for each comparison, with genes being considered as differentially expressed (DE) if receiving a false discovery rate (FDR)-adjusted p-value <0.05 and an estimated log<sub>2</sub> fold change (logFC) beyond the range of ±1. This gave 665 and 527 significantly DE genes in the homozygous (*psen2*<sup>S4Ter/+</sup>) and heterozygous (*psen2*<sup>S4Ter/psen2</sup><sup>S4Ter</sup>) comparisons against wild type (+/+) samples respectively (Figure 5). No DE genes were detected in the comparison between homozygous and heterozygous fish. However, this does not mean that there are no DE genes between these two mutant genotypes, rather, that none were able to be detected given the samples analysed here, as the variability observed between samples was generally greater than the extent of differential gene expression. Estimates of fold-change (logFC) were compared across both mutant versus wild type comparisons, with a strong overall correlation of  $\rho = 0.818$  and 439 common DE genes.

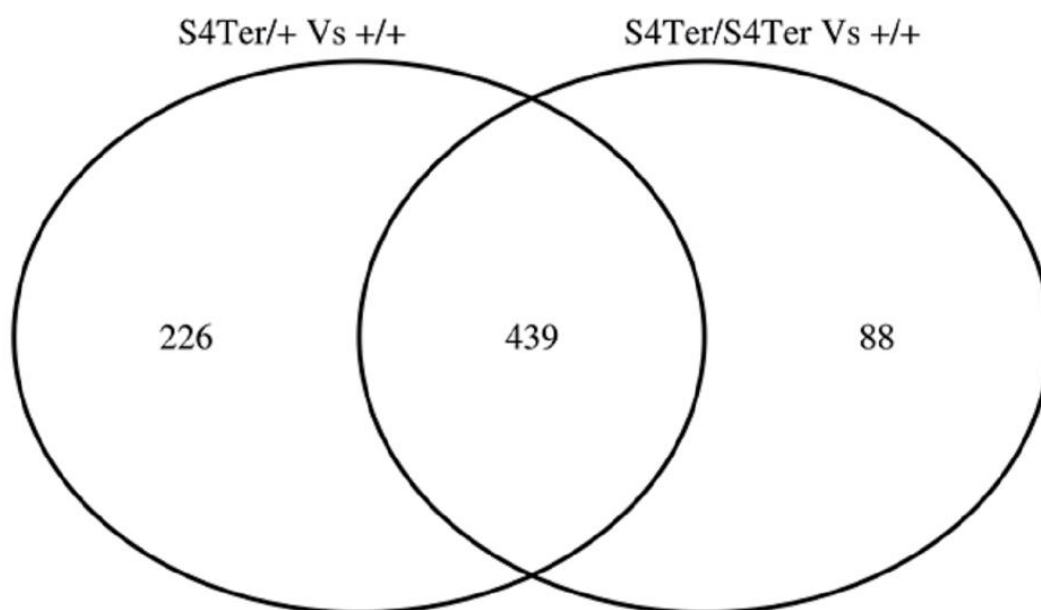


**Figure 5. Numbers of genes differentially expressed in comparisons between mutant and wild type genotypes.** The *psen2* genotypes for each comparison are given in each label. No genes were detected as differentially expressed between the heterozygous and homozygous mutant genotypes.

As seen in Figure 6, many of the genes considered as DE in only one comparison showed similar trends in the alternate comparison, with no genes detected as DE between the two mutant genotypes. Along with the observation that the majority of genes from each comparison were shared with the alternate comparison, this clearly suggests that the *psen2*<sup>S4Ter</sup> mutation acts in a dominant manner for the majority of genes impacted by the presence of the mutation.

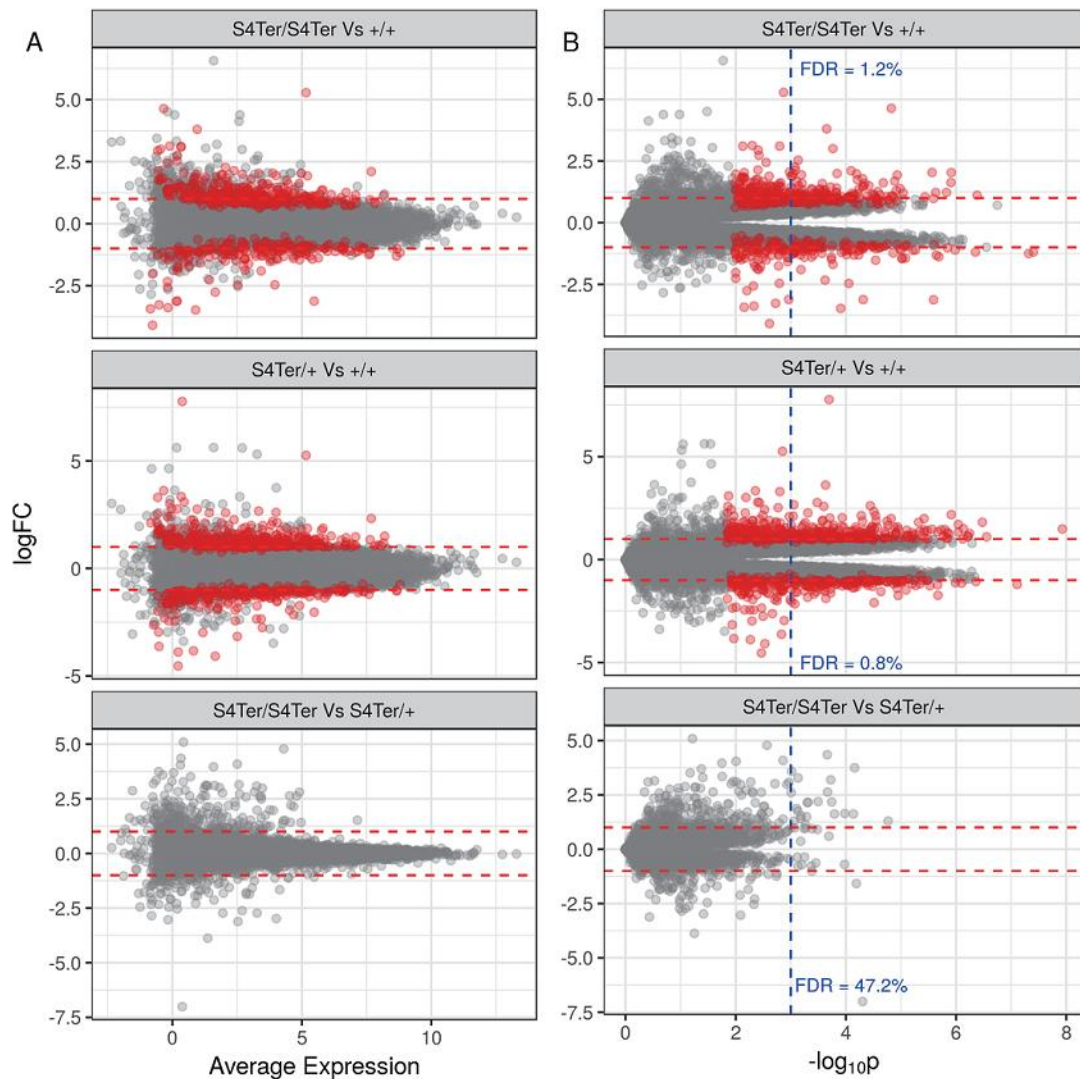


**Figure 6. A) Mean-Difference plots and, B) transposed volcano plots, for each of the three pair-wise comparisons.** Volcano plots are transposed for easier comparison with MD plots. The *psen2* genotypes for each comparison are indicated in the panel strips. Genes considered as differentially expressed are shown in red, corresponding to an FDR of 0.05 and estimated logFC beyond the range  $\pm 1$  in at least one comparison. Red dashed lines indicate a logFC of  $\pm 1$ . Vertical blue lines indicate a raw p-value of 0.001 with the corresponding FDR for each comparison given at this value.

Based on the FDR-adjusted p-value, the top 20 DE genes of each comparison are listed in Tables 1-3, with the full set of results provided in Supplementary File RNAseq\_results.xlsx. Some genes appearing among the top 20 DE genes in both mutant comparisons against wild type (Tables 1 and 2) have functions possibly important in AD pathological processes. These include: *sox11b* (a transcription factor playing a role in adult neurogenesis (Haslinger, Schwarz et al. 2009)), *nr4a1* (nuclear receptor subfamily 4 group A member 1) that has key roles in the cell cycle, inflammation and apoptosis (Pei, Castrillo et al. 2006)), *pcbp3* (Poly(rC)-binding protein 3 that has iron chaperone activity (Leidgens, Bullough et al. 2013)), *nocta* (nocturnin) encoding a protein involved in lipid metabolism, adipogenesis, glucose homeostasis, inflammation and osteogenesis (Stubblefield, Terrien et al. 2012)), and *kdm4aa* (lysine (K)-specific demethylase 4A, genome duplicate a), the human homolog of which has been found to regulate the PDK-dependent metabolic switch between mitochondrial oxidative phosphorylation and glycolysis (Wang, Hung et al. 2016).

**Table 1. Top 20 differentially expressed genes in the comparison between heterozygous mutant (*psen2*<sup>S4Ter/+</sup>) and wild-type (+/+) fish. Average Expression is given using log<sub>2</sub>CPM as the units.**

Gene	Name	logFC	Average Expression	P-Value	FDR
ENSDARG00000095743	<i>sox11b</i>	1.49	5.14	1.18e-08	2.26e-04
ENSDARG00000054378	<i>pcbp3</i>	-1.21	7.59	7.80e-08	7.50e-04
ENSDARG00000075666	<i>tsc22d3</i>	1.11	6.67	2.79e-07	7.86e-04

ENSDARG00000043858	<i>cdk19</i>	-1.06	5.01	4.35e-07	7.86e-04
ENSDARG00000099719	<i>cdkn1d</i>	1.27	5.49	5.68e-07	7.86e-04
ENSDARG00000004187	<i>DNAJB5</i>	1.14	6.89	6.10e-07	7.86e-04
ENSDARG00000092115	<i>EIF4A1A</i>	1.12	6.98	6.17e-07	7.86e-04
ENSDARG00000000796	<i>nr4a1</i>	1.82	3.47	3.33e-07	7.86e-04
ENSDARG00000068708	<i>ifrd1</i>	1.00	6.89	7.50e-07	7.86e-04
ENSDARG00000076239	<i>si:ch211-74f19.2</i>	1.50	5.00	7.36e-07	7.86e-04
ENSDARG00000077810	<i>otud4</i>	-1.15	4.62	7.94e-07	7.86e-04
ENSDARG00000100003	<i>glulb</i>	1.34	7.63	9.10e-07	7.86e-04
ENSDARG00000018782	<i>kdm4aa</i>	-1.12	7.18	1.03e-06	7.87e-04
ENSDARG00000044751	<i>ddt</i>	1.71	4.71	9.11e-07	7.86e-04
ENSDARG00000029500	<i>rpl34</i>	1.03	6.65	1.42e-06	7.87e-04
ENSDARG00000099453	<i>elof1</i>	1.05	5.53	1.53e-06	7.87e-04
ENSDARG00000055760	<i>srm</i>	1.32	4.10	1.45e-06	7.87e-04
ENSDARG00000077726	<i>nocta</i>	2.18	3.87	1.23e-06	7.87e-04
ENSDARG00000054063	<i>arpc4</i>	1.15	3.95	1.68e-06	7.87e-04
ENSDARG00000016200	<i>trib3</i>	1.26	3.35	1.35e-06	7.87e-04

All genes are protein-coding. Genes are ranked by p-value. FDR, FDR-corrected p-value

**Table 2. Top 20 differentially expressed genes in the comparison between homozygous mutant (*psen2<sup>S4Ter</sup>/psen2<sup>S4Ter</sup>*) and wild-type (+/+) fish. Average**

Expression is given using log<sub>2</sub>CPM as the units.

Gene	Name	logFC	Average Expression	P-Value	FDR
ENSDARG00000054378	<i>pcbp3</i>	-1.25	7.59	4.82e-08	4.63e-04
ENSDARG00000075397	<i>cipca</i>	-1.19	5.15	3.95e-08	4.63e-04
ENSDARG00000033160	<i>nr1dl</i>	-1.19	7.63	4.45e-07	1.42e-03
ENSDARG00000095743	<i>sox11b</i>	1.11	5.14	4.17e-07	1.42e-03
ENSDARG00000018782	<i>kdm4aa</i>	-1.11	7.18	1.04e-06	1.43e-03
ENSDARG00000056885	<i>per1a</i>	-1.02	7.34	1.43e-06	1.43e-03
ENSDARG00000036587	<i>cbr1</i>	2.03	4.98	1.22e-06	1.43e-03
ENSDARG00000074337	<i>cbfa2t2</i>	-1.38	5.64	2.06e-06	1.43e-03
ENSDARG00000088882	<i>si:ch211-149b19.2</i>	-1.32	4.30	2.28e-06	1.43e-03
ENSDARG00000000796	<i>nr4a1</i>	1.63	3.47	1.24e-06	1.43e-03
ENSDARG00000019396	<i>rergla</i>	1.22	4.31	2.34e-06	1.43e-03
ENSDARG00000036107	<i>txnipa</i>	1.04	5.36	3.67e-06	1.60e-03
ENSDARG00000040944	<i>ntd5</i>	1.23	2.75	1.49e-06	1.43e-03
ENSDARG00000077726	<i>nocta</i>	2.03	3.87	2.73e-06	1.43e-03
ENSDARG00000098968	<i>RSBN1</i>	-1.11	5.98	5.46e-06	1.83e-03
ENSDARG00000057000	<i>camkvl</i>	-1.12	6.29	6.05e-06	1.83e-03
ENSDARG00000099002	<i>creb5a</i>	-1.43	3.80	8.27e-06	2.10e-03
ENSDARG00000076239	<i>si:ch211-74f19.2</i>	1.20	5.00	9.10e-06	2.16e-03
ENSDARG000000102042	<i>CABZ01004876.1</i>	-1.46	4.91	9.44e-06	2.16e-03
ENSDARG00000061030	<i>vezflb</i>	-1.11	5.12	9.94e-06	2.16e-03



All genes are protein-coding. Genes are ranked by p-value. FDR, FDR-corrected p-value

**Table 3. Top 20 ranked genes in the comparison between homozygous (*psen2<sup>S4Ter</sup>/psen2<sup>S4Ter</sup>*) and heterozygous (*psen2<sup>S4Ter</sup>/+*) mutant fish. Average Expression is given using log<sub>2</sub>CPM as the units.**

Gene	Name	logFC	Average Expression	P-Value	FDR
ENSDARG00000100690	<i>si:ch211-256e16.11</i>	1.29	2.95	1.71e-05	0.281
ENSDARG00000041411	<i>rad51</i>	-1.58	3.08	6.45e-05	0.281
ENSDARG00000005690	<i>slc25a23a</i>	-0.70	5.89	1.06e-04	0.290
ENSDARG00000036840	<i>krt15</i>	1.62	3.43	7.31e-05	0.281
ENSDARG00000019601	<i>coll2a1b</i>	1.65	2.71	1.05e-04	0.290
ENSDARG00000052625	<i>fkbp1b</i>	0.60	4.49	2.03e-04	0.322
ENSDARG00000099197	<i>actc1b</i>	2.63	4.53	2.15e-04	0.322
ENSDARG00000100952	<i>wu:fj16a03</i>	-0.63	5.99	3.51e-04	0.422
ENSDARG00000102744	<i>mgst3a</i>	0.95	3.17	4.08e-04	0.423
ENSDARG00000099420	<i>nme2b.2</i>	2.15	4.68	5.00e-04	0.423
ENSDARG00000088736	<i>si:ch211-250n8.1</i>	-1.01	2.69	4.13e-04	0.423
ENSDARG00000070038	<i>rbp2a</i>	1.62	1.45	1.61e-04	0.322
ENSDARG00000005057	<i>dimt1l</i>	-0.77	2.37	4.25e-04	0.423
ENSDARG00000052515	<i>calcoco2</i>	0.91	2.28	3.30e-04	0.422
ENSDARG00000026726	<i>anxa1a</i>	1.13	3.47	5.41e-04	0.423

ENSDARG00000025325	<i>ccsapa</i>	-0.36	6.29	5.63e-04	0.423
ENSDARG00000090980	<i>apof</i>	-0.71	5.57	6.34e-04	0.423
ENSDARG00000055754	<i>smc1a</i>	0.37	8.17	6.61e-04	0.423
ENSDARG00000001431	<i>actn3b</i>	2.19	2.16	3.20e-04	0.422
ENSDARG00000041402	<i>zc3h14</i>	-0.36	5.37	7.61e-04	0.429

No genes were considered as differentially expressed. All genes are protein-coding.

Genes are ranked by p-value. FDR, FDR-corrected p-value.

Heatmaps of genes with strongest differential expression were constructed showing the top 25 most DE genes unique to each of the mutant comparisons against wild type (Figures 7A and 7B), and the 50 most DE genes shared between the two comparisons (Figure 7C). This showed large numbers of commonly up-regulated genes in both comparisons with many having functions possibly important in AD pathological processes. For example, the human orthologue of *fkbp5* (fk506 binding protein 5), encodes a protein acting as a co-chaperone of the glucocorticoid receptor (Binder 2009) and a negative regulator of glucocorticoid signaling (Stechschulte and Sanchez 2011; Sinclair, Fillman et al. 2013). *fkbp5* transcription is also directly regulated by glucocorticoid receptor (Guidotti, Calabrese et al. 2012; Jubb, Boyle et al. 2017) so increased *fkbp5* transcript levels likely indicate increased glucocorticoid receptor activation of transcription and that mutant brains are under some form of stress. *caspb* (caspase b) was also seen to be upregulated and, in humans, this encodes a cysteine-aspartic protease that plays an essential role in programmed cell death and the innate

immune system (McIlwain, Berger et al. 2013). Upregulated *mt2* (metallothionein 2) provides protection against metal toxicity and oxidative stress (Hidalgo, Penkowa et al. 2006).

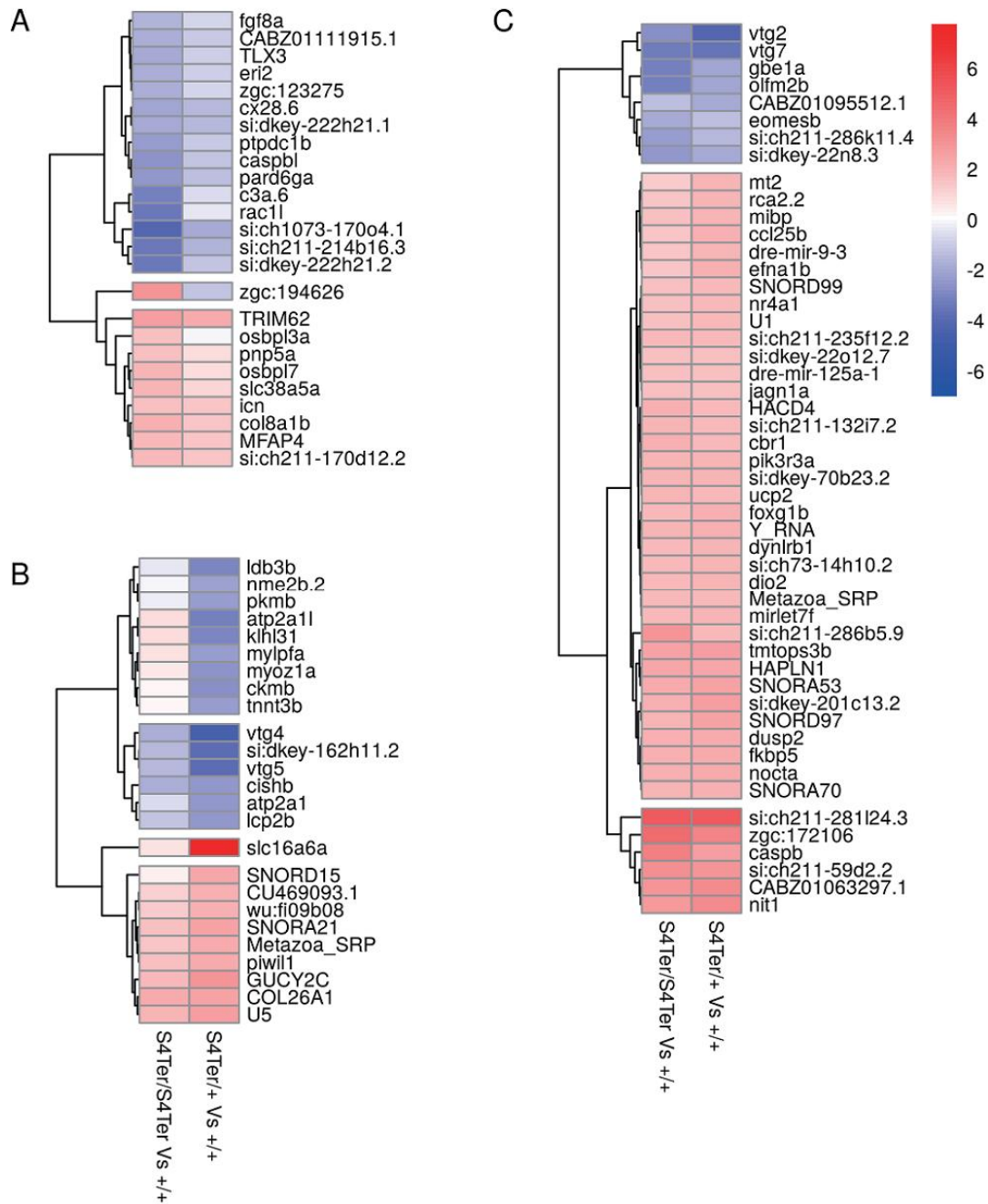


**Figure 7. Overall heatmaps.** Heatmaps showing A) the 25 top-ranked differentially

expressed genes only in homozygous mutants compared to wild type; B) the 25 top-ranked differentially expressed genes only in heterozygous mutants compared to wild type; and, C) the 50 top-ranked genes common to both comparisons between mutant and wild type fish. Genes are ranked by fold-change.

The heatmaps include numerous non-identified genes, with the most strongly upregulated of the common genes being *si:ch211-281124.3*. The protein encoded by gene *si:ch211-281124.3* is predicted to interact with ubiquitin-conjugating enzymes and sirtuin proteins (<http://bit.ly/2Fuyvfh>). Thus, *si:ch211-281124.3* may be involved in the ubiquitin-proteasome system and play a role in inflammation and apoptosis.

According to the heatmap, a number of genes show down-regulation in the *psen2<sup>S4Ter</sup>/+* and *psen2<sup>S4Ter</sup>/psen2<sup>S4Ter</sup>* mutant fish brains compared to their *+/+* siblings, such as *gbe1a*, *olfm2b* and *eomesb* (Figure 7C). Among these down-regulated genes, there are also two “non-identified” genes, *si:ch211-286k11.4* and *si:dkey-22n8.3*. The gene *si:ch211-286k11.4* has subsequently been identified as *cdhr5b* (cadherin-related family member 5b), the human homolog of which, once named *MUCDHL* (*MUCIN AND CADHERIN-LIKE*) has been found to consist of nonpolymorphic tandem repeats similar to mucin proteins and a consensus calcium-binding motif found in all cadherins (Paris and Williams 2000). The gene *si:dkey-22n8.3* encodes an uncharacterised protein, which, according to the prediction of interactors from the STRING database (<https://string-db.org/network/7955.ENSDDARP00000108110>), encodes the

mitochondrial protein ATP synthase, H<sup>+</sup> transporting, mitochondrial Fo complex, subunit F6, consistent with the remarkable effects of putative loss of *psen2* activity on mitochondrial function (see GO analysis below).

It is also interesting to observe members of the *vitellogenin* gene family (*vtg2* and *vtg7*) strongly down-regulated in comparisons of both mutant genotypes against their +/+ siblings (Figure 7C). While these genes are named for their contribution to the protein composition of egg yolk, here their transcripts are expressed in brain. Vitellogenin proteins are thought to contribute, possibly, to antioxidant capacity (Nakamura, Yasuda et al. 1999; Seehuus, Norberg et al. 2006) and the innate immune system (Harman 1956; Gatschenberger, Gimple et al. 2012) and are often responsive to estrogens (Amdam, Simoes et al. 2004) (which may be important in this case since all the brains analysed were from female fish).

Although no gene has been detected as DE between the two mutant genotypes, some genes are seen as DE only in homozygous mutants compared to wild type, or in heterozygous mutants compared to wild type (Figure 7A). Interestingly, the gene *zgc:194626*, now known as *leap2* (*liver-expressed antimicrobial peptide 2*), was found upregulated in homozygous mutants compared to wild type, but downregulated in heterozygous mutants compared to wild type. The human homolog of gene *leap2*, *LEAP2*, encodes a peptide hormone that functions as an endogenous antagonist of the growth hormone secretagogue receptor (GHSR) that, in mammals, binds the hormone

ghrelin to regulate energy homeostasis (Ge, Yang et al. 2018).

The gene *slc16a6a* (*solute carrier family 16, member 6a*) was found apparently greatly upregulated in heterozygous mutants compared to wild type (Figure 7B), while remaining almost unchanged in homozygous mutants compared to wild type. The human homolog of this gene, *SLC16A6*, encodes proton-linked monocarboxylate transporter, a transporter of the major ketone body  $\beta$ -hydroxybutyrate, which is involved in fasting energy metabolism and catalyses the rapid transport across the plasma membrane of many monocarboxylates such as lactate and pyruvate (Hugo, Cruz-Garcia et al. 2012).

### **Gene Ontology (GO) analysis**

A simple GO enrichment analysis was performed on the common DE genes (Table 4) and those considered uniquely DE in one of the two comparisons against wild type (Tables 5 and 6). The most highly ranked GO terms from common DE genes were all associated with mitochondria, i.e. *mitochondrial inner membrane*, *mitochondrial envelope*, *mitochondrial membrane*, *organelle inner membrane*, *mitochondrial protein complex etc.*. Interestingly, the GO terms most significantly enriched from genes considered as uniquely DE in the comparisons between homozygous mutant and wild type brains indicated functions in immune responses. This indicates one area where the effects of homozygosity for *S4Ter* may be quite distinct from those in heterozygous

mutants.

**Table 4. GO terms considered as significantly enriched within the set of 439 DE genes common to both comparisons between mutant and wild-type fish, to an FDR of 5%.**

GOID	Term	Ontology	Total	DE Genes	P-value	FDR
GO:0005743	mitochondrial inner membrane	CC	224	15	6.34e-05	0.014
GO:0005740	mitochondrial envelope	CC	337	19	7.34e-05	0.014
GO:0031966	mitochondrial membrane	CC	318	18	1.08e-04	0.014
GO:0019866	organelle inner membrane	CC	238	15	1.25e-04	0.014
GO:0098798	mitochondrial protein complex	CC	99	9	2.00e-04	0.019
GO:0015980	energy derivation by oxidation of organic compounds	BP	106	9	3.35e-04	0.026
GO:0098800	inner mitochondrial membrane protein complex	CC	88	8	4.50e-04	0.030
GO:0031967	organelle envelope	CC	441	20	8.31e-04	0.039
GO:0044429	mitochondrial part	CC	441	20	8.31e-04	0.039
GO:0005746	mitochondrial respiratory chain	CC	56	6	9.84e-04	0.039
GO:0015849	organic acid transport	BP	77	7	1.02e-03	0.039
GO:0046942	carboxylic acid transport	BP	77	7	1.02e-03	0.039
GO:0000786	nucleosome	CC	59	6	1.30e-03	0.046

The total number of genes matching each term is given for both the set of expressed genes and those considered as differentially expressed (DE). BP, biological process. CC, cellular component. FDR, FDR-corrected p-value.

**Table 5. GO terms considered as significantly enriched within the set of 226 DE genes unique to the comparison between heterozygous mutant and wild-type fish, to an FDR of 5%.**

GOID	Term	Ontology	Total	DE Genes	P-value	FDR
GO:0005578	proteinaceous extracellular matrix	CC	127	8	2.60e-05	0.005
GO:0030017	sarcomere	CC	53	5	1.36e-04	0.010
GO:0030016	myofibril	CC	56	5	1.77e-04	0.010
GO:0043292	contractile fiber	CC	57	5	1.92e-04	0.010

The total number of genes matching each term is given for both the set of expressed genes and those considered as differentially expressed (DE). CC, cellular component. FDR, FDR-corrected p-value.

**Table 6. GO terms considered as significantly enriched within the set of 88 DE genes unique to the comparison between homozygous mutant and wild-type fish, to an FDR of 5%.**

GOID	Term	Ontology	Total	DE Genes	P-value	FDR
GO:0009617	response to bacterium	BP	73	4	2.48e-04	0.020
GO:0006869	lipid transport	BP	91	4	5.76e-04	0.020
GO:0010876	lipid localization	BP	95	4	6.77e-04	0.020
GO:0043207	response to external biotic stimulus	BP	121	4	1.67e-03	0.029



GO:0007186	G-protein coupled receptor signaling pathway	BP	414	7	1.71e-03	0.029
GO:0006952	defense response	BP	212	5	1.95e-03	0.029

The total number of genes matching each term is given for both the set of expressed genes and those considered as differentially expressed (DE). BP, biological process. FDR, FDR-corrected p-value.

## Discussion

Well over 200 mutations causing familial Alzheimer's disease have been identified in the human *PSEN1* and *PSEN2* genes. However, none of these mutations are obviously null (e.g. are frameshift or nonsense mutations) (Jayne, Newman et al. 2016). Knowledge of the molecular effects of null mutations in these genes is, therefore, useful since, by exclusion, it can help us determine the functions critically affected by fAD mutations. Alzheimer's disease takes decades to develop, but we are unable to investigate in detail the molecular changes occurring in the brains of young human carriers of fAD mutations since biopsies cannot be taken. Consequently, analysis in animal models is necessary.

In this study, we generated an 8-bp deletion (*psen2*<sup>S4Ter</sup>) in the zebrafish *psen2* gene. This results in formation of a premature termination codon (PTC) at the fourth codon position downstream of the start codon. This PTC should prevent translation of the protein product of *psen2*. However, three observations suggest caution in this

interpretation. The first is that homozygosity for *S4Ter* does not cause an obvious surface pigmentation phenotype as might be expected for partial loss of  $\gamma$ -secretase activity (Nornes, Newman et al. 2009), although we, and others, have not noted pigmentation defects in apparent *psen1* loss-of-function homozygous mutants ((Sundvik, Chen et al. 2013) and Newman et al. unpublished data). However, *psen2* shows particularly high levels of transcription in melanocytes (Groth, Nornes et al. 2002) and another, yet-to-be-published frameshift mutation in zebrafish *psen2* does show a pigmentation phenotype (Jiang et al. unpublished results). The second reason to suspect that *S4Ter* does not cause a complete loss of *psen2* function is that there is no apparent nonsense-mediated mRNA decay (NMD) of mutant *S4Ter* transcripts despite the presence of the PTC (2). One possible explanation for this might be read-through of the PTC and re-initiation of translation at a second start codon farther downstream. Indeed, it has been reported in mammalian genes that PTCs close to the start codon may cause reduced NMD if there is a downstream AUG codon that can re-initiate translation (Zhang and Maquat 1997; Silva, Ribeiro et al. 2008), and some PTCs close to the start codon may even escape NMD (Romao, Inacio et al. 2000). In fact, a second potential translation start codon exists at codon 34 of the coding sequence. This codon and flanking nucleotides appear closer to the consensus Kozac sequence controlling translation initiation (Kozak 1984) than even the nominal start codon. Thirdly, unlike when *psen2* translation is blocked by morpholino injection, analysis of DoLA neuron number at 24 hpf shows no significant difference between wild type embryos and *S4Ter* homozygotes, (although genetic compensation might be suppressing a loss-of-function

*psen2* phenotype in this case). Since we do not currently possess an antibody that recognises zebrafish *Psen2* protein, additional tests should be performed to investigate whether or not the *S4Ter* mutation represents a loss of function.

### **Dominance due to haploinsufficiency or neomorphism?**

The molecular phenotype of the *S4Ter* mutation (as reflected in our transcriptome analyses) is remarkable in that heterozygous and homozygous mutant fish show broadly similar effects on gene expression. If *S4Ter* is a loss-of-function mutation then this reflects very widespread haploinsufficiency of *psen2* function. An alternative is that the mutation is neomorphic and causes a gain of function. Conceivably, *S4Ter* may be acting in a dominant negative manner although, in that case, only on *psen2* activity since, if the activity of both *psen1* and *psen2* were suppressed, this would most likely be lethal during embryo development.

Remarkably, the GO analysis of the transcriptomic data (Table 4) revealed that the common changes in *psen2* activity caused by *S4Ter* mainly affect mitochondrion formation and function, including alterations proposed to contribute to the neuronal death associated with AD pathology (Hedskog, Pinho et al. 2013). Of particular importance to mitochondrial function may be decreased expression of the gene *pcbp3*, the human orthologue of which encodes Poly(rC)-binding protein 3 that has an iron chaperone activity toward ferritin (Leidgens, Bullough et al. 2013). *pcbp3* may play an

important role in the distribution of iron in the cytosolic labile iron pool to various destinations including mitochondria (Philpott and Ryu 2014). Iron is essential to normal mitochondrial function due to the many iron-sulfur cluster binding proteins mitochondria contain, including many involved in oxidative phosphorylation.

Two reports have shown that loss of *PSEN2* activity in mammalian cells causes increased juxtaposition between mitochondria and the endoplasmic reticulum (the mitochondrial associated membranes, MAM) (Zampese, Fasolato et al. 2011; Filadi, Greotti et al. 2016) and this can inhibit respiration by mitochondria (Contino, Porporato et al. 2017). It may be that the widespread effects we have observed on mitochondria due to *S4Ter* are partially a reflection of decreased delivery to them of  $\text{Fe}^{2+}$  from the labile iron pool. Alternatively, many other genes involved in mitochondrial function are affected by the *S4Ter* mutation of *psen2* and may also play a significant role in regulating the transcriptomic changes we have observed.

In conclusion, we found that the *S4Ter* mutation of zebrafish *psen2* acts in a dominant manner to affect significantly mitochondrial function but does not induce NMD of mutant transcripts. Our results support previous findings on the importance of mammalian *PSEN2* in control of mitochondrial function via MAM formation. Future work should involve detailed analysis of the ability of the *psen2*<sup>*S4Ter*</sup> transcript to be translated into protein and the function of any protein produced. This work contributes to our analysis of the effects of fAD mutations on brain biology.

## **Acknowledgments**

The authors wish to thank Seyyed Hani Moussavi Nik for kind assistance in adjusting the conditions for the dqPCR.

## References

- Agrawal, V., N. Sawhney, et al. (2016). "Loss of Presenilin 2 Function Is Associated with Defective LPS-Mediated Innate Immune Responsiveness." Molecular Neurobiology **53**(5): 3428-3438.
- Amdam, G. V., Z. L. Simoes, et al. (2004). "Hormonal control of the yolk precursor vitellogenin regulates immune function and longevity in honeybees." Exp Gerontol **39**(5): 767-773.
- Area-Gomez, E., A. J. de Groof, et al. (2009). "Presenilins are enriched in endoplasmic reticulum membranes associated with mitochondria." Am J Pathol **175**(5): 1810-1816.
- Babon, J. J., M. McKenzie, et al. (2003). "The use of resolvases T4 endonuclease VII and T7 endonuclease I in mutation detection." Molecular Biotechnology **23**(1): 73-81.
- Behbahani, H., I. G. Shabalina, et al. (2006). "Differential role of Presenilin-1 and -2 on mitochondrial membrane potential and oxygen consumption in mouse embryonic fibroblasts." J Neurosci Res **84**(4): 891-902.
- Benjamini, Y. and Y. Hochberg (1995). Controlling The False Discovery Rate - A Practical And Powerful Approach To Multiple Testing.
- Binder, E. B. (2009). "The role of FKBP5, a co-chaperone of the glucocorticoid receptor in the pathogenesis and therapy of affective and anxiety disorders." Psychoneuroendocrinology **34**(1): 021.
- Brogna, S. and J. Wen (2009). "Nonsense-mediated mRNA decay (NMD) mechanisms." Nat Struct Mol Biol **16**(2): 107-113.
- Contino, S., P. E. Porporato, et al. (2017). "Presenilin 2-Dependent Maintenance of Mitochondrial Oxidative Capacity and Morphology." Front Physiol **8**(796).
- De Strooper, B., P. Saftig, et al. (1998). "Deficiency of presenilin-1 inhibits the normal cleavage of amyloid precursor protein." Nature **391**(6665): 387-390.
- Donoviel, D. B., A. K. Hadjantonakis, et al. (1999). "Mice lacking both presenilin genes exhibit early embryonic patterning defects." Genes Dev **13**(21): 2801-2810.
- Ebrahimie, E., S. H. Moussavi Nik, et al. (2016). "The Zebrafish Equivalent of Alzheimer's Disease-Associated PRESENILIN Isoform PS2V Regulates Inflammatory and Other Responses to Hypoxic Stress." J Alzheimers Dis **52**(2): 581-608.
- Ferjentsik, Z., S. Hayashi, et al. (2009). "Notch Is a Critical Component of the Mouse Somitogenesis Oscillator and Is Essential for the Formation of the Somites." PLOS Genetics **5**(9): e1000662.
- Filadi, R., E. Greotti, et al. (2016). "Presenilin 2 Modulates Endoplasmic Reticulum-Mitochondria Coupling by Tuning the Antagonistic Effect of Mitofusin 2." Cell Reports **15**(10): 2226-2238.
- Gao, L., S. Tian, et al. (2013). "Hypoxia increases A $\beta$ -induced tau phosphorylation by calpain and promotes behavioral consequences in AD transgenic mice." J Mol Neurosci **51**(1): 138-147.
- Gatschenberger, H., O. Gimple, et al. (2012). "Honey bee drones maintain humoral immune competence throughout all life stages in the absence of vitellogenin production." J Exp Biol **215**(Pt 8): 1313-1322.
- Ge, X., H. Yang, et al. (2018). "LEAP2 Is an Endogenous Antagonist of the Ghrelin Receptor." Cell Metab **27**(2): 461-469.
- Groth, C., S. Nornes, et al. (2002). "Identification of a second presenilin gene in zebrafish with similarity to the human Alzheimer's disease gene presenilin2." Development Genes and Evolution

- 212**(10): 486-490.
- Guidotti, G., F. Calabrese, et al. (2012). "Glucocorticoid Receptor and FKBP5 Expression Is Altered Following Exposure to Chronic Stress: Modulation by Antidepressant Treatment." Neuropsychopharmacology **38**: 616.
- Handler, M., X. Yang, et al. (2000). "Presenilin-1 regulates neuronal differentiation during neurogenesis." Development **127**(12): 2593-2606.
- Harman, D. (1956). "Aging: a theory based on free radical and radiation chemistry." J Gerontol **11**(3): 298-300.
- Haslinger, A., T. J. Schwarz, et al. (2009). "Expression of Sox11 in adult neurogenic niches suggests a stage-specific role in adult neurogenesis." Eur J Neurosci **29**(11): 2103-2114.
- Hedskog, L., C. M. Pinho, et al. (2013). "Modulation of the endoplasmic reticulum-mitochondria interface in Alzheimer's disease and related models." Proc Natl Acad Sci U S A **110**(19): 7916-7921.
- Herreman, A., D. Hartmann, et al. (1999). "Presenilin 2 deficiency causes a mild pulmonary phenotype and no changes in amyloid precursor protein processing but enhances the embryonic lethal phenotype of presenilin 1 deficiency." Proceedings of the National Academy of Sciences **96**(21): 11872-11877.
- Herreman, A., L. Serneels, et al. (2000). "Total inactivation of gamma-secretase activity in presenilin-deficient embryonic stem cells." Nat Cell Biol **2**(7): 461-462.
- Hidalgo, J., M. Penkowa, et al. (2006). "Expression of metallothionein-I, -II, and -III in Alzheimer disease and animal models of neuroinflammation." Exp Biol Med **231**(9): 1450-1458.
- Hroudova, J., N. Singh, et al. (2014). "Mitochondrial dysfunctions in neurodegenerative diseases: relevance to Alzheimer's disease." Biomed Res Int **175062**(10): 12.
- Hugo, S. E., L. Cruz-Garcia, et al. (2012). "A monocarboxylate transporter required for hepatocyte secretion of ketone bodies during fasting." Genes & Development **26**(3): 282-293.
- Hwang, W. Y., Y. Fu, et al. (2013). "Efficient genome editing in zebrafish using a CRISPR-Cas system." Nat Biotechnol **31**(3): 227-229.
- Jayadev, S., A. Case, et al. (2013). "Presenilin 2 influences miR146 level and activity in microglia." Journal of Neurochemistry **127**(5): 592-599.
- Jayadev, S., A. Case, et al. (2010). "Presenilin 2 is the predominant gamma-secretase in microglia and modulates cytokine release." PLoS ONE **5**(12): 0015743.
- Jayadev, S., J. B. Leverenz, et al. (2010). "Alzheimer's disease phenotypes and genotypes associated with mutations in presenilin 2." Brain **133**(Pt 4): 1143-1154.
- Jayne, T., M. Newman, et al. (2016). "Evidence For and Against a Pathogenic Role of Reduced gamma-Secretase Activity in Familial Alzheimer's Disease." J Alzheimers Dis **52**(3): 781-799.
- Jubb, A. W., S. Boyle, et al. (2017). "Glucocorticoid Receptor Binding Induces Rapid and Prolonged Large-Scale Chromatin Decompaction at Multiple Target Loci." Cell Rep **21**(11): 3022-3031.
- Kang, D. E., I. S. Yoon, et al. (2005). "Presenilins mediate phosphatidylinositol 3-kinase/AKT and ERK activation via select signaling receptors. Selectivity of PS2 in platelet-derived growth factor signaling." J Biol Chem **280**(36): 31537-31547.
- Kim, D., B. Langmead, et al. (2015). "HISAT: a fast spliced aligner with low memory requirements." Nature methods **12**: 357.
- Kozak, M. (1984). "Compilation and analysis of sequences upstream from the translational start site in eukaryotic mRNAs." Nucleic Acids Res **12**(2): 857-872.

- Law, C. W., Y. Chen, et al. (2014). "voom: precision weights unlock linear model analysis tools for RNA-seq read counts." *Genome Biology* **15**(2): R29.
- Lee, M. K., H. H. Slunt, et al. (1996). "Expression of presenilin 1 and 2 (PS1 and PS2) in human and murine tissues." *J Neurosci* **16**(23): 7513-7525.
- Leidgens, S., K. Z. Bullough, et al. (2013). "Each member of the poly-r(C)-binding protein 1 (PCBP) family exhibits iron chaperone activity toward ferritin." *J Biol Chem* **288**(24): 17791-17802.
- Levy-Lahad, E., W. Wasco, et al. (1995). "Candidate gene for the chromosome 1 familial Alzheimer's disease locus." *Science* **269**(5226): 973-977.
- Liao, Y., G. K. Smyth, et al. (2013). "The Subread aligner: fast, accurate and scalable read mapping by seed-and-vote." *Nucleic Acids Research* **41**(10): e108-e108.
- Marchi, S., S. Patergnani, et al. (2014). "The endoplasmic reticulum–mitochondria connection: One touch, multiple functions." *Biochimica et Biophysica Acta (BBA) - Bioenergetics* **1837**(4): 461-469.
- McIlwain, D. R., T. Berger, et al. (2013). "Caspase functions in cell death and disease." *Cold Spring Harb Perspect Biol* **5**(4).
- Meeker, N. D., S. A. Hutchinson, et al. (2007). "Method for isolation of PCR-ready genomic DNA from zebrafish tissues." *Biotechniques* **43**(5): 614.
- Mohuczy, D., K. Qian, et al. (2002). "Presenilins in the heart: presenilin-2 expression is increased by low glucose and by hypoxia in cardiac cells." *Regul Pept* **110**(1): 1-7.
- Nakamura, A., K. Yasuda, et al. (1999). "Vitellogenin-6 is a major carbonylated protein in aged nematode, *Caenorhabditis elegans*." *Biochem Biophys Res Commun* **264**(2): 580-583.
- Naruse, S., G. Thinakaran, et al. (1998). "Effects of PS1 deficiency on membrane protein trafficking in neurons." *Neuron* **21**(5): 1213-1221.
- Newman, M., I. F. Musgrave, et al. (2007). "Alzheimer disease: amyloidogenesis, the presenilins and animal models." *Biochim Biophys Acta* **3**: 285-297.
- Nornes, S., M. Newman, et al. (2008). "Interference with splicing of Presenilin transcripts has potent dominant negative effects on Presenilin activity." *Human molecular genetics* **17**(3): 402-412.
- Nornes, S., M. Newman, et al. (2009). "Independent and cooperative action of Psen2 with Psen1 in zebrafish embryos." *Experimental Cell Research* **315**(16): 2791-2801.
- Paris, M. J. and B. R. Williams (2000). "Characterization of a 500-kb contig spanning the region between c-Ha-Ras and MUC2 on chromosome 11p15.5." *Genomics* **69**(2): 196-202.
- Pei, L., A. Castrillo, et al. (2006). "Regulation of macrophage inflammatory gene expression by the orphan nuclear receptor Nur77." *Mol Endocrinol* **20**(4): 786-794.
- Philpott, C. C. and M. S. Ryu (2014). "Special delivery: distributing iron in the cytosol of mammalian cells." *Front Pharmacol* **5**(173).
- Quast, C., E. Pruesse, et al. (2013). "The SILVA ribosomal RNA gene database project: improved data processing and web-based tools." *Nucleic Acids Research* **41**(D1): D590-D596.
- Romao, L., A. Inacio, et al. (2000). "Nonsense mutations in the human beta-globin gene lead to unexpected levels of cytoplasmic mRNA accumulation." *Blood* **96**(8): 2895-2901.
- Rossi, A., Z. Kontarakis, et al. (2015). "Genetic compensation induced by deleterious mutations but not gene knockdowns." *Nature* **524**: 230.
- Ryman, D. C., N. Acosta-Baena, et al. (2014). "Symptom onset in autosomal dominant Alzheimer disease: a systematic review and meta-analysis." *Neurology* **83**(3): 253-260.
- Seehuus, S. C., K. Norberg, et al. (2006). "Reproductive protein protects functionally sterile honey bee



- workers from oxidative stress." *Proc Natl Acad Sci U S A* **103**(4): 962-967.
- Shen, J., R. T. Bronson, et al. (1997). "Skeletal and CNS defects in Presenilin-1-deficient mice." *Cell* **89**(4): 629-639.
- Silva, A. L., P. Ribeiro, et al. (2008). "Proximity of the poly(A)-binding protein to a premature termination codon inhibits mammalian nonsense-mediated mRNA decay." *Rna* **14**(3): 563-576.
- Sinclair, D., S. G. Fillman, et al. (2013). "Dysregulation of glucocorticoid receptor co-factors FKBP5, BAG1 and PTGES3 in prefrontal cortex in psychotic illness." *Scientific reports* **3**: 3539.
- Stechschulte, L. A. and E. R. Sanchez (2011). "FKBP51-a selective modulator of glucocorticoid and androgen sensitivity." *Curr Opin Pharmacol* **11**(4): 332-337.
- Stubblefield, J. J., J. Terrien, et al. (2012). "Nocturnin: at the crossroads of clocks and metabolism." *Trends Endocrinol Metab* **23**(7): 326-333.
- Sundvik, M., Y. C. Chen, et al. (2013). "Presenilin1 regulates histamine neuron development and behavior in zebrafish, danio rerio." *J Neurosci* **33**(4): 1589-1597.
- Tamme, R., S. Wells, et al. (2002). "The identity and distribution of neural cells expressing the mesodermal determinant spadetail." *BMC Developmental Biology* **2**(1): 9.
- Wang, L.-Y., C.-L. Hung, et al. (2016). "KDM4A Coactivates E2F1 to Regulate the PDK-Dependent Metabolic Switch between Mitochondrial Oxidation and Glycolysis." *Cell Reports* **16**(11): 3016-3027.
- Wang, P., F. A. Pereira, et al. (2003). "Presenilins are required for the formation of comma- and S-shaped bodies during nephrogenesis." *Development* **130**(20): 5019-5029.
- Zampese, E., C. Fasolato, et al. (2011). "Presenilin 2 modulates endoplasmic reticulum (ER)-mitochondria interactions and Ca<sup>2+</sup> cross-talk." *Proc Natl Acad Sci U S A* **108**(7): 2777-2782.
- Zetterberg, H., E. Mortberg, et al. (2011). "Hypoxia due to cardiac arrest induces a time-dependent increase in serum amyloid beta levels in humans." *PLoS ONE* **6**(12): 14.
- Zhang, J. and L. E. Maquat (1997). "Evidence that translation reinitiation abrogates nonsense-mediated mRNA decay in mammalian cells." *Embo J* **16**(4): 826-833.
- Zhang, Z., P. Nadeau, et al. (2000). "Presenilins are required for gamma-secretase cleavage of beta-APP and transmembrane cleavage of Notch-1." *Nat Cell Biol* **2**(7): 463-465.

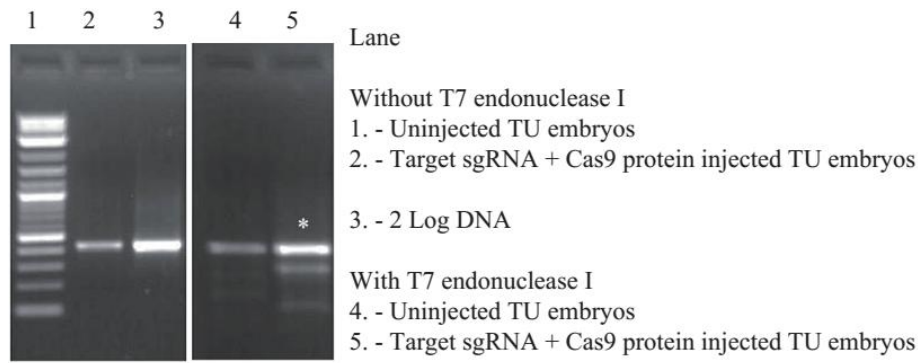
### 2.3 Supplementary Information

This section is included in the thesis as information supplementary to Section 2.2. It contains additional information not included in the main text of the manuscript.

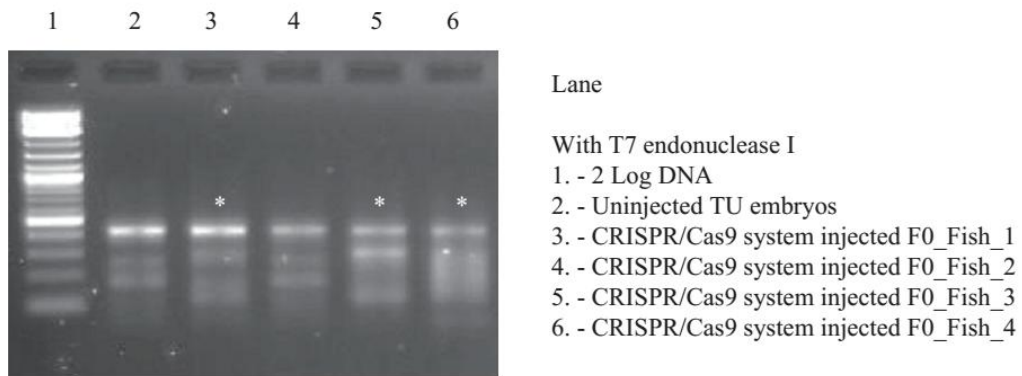
#### **File S1. Mutation screening and breeding of CRISPR/Cas9-injected fish.**

The T7 endonuclease I assay was applied to G0 embryos injected with the CRISPR Cas9 mutagenesis system components to test whether double-stranded breaks (DSBs) were generated at the target site. DNA amplified from uninjected wild type Tübingen embryos showed cleavage products, one of ~180 bp and the other ~280 bp (Figure S1A), which were not the sizes expected for mutations at the target site. However, the CRISPR/Cas9-injected G0 embryos showed two different cleavage bands, one of ~150 bp and the other ~300 bp (Figure S1A), which were close to the sizes expected. Thus, we assumed that this CRISPR/Cas9 system could generate DSBs at the appropriate locus in the genomes of the injected G0 embryos. The cleavage products detected in the wild type Tübingen embryos may have been caused by single nucleotide polymorphisms (SNPs) (Babon, McKenzie et al. 2003).

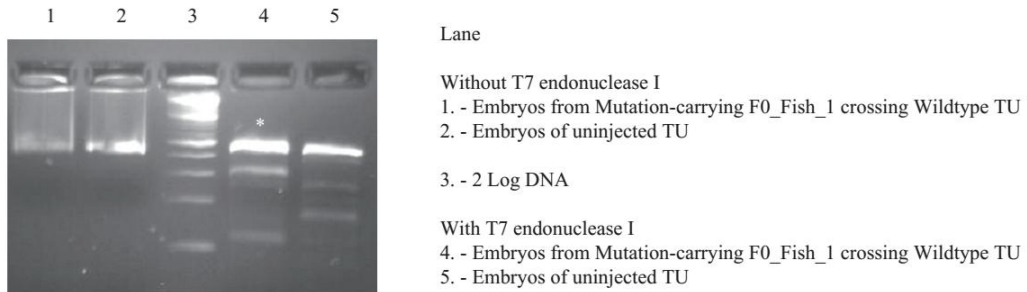
**A**



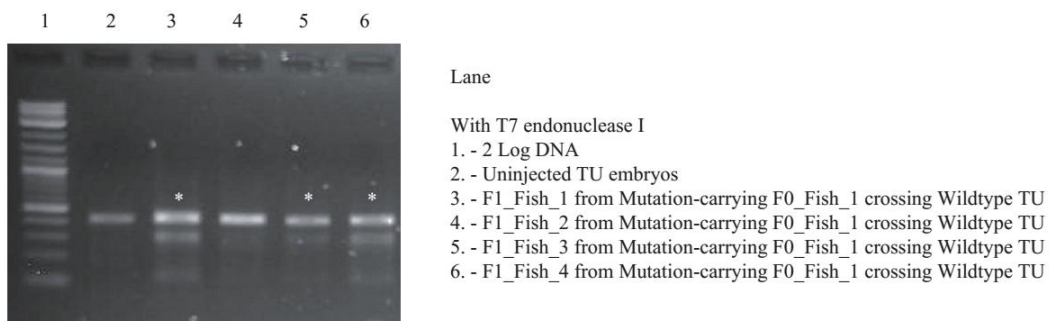
**B**



**C**



**D**



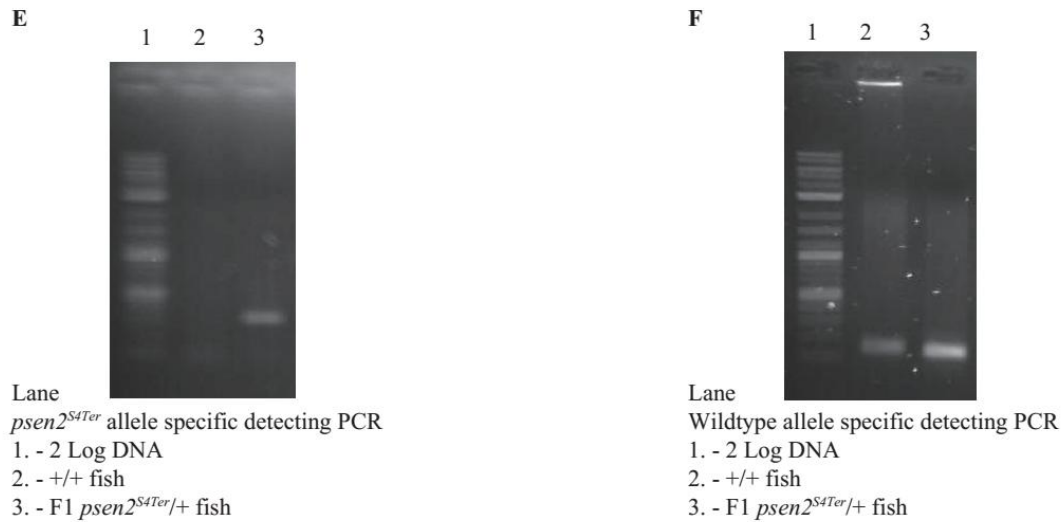


**Figure S1. T7 endonuclease assays and PCRs for fish from different generations.**

(A) 10 of the CRISPR/Cas9-injected G0 embryos were pooled together and then tested with the T7 endonuclease I assay. The positive cleavage pattern was detected.

(B) 39 of the CRISPR/Cas9-injected G0 fish were tested, and 13 out of these showed positive cleavage patterns, indicating that they carried mutations.

(C) 10 F1 embryos were pooled before testing with the T7 endonuclease I assay. The positive cleavage patterns observed indicated that mutations have been passed through the germline.

(D) 5 out of 10 tested F1 fish showed positive cleavage in the T7 endonuclease I assay.

(E)  $psen2^{S4Ter}$  allele-specific detection PCR.

(F) Wild type allele-specific detection PCR.

When injected G0 embryos had become adults, DNA from tail fin biopsies was tested using the T7 endonuclease I assay to detect for mutations generated through non-homologous end joining (NHEJ) pathway repair of DSBs at the target site (Hwang, Fu

et al. 2013). Some of the G0 fish showed similar cleavage patterns to that of the pooled G0 embryos (S1B Fig), indicating the presence of cells with mutations at the target site. 39 injected G0 fish were tested, with 13 of these showing the cleavage pattern indicating the presence of mutations. However, since different cells in each mutated G0 fish may carry different mutations, each of the positive G0 fish was outbred to a wild type Tübingen fish, so that any mutant F1 progeny would be completely heterozygous for a single mutation at the intended site. 10 F1 embryos were pooled and then tested using the T7 endonuclease I assay, and the expected cleavage pattern observed (S1C Fig) indicated that these mutations had passed through the germline. When the F1 progeny had become adult, DNA from biopsies was tested again using the T7 endonuclease I assay to detect mutation-carrying heterozygous fish. 5 out of 10 tested F1 fish showed the expected cleavage pattern (S1D Fig). After sequencing genomic DNA from these 5 heterozygous mutants, 3 different mutations were identified. One of these was an 8-bp deletion resulting in a premature termination codon close downstream of the start codon of *psen2* (Figure 1). It is designated *psen2*<sup>S4Ter</sup>.

**File S2. Additional discussion on the members of the *vitellogenin* gene family.**

Since vitellogenin is a major target of oxidative carbonylation (Seehuus, Norberg et al. 2006), the binding of it to live cells is suggested to improve cell oxidative stress tolerance (Havukainen, Munch et al. 2013). Based on the free radical theory of aging, the balance between reactive oxygen species (ROS) and antioxidants is an important factor in chronic inflammation and aging-associated diseases (Harman 1956). It was also found that the levels of vitellogenin in honey bee are negatively correlated with the aging rate in workers (Seehuus, Norberg et al. 2006; Havukainen, Munch et al. 2013; Munch, Ihle et al. 2015). This antioxidant activity of vitellogenin is also found in the nematode (*Caenorhabditis elegans*) (Nakamura, Yasuda et al. 1999). Studies in some fish species found that vitellogenin acts as an antimicrobial agent involved in immune defense (Wang, Wang et al. 2011; Zhang, Wang et al. 2011). Furthermore, phosvitin, a vitellogenin-derived protein, is also able to recognise pathogen-associated molecular patterns (PAMPs) and to inhibit the growth of Gram-negative bacteria (*Escherichia coli* strain was used as test bacterium) by chelating ions through its numerous phosphorylated serine residues (Sattar Khan, Nakamura et al. 2000). In our study, members of the *vitellogenin* gene family were found strongly down-regulated in both homozygous and heterozygous mutant genotypes compared to their wild type siblings (Figure 7). Since the total RNA purified for RNA-seq was extracted from the brains of zebrafish, the down-regulating of *vitellogenin* genes observed in mutants seems more likely related to reduced antioxidant activity or antimicrobial activity rather than

reproduction.

- Babon, J. J., M. McKenzie, et al. (2003). "The use of resolvases T4 endonuclease VII and T7 endonuclease I in mutation detection." Molecular Biotechnology **23**(1): 73-81.
- Harman, D. (1956). "Aging: a theory based on free radical and radiation chemistry." J Gerontol **11**(3): 298-300.
- Havukainen, H., D. Munch, et al. (2013). "Vitellogenin recognizes cell damage through membrane binding and shields living cells from reactive oxygen species." J Biol Chem **288**(39): 28369-28381.
- Hwang, W. Y., Y. Fu, et al. (2013). "Heritable and Precise Zebrafish Genome Editing Using a CRISPR-Cas System." PLoS ONE **8**(7): e68708.
- Munch, D., K. E. Ihle, et al. (2015). "Vitellogenin in the honey bee brain: Atypical localization of a reproductive protein that promotes longevity." Exp Gerontol **71**: 103-108.
- Nakamura, A., K. Yasuda, et al. (1999). "Vitellogenin-6 is a major carbonylated protein in aged nematode, *Caenorhabditis elegans*." Biochem Biophys Res Commun **264**(2): 580-583.
- Sattar Khan, M. A., S. Nakamura, et al. (2000). "Bactericidal action of egg yolk phosvitin against *Escherichia coli* under thermal stress." J Agric Food Chem **48**(5): 1503-1506.
- Seehuus, S. C., K. Norberg, et al. (2006). "Reproductive protein protects functionally sterile honey bee workers from oxidative stress." Proc Natl Acad Sci U S A **103**(4): 962-967.
- Wang, S., Y. Wang, et al. (2011). "Phosvitin plays a critical role in the immunity of zebrafish embryos via acting as a pattern recognition receptor and an antimicrobial effector." J Biol Chem **286**(25): 22653-22664.
- Zhang, S., S. Wang, et al. (2011). "Vitellogenin, a multivalent sensor and an antimicrobial effector." Int J Biochem Cell Biol **43**(3): 303-305.

**File S3. Supporting tables.**

**Table S1. Expression levels of the wild type *psen2* allele in 25ng total adult brain cDNA.**

+/+ fish under normoxia	<i>psen2<sup>S4Ter</sup>/+</i> fish under normoxia	<i>psen2<sup>S4Ter</sup>/psen2<sup>S4Ter</sup></i> fish under normoxia
1241.5	696.48	2.538
1116.2	658.88	2.765
1539.4	793.29	3.445
+/+ fish under hypoxia	<i>psen2<sup>S4Ter</sup>/+</i> fish under hypoxia	<i>psen2<sup>S4Ter</sup>/psen2<sup>S4Ter</sup></i> fish under hypoxia
1739.8	893.43	2.862
1667.6	837.51	3.562
1925.9	1280.4	0.966

**Table S2. Expression levels of the *psen2<sup>S4Ter</sup>* allele in 25ng total adult brain cDNA.**

+/+ fish under normoxia	<i>psen2<sup>S4Ter</sup>/+</i> fish under normoxia	<i>psen2<sup>S4Ter</sup>/psen2<sup>S4Ter</sup></i> fish under normoxia
0.11	818.48	832.91
0.364	561.92	1144.2
0.108	655.45	1204.1
+/+ fish under hypoxia	<i>psen2<sup>S4Ter</sup>/+</i> fish under hypoxia	<i>psen2<sup>S4Ter</sup>/psen2<sup>S4Ter</sup></i> fish under hypoxia
5.432	940.09	1721.5
4.297	855.15	2048.8
4.732	1289.4	1931.8

**Table S3. Numbers of DoLA neurons in 24 hpf embryos (revealed by *in situ* transcript hybridization against *tbx16*).**

+/+	<i>psen2<sup>S4Ter</sup>/+</i>	<i>psen2<sup>S4Ter</sup>/psen2<sup>S4Ter</sup></i>
20	16	19
23	9	20



22	17	18
17	23	27
17	21	22
	18	23
	22	20
	26	17
	24	27
	23	23
	26	17
	23	18
	18	22
	14	20
	17	20
	16	24
	23	
	17	
	17	
	17	
	16	

**File S4 Gene-Level report.html**

**File S5 RNAseq\_results.xlsx**

## Chapter 3 Generation of familial Alzheimer's disease-like mutations in zebrafish *psen2* using the CRISPR/Cas9 system

### 3.1 Introduction, Significance and Commentary

In the work described in this chapter, we attempted to generate two fAD-related mutations in the zebrafish *psen2* gene using the CRISPR/Cas9 system. However, due (most likely) to the low efficiency of homology-directed repair, we failed to identify any of these mutations. Instead, an in-frame mutation, *psen2*<sup>T141\_L142delinsMISLISV</sup>, and a coding sequence-truncating mutation, *psen2*<sup>NI40fs</sup>, were generated in zebrafish. Nonsense-mediated decay was found occur for the *psen2*<sup>NI40fs</sup> mutant transcript, while the *psen2*<sup>T141\_L142delinsMISLISV</sup> mutant transcript is stable. Gross loss of melanotic pigmentation was observed in the skin of *NI40fs* homozygous adults, indicating a loss of  $\gamma$ -secretase activity, while *T141\_L142delinsMISLISV* homozygous adults retain faint melanotic pigmentation, most likely indicating that weak  $\gamma$ -secretase activity still retains. Therefore, *NI40fs* is most likely a true null mutation while, *T141\_L142delinsMISLISV* appears to be a fAD-like mutation in zebrafish.

The significances of this work includes:

1. *NI40fs* most likely represents a true null (or severely hypomorphic) allele of zebrafish *psen2*, in contrast to another frameshift mutation, *S4Ter*, described in Chapter 2, that shows grossly normal adult pigmentation.

2. This is the first time that a fAD-like mutation has been identified in zebrafish *psen2*, *T141\_L142delinsMISLISV*. This can be exploited in future analyses, such as in comparison of the transcriptomic effects of this mutation relative to the wild type allele and to those of a *psen2* null mutation (either *NI40fs* or *S4Ter*).

**3.2** The zebrafish orthologue of familial Alzheimer's disease gene *PRESENILIN 2* is required for normal adult melanotic skin pigmentation.

This chapter is included in the thesis in the form of a research paper manuscript authored by H. Jiang, M. Newman, and M. Lardelli, and which is ready for submission for peer review by a scientific journal.

## Statement of Authorship

### Statement of Authorship

Title of Paper	The zebrafish orthologue of familial Alzheimer's disease gene <i>PRESENILIN 2</i> is required for normal adult melanotic skin pigmentation.
Publication Status	<input type="checkbox"/> Published <input type="checkbox"/> Accepted for Publication <input type="checkbox"/> Submitted for Publication <input checked="" type="checkbox"/> Unpublished and Unsubmitted work written in manuscript style
Publication Details	Has been prepared for submission.

#### Principal Author

Name of Principal Author (Candidate)	Haowei Jiang		
Contribution to the Paper	Research plan, most of the experiments, data analysis, manuscript drafting.		
Overall percentage (%)	80%		
Certification:	This paper reports on original research I conducted during the period of my Higher Degree by Research candidature and is not subject to any obligations or contractual agreements with a third party that would constrain its inclusion in this thesis. I am the primary author of this paper.		
Signature		Date	1/5/18

#### Co-Author Contributions

By signing the Statement of Authorship, each author certifies that:

- i. the candidate's stated contribution to the publication is accurate (as detailed above);
- ii. permission is granted for the candidate to include the publication in the thesis; and
- iii. the sum of all co-author contributions is equal to 100% less the candidate's stated contribution.

Name of Co-Author	Morgan Newman		
Contribution to the Paper	Supervision and help with the experiments.		
Signature		Date	1/5/2018

Name of Co-Author	Michael Lardelli		
Contribution to the Paper	Supervision, help with data analysis, manuscript drafting.		
Signature		Date	1/5/2018

**Title: The zebrafish orthologue of familial Alzheimer's disease gene *PRESENILIN 2* is required for normal adult melanotic skin pigmentation.**

**Authors:** Haowei Jiang<sup>1,\*</sup>, Morgan Newman<sup>1</sup>, Michael Lardelli<sup>1</sup>

**Affiliations:** <sup>1</sup>University of Adelaide, School of Biological Sciences, Alzheimer's Disease Genetics Laboratory, North Terrace, Adelaide, SA 5005, AUSTRALIA

**\*Corresponding Author:** Haowei Jiang, University of Adelaide, School of Biological Sciences, Alzheimer's Disease Genetics Laboratory, North Terrace, Adelaide, SA 5005, AUSTRALIA. Email: [haowei.jiang@adelaide.edu.au](mailto:haowei.jiang@adelaide.edu.au)

**Key words:** CRISPR/Cas9, familial Alzheimer's disease, *PRESENILIN 2*, pigmentation, zebrafish

**Abbreviations:** AD, Alzheimer's Disease; CRISPR, clustered regularly interspaced short palindromic repeats; DSB, double-strand break; HDR, homology-directed repair ; NHEJ, nonhomologous end joining; NMD, nonsense-mediated decay; PSEN, *PRESENILIN*; PTC, premature translation-termination codon; TMD, transmembrane domain;

**Financial Disclosure Statement:** This research was supported by grants from the National Health and Medical Research Council of Australia, GNT1061006 and GNT1126422, and by funds from the School of Biological Sciences of the University of Adelaide. HJ is supported by an Adelaide Scholarship International from the University of Adelaide.

**Conflict of Interest Statement:** The authors declare no conflict of interest.

## Abstract

Alzheimer's disease is the most common form of age-related dementia. At least 15 mutations in the human gene *PRESENILIN 2* (*PSEN2*) have been found to cause familial Alzheimer's disease (fAD). Zebrafish possess an orthologous gene, *psen2*, and present opportunities for investigation of *PRESENILIN* function related to Alzheimer's disease. The most prevalent and best characterized fAD mutation in *PSEN2* is *N141I*. The equivalent codon in zebrafish *psen2* is N140. We used genome editing technology in zebrafish to target generation of mutations to the N140 codon. We isolated two mutations: *N140fs*, causing truncation of the coding sequence, and *T141\_L142delinsMISLISV*, that deletes the two codons immediately downstream of N140 and replaces them with seven codons coding for amino acid residues MISLISV. Thus, like almost every fAD mutation in the *PRESENILIN* genes, this latter mutation does not truncate the gene's open reading frame. Both mutations are homozygous viable although *N140fs* transcripts are subject to nonsense-mediated decay and lack any possibility of coding for an active  $\gamma$ -secretase enzyme. *N140fs* homozygous larvae initially show grossly normal melanotic skin pigmentation but subsequently lose this by age while retaining pigmentation in the retinal pigmented epithelium. *T141\_L142delinsMISLISV* homozygotes retain faint skin melanotic pigmentation as adults, most likely indicating that the protein encoded by this allele retains weak  $\gamma$ -secretase activity. Null mutations in the human *PRESENILIN* genes do not cause Alzheimer's disease so these two mutations may be useful for future investigation of

the differential effects of null and fAD-like *PRESENILIN* mutations on brain aging.

## **Introduction**

Alzheimer's disease (AD) is a progressive neurodegenerative disorder, and is the most common form of age-related dementia, accounting for 50-75% of dementia cases worldwide (alz.co.uk 2014). Most AD occurs after the age of 65 years (late onset) and is sporadic. Early onset AD is far less common and approximately 13% of early onset cases are familial AD (fAD) (Campion, Dumanchin et al.). Autosomal dominant inheritance of mutations in the *AMYLOID BETA A4 PRECURSOR PROTEIN* gene (*APP*) (Guerreiro and Hardy 2014), *PRESENILIN 1* and *2* genes (*PSENI*, *PSEN2*) (Jayadev, Leverenz et al. 2010), and *SORTILIN-RELATED RECEPTOR* gene (*SORL1*) (Scherzer, Offe et al. 2004; Pottier, Hannequin et al. 2012) are considered to be the major cause of fAD. Of the two *PRESENILIN* genes, *PSEN2* is a less common locus for fAD mutations than *PSENI*. Only around 15 fAD mutations have been reported in *PSEN2* to date, compared to over two hundred mutations reported in *PSENI* (Jayadev, Leverenz et al. 2010). All but one of the many different fAD mutations in the *PSEN* genes do not cause truncation of coding sequences, a phenomenon we have previously described as the "fAD mutation reading frame preservation rule" (Jayne, Newman et al. 2016).

*PSEN* proteins become endoproteolytically cleaved during activation of  $\gamma$ -secretase



activity to form N- and C-terminal fragments (NTF and CTF respectively) (Jumpertz, Rennhack et al. 2012). The NTFs and CTFs of PSEN2 predominantly localise to the endoplasmic reticulum (ER) (Area-Gomez, de Groof et al. 2009), and the first two transmembrane domains (TMDs) of PSEN2 are thought to be necessary for ER localisation (Tomita, Tokuhiko et al. 1998). The first fAD mutation reported in *PSEN2* was *N141I*, caused by an A-to-T transition at the second position of codon 141 (Levy-Lahad, Wasco et al. 1995). The *N141I* mutation alters the N-terminal flank of the second TMD (TMD2) of PSEN2 by substituting a hydrophobic isoleucine residue for the hydrophilic asparagine residue immediately downstream of the first residue of TMD2. This position is thought to be important for accurate positioning of the transmembrane  $\alpha$ -helix structure (Hardy 1997). A PolyPhen-2 (Adzhubei, Schmidt et al.) analysis of the *N141I* mutation indicates probable damage to protein structure with a score of 0.934 (sensitivity: 0.80; specificity: 0.94). The mean age of Alzheimer's disease onset for carriers of *N141I* is 53.7 years old, but with a very wide range of 39 to 75 years (Jayadev, Leverenz et al. 2010). Thus, *N141I* has an age of onset overlapping those of *PSEN1* fAD families (mean age of onset of 45.5 years) and sporadic AD (mean age of onset of 71.5) (Jayadev, Leverenz et al. 2010). The *N141I* mutation is thought to increase the ratio of A $\beta$ 42 to A $\beta$ 40 via abnormal  $\gamma$ -secretase activity (Tomita, Maruyama et al. 1997). A more recent transgenic mouse model of AD suggested that both A $\beta$ 42 and A $\beta$ 40 production are enhanced by *N141I*, and this can significantly accelerate A $\beta$ -dependent dysfunction in spatial learning and memory (Toda, Noda et al. 2011).

Mammalian PRESENILINs have also been found necessary for tyrosinase trafficking and melanin formation by a  $\gamma$ -secretase-dependent mechanism (Wang, Tang et al. 2006). TYROSINASE is a key enzyme in melanin synthesis (Tief, Hahne et al. 1996). The two TYROSINASE-related proteins, TYROSINASE-related protein 1 (Tyrp1) and DOPACHROME TAUTOMERASE (DCT) (also known as TYROSINASE-related protein 2 (Tyrp2)) (del Marmol and Beermann 1996), are implicated in the activity of the intramembrane protease,  $\gamma$ -secretase (Vetrivel, Zhang et al. 2006; Wang, Tang et al. 2006). A partial loss-of-function in melanotic pigment formation has been observed in a mouse model of the *PSEN1* fAD mutation *M146V* (Wang, Tang et al. 2006).

In mammals, the protein SILVER, MOUSE, HOMOLOG OF (SILV, also known as PREMELANOSOMAL PROTEIN, PMEL) (Watt, van Niel et al. 2013) is another type 1 membrane protein that can be cleaved by proteases including  $\gamma$ -secretase (Kummer, Maruyama et al. 2009) to form a natural functional amyloid that facilitates melanin formation (Bissig, Rochin et al. 2016). SILV is expressed in pigment cells of the eye and skin, which synthesise melanin pigments within melanosomes (Raposo and Marks 2007). After a juxtamembrane cleavage, the C-terminal fragment of SILV is then processed by the  $\gamma$ -secretase complex to release an intracellular domain fragment (Kummer, Maruyama et al. 2009) into endosomal precursors to form amyloid fibrils. These ultimately become melanosomes (Fowler, Koulov et al. 2005; Rochin, Hurbain et al. 2013).

Zebrafish are a versatile system in which to investigate, at the molecular level, the effects on the brain and other tissues of fAD mutations (Hin, Newman et al. 2018). The ability to generate large families of siblings and then raise these in a near identical environment (the same tank or the same recirculated-water system) can reduce genetic and environmental variability to allow more sensitive detection of mutation-dependent changes. The organisation of the genome and the genetic pathways controlling signal transduction and development of zebrafish and humans are highly conserved (Postlethwait, Woods et al. 2000). Despite ~420 million years of divergent evolution of the human and zebrafish lineages (Ravi and Venkatesh 2008), most human genes have clearly identifiable orthologues in zebrafish. Thus, the zebrafish genes *psen1* (Leimer, Lun et al. 1999) and *psen2* (Groth, Nornes et al. 2002) are orthologues of human *PSEN1* and *PSEN2*, respectively. The Presenilin protein sequences of zebrafish show considerable identity with those of humans. The zebrafish Psen1 protein shows 73.9% amino acid residue (aa) identity with human PSEN1 (Leimer, Lun et al. 1999), while zebrafish Psen2 shows 74% identity with human PSEN2 (Groth, Nornes et al. 2002).

In this paper we describe an attempt to generate a zebrafish model of the *N141I* fAD mutation of human *PSEN2* by introducing an equivalent mutation into the zebrafish *psen2* gene. While homology-directed repair (HDR) after CRISPR Cas9 cleavage at the relevant site in zebrafish *psen2* was not successful, we did find products of non-homologous end joining (NHEJ) that will prove useful in future analyses. We identified both a frameshift mutation and a reading frame-preserving indel mutation close to the

N141-equivalent codon of zebrafish *psen2*. Surprisingly, we discovered that the  $\gamma$ -secretase activity of Psen2 (unlike that of Psen1) appears essential for melanotic pigment formation in the skin of zebrafish adults but not in their retinal pigmented epithelium.

## Materials and Methods

### Animal ethics

All experiments using zebrafish were conducted under the auspices of the Animal Ethics Committee of the University of Adelaide. Permits S-2014-108 and S-2017-073.

### CRISPR guide RNA (sgRNA) design and synthesis

The target sequence of the sgRNA used to generate double-stranded breaks near the N140 codon in zebrafish *psen2* is 5'-GAATTCGGTGCTCAACACTC *TGG*-3'. The template for sgRNA transcription was synthesised by PCR (Bassett and Liu 2014). The forward primer for this template synthesis PCR contains a T7 polymerase binding site (the underlined region), the target sequence (bold) and a region complementary to a common reverse primer (italicised): 5'-  
GAAATTAATACGACTCACTATAGGG**GAATTCGGTGCTCAACACTC***GTTTTAG*  
*AGCTAGAAATAGC*-3'. The sequence of the reverse primer is 5'-

AAAAGCACCGACTCGGTGCCACTTTTTCAAGTTGATAACGGACTAGCCTTA  
TTTAACTTGCTATTTCTAGCTCTAAAAC-3'. This synthesis PCR used Phusion®  
High-Fidelity DNA Polymerase (NEB, Ipswich, Massachusetts, USA, M0530S) and  
cycle conditions of 98°C for 30 s and then 35 cycles of [98°C, 10 s; 60°C, 30 s; 72°C,  
15 s] then 72°C, 10 min. The template was then gel-purified using the Wizard® SV Gel  
and PCR Clean-Up System (Promega, Madison, Wisconsin, USA, A9281). The target  
sgRNA was synthesized from this template using the HiScribe™ T7 Quick High Yield  
RNA Synthesis Kit (NEB, Ipswich, Massachusetts, USA, E2050S).

### **Design of single-stranded oligonucleotide templates for homology-directed repair (HDR)**

To attempt to introduce the *N140I* mutation into zebrafish *psen2* (equivalent to human  
*PSEN2 N141I*), a single stranded oligonucleotide template (“N140I oligo”) containing  
the N>I mutation (A>T, bold italics and underlined) followed by two silent  
(synonymous codon) mutations (T>C and G>C, italicised and underlined) was designed:

5’-

ACTCAGTGGGCCAGCGTCTGCTGAATTCGGTGCTC**ATC**ACCCTCGCATGAT  
CAGTGTGATTGTCTTCATGACC-3’.

We also attempted (unsuccessfully) to introduce the *V147I* mutation into zebrafish  
*psen2*, (equivalent to *V148I* in human *PSEN2*) using a single-stranded oligonucleotide

template (“V147I oligo”), containing the V>I mutation (G>A and G>C, bold italics and underlined) followed by two silent (synonymous codon) mutations (T>A and C>G, italicised and underlined): 5’-CTGAATTCGGTGCTCAACACTCTGGTCATGATCAGT**ATCATAGT**GTTTCATGACCATCATCCTGGTGCTGCTCTAC-3’. The attempted mutation of the *VI47* site in *psen2* is only describe and discussed in Supplemental Information.

The single-stranded oligonucleotide templates were co-injected with their corresponding CRISPR/Cas9 systems, so that any induced double-stranded DNA breaks (DSBs) might be repaired through the HDR pathway (Bassett and Liu 2014) to insert desired mutations into the zebrafish genome.

### **Injection of zebrafish embryos**

Tübingen (TU) strain wildtype embryos were collected from mass spawning. The target sgRNA (70 ng/μL final concentration) was mixed with “N140I oligo” (30 ng/μL for final concentration) and Cas9 nuclease (1μg/μL for final concentration) (Invitrogen, Carlsbad, California, USA, B25640), and then incubated at 37°C for 15 min to maximize formation of active CRISPR Cas9 complexes. 5-10 nL of the mixture was then injected into zebrafish embryos at the one-cell stage. The injected embryos were subsequently raised for mutation screening.

## Mutation detection in CRISPR Cas9-injected G0 fish

From each batch of injected embryos, 10 embryos were selected at random at ~24 hpf and pooled for genomic DNA extraction. The genomic DNA of these embryos was extracted using sodium hydroxide (Meeker, Hutchinson et al. 2007). The 10 embryos were placed in 100  $\mu$ L of 50 mM NaOH and then heated to 95°C for 15 min. They were then cooled to 4°C followed by addition of 1/10th volume of 1 M Tris-HCl, pH 8.0 to neutralize the basic solution (Meeker, Hutchinson et al. 2007).

Mutation-specific primers were designed to detect mutation-carrying fish by PCR. For the “N140I oligo”-injected embryos, a mutation-specific forward primer was designed: 5'-TCGGTGCTCATCACCTC-3'. A wild type-specific forward primer (5'-TCGGTGCTCAACACTCTG-3') and a common reverse primer (5'-ACCAAGGACCACTGATTCAGC-3') were also designed. The PCR conditions for both these reactions are: 95°C, 2 min and then 31 cycles of [95°C, 30 s; 58°C, 30 s; 72°C 30 s], then 72°C, 5 min. The lengths of the expected PCR products of these reactions are all ~300 nucleotides.

For the “V147I oligo”-injected embryos, a mutation-specific forward primer was designed: 5'-TCTGGTCATGATCAGTATCATAGTG-3'. A wild type-specific forward primer (5'-TCTGGTCATGATCAGTGTGATTGTC-3') and a common reverse primer (5'-TCACCAAGGACCACTGATTCAGC-3') were also designed. The PCR

conditions for all these three reactions are: 95°C, 2 min, and then 31 cycles of [95°C, 30 s; 58°C, 30 s; 72°C, 30 s], then 72°C 5 min. The lengths of the PCR products of these reactions are ~280 nucleotides.

The F1 progeny of the mosaic, mutation-carrying G0 fish were also screened with these mutation-specific PCR reactions.

### **Mutation detection in F1 fish using the T7 endonuclease I assay**

Since the DSBs induced by the CRISPR/Cas9 system may also be repaired through the NHEJ pathway (Bibikova, Golic et al. 2002; Bassett and Liu 2014), random mutations may also be generated at the DSB sites. Thus, the F1 progeny of the mosaic, mutation-carrying G0 fish may be heterozygous for such random mutations.

To screen for these mutations, the genomic DNA of tail biopsies from F1 fish was extracted using sodium hydroxide as above, followed by analysis using the T7 endonuclease I assay (since T7 endonuclease I is able to recognize and cleave at the sites of mismatches in DNA heteroduplexes (Babon, McKenzie et al. 2003)).

A pair of amplification primers binding in the regions flanking the N140 target site was designed: 5'-AGCATCACCTTGATTCAAGG-3' and 5'-GGTTCCTGATGACACACTGA-3'. The PCR conditions for this amplification



reaction are 95°C, 2 min and then 31 cycles of [95°C, 30 s; 58°C, 30 s; 72°C, 30 s], then 72°C, 5 min and the amplified fragment is predicted to be 473 nucleotides in length. The PCR products were purified using the Wizard® SV Gel and PCR Clean-Up System (Promega, Wisconsin, USA, A9281) and then denatured and annealed (denaturation at 95°C for 5 min and then annealing by slow cooling of the samples at -2°C/sec from 95°C to 85°C and then -0.1°C/sec from 85°C to 25°C) before addition of the T7 endonuclease I (NEB, Ipswich, Massachusetts, USA, M0302S). If reannealed fragments contained mismatches due to mutations, they would be cleaved by T7 endonuclease I into two fragments; ~109 nucleotides (upstream) and ~364 nucleotides (downstream). Those amplified and reannealed fragments showing positive signals (cleavage) in T7 endonuclease I assays were then sent to the Australian Genome Research Facility (AGRF, North Melbourne, VIC, Australia) for Sanger sequencing to identify the mutations.

### **Mutation detection in F2 fish using PCR**

Mutation-specific PCR primers were designed to detect the two mutations (*NI40fs* and *T141\_L142delinsMISLISV*) identified in F1 fish. For *NI40fs*, a mutation-specific forward primer (5'-TGCTGAATTCGGTGCTCTG-3') was designed. For *T141\_L142delinsMISLISV*, another mutation-specific forward primer (5'-TGAATTCGGTGCTCAACATG-3') was designed. A wild type-specific forward primer (5'-TGAATTCGGTGCTCAACACTC-3') was designed as a control. A

common reverse primer (5'-TCACCAAGGACCACTGATTCAGC-3') was used with these three different forward primers. The temperature cycling conditions for these PCRs are identical for the wild type and *N140fs* alleles: 95°C, 2 min, and then 31 cycles of [95°C, 30 s; 60°C, 30 s; 72°C, 30 s], then 72°C, 5 min. For detection of the *T141\_L142delinsMISLISV* allele, the annealing temperature was altered to 61.5°C. The PCR products of these reactions are all predicted to be ~320 nucleotides in length.

### **Breeding of mutant fish**

Since the mutation-carrying G0 fish were mosaic for mutations, these were outbred with wildtype TU fish so that their progeny (F1 fish) would be completely heterozygous for any mutations.

The F1 fish carrying the *psen2*<sup>*T141\_L142delinsMISLISV*</sup> or *psen2*<sup>*N140fs*</sup> alleles were outbred with wild type TU fish to generate additional individuals heterozygous for the mutations. (The families of progeny of such matings would consist of 50% heterozygous mutants and 50% wild type fish). When these F2 progeny were sexually mature, pairs of heterozygous individuals were in-crossed to generate F3 families containing homozygous mutant, heterozygous mutant and wild type siblings for further analysis.

### **Imaging of skin pigmentation in zebrafish**

The pigmentation patterns of mutant zebrafish were imaged using a Leica Microsystems, Type DFC450 C microscope, and the software Leica Application Suite, Version 4.9.0 (Leica Microsystems, Wetzlar, Germany).

### **Total RNA extraction from 6-month-old zebrafish brains**

When F2 fish families from outcrossed heterozygous mutant F1 fish were 6 months of age, eight female fish of each genotype (i.e. eight wild type and eight heterozygous mutant individuals) were selected for brain removal and total RNA extraction. From these fish, four of each genotype were exposed to hypoxia (the dissolved oxygen content of the water was ~1.00 mg/L) for ~2.5 h, while the other four of each genotype were exposed to normoxia (the dissolved oxygen content of the water was ~6.60 mg/L). Total RNA was extracted from these brains using the *mirVana*<sup>™</sup> miRNA Isolation Kit (Ambion, Inc, Foster City, California, USA, AM1560). cDNA was synthesised from the RNA using the SuperScript<sup>™</sup> III First-Strand Synthesis System (Invitrogen, Carlsbad, California, USA, 18080051) and Random Primers (Promega, Madison, Wisconsin, USA, C1181).

### **Allele-specific expression analysis by digital quantitative PCR (dqPCR)**

PCR primer pairs detecting specific alleles were designed for dqPCR: a specific

forward primer for mutation *psen2*<sup>T141\_L142delinsMISLISV</sup> (5'-TGAATTCGGTGCTCAACATG-3'), a specific forward primer for mutation *psen2*<sup>N140fs</sup> (5'-TGCTGAATTCGGTGCTCTG-3'), and a specific forward primer for the wild type allele (5'-TGAATTCGGTGCTCAACACTC-3'). A common reverse primer (5'-AAGAGCAGCATCAGCGAGG-3') was used with all these three forward primers. Allele-specific dqPCR was performed using the QuantStudio™ 3D Digital PCR System (Life Sciences, Waltham, MA, USA) with QuantStudio™ 3D Digital PCR 20K Chip Kit v2 and Master Mix (Life Sciences, Waltham, MA, USA, A26317) and SYBR™ Green I Nucleic Acid Gel Stain (Life Sciences, Waltham, MA, USA, S7563). The dqPCR conditions for allele-specific expression detection are 96°C, 10 min, then 49 cycles of [62°C, 2 min; 98°C, 30 s], then 62°C 2 min. The expected length of the PCR products is ~130 bp. 25ng of cDNA (based on quantification of RNA concentration and the assumption of complete reverse transcription into cDNA) of each sample was loaded into each chip. The chips were analysed using QuantStudio™ 3D AnalysisSuite Cloud Software (Life Sciences, Waltham, MA, USA).

## Results

### fAD-like and coding sequence-truncating mutations in *psen2*

Our initial aim was to create mutations in zebrafish *psen2* equivalent to the fAD mutations of human *PSEN2*, *N141I* and *V148I* (*N140I* and *V147I* in zebrafish

respectively). However, while CRISPR Cas9-targeting of these sites appeared feasible, no incorporation of desired mutations via homology-directed repair was found. Nevertheless, two mutations at the N140 site were ultimately identified. One of these is an indel mutation removing two codons (T141 and L142) and replacing these with seven novel codons (MISLISV). Consequently, this allele is designated *psen2*<sup>T141\_L142delinsMISLISV</sup> and may be considered EOfAD-like in that it does not truncate the coding sequence (Figure 1). The second mutation is a deletion of 7 nucleotides causing a frameshift that does truncate the coding sequence (CDS), *psen2*<sup>N140fs</sup>, due to a premature termination codon (PTC) at the 142<sup>nd</sup> codon position.

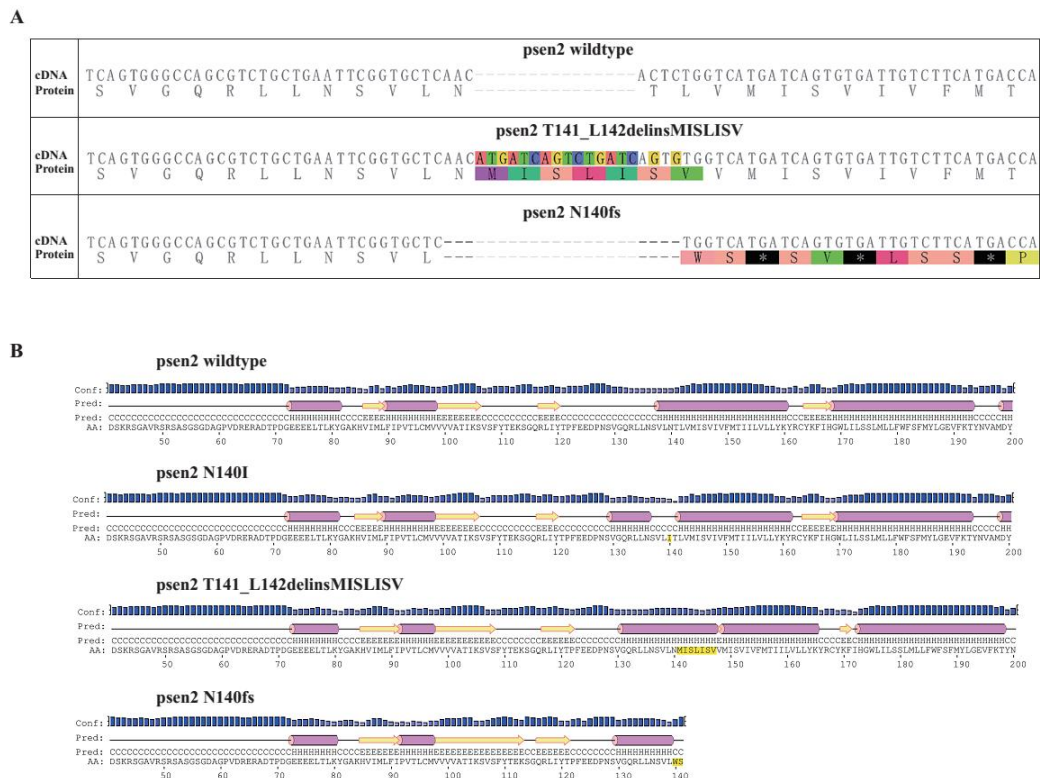


**Figure 1. Predicted protein primary and secondary structures.**

(A) The protein coding sequence of zebrafish *Psen2* is altered by the mutations.

(B) The predicted protein structures of zebrafish *Psen2* are also changed by the two identified mutations (and are shown relative to the wild type structure and a structure incorporating a hypothetical *NI40I* mutation. Purple bar: helix; yellow arrow: strand; black line: coil; Conf: confidence of prediction; Pred: predicted secondary structure; AA: target sequence.

Inbreeding of *T141\_L142MISLISV* and *NI40fs* mutant fish showed both mutations to be homozygous viable although both showed severe defects in skin pigmentation in post-larval stages (described later).

### **Changes of protein structure caused by the mutations**

PRESENILINs have a complex structure with multiple TMDs. Therefore, mutations have the potential to greatly disturb protein structure by interfering with normal membrane insertion. To understand the possible consequences of, in particular, the *T141\_L142delinsMISLISV* mutation, we compared theoretical hydropathicity plots (Gasteiger, Hoogland et al. 2005) for our isolated mutations with those for wild type *psen2* and a mutation equivalent to human *NI41I* (Figure 2). The *T141\_L142delinsMISLISV* mutation contributes only non-polar (M, I, L, V) or, at least, uncharged, polar (S) amino acid residues (aa) to the protein structure, presumably expanding the hydrophobic stretch of aas that form TMD2. Presumably, this mutation allows overall correct membrane insertion but disrupts the conformation of the protein

sufficiently to almost entirely, but not completely, destroy its  $\gamma$ -secretase activity (see later).

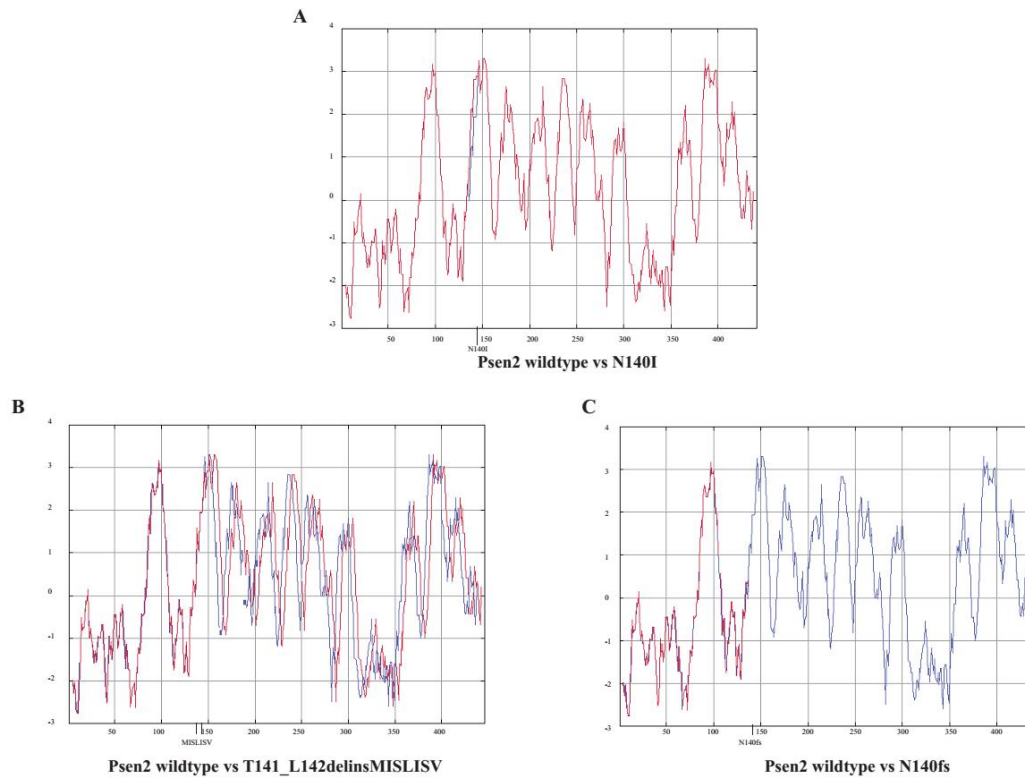


**Figure 2. Predicted protein hydropathicity plots.**

The blue line refers to wild type Psen2. The red lines refer to the mutants.

The *N140fs* mutation cannot possibly express a catalytically active  $\gamma$ -secretase enzyme since it truncates the CDS at the start of TMD2. Thus, it lacks both the aspartate residues required for the  $\gamma$ -secretase catalytic domain (Wolfe, Xia et al. 1999; Fraering 2007).

***N140fs* transcripts are subject to nonsense-mediated decay**

Mutations creating premature termination codons (PTCs) in coding sequences upstream of exon-exon junctions in spliced transcripts can result in destabilisation of the transcripts through nonsense-mediated decay (NMD, reviewed by (Chang, Imam et al. 2007)). Therefore, we expected that transcripts from the *T141\_L142delinsMISLISV* allele might be similarly stable to wild type transcripts while *NI40fs* allele transcripts would show decreased stability and abundance. To test this we performed dqPCR that allows direct comparison of transcript abundances. We extracted total RNA from the brains of 6-month-old adult zebrafish, reverse transcribed this to cDNA, and then performed dqPCR with primers specifically detecting the wild type or mutant alleles. The results confirmed similar levels of *T141\_L142delinsMISLISV* and wild type transcripts in heterozygous mutant brains but levels of *NI40fs* transcripts are only approximately 25% of those for wild type transcripts in heterozygous mutant brains (Figure 4). The first round of translation of a transcript is critical for NMD and so inhibition of translation (e.g. with cycloheximide) can increase the stability of transcripts with PTCs (Carter, Doskow et al. 1995; Hurt, Robertson et al. 2013). Cycloheximide treatment of a group of embryos heterozygous for *NI40fs* caused an approximately 5-fold increase in *NI40fs* allele-derived transcripts but only an approximately 2-fold increase in wild type transcripts (File S4) supporting that NMD destabilises *NI40fs* transcripts.

### **Stability of mutant allele transcripts under normoxia compared to hypoxia**



Numerous lines of evidence support that hypoxia is an important factor in the development of AD (reviewed in (Salminen, Kauppinen et al. 2017)). This includes that expression of the fAD genes, *PSEN1*, *PSEN2* and *APP* are upregulated under hypoxia (Sato, Hori et al. 1999; Nishikawa, Manabe et al. 2004; Zhang, Zhou et al. 2007; De Gasperi, Sosa et al. 2010), phenomena that are conserved in zebrafish (Moussavi Nik, Wilson et al. 2012) despite ~420 million years of divergent evolution from mammals (Detrich III, Zon et al. 2009). Also, hypoxia has previously been observed to inhibit NMD (Gardner 2008). Therefore, to observe how hypoxia might affect the levels of transcripts from our mutant alleles we performed dqPCR using total RNA extracted from the brains of 6-month-old zebrafish exposed to normoxia or hypoxia (Figures 3 and 4). This revealed little effect of hypoxia on the levels of transcripts from wild type or *T141\_L142delinsMISLISV* alleles (Figure 3) in heterozygous fish brains (that is most likely due to the young age of the fish, see Discussion) and a small, but apparently statistically significant increase in the levels of *N140fs* allele transcripts (Figure 4). However, we cannot distinguish whether this increase is due to induction of transcription, or inhibition of NMD, or both (or other factors that could increase transcript levels).

*psen2* wild type allele and *psen2*<sup>T141\_L142delinsMISLISV</sup> allele-specific expression in 25 ng total brain cDNA

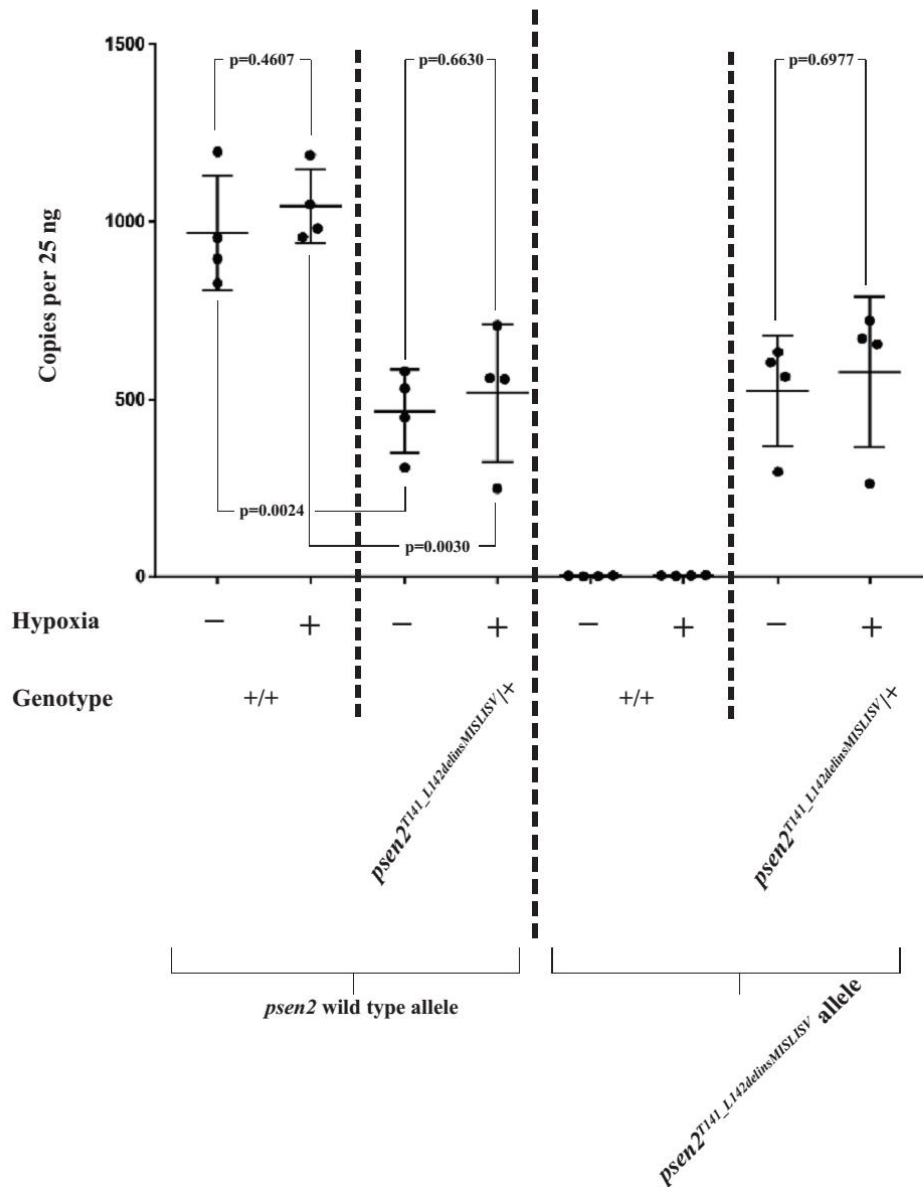


**Figure 3.** *psen2* wild type and *psen2*<sup>T141\_L142delinsMISLISV</sup> allele-specific expression (as copies per the 25 ng of total brain cDNA in each dqPCR).

The expression levels of wild type *psen2* alleles in *psen2*<sup>T141\_L142delinsMISLISV</sup>/+ fish (~460 copies) were significantly ( $p=0.0024$ ) lower than in their wild type siblings (~950 copies) under normoxia. Under hypoxia, the expression levels of wild type *psen2* alleles in both *psen2*<sup>T141\_L142delinsMISLISV</sup>/+ fish (~1,000 copies) and their wild type siblings (~510 copies) were up-regulated, but neither of the genotypes showed statistically

significant differences compared to their normoxic controls. The expression levels of the *psen2*<sup>T141\_L142delinsMISLISV</sup> alleles in *psen2*<sup>T141\_L142delinsMISLISV/+</sup> fish (~520 copies under normoxia) were increased by acute hypoxia (~580 copies), but without statistical significance. Means with SDs are indicated.

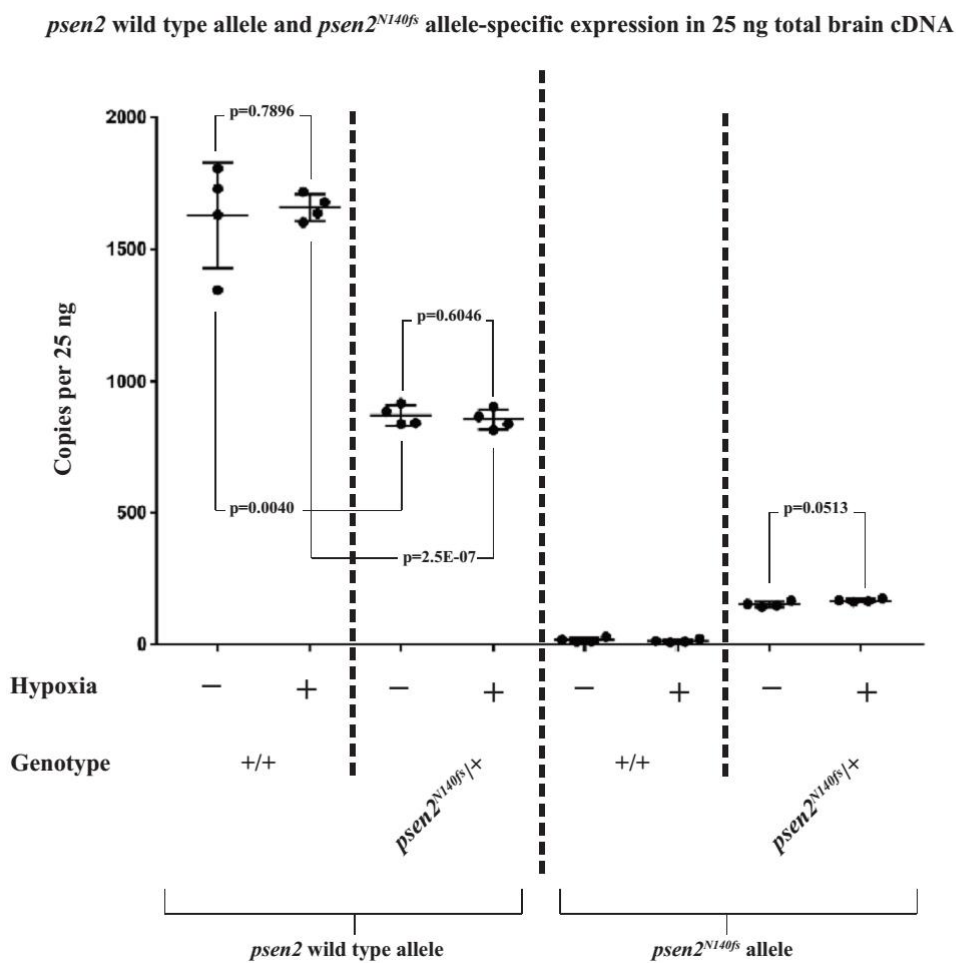


**Figure 4.** *psen2* wild type allele and *psen2*<sup>N140fs</sup> allele-specific expression (as copies per the 25 ng of total brain cDNA in each dqPCR).

The expression levels of wild type *psen2* alleles in *psen2*<sup>N140fs/+</sup> fish (~860 copies) were significantly (p=0.0024) lower than in their wild type siblings (~1,600 copies) under

normoxia. Under hypoxia, the expression levels of wild type *psen2* alleles in both *psen2*<sup>N140fs/+</sup> fish (~860 copies) and their wild type siblings (~1,700 copies) were slightly up-regulated, but not with statistical significance compared to these genotypes under normoxia. The expression levels of *psen2*<sup>N140fs</sup> alleles in *psen2*<sup>N140fs/+</sup> fish (~150 copies under normoxia) were increased (p=0.0513) by acute hypoxia (~160 copies). Means with SDs are indicated.

### **Pigment phenotypes of mutation-carrying fish**

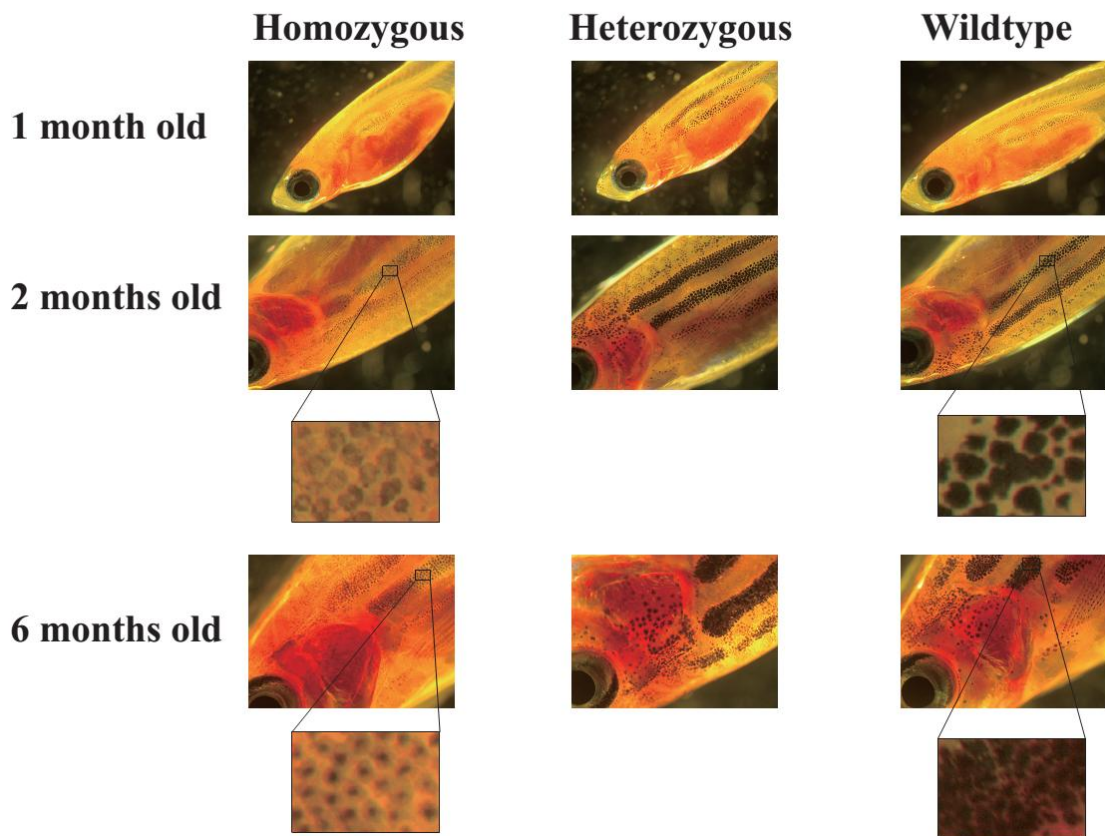
During the process of isolating mutations in *psen2*, we observed that some of the G0 CRISPR Cas9-injected, mosaic, mutation-carrying fish showed unique patches of pigmentation loss in their skin (Figure 5A). (Four of 12 G0 fish injected with the CRISPR Cas9 complex targeting the N140 codon showed this phenotype). None of the F1 progeny of these fish (heterozygous for either of the mutations in *psen2*) showed apparent pigmentation loss. However, when inbreeding F2 heterozygous mutant fish we found that some of the F3 progeny for either the *T141\_L142delinsMISLISV* mutation or the *N140fs* mutation showed differences in surface melanotic pigmentation pattern obvious to the unaided eye by one month of age. Genotyping of these fish using allele-specific PCR on tail biopsies showed them to be homozygous mutants. Subsequently, we observed the development of surface pigmentation with age for these fish families and saw that fish heterozygous for either the *T141\_L142delinsMISLISV* or *N140fs* mutation were indistinguishable from wild type fish in surface pigmentation but

that homozygous *T141\_L142delinsMISLISV* fish had much fainter melanotic pigmentation, with many faintly melanotic cells arranged in apparently normal stripes (Figure 5B). In contrast, homozygous *NI40fs* fish appeared to lack surface melanotic stripes (although a very faint impression of striping was still visible, Figure 5C). Since  $\gamma$ -secretase activity is required for melanin formation (Wang, Tang et al. 2006; Kummer, Maruyama et al. 2009), and *psen2* appears relatively highly expressed in melanocytes (Groth, Nornes et al. 2002) it is likely that *NI40fs* homozygous fish lack melanin due to absence of  $\gamma$ -secretase activity from *psen2* while *T141\_L142delinsMISLISV* homozygous fish retain low levels of *psen2*-derived  $\gamma$ -secretase activity.

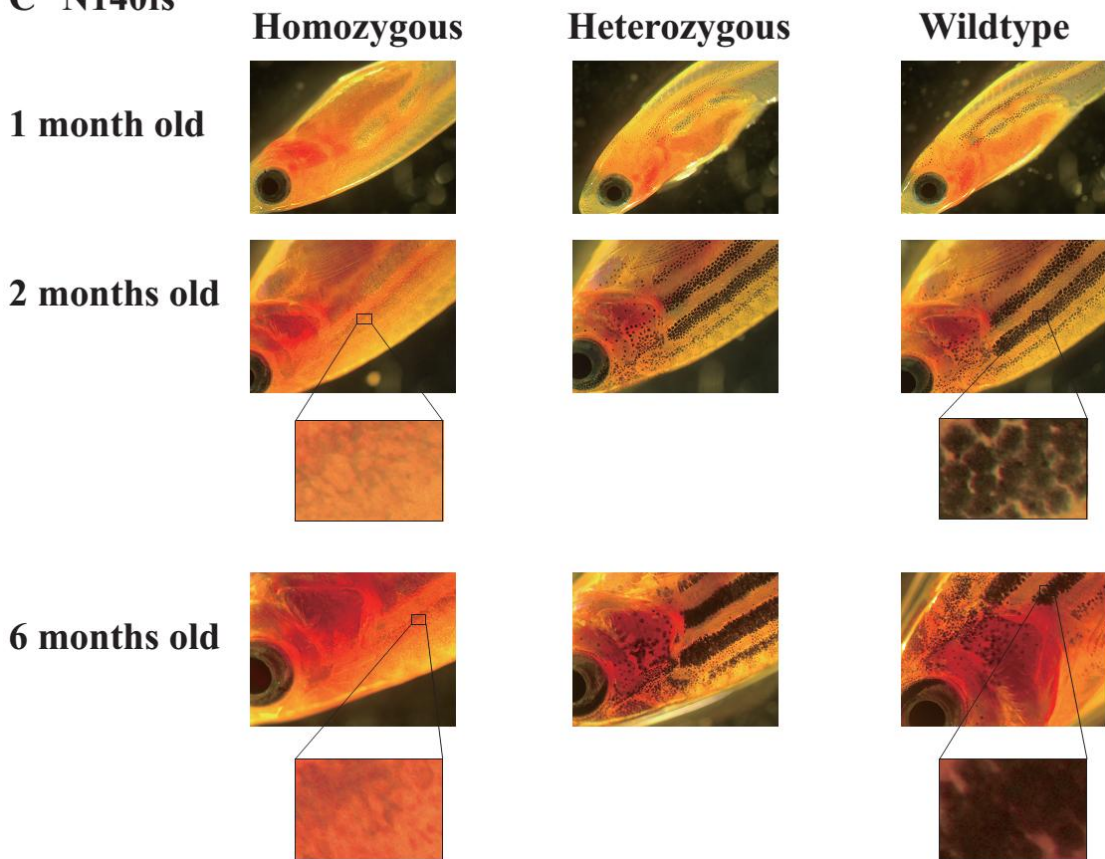
## A G0 fish



**B T141\_L142delinsMISLISV**



**C N140fs**



**D**

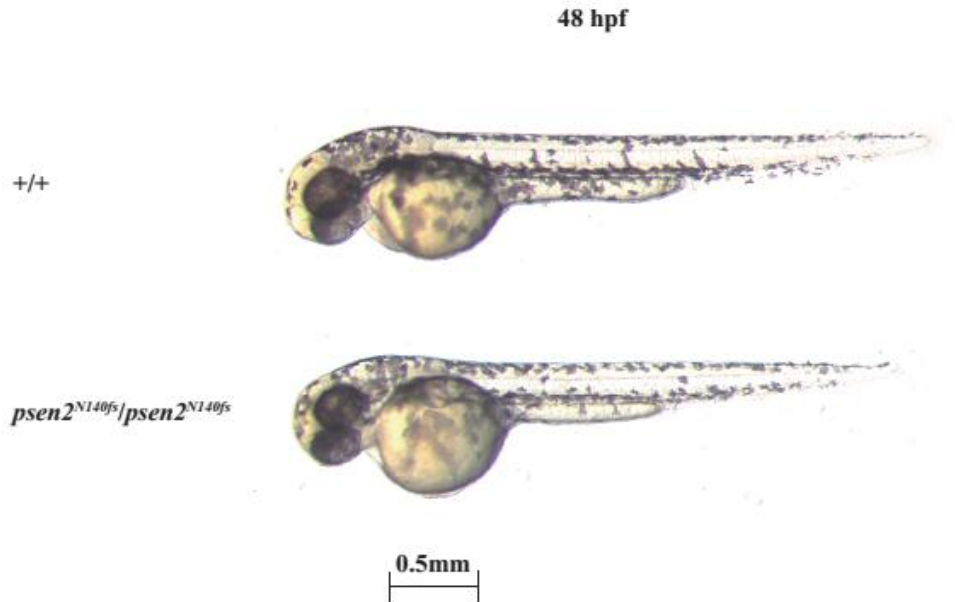


**Figure 5. Surface melanotic pigmentation phenotypes.**

(A) Patches of pigmentation loss in the skin of mosaic mutant G0 fish.

(B) *psen2<sup>T141\_L142delinsMISLISV</sup>* mutants and +/+ sibling fish.

(C) *psen2<sup>N140fs</sup>* mutants and +/+ sibling fish.

(D) No gross melanotic pigmentation phenotype was observed in *psen2<sup>N140fs</sup>* homozygous embryos at 50 hpf.

The intracellular distribution of pigment also appeared to change with age in the skin melanophores of *T141\_L142delinsMISLISV* homozygous fish. At two months of age pigment appeared evenly distributed in these cells but excluded from their central, presumably nuclear, regions (Figure 5B). However, by six months of age, the pigment appeared concentrated at the centre of cells and was, presumably, perinuclear. The

density of pigment formation in heterozygous and wild type fish made it difficult to see whether a similar phenomenon was also occurring in those.

Curiously, the *NI40fs* homozygous fish lacking surface melanotic pigmentation retained strong melanotic pigmentation in their retinal pigmented epithelium. This is obvious as the dark eyes of the fish shown in Figure 5C and was confirmed by dissection of these eyes (not shown). Also, the 48 hpf larval *NI40fs* homozygous progeny of homozygous parents showed abundant surface melanocytes that cannot be due to maternal inheritance of wild type *psen2* function (Figure 5D). Thus, the dependence of zebrafish adult skin melanotic pigmentation on *psen2* function is both cell type- and age-specific.

## Discussion

Our attempts at generation of point mutations in the zebrafish *psen2* gene by HDR were unsuccessful. However, we did succeed in identifying two mutations (formed by the NHEJ pathway) that may prove useful in analysing the role of the human *PSEN2* gene in familial Alzheimer's disease; an in-frame mutation, *psen2*<sup>T141\_L142delinsMISLISV</sup>, and a frame-shift mutation, *psen2*<sup>NI40fs</sup>.

The in-frame mutation *psen2*<sup>T141\_L142delinsMISLISV</sup> is an indel mutation altering two codons and inserting an additional 5 codons. Although this mutation changes the length of the



protein coding sequence, the predicted protein hydrophobicity plot of the putative mutant protein (Figure 2) supports that the mutation does not completely destroy the transmembrane structure of Psen2. Since most of the fAD mutations in human *PSEN2* are in-frame mutations that may change hydrophobicity without destroying the overall transmembrane structure of the protein (Jayadev, Leverenz et al. 2010), the *T141\_L142delinsMISLISV* mutation would appear to be more fAD-like than null.

The frame-shift mutation *psen2*<sup>N140fs</sup> was caused by a deletion of 7 nucleotides and results in a PTC at the 142<sup>nd</sup> codon position. This mutation causes truncation of the coding sequence at the upstream end of TMD2 of zebrafish Psen2. The first two TMDs of human PSEN2 are thought to be necessary for ER localisation (Tomita, Tokuhiko et al. 1998). Since coding sequence truncation occurs at the upstream end of TMD2, if this mutant allele expressed a protein, it would most likely not be able to form TMD structures for ER localization. Neither could it possibly have  $\gamma$ -secretase activity since it lacks the aspartate residues required (Wolfe, Xia et al. 1999; Fraering 2007). Moreover, since dqPCR showed that the levels of *N140fs* transcripts are only approximately 25% of those for wild type transcripts in heterozygous mutant brains, *N140fs* expression appears limited by NMD (a fact supported by the ~5-fold increased N140fs transcript level in the presence of the translation inhibitor, cycloheximide (File S4). Our previous work has shown that zebrafish *psen2* does not express a truncated isoform equivalent to the PS2V isoform of human *PSEN2* (Moussavi Nik, Newman et al. 2011) and that a PS2V-like truncation of zebrafish Psen2 does not have PS2V-like

activity (Moussavi Nik, Newman et al. 2015). (Instead a PS2V-like function is expressed from zebrafish *psen1* (Moussavi Nik, Newman et al. 2015)). Therefore, *NI40fs* most likely represents a true null (or severely hypomorphic) allele of zebrafish *psen2*, unlike another frameshift mutation, *S4Ter*, that we recently analysed and that shows grossly normal adult pigmentation (Jiang et al., manuscript submitted).

In human cells, expression of the *APP*, *PSEN1* and *PSEN2* genes can be upregulated by hypoxia (Moussavi Nik, Wilson et al. 2012) and we previously showed that this phenomenon has been conserved during the nearly half a billion years since the divergence of the zebrafish and human evolutionary lineages (Moussavi Nik, Wilson et al. 2012). In that earlier paper we saw nearly a two-fold increase in zebrafish brain *psen2* mRNA levels under hypoxia compared to normoxia while, in this work, no significant differences were seen (except for *NI40fs* allele transcripts where hypoxia may be inhibiting NMD (Gardner 2008)). Upon checking our laboratory records we found that the fish used in the earlier publication were around 12 months old compared to the six months of age in this work. In other, yet unpublished work we have observed that differences in adult age make very significant differences to brain transcriptional responses to hypoxia with young adult fish showing the mildest responses (Newman et al. unpublished results).

In previous research we showed that blockage of *psen2* function using morpholino antisense nucleotides injected into zebrafish zygotes increases the number of DoLA

neurons at 24 hpf (Nornes, Newman et al. 2009). Despite the evidence that the *NI40fs* mutation is null, we did not see increased DoLA neuron numbers in *NI40fs* homozygous embryos at 24 hpf (See S3 Files for experiment description and data). The observation of differing developmental phenotypes from decreased gene function due to mutation or morpholino injection is a common occurrence (Kok, Shin et al. 2015). It is thought to be due to the phenomenon of “genetic compensation” whereby only decreased gene function through mutation, (and not by morpholino injection), causes compensatory upregulation of other genes with similar activities (Rossi, Kontarakis et al. 2015). It is likely that genetic compensation is causing the lack of response of DoLA neuron number to the *NI40fs* mutation. An alternative explanation would be a maternal contribution of wild type *psen2* activity from the heterozygous *NI40fs* mother of the embryos examined. Further experimentation such as blockage of *psen1* translation by morpholino injection into *psen2<sup>NI40fs</sup>* homozygous embryos or analysis of DoLA numbers in *psen2<sup>NI40fs</sup>* homozygous embryos from homozygous parents might resolve this question.

Skin pigmentation pattern is severely affected in adult fish homozygous for the mutation *T141\_L142delinsMISLISV*. These fish show surface melanotic stripes that appear approximately the same width as in wild type fish but are much fainter. Closer examination of these stripes at 6 months of age reveals cells with vestigial, and likely perinuclear, pigment. The number of cells is not obviously affected, only the pigmentation they show. Thus, loss of *psen2* function does not appear to affect

melanophore viability (although, in an animal as highly regenerative as the zebrafish, further tests would be required to conclude this with certainty). By extrapolation it appears likely that *NI40fs* homozygous adult fish still possess skin melanophores but that these lack melanin. The retention of some adult skin melanin formation in *T141\_L142delinsMISLISV* homozygotes but not *NI40fs* homozygotes, and the roles played by  $\gamma$ -secretase in melanosome function (Kumano, Masuda et al. 2008; Yang, Arslanova et al. 2010; Rochin, Hurbain et al. 2013), support that *T141\_L142delinsMISLISV* mutant Psen2 protein molecules retain some level of  $\gamma$ -secretase activity. This supports that the *T141\_L142delinsMISLISV* mutation of zebrafish Psen2 does not seriously disrupt the protein's overall pattern of folding for membrane insertion, but does distort its conformation sufficiently to reduce  $\gamma$ -secretase activity. Partial loss of  $\gamma$ -secretase activity is a commonly observed characteristic of fAD-like mutations in *PRESENILIN* genes. For example, mouse skin completely lacking expression of wild type *Psen1* and *Psen2* genes but with a single knock-in M146V fAD-like allele of *Psen1* show lighter skin and coat colour than similar mice possessing a single wild type allele of *Psen1* (Wang, Tang et al. 2006). These data, and the fact that the *T141\_L142delinsMISLISV* mutation obeys the "fAD mutation reading frame preservation rule" (Jayne, Newman et al. 2016), support that this mutation should be investigated for its utility in zebrafish-based fAD research.

Intriguingly, only the melanotic pigmentation of adult zebrafish skin is dependent on *psen2* function while larvae and cells of the retinal pigmented epithelium do not show

this dependency. This most likely indicates that the Psen1 protein (or, possibly, another protein with  $\gamma$ -secretase-like activity (Jayne, Newman et al. 2016)) contributes to normal melanosome formation in these remaining pigmented cells. That different PRESENILIN proteins might contribute to melanosome formation in different cells or in the same cell type at different ages is a level of developmental complexity that has not previously been appreciated. Alternatively, the skin melanophores of adult fish might, for some unknown reason, be incapable of genetic compensation (e.g. upregulation of *psen1* activity when *psen2* activity is lost through mutation). The possibility of cell type-specificity of genetic compensation has also not previously been considered. The lack of an obvious larval pigmentation phenotype explains why *psen2* was not identified by the large mutation screens for developmental phenotypes conducted by the laboratories of Christiane Nüsslein-Volhard (Kelsh, Brand et al. 1996) and Wolfgang Driever (Driever, Solnica-Krezel et al. 1996) and published in 1996.

In conclusion, we have generated in zebrafish an EOfAD-like mutation, *psen2*<sup>T141\_L142delinsMISLISV</sup>, and an apparent null, loss-of-function mutation *psen2*<sup>N140fs</sup>. Since none of the over 200 human fAD mutations in *PSEN1* and *PSEN2* are obviously null alleles, these two zebrafish mutations may prove useful for defining the gene regulatory and other molecular changes that are particular to fAD mutations in the *PRESENILIN* genes. Our future work will use these and other zebrafish mutation models to dissect how fAD-like mutations cause Alzheimer's disease.

## Acknowledgments

The authors wish to thank Seyyed Hani Moussavi Nik for kind assistance in adjusting the conditions for the dqPCR.

## References

- Adzhubei, I. A., S. Schmidt, et al. A method and server for predicting damaging missense mutations, *Nat Methods*. 2010 Apr;7(4):248-9. doi: 10.1038/nmeth0410-248.
- alz.co.uk (2014). World Alzheimer Report 2014: Dementia and Risk Reduction, Alzheimer's Disease International.
- Area-Gomez, E., A. J. de Groof, et al. (2009). "Presenilins are enriched in endoplasmic reticulum membranes associated with mitochondria." *Am J Pathol* **175**(5): 1810-1816.
- Babon, J. J., M. McKenzie, et al. (2003). "The use of resolvases T4 endonuclease VII and T7 endonuclease I in mutation detection." *Molecular Biotechnology* **23**(1): 73-81.
- Bassett, A. and J.-L. Liu (2014). "CRISPR/Cas9 mediated genome engineering in Drosophila." *Methods* **69**(2): 128-136.
- Bassett, A. R. and J.-L. Liu (2014). "CRISPR/Cas9 and Genome Editing in Drosophila." *Journal of Genetics and Genomics* **41**(1): 7-19.
- Bibikova, M., M. Golic, et al. (2002). "Targeted chromosomal cleavage and mutagenesis in Drosophila using zinc-finger nucleases." *Genetics* **161**(3): 1169-1175.
- Bissig, C., L. Rochin, et al. (2016). "PMEL Amyloid Fibril Formation: The Bright Steps of Pigmentation." *Int J Mol Sci* **17**(9).
- Campion, D., C. Dumanchin, et al. "Early-Onset Autosomal Dominant Alzheimer Disease: Prevalence, Genetic Heterogeneity, and Mutation Spectrum." *The American Journal of Human Genetics* **65**(3): 664-670.
- Carter, M. S., J. Duskow, et al. (1995). "A regulatory mechanism that detects premature nonsense codons in T-cell receptor transcripts in vivo is reversed by protein synthesis inhibitors in vitro." *J Biol Chem* **270**(48): 28995-29003.
- Chang, Y. F., J. S. Imam, et al. (2007). "The nonsense-mediated decay RNA surveillance pathway." *Annu Rev Biochem* **76**: 51-74.
- De Gasperi, R., M. A. Sosa, et al. (2010). "Presenilin-1 regulates induction of hypoxia inducible factor-1alpha: altered activation by a mutation associated with familial Alzheimer's disease." *Mol Neurodegener* **5**(38): 1750-1326.
- del Marmol, V. and F. Beermann (1996). "Tyrosinase and related proteins in mammalian pigmentation." *FEBS Lett* **381**(3): 165-168.
- Detrich III, H. W., L. I. Zon, et al. (2009). Essential zebrafish methods: Genetics and genomics, Academic Press.
- Driever, W., L. Solnica-Krezel, et al. (1996). "A genetic screen for mutations affecting embryogenesis in

- zebrafish." Development **123**: 37-46.
- Fowler, D. M., A. V. Koulov, et al. (2005). "Functional Amyloid Formation within Mammalian Tissue." PLoS Biology **4**(1): e6.
- Fraering, P. C. (2007). "Structural and Functional Determinants of gamma-Secretase, an Intramembrane Protease Implicated in Alzheimer's Disease." Curr Genomics **8**(8): 531-549.
- Gardner, L. B. (2008). "Hypoxic Inhibition of Nonsense-Mediated RNA Decay Regulates Gene Expression and the Integrated Stress Response." Molecular and Cellular Biology **28**(11): 3729-3741.
- Gasteiger, E., C. Hoogland, et al. (2005). Protein identification and analysis tools on the ExPASy server. The proteomics protocols handbook, Springer: 571-607.
- Groth, C., S. Nornes, et al. (2002). "Identification of a second presenilin gene in zebrafish with similarity to the human Alzheimer's disease gene presenilin2." Development Genes and Evolution **212**(10): 486-490.
- Guerreiro, R. and J. Hardy (2014). "Genetics of Alzheimer's disease." Neurotherapeutics **11**(4): 732-737.
- Hardy, J. (1997). "Amyloid, the presenilins and Alzheimer's disease." Trends in Neurosciences **20**(4): 154-159.
- Hin, N., M. Newman, et al. (2018). "Accelerated brain aging towards transcriptional inversion in a zebrafish model of familial Alzheimer's disease." bioRxiv.
- Hurt, J. A., A. D. Robertson, et al. (2013). "Global analyses of UPF1 binding and function reveal expanded scope of nonsense-mediated mRNA decay." Genome Res **23**(10): 1636-1650.
- Jayadev, S., J. B. Leverenz, et al. (2010). "Alzheimer's disease phenotypes and genotypes associated with mutations in presenilin 2." Brain **133**(Pt 4): 1143-1154.
- Jayne, T., M. Newman, et al. (2016). "Evidence For and Against a Pathogenic Role of Reduced gamma-Secretase Activity in Familial Alzheimer's Disease." J Alzheimers Dis **52**(3): 781-799.
- Jumpertz, T., A. Rennhack, et al. (2012). "Presenilin is the molecular target of acidic gamma-secretase modulators in living cells." PLoS ONE **7**(1): 6.
- Kelsh, R. N., M. Brand, et al. (1996). "Zebrafish pigmentation mutations and the processes of neural crest development." Development **123**: 369-389.
- Kok, F. O., M. Shin, et al. (2015). "Reverse genetic screening reveals poor correlation between morpholino-induced and mutant phenotypes in zebrafish." Dev Cell **32**(1): 97-108.
- Kumano, K., S. Masuda, et al. (2008). "Both Notch1 and Notch2 contribute to the regulation of melanocyte homeostasis." Pigment Cell Melanoma Res **21**(1): 70-78.
- Kummer, M. P., H. Maruyama, et al. (2009). "Formation of Pmel17 amyloid is regulated by juxtamembrane metalloproteinase cleavage, and the resulting C-terminal fragment is a substrate for gamma-secretase." J Biol Chem **284**(4): 2296-2306.
- Leimer, U., K. Lun, et al. (1999). "Zebrafish (Danio rerio) Presenilin Promotes Aberrant Amyloid  $\beta$ -Peptide Production and Requires a Critical Aspartate Residue for Its Function in Amyloidogenesis." Biochemistry **38**(41): 13602-13609.
- Levy-Lahad, E., W. Wasco, et al. (1995). "Candidate gene for the chromosome 1 familial Alzheimer's disease locus." Science **269**(5226): 973-977.
- Meeker, N. D., S. A. Hutchinson, et al. (2007). "Method for isolation of PCR-ready genomic DNA from zebrafish tissues." Biotechniques **43**(5): 614.
- Moussavi Nik, S. H., M. Newman, et al. (2011). "The response of HMGA1 to changes in oxygen availability is evolutionarily conserved." Exp Cell Res **317**(11): 1503-1512.
- Moussavi Nik, S. H., M. Newman, et al. (2015). "Alzheimer's disease-related peptide PS2V plays ancient,

- conserved roles in suppression of the unfolded protein response under hypoxia and stimulation of gamma-secretase activity." Hum Mol Genet **26**.
- Moussavi Nik, S. H., L. Wilson, et al. (2012). "The BACE1-PSEN-AbetaPP regulatory axis has an ancient role in response to low oxygen/oxidative stress." J Alzheimers Dis **28**(3): 515-530.
- Nishikawa, A., T. Manabe, et al. (2004). "Novel function of PS2V: change in conformation of tau proteins." Biochem Biophys Res Commun **318**(2): 435-438.
- Nornes, S., M. Newman, et al. (2009). "Independent and cooperative action of Psen2 with Psen1 in zebrafish embryos." Experimental Cell Research **315**(16): 2791-2801.
- Postlethwait, J. H., I. G. Woods, et al. (2000). "Zebrafish Comparative Genomics and the Origins of Vertebrate Chromosomes." Genome Research **10**(12): 1890-1902.
- Pottier, C., D. Hannequin, et al. (2012). "High frequency of potentially pathogenic SORL1 mutations in autosomal dominant early-onset Alzheimer disease." Mol Psychiatry **17**(9): 875-879.
- Raposo, G. and M. S. Marks (2007). "Melanosomes--dark organelles enlighten endosomal membrane transport." Nat Rev Mol Cell Biol **8**(10): 786-797.
- Ravi, V. and B. Venkatesh (2008). "Rapidly evolving fish genomes and teleost diversity." Current Opinion in Genetics & Development **18**(6): 544-550.
- Rochin, L., I. Hurbain, et al. (2013). "BACE2 processes PMEL to form the melanosome amyloid matrix in pigment cells." Proc Natl Acad Sci U S A **110**(26): 10658-10663.
- Rossi, A., Z. Kontarakis, et al. (2015). "Genetic compensation induced by deleterious mutations but not gene knockdowns." Nature **524**: 230.
- Salminen, A., A. Kauppinen, et al. (2017). "Hypoxia/ischemia activate processing of Amyloid Precursor Protein: impact of vascular dysfunction in the pathogenesis of Alzheimer's disease." Journal of Neurochemistry **140**(4): 536-549.
- Sato, N., O. Hori, et al. (1999). "A novel presenilin-2 splice variant in human Alzheimer's disease brain tissue." J Neurochem **72**(6): 2498-2505.
- Scherzer, C. R., K. Offe, et al. (2004). "Loss of apolipoprotein E receptor LR11 in Alzheimer disease." Arch Neurol **61**(8): 1200-1205.
- Tief, K., M. Hahne, et al. (1996). "Tyrosinase, the key enzyme in melanin synthesis, is expressed in murine brain." Eur J Biochem **241**(1): 12-16.
- Toda, T., Y. Noda, et al. (2011). "Presenilin-2 Mutation Causes Early Amyloid Accumulation and Memory Impairment in a Transgenic Mouse Model of Alzheimer's Disease." Journal of Biomedicine and Biotechnology **2011**.
- Tomita, T., K. Maruyama, et al. (1997). "The presenilin 2 mutation (N141I) linked to familial Alzheimer disease (Volga German families) increases the secretion of amyloid  $\beta$  protein ending at the 42nd (or 43rd) residue." Proceedings of the National Academy of Sciences **94**(5): 2025-2030.
- Tomita, T., S. Tokuhira, et al. (1998). "Molecular dissection of domains in mutant presenilin 2 that mediate overproduction of amyloidogenic forms of amyloid beta peptides. Inability of truncated forms of PS2 with familial Alzheimer's disease mutation to increase secretion of A $\beta$ 42." J Biol Chem **273**(33): 21153-21160.
- Vetrivel, K. S., Y.-w. Zhang, et al. (2006). "Pathological and physiological functions of presenilins." Molecular Neurodegeneration **1**(1): 4.
- Wang, R., P. Tang, et al. (2006). "Regulation of tyrosinase trafficking and processing by presenilins: partial loss of function by familial Alzheimer's disease mutation." Proc Natl Acad Sci U S A **103**(2): 353-358.



- Watt, B., G. van Niel, et al. (2013). "PMEL: a pigment cell-specific model for functional amyloid formation." Pigment Cell Melanoma Res **26**(3): 300-315.
- Wolfe, M. S., W. Xia, et al. (1999). "Two transmembrane aspartates in presenilin-1 required for presenilin endoproteolysis and gamma-secretase activity." Nature **398**(6727): 513-517.
- Yang, T., D. Arslanova, et al. (2010). "In vivo manifestation of Notch related phenotypes in zebrafish treated with Alzheimer's amyloid reducing gamma-secretase inhibitors." J Neurochem **113**(5): 1200-1209.
- Zhang, X., K. Zhou, et al. (2007). "Hypoxia-inducible Factor 1 $\alpha$  (HIF-1 $\alpha$ )-mediated Hypoxia Increases BACE1 Expression and  $\beta$ -Amyloid Generation." Journal of Biological Chemistry **282**(15): 10873-10880.

### 3.3 Supplementary Information

This section is included in the thesis as information supplementary to Section 3.2. It contains additional information not included in the main text of the manuscript.

#### **File S1. Mutation screening and breeding.**

In addition to the mutation *NI4II*, another missense mutation in the human *PSEN2* gene, *VI48I*, was also considered for introduction into zebrafish *psen2*. *VI48I* is a missense mutation caused by a G-to-A transition at the first position of codon 148 of *PSEN2* (Lao, Beyer et al. 1998). Like *NI4II*, this mutation is also located within TMD2. However, since both valine and isoleucine are hydrophobic (with the hydrophobicity of isoleucine slightly stronger than that of valine), the PolyPhen-2 prediction score (Adzhubei, Schmidt et al.) for V148I (0.222 with sensitivity of 0.91 and specificity of 0.88) is more benign than that for *NI4II* (i.e. 0.934). The age of onset of Alzheimer's disease in the individual with the *VI48I* mutation was age 71 (Lao, Beyer et al. 1998), which is also much later than the mean onset age for the *NI4II* mutation (age 53.7). It is also reported that *VI48I* does not significantly change the A $\beta$  42/40 ratio (Walker, Martinez et al. 2005).

#### **Mutation screening and breeding of the CRISPR/Cas9 and template oligo-injected G0 fish**

The *in vivo* cleavage activity of the CRISPR/Cas9 system used in this study was tested using the T7 endonuclease I assay. It is interesting that even the uninjected TU embryos showed two cleavage bands in a T7 endonuclease I assay, although the sizes of these bands were different to those expected for the samples injected with the CRISPR/Cas9 system (Figure S1A). This may be due to that the T7 endonuclease I assay system is so sensitive that it cleavage can occur at sites of single mismatched bases heteroduplexes (Babon, McKenzie et al. 2003), i.e. due to single nucleotide polymorphisms (SNPs). The CRISPR/Cas9 system-injected TU embryos showed four cleavage bands in the T7 endonuclease I assay (Figure S1A), two of which were the same as those for the uninjected TU embryos (possibly caused by SNPs in the TU genome), while the other two were the sizes expected for mutation produced by the DNA cleavage activity of the CRISPR/Cas9 system. Therefore, the CRISPR/Cas9 system used in this study showed cleavage activity in the TU genome, and we could use this system to attempt to generate the mutations desired by co-injecting it together with homology-directed repair (HDR) oligonucleotide templates.

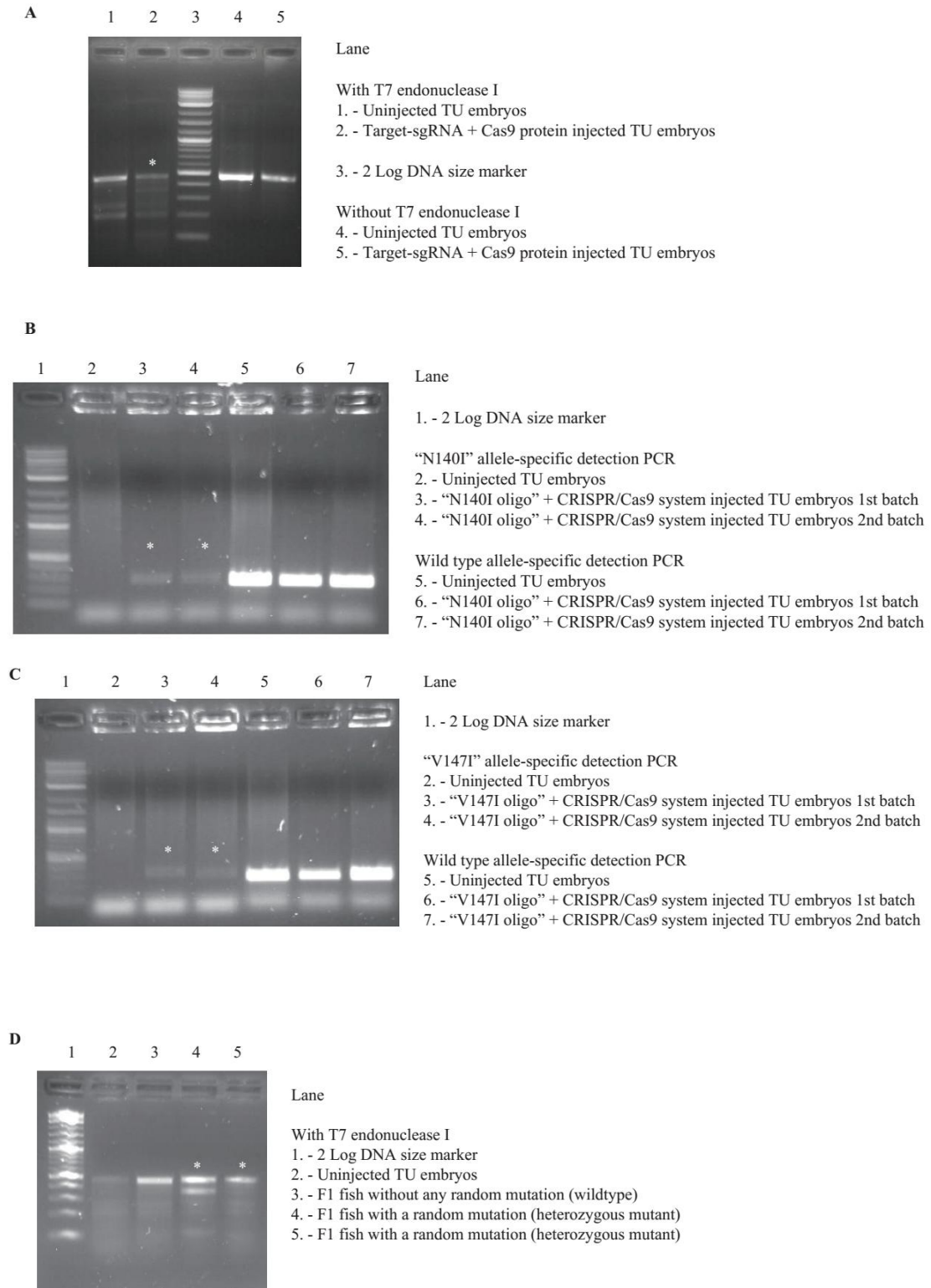


**Figure S1. T7 endonuclease assays and mutation-specific PCRs for embryos at 24 hpf.**

(A) T7 endonuclease I assay for testing the cleavage activity of the CRISPR/Cas9

system.

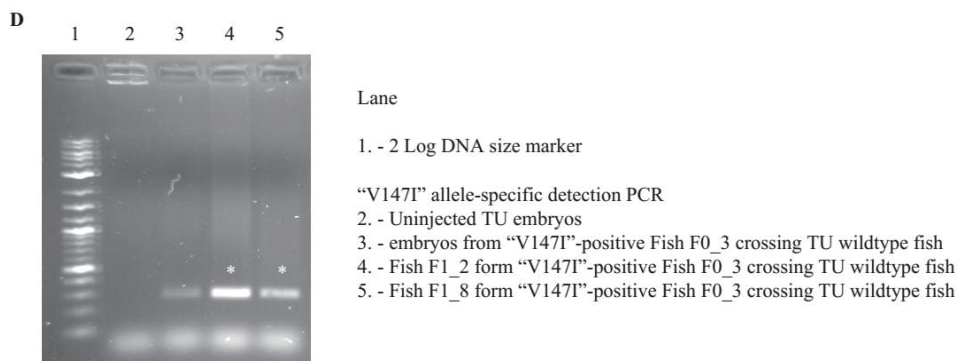
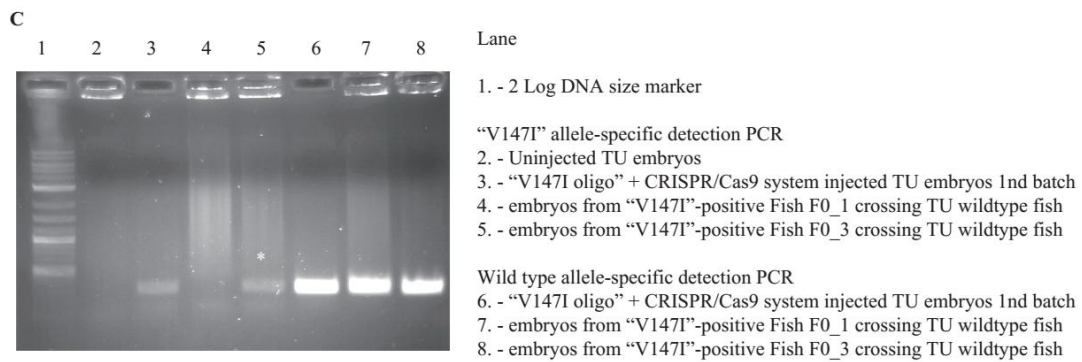
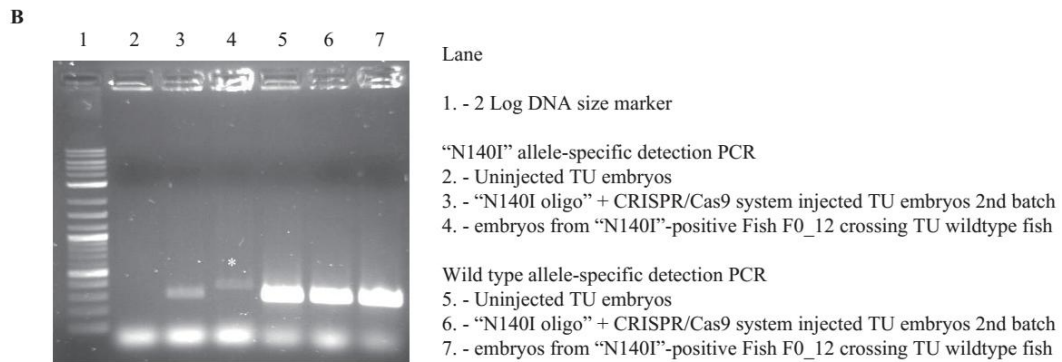
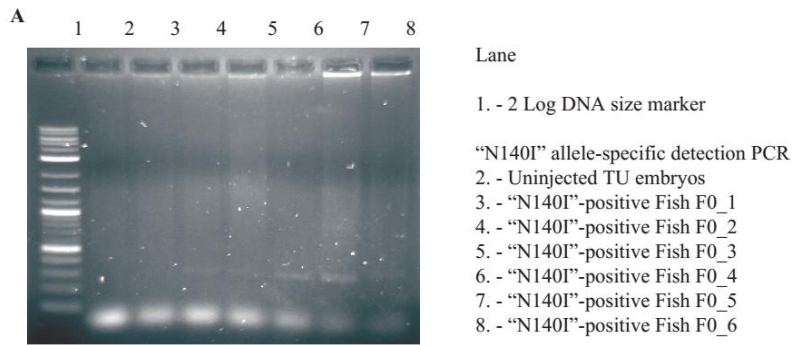
(B) “*N140I*” allele-detection PCR for testing of CRISPR/Cas9 plus “N140I oligo” co-injected TU embryos. 10 embryos from each injection batch were pooled for these tests. Both batches of the injected TU embryos showed positive signals in the “N140I” allele-detection PCR. Therefore, some of these “N140I oligo” injected TU embryos may have carried the “N140I” allele in the genomes of some cells.

(C) “*V147I*” allele-detection PCR for testing the CRISPR/Cas9 plus “V147I oligo” injected TU embryos. 10 embryos from each batch were pooled for these tests. Both batches of the injected TU embryos showed positive signals from the “*V147I*” allele-detection PCR. Therefore, some of these “V147I oligo” injected TU embryos may have carried the “*V147I*” allele in the genomes of some cells.

(D) T7 endonuclease I assay for detecting random mutations at the CRISPR/Cas9 target site in the F1 progeny. Tail-clip biopsies from 46 of the F1 progeny from the CRISPR/Cas9 plus “V147I oligo” injected mosaic G0 fish were tested using the T7 endonuclease I assay to screen for the presence of cells with mutations at the target site. Only 5 fish showed cleavage patterns indicating the presence of mutations.

For the “N140I oligo” injected TU embryos, 10 embryos from each batch were pooled and tested using the “*N140I*” allele-specific detection PCR (Figure S1B). Positive signals showed that there should be mutant fish carrying the “*N140I*” mutation in both batches. The remaining G0 embryos were raised to adulthood and then genotyped using the “*N140I*” allele-specific detection PCR (Figure S2A). Twelve of these genotyped G0

fish (from a total of 120) showed positive signals in the “*NI40I*” allele-specific detection PCR (Figure S2A). All these “*NI40I*” allele-carrying G0 fish were then outbred with TU wild type fish to generate F1 fish potentially heterozygous for the “*NI40I*” allele. 10 F1 embryos from each “*NI40I*” allele carrying G0 fish crossed with a TU wild type fish were pooled for the “*NI40I*” allele-specific detection PCR. Unfortunately, none of these progeny showed any positive signal from the “*NI40I*” allele-specific detection PCR, indicating that the “*NI40I*” allele was not present in the F1 progeny. Interestingly, the “*NI40I*” allele-specific detection PCR for the F1 progeny from one “*NI40I*” allele-carrying G0 fish produced a DNA fragment of ~400 nucleotides in size (Figure S2B), while the positive signal for the “*NI40I*” allele-specific detection PCR was calculated to be ~300 nucleotides. This probably indicates the existence of a DNA rearrangement at the cleavage site that incorporated all or part of the oligonucleotide sequence in an unintended manner.



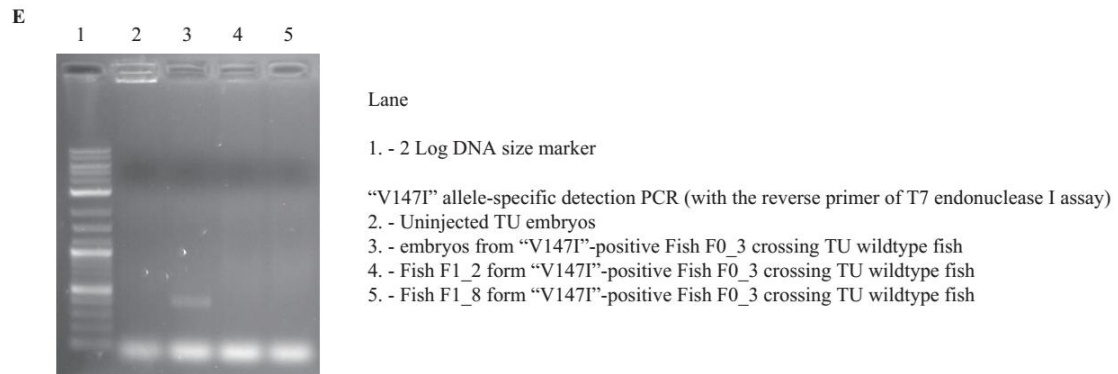


**Figure S2. Mutation-specific PCR tests of G0 and F1 fish.**

(A) “*N140I*” allele-specific detection PCRs on tail-clip biopsies from G0 fish. Twelve G0 fish (120 in total) showed positive signals in the “*N140I*” allele-specific detection PCR.

(B) “*N140I*” allele-specific detection PCRs from F1 embryos of the G0 mosaic fish showing “*N140I*” allele-positive signals. 10 F1 embryos at 24 hpf from each “*N140I*” allele-carrying G0 fish were pooled for testing. The F1 progeny from one “*N140I*” allele-carrying G0 fish showed a signal at ~400 bp, which may result from imperfect incorporation of the “*N140I* oligo” sequence into the target site of the CRISPR/Cas9 system.

(C) “*V147I*” allele-specific PCRs from F1 embryos of the G0 mosaic fish showing “*V147I*” allele-positive signals. 10 F1 embryos at 24 hpf from each “*V147I*” allele carrying G0 fish were pooled for testing. The F1 progeny from one of the “*V147I*” allele-carrying G0 fish showed the same positive signal as the injected G0 embryos.

(D) “*V147I*” allele-specific detection PCR from tail-clip biopsies of F1 fish. Two out of twelve tested F1 fish (raised from the positive batch of embryos observed above in D) showed positive signals, indicating they might carry the desired “*V147I*” allele.



(E) “*V147P*” allele-specific detection PCR using the same forward primer as in (E) but a different reverse primer binding farther downstream in *psen2* DNA. While the pooled F1 embryos still gave a positive signal, the two F1 fish no longer showed a positive signal using this PCR, revealing that the previously seen positive signals (in E) were artefacts.

For the “V147I oligo” injected TU embryos, positive signals were also detected using the “*V147P*” allele-specific detection PCR (Figure S1C, signal from 10 embryos pooled). Six of the 36 tested G0 fish showed positive signals using the “*V147P*” allele-specific detection PCR. The six “*V147P*” allele-carrying G0 fish were then outbred with TU wild type fish. 10 embryos from the F1 progeny from each “*V147P*” allele-carrying G0 fish with a TU wild type fish were pooled for the “*V147P*” allele-specific detection PCR. The F1 progeny from one of the “*V147P*” allele carrying G0 fish showed the same positive signal as the injected G0 embryos (Figure S2C). It seemed that these F1 progeny might carry the “*V147P*” allele. When these F1 progeny were raised, they were genotyped using the “*V147P*” allele-specific detection PCR. Two out of twelve tested F1 fish showed positive signals, indicating they might carry the “*V147P*” allele. To verify these results, a region encompassing the intended mutation site in these two fish was amplified by PCR using the primers for the T7 endonuclease assay, and then sequenced. However, only wild type DNA sequences were seen. To check subsequently the previous positive “*V147P*” allele-specific detection PCR, the PCR was modified to use the same forward primer (specific to the desired mutation) but a different reverse

primer (farther downstream of the previously used reverse primer). Interestingly, although the genomic DNA from the pooled F1 embryos still showed a positive signal, the DNAs from the two F1 positive fish no longer showed a positive signal using this PCR test (Figure S2E). Thus, the previous positive signals detected for these two fish were artefacts. It seems that, in the pooled F1 embryos, the “*V147P*” allele did exist, but the allele was either at too low a frequency to be likely to be detected using the number of fish that we observed or, possibly, cannot be passed through the germline (i.e. for some reason it may be lethal to gamete formation or embryo development).

In conclusion, in this study we used the CRISPR/Cas9 system to attempt to insert fAD mutations (point mutations) into the zebrafish genome to investigate the pathological changes caused by these mutations. However, while we could detect the likely existence of these point mutations in the G0 fish, we did not see them transmitted to F1 progeny.

#### **NHEJ-generated mutations at the CRISPR/Cas9 target site in F1 progeny**

46 of the F1 progeny from the “*V147P*” allele-carrying mosaic G0 fish were tested using T7 endonuclease I assays to detect mutations generated through NHEJ. The mutation-carrying F1 progeny showed different cleavage patterns to the wild type fish (Figure S1D), but similar patterns to that from embryos injected only with the CRISPR/Cas9 system without mutation-containing oligonucleotides (Figure S1A), indicating these mutations were likely induced by the injected CRISPR/Cas9 system alone. Among the

46 F1 fish tested, only five fish showed cleavage patterns indicating the presence of mutations. Sequencing across the target site in these five fish showed the presence of only two different mutations. One mutation (carried by two of the fish) was a 15 nucleotide-indel mutation (an in-frame mutation) that deleted two codons (T141 and L142) with an insertion of another seven codons (MISLISV) and was consequently named *psen2*<sup>T141\_L142delinsMISLISV</sup> (Figure 1A). The other mutation (carried by three of the fish) was a seven nucleotide -deletion resulting in a frameshift mutation downstream from N140 leading to a premature termination codon at the 142<sup>th</sup> codon position. It was consequently named *psen2*<sup>N140fs</sup> (Figure 1A).

**File S2. dqPCR results for allele-specific transcript quantification in six month old brains.**

**Table S1. Allele-specific transcript quantification in six month old *psen2*<sup>T141\_L142delinsMISLISV/+</sup> and wild type sibling brains. Copies per 25ng of total brain cDNA (assuming complete reverse transcription of total brain RNA).**

<i>psen2</i> wild type allele	
+/+ wild type allele under normoxia	<i>psen2</i> <sup>T141_L142delinsMISLISV/+</sup> wild type allele under normoxia
895.88	450.69
954.56	579.27
827.13	309.93
1196.3	531.43
+/+ wild type allele under hypoxia	<i>psen2</i> <sup>T141_L142delinsMISLISV/+</sup> wild type allele under hypoxia
1187.5	250.22
1048.5	561.6
981.92	557.32
956.9	709.39
<i>psen2</i> <sup>T141_L142delinsMISLISV</sup> mutant allele	
+/+ mutant allele under normoxia	<i>psen2</i> <sup>T141_L142delinsMISLISV/+</sup> mutant allele under normoxia
2.862	565.52
0.103	634.11
1.2	297.33
2.963	604.62
+/+ mutant allele under hypoxia	<i>psen2</i> <sup>T141_L142delinsMISLISV/+</sup> mutant allele under hypoxia
4.137	264.77
3.156	671.13
2.232	656.45
2.972	722.62

**Table S2. Allele-specific transcript quantification in six month old *psen2*<sup>N140fs/+</sup> fish and wild type sibling brains. Copies per 25ng of total brain cDNA (assuming complete**

reverse transcription of total brain RNA).

<i>psen2</i> wild type allele	
+/+ wild type allele under normoxia	<i>psen2</i> <sup>N140fs</sup> /+ wild type allele under normoxia
1346.8	918.15
1806.9	885.32
1729.6	842.01
1630.9	837.78
+/+ wild type allele under hypoxia	<i>psen2</i> <sup>N140fs</sup> /+ wild type allele under hypoxia
1678.6	838.53
1601.3	903.36
1635.7	815.97
1718.4	866.78
<i>psen2</i> <sup>N140fs</sup> mutant allele	
+/+ mutant allele under normoxia	<i>psen2</i> <sup>N140fs</sup> /+ mutant allele under normoxia
11.017	154.64
29.408	165.58
18.746	141.68
10.673	148.65
+/+ mutant allele under hypoxia	<i>psen2</i> <sup>N140fs</sup> /+ mutant allele under hypoxia
7.767	164.15
12.353	167.54
22.487	174.94
10.041	161.02

**File S3. *In situ* transcript hybridization analysis of DoLA neuron number.**

Blockage of the expression of *psen2* using a morpholino has been shown to increase the number of a particular spinal cord interneuron – the Dorsal Longitudinal Ascending (DoLA) neuron (Nornes, Newman et al. 2009). Since the loss of pigmentation phenotype in homozygous *NI40fs* mutants is suggestive of loss of  $\gamma$ -secretase activity, we assumed this mutation might result in loss of all *psen2* function. As there is currently no antibody detecting zebrafish Psen2 protein available, we attempted to demonstrate loss of *psen2* function for *NI40fs* by observing DoLA neuron number in embryos at 24 hpf.

To examine the effect of *NI40fs* on DoLA number, embryos from mating of a pair of heterozygous fish were collected. Theoretically, this family would be comprised of approximately 50% heterozygous mutant, 25% homozygous mutant and 25% wild type genotypes. *In situ* transcript hybridization against transcripts of the gene *tbx16* that labels DoLA neurons (Tamme, Wells et al. 2002) was then performed on these embryos at 24 hpf. Genotyping of each embryo was performed after the number of DoLA neurons in each embryo had been recorded by direct observation, using PCRs specific for the mutant and wild type alleles. However, two-tailed t-tests assuming either equal or unequal variances found no significant differences in DoLA number between any two genotypes (Figure S3), (similar to observations for the *S4Ter* mutation, Jiang, unpublished results), suggesting that genetic compensation may be induced by these

endogenous mutations to suppress the phenotype of increased DoLA number after loss of *psen2* activity from morpholino injection (Rossi, Kontarakis et al. 2015).

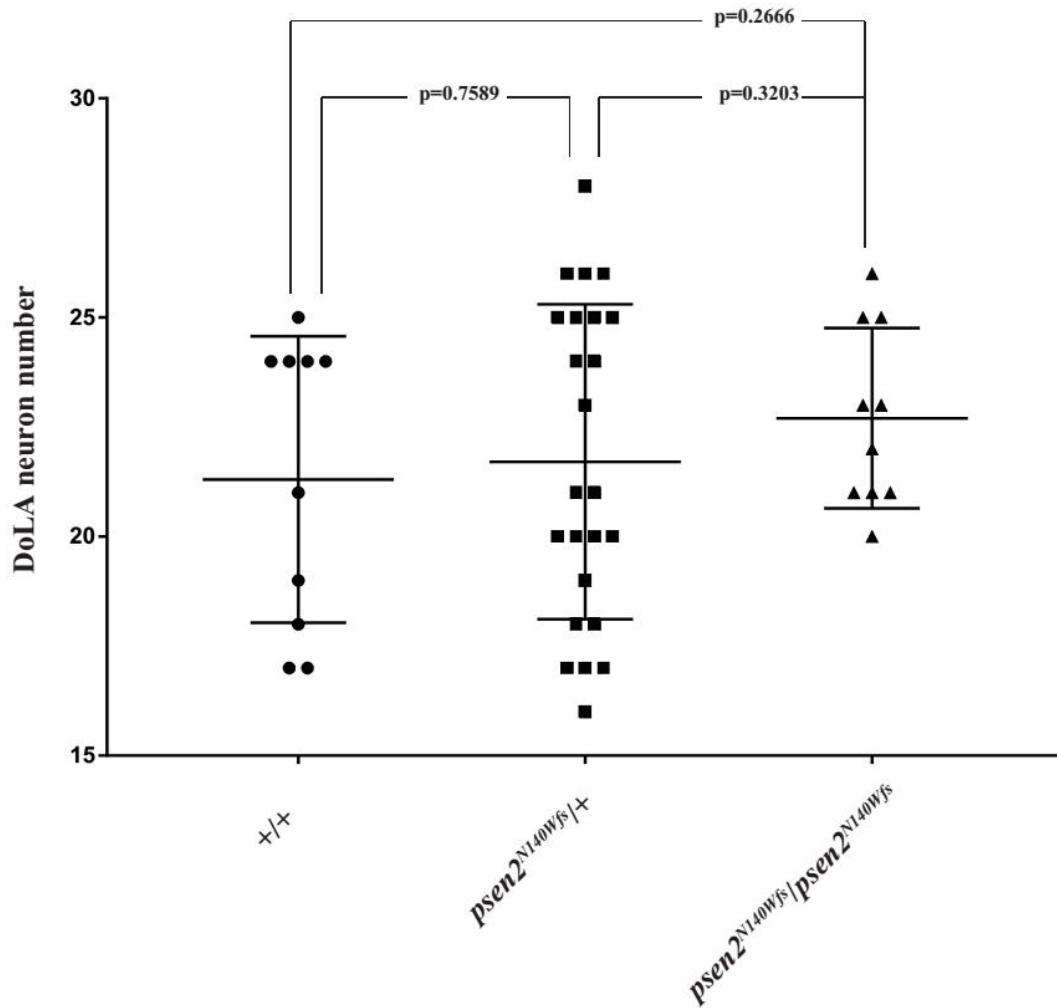


**Figure S3. DoLA neuron numbers.**

DoLA neuron numbers in wild type and *psen2*<sup>N140fs</sup> mutant embryos as revealed by *in situ* hybridisation against *tbx16* transcripts.

44 embryos from a pair-mating of fish heterozygous for the *psen2*<sup>N140fs</sup> mutation were subjected to *in situ* transcript hybridisation at 24 hpf. Genotyping subsequent to DoLA

quantification showed that this family included 24 heterozygous mutants, 10 homozygous mutants and 10 wild type sibling embryos. Values of p were determined in two-tailed t-tests.

**S3 Table. *In situ* hybridization against *tbx16* transcripts in DoLA neurons.**

DoLA numbers in +/+	DoLA numbers in <i>psen2<sup>N140fs</sup>/+</i>	DoLA numbers in <i>psen2<sup>N140fs</sup>/psen2<sup>N140fs</sup></i>
18	18	25
24	20	21
24	25	23
25	19	26
24	20	25
21	21	21
17	28	21
19	26	22
24	24	23
17	20	20
	17	
	17	
	17	
	26	
	25	
	24	
	21	
	25	
	20	
	23	
	25	
	18	
	16	
	26	



#### **S4 File. Cycloheximide treatment of *psen2*<sup>N140fs/+</sup> embryos from 48 to 50 hpf.**

To verify whether NMD is occurring for *psen2*<sup>N140Wfs</sup> allele transcripts we treated *psen2*<sup>N140Wfs/+</sup> embryos with cycloheximide at 48 hpf for two hours to stabilize any NMD-targeted mRNA (Carter, Doskow et al. 1995; Hurt, Robertson et al. 2013). Cycloheximide (CHX) is a potent translation elongation inhibitor, and a short treatment with this drug can be used to stabilize NMD-targeted mRNAs (Carter, Doskow et al. 1995; Hurt, Robertson et al. 2013). In our study, we treated *psen2*<sup>N140fs/+</sup> embryos (generated by pair-mating of a *psen2*<sup>N140fs/psen2</sup><sup>N140fs</sup> female and a +/+ male fish) at 48 hpf with 200 µg/mL of cycloheximide (Sigma-Aldrich, St. Louis, Missouri, USA, C4859) at 28.5°C for two hours. 20 of the treated *psen2*<sup>N140fs/+</sup> embryos were pooled for total RNA extraction with the RNeasy Mini Kit (QIAGEN, Venlo, Netherlands, 74104). 20 non-treated *psen2*<sup>N140fs/+</sup> embryos were used as a control group. The RNAs from the pooled embryos were used to prepare cDNA using the SuperScript™ III First-Strand Synthesis System (Invitrogen, Carlsbad, California, USA, 18080051) and Random Primers (Promega, Madison, Wisconsin, USA, C1181). A pair of PCR primers (forward primer 5'-AAGAAGACCCGAACTCAGTGG-3', reverse primer: 5'-CTTGTAGAGCAGCACCAGGATG-3') were used to amplify a region spanning the mutation site. The PCR cycling conditions were: 95°C, 2 min, and then 31 cycles of [95°C, 30 s; 60°C, 30 s; 72°C, 30 s], 72°C 5 min. The PCR products were predicted to be ~110 nucleotides in length (with fragments amplified from the N140fs deletion mutation allele cDNA being 7 nucleotides shorter than from the wild type allele). The

PCR products were separated by electrophoresis through a 20% polyacrylamide gel, at 120V for five hours.

As shown in Figure S4A, PCR on cDNA from the CHX-treated *psen2*<sup>N140fs/+</sup> embryos, resulted in two bands in the electrophoretic gel of approximately equal intensity, while PCR on cDNA from non-treated *psen2*<sup>N140fs/+</sup> embryos resulted in only one band at the apparent same size as the upper band of the treated group. However, the bands in Figure S4A are not well resolved probably due to limitations of the separation technique. Therefore, digital quantitative PCR (dqPCR) designed for allele-specific expression analysis (see Materials and Methods) was performed on the same cDNAs from these samples. As show in Figure S4B, expression of both the wild type *psen2* allele and the *psen2*<sup>N140fs</sup> allele was upregulated after CHX-treatment, but the fold change (FC) of the upregulation of the *psen2*<sup>N140fs</sup> allele (FC=5.601) was significantly higher than that for the wild type *psen2* allele (FC=2.373), indicating that the NMD-targeted mutant mRNAs were stabilized by CHX in the *psen2*<sup>N140fs/+</sup> embryos.

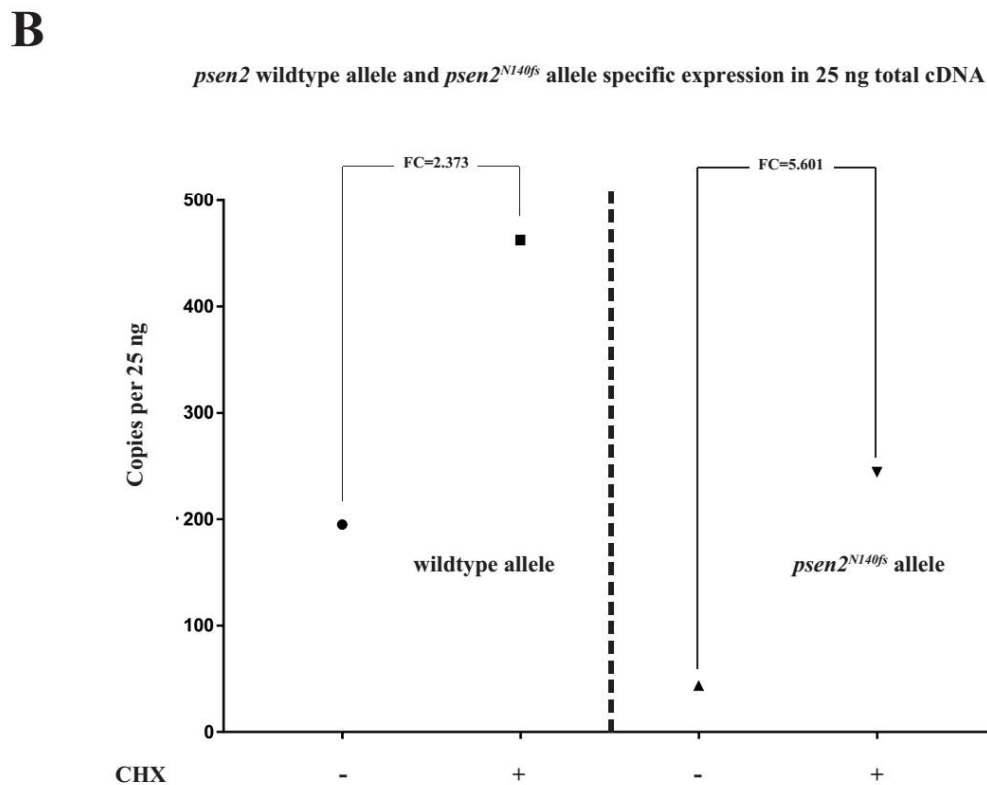
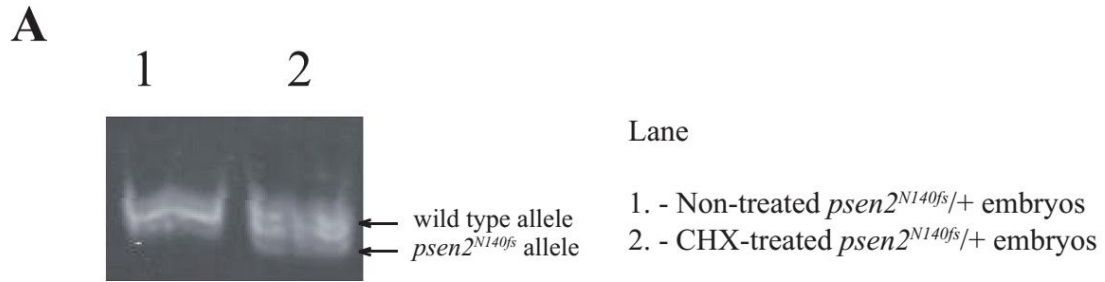


**Figure S4. dqPCRs detecting wild type and mutant alleles in *psen2*<sup>N140fs/+</sup> embryos at 50 hpf after two hours of cycloheximide treatment relative to untreated embryos.**

(A) In a 20% polyacrylamide gel, amplification of cDNA fragments spanning the mutation (7 nucleotides shorter than wild type) was only observed in the CHX-treated group, while only one higher molecular weight band (from the wild type allele) was observed in the non-treated group. This supports that NMD is destabilising the mutant transcript in heterozygous embryos.

(B) In dqPCR, both the wild type *psen2* allele and the *psen2*<sup>N140fs</sup> allele were observed to be upregulated after the CHX-treatment. The fold change (FC) of the upregulation of the *psen2*<sup>N140fs</sup> allele transcripts (FC=5.601) was significantly higher than that for the wild type *psen2* allele transcripts (FC=2.373).

**S4 Table. Allele-specific expression analysis on the *psen2*<sup>N140fs/+</sup> embryos (non-treated and CHX-treated) at 50 hpf in 25ng of total embryo cDNA. Copies per 25ng (assuming complete reverse transcription of total RNA).**

<i>psen2</i> wild type allele	
Non-treated <i>psen2</i> <sup>N140fs/+</sup>	CHX-treated <i>psen2</i> <sup>N140fs/+</sup>
194.99	462.66
<i>psen2</i> <sup>N140fs</sup> mutant allele	
Non-treated <i>psen2</i> <sup>N140fs/+</sup>	CHX-treated <i>psen2</i> <sup>N140fs/+</sup>
43.63	244.37

## Supporting references

- Adzhubei, I. A., S. Schmidt, et al. A method and server for predicting damaging missense mutations, Nat Methods. 2010 Apr;7(4):248-9. doi: 10.1038/nmeth0410-248.
- Babon, J. J., M. McKenzie, et al. (2003). "The use of resolvases T4 endonuclease VII and T7 endonuclease I in mutation detection." Molecular Biotechnology **23**(1): 73-81.
- Carter, M. S., J. Doskow, et al. (1995). "A regulatory mechanism that detects premature nonsense codons in T-cell receptor transcripts in vivo is reversed by protein synthesis inhibitors in vitro." J Biol Chem **270**(48): 28995-29003.
- Hurt, J. A., A. D. Robertson, et al. (2013). "Global analyses of UPF1 binding and function reveal expanded scope of nonsense-mediated mRNA decay." Genome Res **23**(10): 1636-1650.
- Lao, J. I., K. Beyer, et al. (1998). "A novel mutation in the predicted TM2 domain of the presenilin 2 gene in a Spanish patient with late-onset Alzheimer's disease." Neurogenetics **1**(4): 293-296.
- Nornes, S., M. Newman, et al. (2009). "Independent and cooperative action of Psen2 with Psen1 in zebrafish embryos." Experimental Cell Research **315**(16): 2791-2801.
- Rossi, A., Z. Kontarakis, et al. (2015). "Genetic compensation induced by deleterious mutations but not gene knockdowns." Nature **524**: 230.

- Tamme, R., S. Wells, et al. (2002). "The identity and distribution of neural cells expressing the mesodermal determinant spadetail." BMC Developmental Biology **2**(1): 9.
- Walker, E. S., M. Martinez, et al. (2005). "Presenilin 2 familial Alzheimer's disease mutations result in partial loss of function and dramatic changes in A $\beta$  42/40 ratios." Journal of Neurochemistry **92**(2): 294-301.

## **Chapter 4 Ratiometric assays of autophagic flux in zebrafish for analysis of familial Alzheimer's disease-like mutations**

### **4.1 Introduction, Significance and Commentary**

To detect possible changes in autophagic flux in zebrafish models of fAD mutations, we designed a GFP-based assay construct, GFP-Lc3a-GFP, which is able to generate equimolar amounts of GFP-Lc3a and a free GFP internal control within cells. This assay construct was expressed in zebrafish larvae of different genotypes, including larvae homozygous for a putative *psen2* null mutation (*S4Ter*), heterozygous for the same putative *psen2* null mutation, heterozygous for a fAD-like and reading-frame-preserving mutation in zebrafish *psen1*, and heterozygous for a fAD-related, reading-frame-truncating mutation in *psen1*. Significantly decreased autophagic flux was detected in larvae both heterozygous and homozygous for the putative *psen2* null mutation, as well as larvae heterozygous for the fAD-like, reading-frame-preserving *psen1* mutation, while a trend of increased autophagic flux was seen in larvae heterozygous for the fAD-related reading-frame-truncating mutation of *psen1*.

The significances of this work includes:

1. We designed an internally controlled GFP-based assay to monitor autophagic flux in the zebrafish model, such that results from separate western immunoblots are

comparable and providing a higher throughput for measurement of autophagic flux via western immunoblotting.

2. This is the first measurement of changes in autophagic flux caused by fAD-related mutations in the zebrafish model.

3. The similar changes in autophagic flux observed in larvae heterozygous or homozygous for the putative *psen2* null mutation *S4Ter* provide evidence supporting the transcriptomic observations made in a previous paper (Chapter 2).

#### 4.2 Ratiometric assays of autophagic flux in zebrafish for analysis of familial Alzheimer's disease-like mutations

This chapter is included in the thesis in the form of a research paper manuscript authored by H. Jiang, M. Newman, D. Ratnayake, and M. Lardelli, and which is ready for submission for peer review by a scientific journal.

## Statement of Authorship

### Statement of Authorship

Title of Paper	Ratiometric assays of autophagic flux in zebrafish for analysis of familial Alzheimer's disease-like mutations
Publication Status	<input type="checkbox"/> Published <input type="checkbox"/> Accepted for Publication <input type="checkbox"/> Submitted for Publication <input checked="" type="checkbox"/> Unpublished and Unsubmitted work written in manuscript style
Publication Details	doi.org/10.1101/272351

#### Principal Author

Name of Principal Author (Candidate)	Haowei Jiang			
Contribution to the Paper	Research plan, most of the experiments and data analysis, manuscript drafting.			
Overall percentage (%)	80%			
Certification:	This paper reports on original research I conducted during the period of my Higher Degree by Research candidature and is not subject to any obligations or contractual agreements with a third party that would constrain its inclusion in this thesis. I am the primary author of this paper.			
Signature	<table border="1"> <tr> <td></td> <td>Date</td> <td>1/5/18</td> </tr> </table>		Date	1/5/18
	Date	1/5/18		

#### Co-Author Contributions



By signing the Statement of Authorship, each author certifies that:

- i. the candidate's stated contribution to the publication is accurate (as detailed above);
- ii. permission is granted for the candidate to include the publication in the thesis; and
- iii. the sum of all co-author contributions is equal to 100% less the candidate's stated contribution.

Name of Co-Author	Morgan Newman			
Contribution to the Paper	Supervision and help with the experiments			
Signature	<table border="1"> <tr> <td></td> <td>Date</td> <td>1/5/2018</td> </tr> </table>		Date	1/5/2018
	Date	1/5/2018		

Name of Co-Author	Dhanushika Ratnayake			
Contribution to the Paper	Characterize the polyQ80-GFP-v2A-GFP construct			
Signature	<table border="1"> <tr> <td></td> <td>Date</td> <td>30-04-2018</td> </tr> </table>		Date	30-04-2018
	Date	30-04-2018		



Name of Co-Author	Michael Lardelli
Contribution to the Paper	Design of the constructs, supervision, manuscript drafting 
Signature	
Date	1/5/2018

**Title: Ratiometric assays of autophagic flux in zebrafish for analysis of familial Alzheimer's disease-like mutations**

**Authors:** Haowei Jiang<sup>1,\*</sup>, Morgan Newman<sup>1</sup>, Dhanushika Ratnayake<sup>1,2</sup>, Michael Lardelli<sup>1</sup>

**Affiliations:** <sup>1</sup>University of Adelaide, School of Biological Sciences, Alzheimer's Disease Genetics Laboratory, North Terrace, Adelaide, SA 5005, AUSTRALIA

<sup>2</sup>Current Address: Monash University, Australian Regenerative Medicine Institute, Wellington Road, Clayton 3800, AUSTRALIA

**\*Corresponding Author:** Haowei Jiang, University of Adelaide, School of Biological Sciences, Alzheimer's Disease Genetics Laboratory, North Terrace, Adelaide, SA 5005, AUSTRALIA. Email: [haowei.jiang@adelaide.edu.au](mailto:haowei.jiang@adelaide.edu.au)

**Key words:** autophagy, familial Alzheimer's disease, PRESENILIN genes, zebrafish

**Abbreviations:** A $\beta$ , amyloid- $\beta$ ; AD, Alzheimer's Disease; APP, Amyloid beta A4 protein; Atg, autophagy-related gene; AV, autophagic vacuole; CQ, chloroquine; GFP, green fluorescent protein; LC3, microtubule-associated protein 1 light chain 3; PE, phosphatidylethanolamin; polyQ, poly-glutamine; PSEN, presenilin; Rapa, rapamycin

**Financial Disclosure Statement:** This research was supported by grants from the National Health and Medical Research Council of Australia, GNT1061006 and GNT1126422, and by funds from the School of Biological Sciences of the University of Adelaide. HJ is supported by an Adelaide Scholarship International from the University of Adelaide.

**Conflict of Interest Statement:** The authors declare no conflict of interest.

## Abstract

Protein aggregates such as those formed in neurodegenerative diseases can be degraded via autophagy. To assess changes in autophagic flux in zebrafish models of familial Alzheimer's disease (fAD) mutations, we first developed a transgene, polyQ80-GFP-v2A-GFP, expressing equimolar amounts of aggregating polyQ80-GFP and a free GFP internal control in zebrafish embryos and larvae. This assay detects changes in autophagic flux by comparing the relative strength of polyQ80-GFP and free GFP moiety signals on western immunoblots probed with an antibody detecting GFP. However, the assay's application is limited by the toxicity of polyQ80-GFP, and because aggregation of this protein may, itself, induce autophagy. To overcome these issues, we subsequently developed a similar ratiometric assay where expression of a GFP-Lc3a-GFP transgene generates initially equimolar amounts of GFP-Lc3a (directed to autophagic degradation) and a free GFP internal control. The sensitivity of this latter assay is reduced by a cellular protease activity that separates Lc3a from GFP-Lc3a, thus contributing to the apparent free GFP signal and somewhat masking decreases in autophagic flux. Nevertheless, the assay demonstrates significantly decreased autophagic flux in zebrafish lacking *presenilin2* gene activity supporting that the Presenilin2 protein, like human PRESENILIN1, plays a role(s) in autophagy. Zebrafish heterozygous for a typical fAD-like, reading-frame-preserving mutation in *psen1* show decreased autophagic flux consistent with observations in mammalian systems. Unexpectedly, a zebrafish model of the only confirmed reading-frame-truncating fAD

mutation in a human *PRESENILIN* gene, the K115Efs mutation of human *PSEN2*, shows possibly increased autophagic flux in young zebrafish (larvae).

## **Introduction**

Autophagic/lysosomal dysfunction is thought to be involved in the neurodegenerative process of Alzheimer's disease (AD) (Boland, Kumar et al. 2008). The endosomal-lysosomal system is a prominent site for the processing of the AMYLOID BETA A4 PRECURSOR PROTEIN (APP) to form the aggregating peptide amyloid $\beta$  (A $\beta$ ) (Orr and Oddo 2013), which is the major component of the amyloid plaques observed in AD brains. Autophagic vacuoles (AVs) are thought to be the major reservoirs of intracellular A $\beta$ , and accumulation of immature AVs has been detected in AD brains, suggesting that the maturation of AVs to lysosomes may be impaired (Nixon, Wegiel et al. 2005; Yu, Cuervo et al. 2005). Both full-length APP and  $\beta$ -secretase-cleaved APP are found in such AVs, which are also highly enriched in PRESENILIN (PSEN) proteins (Area-Gomez, de Groof et al. 2009) (components of the  $\gamma$ -secretase complexes that cleave APP to form A $\beta$ ) suggesting that a link may exist between A $\beta$  production and cell survival pathways through activated autophagy in AD. The A $\beta$  accumulation is thought to be induced by the combination of increased autophagy induction and defective clearance of A $\beta$ -generating AVs (Boland, Kumar et al. 2008).

Dominant mutations in the *PRESENILIN (PSEN)* genes cause the majority of familial, early onset AD (fAD, (Pottier, Hannequin et al. 2012)). We have previously argued that a body of evidence supports that the AD-relevant effect of these mutations may be to alter the activity of PSEN holoproteins rather than the endoproteolysed forms that are active in the  $\gamma$ -secretase complexes that cleave APP (Jayne, Newman et al. 2016). Indeed, in 2010 Lee et al. showed that changes in PSEN1 holoprotein function, rather than  $\gamma$ -secretase activity, appear to affect lysosomal function in *PSEN1* fAD mutant human fibroblasts (Lee, Yu et al. 2010). However, the effects of *PSEN* fAD mutations on autophagy are currently debated (Zhang, Garbett et al. 2012) and it has not yet been shown that the related protein, PSEN2, plays a role in autophagic flux. Thus, the roles of the multifunctional PSEN proteins in cellular function and AD require further investigation.

Non-mammalian animal models including the zebrafish can facilitate AD research through development of rapid, novel assays for cellular processes such as autophagy. An excellent example is the fluorescent protein-based assay published by Kaizuka et al in 2016 that allows qualitative visualization of differences in autophagic flux within cells (Kaizuka, Morishita et al. 2016). However, it is also desirable to make simple, quantitative assessments of relative differences in autophagic flux in whole tissues/animals e.g. when these are subjected to different drug treatments or have different genotypes. In this paper we describe the development of two, internally-controlled assays using zebrafish embryos/larvae that allow rapid quantitative

comparison of relative autophagic flux using western immunoblotting. We describe exploitation of the superior of these two assays to demonstrate that activity of the zebrafish *PSEN2*-orthologous gene, *psen2*, is required for efficient autophagy. We also investigate changes in autophagic flux in two novel zebrafish models of fAD-like mutations in the human *PSEN* genes. While a typical, reading frame-preserving fAD-like mutation in zebrafish *psen1* significantly decreases autophagic flux, a model of the only known reading frame-truncating *PSEN* fAD mutation does not and may possibly increase autophagic flux in young fish.

## **Methods and Materials**

### **Zebrafish husbandry and animal ethics**

All the wild-type and mutant zebrafish were maintained in a recirculated water system. All work with zebrafish was conducted under the auspices of the Animal Ethics Committee of the University of Adelaide.

### **Construction of the polyQ80-GFP-v2A-GFP transgene**

A DNA sequence coding for polyQ80-GFP-v2A-GFP (Figure 2A and S1 File A) was synthesized by Biomatik Corp. and subsequently ligated into the pT2AL200R150G (Tol2 transposon-based) (S1 File D) gene transfer vector for expression from the

ubiquitously-transcribed elongation factor 1 alpha promoter (EF1 $\alpha$ -p) (Clark, Urban et al. 2011). The polyQ80-GFP-v2A-GFP transgene codes for two proteins, an 80-residue polyglutamine repeat sequence (polyQ80) fused to the N-terminal of GFP protein as well as a free GFP protein. A viral 2A peptide (v2A) sequence between the two GFP sequences allows their synthesis as separate entities by a “ribosomal-skip” mechanism (Provost, Rhee et al. 2007). Thus, translation of polyQ80-GFP-v2A-GFP mRNA gives 1:1 stoichiometric synthesis of polyQ80-GFP and free GFP. PolyQ80-GFP subsequently aggregates and should be degraded by autophagy, while the free GFP remains soluble in the cytosol to act as an internal control.



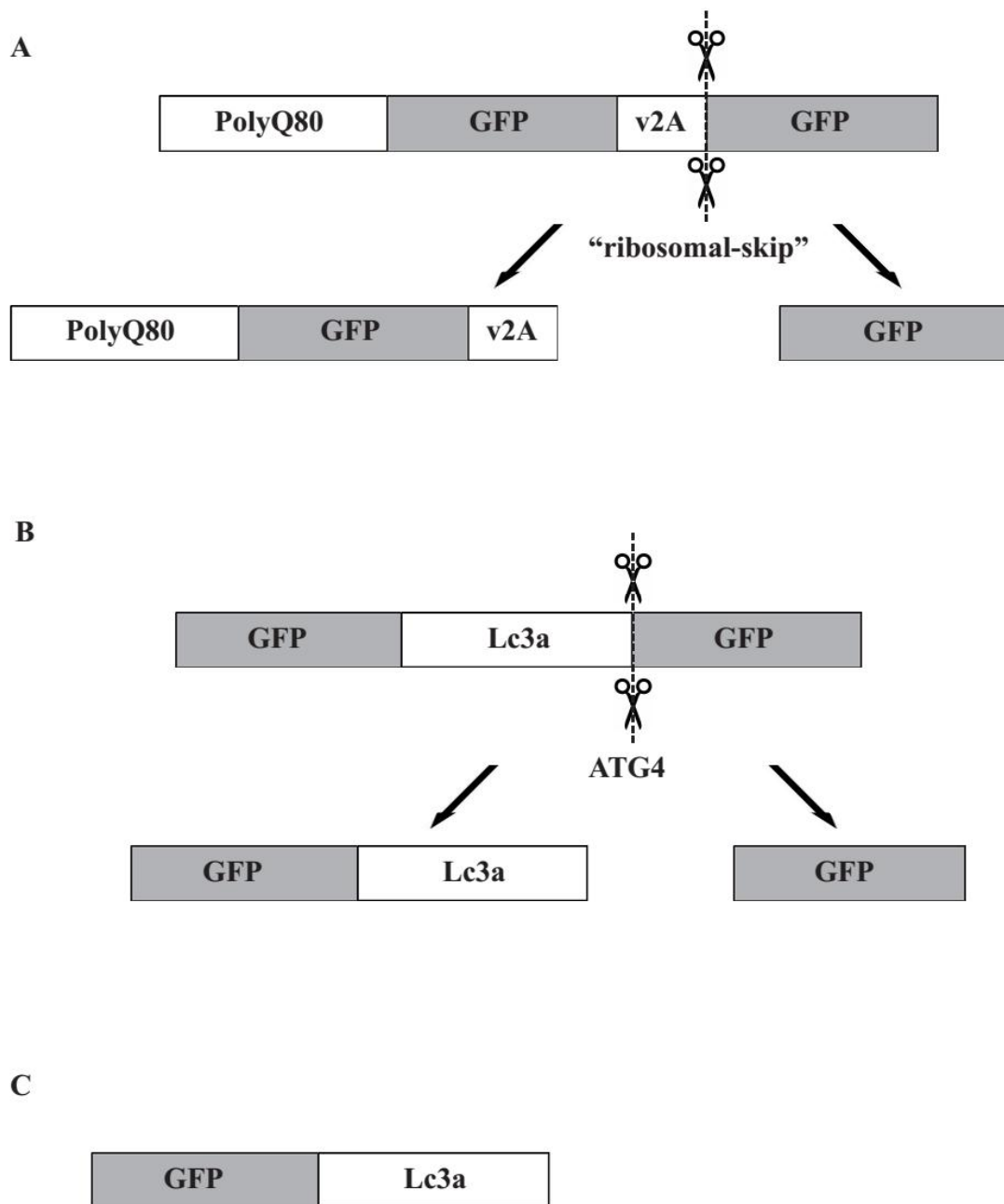


**Figure 2. Design of three GFP-based constructs for assay of autophagic flux.**

(A) Transgene PolyQ80-GFP-v2A-GFP.

(B) Transgene GFP-Lc3a-GFP.

(C) Transgene GFP-Lc3a.

**Construction of the GFP-Lc3a-GFP transgene**

A sequence coding for GFP-Lc3a-GFP (Figure 2B and S1 File B) was synthesized by Biomatik and ligated into the pT2AL200R150G (Kawakami 2007) gene transfer vector (S1 File D). This construct encodes a fusion protein where GFP is linked to the N-terminal of zebrafish Lc3a which, at its C-terminal, is linked to an additional GFP. When this transgene is expressed in cells, the most C-terminal glycine residue of Lc3a is cleaved by an endogenous ATG4 family protease, producing equimolar amounts of GFP-Lc3a and free GFP. GFP-Lc3a is conjugated to PE and localizes to autophagosomes (Kaizuka, Morishita et al. 2016). The GFP-Lc3a molecules attached to the autophagosomal inner membrane are subsequently degraded after fusion with lysosomes, while those on the outer membrane are deconjugated by Atg4 proteins and recycled back to the cytosol. The free GFP exists in the cytoplasm and functions as an internal control. Relative autophagic activity is measured as changes in the ratio of GFP-Lc3a / free GFP via western immunoblotting.

### **Construction of the GFP-Lc3a transgene**

The GFP-Lc3a transgene (Figure 2C and S1 File C) in the pT2AL200R150G vector was derived from GFP-Lc3a-GFP by PCR amplification using 5'-phosphorylated primers to exclude the downstream GFP coding sequence followed by ligation to recircularise the plasmid. The sequences of the PCR primers used were 5'-TAGATCGATGATGATCCAGACATGA-3' and 5'-GCAGCCGAAGGTCTCCT-3'.

## Zebrafish embryos

Three mutations were involved in our research, a putatively null mutation in zebrafish *psen2*, *psen2*<sup>S4Ter</sup>, a model of a typical reading-frame-preserving fAD-type mutation in *psen1*, *psen1*<sup>Q96K97del</sup>, and a model of human *PSEN2*<sup>K115Efs</sup> (Jayadev, Leverenz et al. 2010), *psen1*<sup>K97Gfs</sup>. Descriptions of the generation of these mutations were listed in S3 File.

Five different genotypes of zebrafish embryos, Tübingen (TU) wildtype (+/+), putatively *psen2* null heterozygous (*psen2*<sup>S4Ter/+</sup>), putatively *psen2* null homozygous (*psen2*<sup>S4Ter/psen2</sup><sup>S4Ter</sup>), *psen1*<sup>Q96K97del</sup> heterozygous (*psen1*<sup>Q96K97del/+</sup>), and *psen1*<sup>K97Gfs</sup> heterozygous (*psen1*<sup>K97Gfs/+</sup>), were spawned either by mass mating or pair-mating of individuals.

## Microinjection of zebrafish embryos

For the polyQ80-GFP-v2A-GFP assay, zebrafish zygotes were injected with ~5-10 nL of a solution containing 25ng/μL of the polyQ80-GFP-v2A-GFP transgene with 25ng/μL of Tol2 transposase mRNA (Clark, Urban et al. 2011). For the GFP-Lc3a-GFP and GFP-Lc3a assays, zebrafish zygotes were injected with ~5-10 nL of a solution of 50ng/μL of the GFP-Lc3a-GFP or GFP-Lc3a transgenes respectively with 25ng/μL of

the Tol2 transposase mRNA. The injected embryos were incubated at 28.5°C in E3 medium (2011). At ~24 hours post fertilization (hpf), embryos showing widely distributed GFP expression (as visualized by fluorescence microscopy) were selected for subsequent analysis (Figure 1).

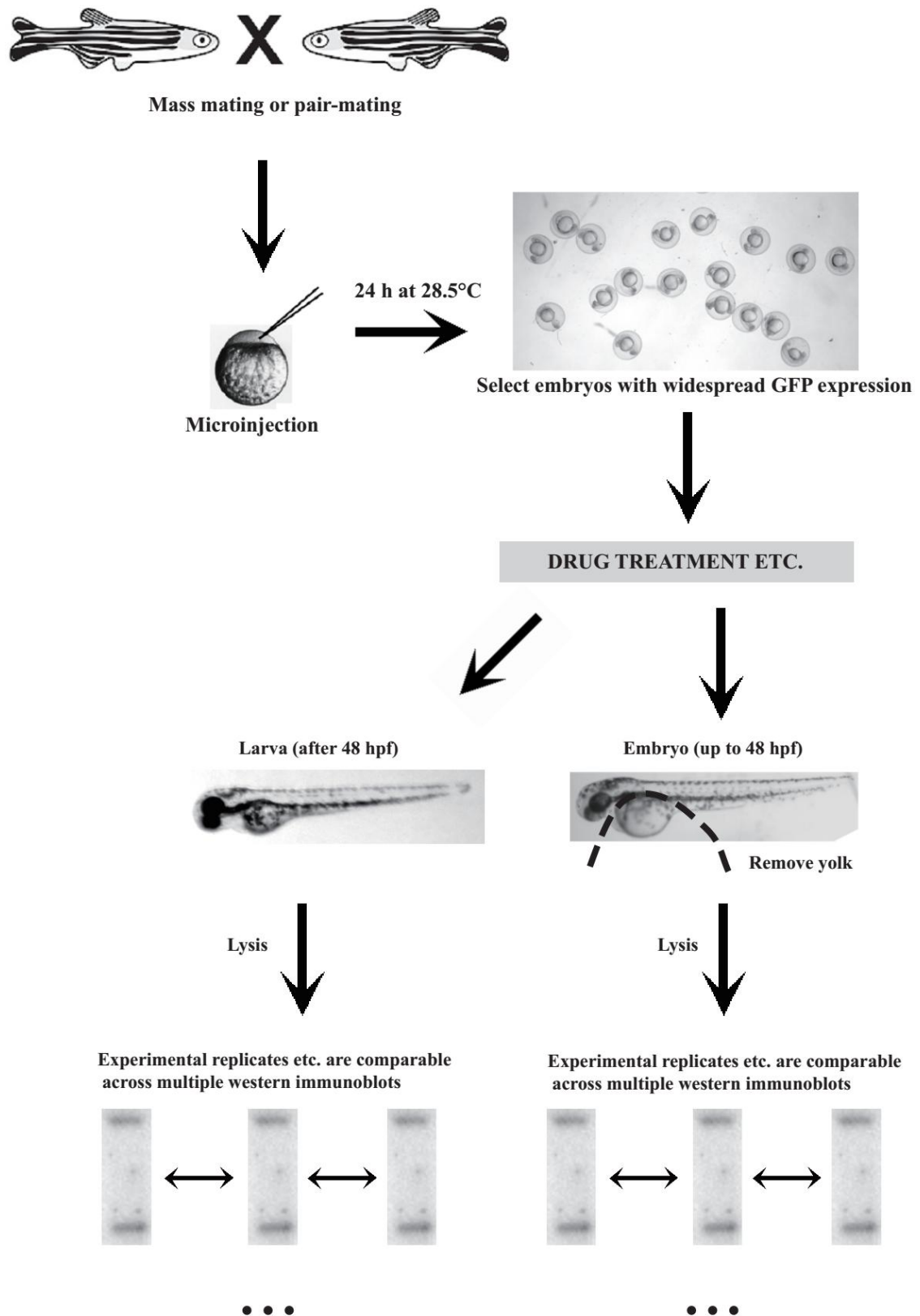


**Figure 1. Experimental flow chart.**

## **Rapamycin and Chloroquine treatments**

For the PolyQ80-GFP-v2A-GFP assay, GFP-expressing zebrafish embryos from microinjection of polyQ80-GFP-v2A-GFP were separated randomly into three groups at ~30 hpf. Two groups were treated with either 1 $\mu$ M rapamycin (Rapa) (SIGMA, R8781) or 50mM chloroquine (CQ) (SIGMA, C6628) from 30 hpf until 48 hpf, with one group remaining untreated as a control. The embryos were chilled and then lysed for western immunoblotting at ~48 hpf.

For the GFP-Lc3a-GFP assay (or GFP-Lc3a expression analysis) at 48 hpf in +/+ embryos, GFP-expressing zebrafish embryos from microinjection were separated randomly into four groups at ~24 hpf. Three of these groups were treated with rapamycin (1 $\mu$ M) or chloroquine (50 $\mu$ M or 50mM) from 30 hpf until 48 hpf, and the remaining group remained untreated as a control. The embryos were chilled and then lysed immediately for western immunoblotting at ~48 hpf.

For the GFP-Lc3a-GFP assay (or GFP-Lc3a expression analysis) at 96 hpf in +/+ larvae, GFP-expressing zebrafish embryos from microinjection were selected at ~24 hpf and randomly separated into several groups for treatment with rapamycin (1 $\mu$ M) or chloroquine (various concentrations) from 78 hpf until 96 hpf. Larvae were then chilled and lysed immediately for western immunoblotting at ~96 hpf.

## **Western immunoblot analyses**

48 and 52 hpf-old embryos were firstly dechorionated and deyolked and then placed in sample buffer (2% sodium dodecyl sulphate (SDS), 5%  $\beta$ -mercaptoethanol, 25% v/v glycerol, 0.0625 M Tris-HCl [pH 6.8], and bromophenol blue) (Ganesan, Moussavi Nik et al. 2014), heated immediately to 95°C for 10 min and then sonicated (Diagenode Bioruptor UCD-200) in an ice-water bath at high power mode for 10 min before loading onto polyacrylamide gels for electrophoresis (see below). The 96 hpf-old larvae were not deyolked before lysis in sample buffer.

Samples were loaded onto NuPAGE™ 4-12% Bis-Tris Protein Gels (Invitrogen, NP0323BOX), and the separated proteins were subsequently transferred to nitrocellulose membrane (BIO-RAD, 1620115) using the Mini Gel Tank and Blot Module Set (Life technologies, NW2000). The nitrocellulose membranes were subsequently blocked with blocking reagent (Roche, 11921681001) and then probed with the primary antibody, polyclonal anti-GFP goat (ROCKLAND™, 600-101-215), followed by secondary antibody, horseradish peroxidase (HRP) conjugated anti-goat antibody (ROCKLAND™, 605-703-125). Finally, bound antibody was detected by chemiluminescence using SuperSignal™ West Pico PLUS Chemiluminescent Substrate (ThermoFisher, 34580). The ChemiDoc™ MP Imaging System (Bio-Rad) was used to image all the western immunoblots. The intensity of each band from western immunoblots was measured by Image Lab™ Software (Bio-Rad). All these

intensity data are presented in S2 File.

### **Statistical tests**

For data sets with non-independent variables, one-way ANOVA was used if the data showed equal variances (Welch's ANOVA was used instead if the data showed unequal variances), followed by Games-Howell tests of significance between pairs of data columns.

For data sets with independent variables, F-tests were first applied between different groups of data. If the p value of the F-test was  $>0.05$ , reflecting no significant difference between the variances of two groups, then a two-tailed t-test assuming equal variances was applied to the two groups. If the p value of the F-test was  $<0.05$ , reflecting a significant difference between the variances of two groups, then a two-tailed t-test assuming unequal variances was applied to the two groups.

## **Results**

### **PolyQ80-based autophagy assay in zebrafish**

The viral 2A (v2A) system for simultaneous, stoichiometric expression of two peptides from single mRNA transcripts was first applied in zebrafish by Provost et al. (Provost,



Rhee et al. 2007). The presence of the v2A linker in a coding sequence causes ribosomes to “skip” production of a peptide bond without terminating translation. We sought to exploit this to adapt Ju et al.’s polyQ80-based assay of autophagic flux (described in 2009) to zebrafish. Ju et al expressed fusions to luciferase of aggregating polyQ80 and non-aggregating polyQ21 in separate thigh muscles of mice (Ju, Miller et al. 2009). As a more direct measure of protein concentration we sought to measure by western immunoblotting the relative amounts of a polyQ80-GFP fusion and free GFP when these are translated in a 1:1 ratio from a single mRNA (Figureures 1 and 2A). The polyQ80-GFP-v2A-GFP transgene expressing these proteins is carried in a Tol2 transposon vector and introduced into fertilized zebrafish eggs by microinjection together with transposase mRNA (see Materials and Methods, Figure 2A) (Note: We initially developed a polyQ80-GFP-v2A-mCherry-based system but this required immunoblotting against GFP followed by stripping and reprobing the blot to detect mCherry, and the expression ratios thus produced were then only comparable between the samples on individual blots – data not shown.) To allow stable propagation of the polyQ80-GFP-v2A-GFP transgene in *Escherichia coli* (i.e. to avoid recombination between the directly repeated GFP coding sequences) we introduced numerous silent mutations into the degenerate codon positions in the downstream, free GFP coding sequence (see Supplementary Data File 1).

Injection of the polyQ80-GFP-v2A-GFP transgene into fertilized zebrafish eggs results in its widespread insertion into the chromosomes of embryonic cells. Expression of

GFP is detectable for weeks afterwards although the transgene does not appear to transmit through the germline (data not shown). Western immunoblotting of embryos (up to 48 hours post fertilization, hpf) or larvae (after 48 hpf) from these injected eggs identified three expected bands of protein: a small fraction of full-length polyQ80-GFP-v2A-GFP, and greater amounts of separated polyQ80-GFP and free GFP proteins (Figure 3A).

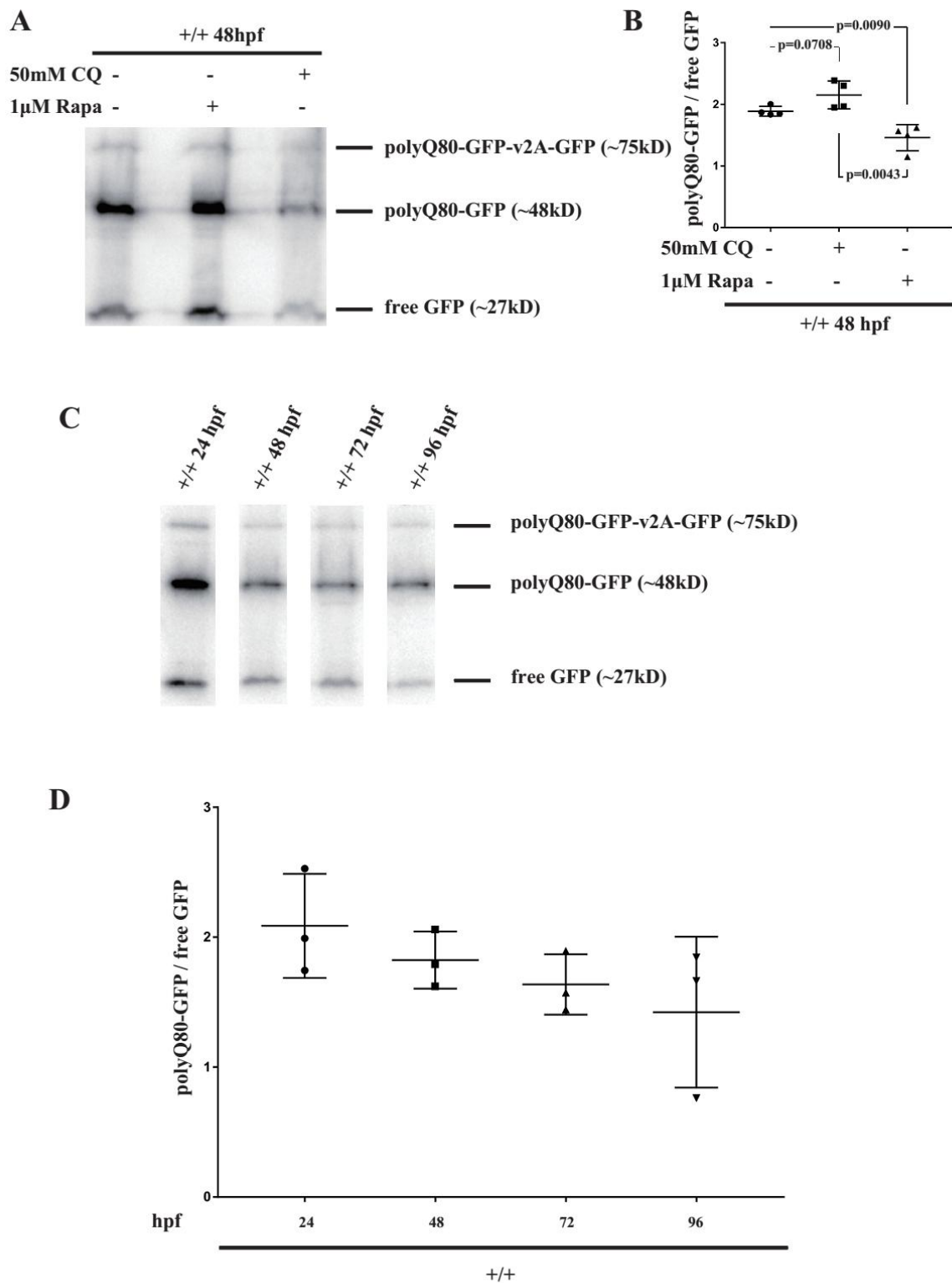


**Figure 3. polyQ80-GFP-v2A-GFP assay of autophagy.**

(A) Western immunoblots from polyQ80-GFP-v2A-GFP-injected +/+ embryos at 48 hpf after treatment with rapamycin (Rapa) or chloroquine (CQ).

(B) Ratios (polyQ80-GFP / free GFP) in polyQ80-GFP-v2A-GFP-injected +/+ embryos at 48hpf after treatment with Rapa or CQ. Means with standard deviations (SDs) are shown. p-values are from two-tailed t-tests assuming equal variance (shown by results of F-tests).

(C) Western immunoblots from polyQ80-GFP-v2A-GFP-injected +/+ embryos at 24 hpf, 48 hpf, 72 hpf, and 96 hpf.

(D) Ratios (polyQ80-GFP / free GFP) in polyQ80-GFP-v2A-GFP-injected +/+ embryos at 24 hpf, 48 hpf, 72 hpf, and 96 hpf. Means with SDs are indicated. The p value from a one-way ANOVA is  $0.266 > 0.05$ , indicating that no significant difference in autophagic flux was found over the different time points.

An advantage of zebrafish over mammalian models is the easy treatment of their living embryos with drugs by placement of these in the embryos' aqueous support medium for direct absorption. (The absorption of less soluble drugs can be facilitated by co-exposure to 1% DMSO, e.g. (Grunwald and Eisen 2002)). To test whether polyQ80-GFP was being degraded by autophagy selectively relative to free GFP we sought to enhance autophagy induction or block autophagic flux using rapamycin, (Fleming and Rubinsztein 2011) or chloroquine (Yoon, Cho et al. 2010). Both drugs have previously been used successfully to modulate autophagy in zebrafish (Fleming and Rubinsztein 2011; Cui, Sim et al. 2012).

In zebrafish embryos, autophagy is up-regulated at the pharyngula stage (24~48 hpf), and the earliest time point at which the phosphatidylethanolamin (PE)-Lc3-II conjugate (critical for autophagy induction) has been detected is 32 hpf (He, Bartholomew et al. 2009). Therefore, in our research, injected embryos were exposed to 1 $\mu$ M rapamycin or 50mM chloroquine from 30 hpf before lysis at 48 hpf for analysis. The ratios of polyQ80-GFP to free GFP observed from both drug treatments compared to non-treatment controls are presented in Figure 3B. The ratio (poly80Q-GFP / free GFP) was significantly reduced through rapamycin treatment ( $p=0.0090$ ), indicating that autophagy was induced. The ratio (poly80Q-GFP / free GFP) was apparently increased through chloroquine treatment ( $p=0.0708$ ), consistent with inhibition of autophagy. Since the changes in the ratios of poly80Q-GFP / free GFP are consistent with the changes in autophagy expected from these different drug treatments, the polyQ80-GFP-v2A-GFP assay appears able to measure autophagic flux in zebrafish.

The polyQ80-GFP / free GFP ratio observed from the polyQ80-GFP-v2A-GFP transgene possibly decreases between 24 hpf and 96 hpf as indicated by a statistically non-significant trend (Figure 3C and 3D) Also, we noticed that this assay itself is somewhat toxic to zebrafish embryos with approximately half of the injected embryos showing abnormal development at 24 hpf (data not shown). This may be due to the previously observed toxicity of polyglutamine proteins in zebrafish (Schiffer, Broadley et al. 2007; van Bebber, Paquet et al. 2010). Furthermore, in 2007, Schiffer et al. reported that polyQ102-GFP could aggregate to form large SDS-insoluble inclusions,

while free GFP was observed to be produced by removal of polyQ moieties from polyQ-GFP fusion proteins (Schiffer, Broadley et al. 2007). All these phenomena might introduce unanticipated variability into observed polyQ80 / free GFP ratios (although this can be overcome somewhat by the extensive experimental replication that is facilitated by use of the zebrafish model system). For this reason we sought a less-toxic, aggregation-independent, but still internally-controlled alternative assay system.

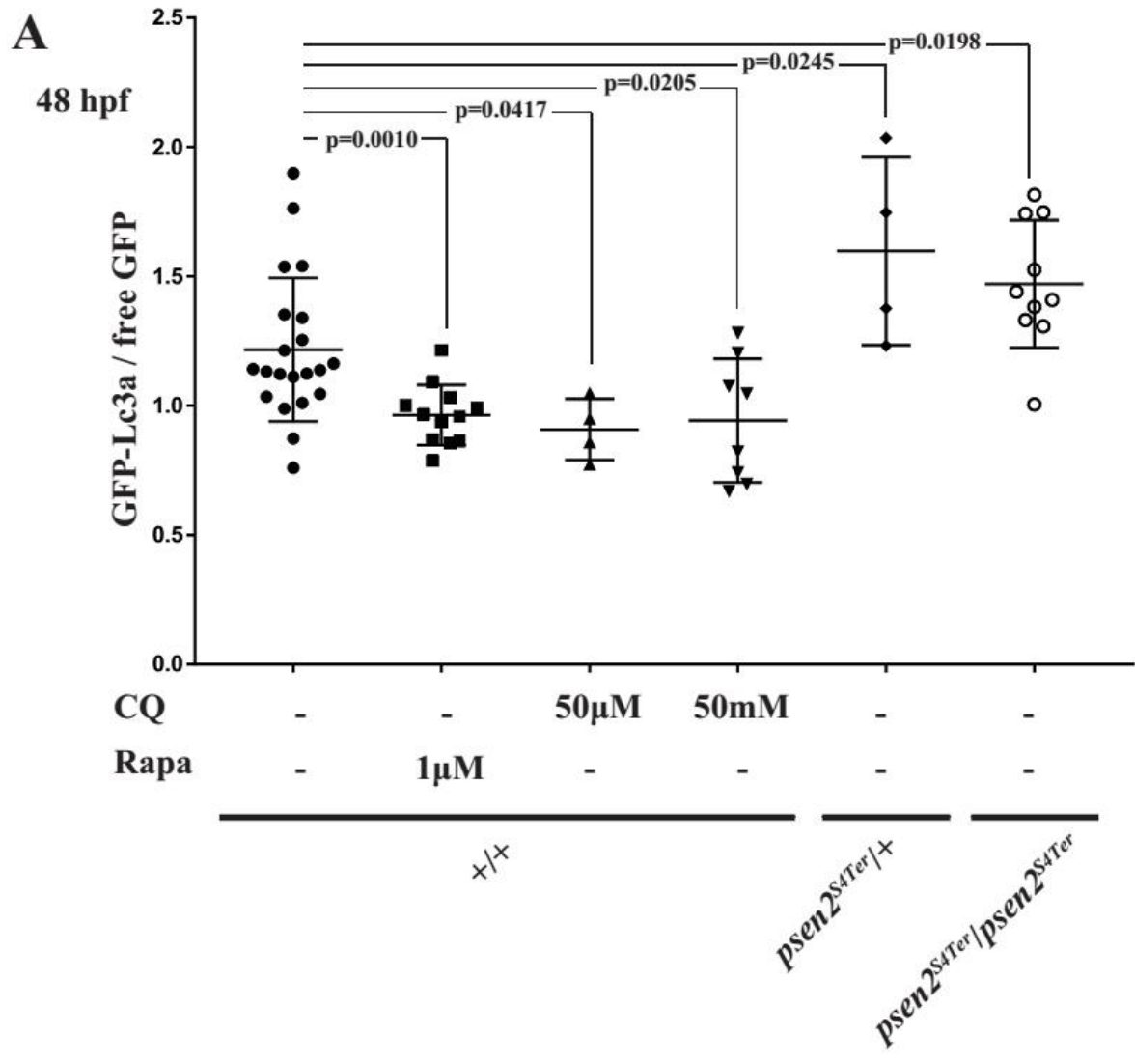
### **GFP-LC3-GFP probe to quantify autophagic flux by western immunoblotting**

In 2016, Kaizuka et al. (Kaizuka, Morishita et al. 2016) described constructs to visualize autophagic flux in zebrafish embryos. Their GFP-LC3-RFP fusion protein is cleaved into separate GFP-LC3 and RFP proteins by embryos' endogenous ATG4 activity. The GFP-LC3 then associates with autophagosomes while the RFP acts as an internal control.

We wished to adapt the assay from Kaizuka et al. to allow quantification of autophagic flux by western immunoblotting while avoiding the difficulties posed by use of polyQ80-GFP. However, we knew from previous unpublished work with GFP-v2A-RFP fusion proteins that use of an RFP internal control for normalization of GFP expression is problematic since results are only comparable between samples on the same immunoblot. This difficulty could be overcome if GFP served both as autophagy target and as the internal control. Therefore we applied the tandem GFP principle of the

polyQ80-GFP-v2A-GFP construct to create GFP-LC3-GFP. This is cleaved by ATG4 within cells to give, initially, equimolar amounts of GFP-LC3 and free GFP proteins (Figure 2B). When assayed, these proteins have discernibly different molecular masses identifiable on western immunoblots probed with a single anti-GFP primary antibody (Figure 2B). The mean GFP-Lc3a / free GFP ratio observed in wild type (+/+) embryos at 48 hpf is slightly higher than at 96 hpf (1.22 vs 1.13 in Figure 5A and 5B respectively). However, similar to the polyQ80-GFP-v2A-GFP assay, this difference is not statistically significant ( $p=0.42$ ).

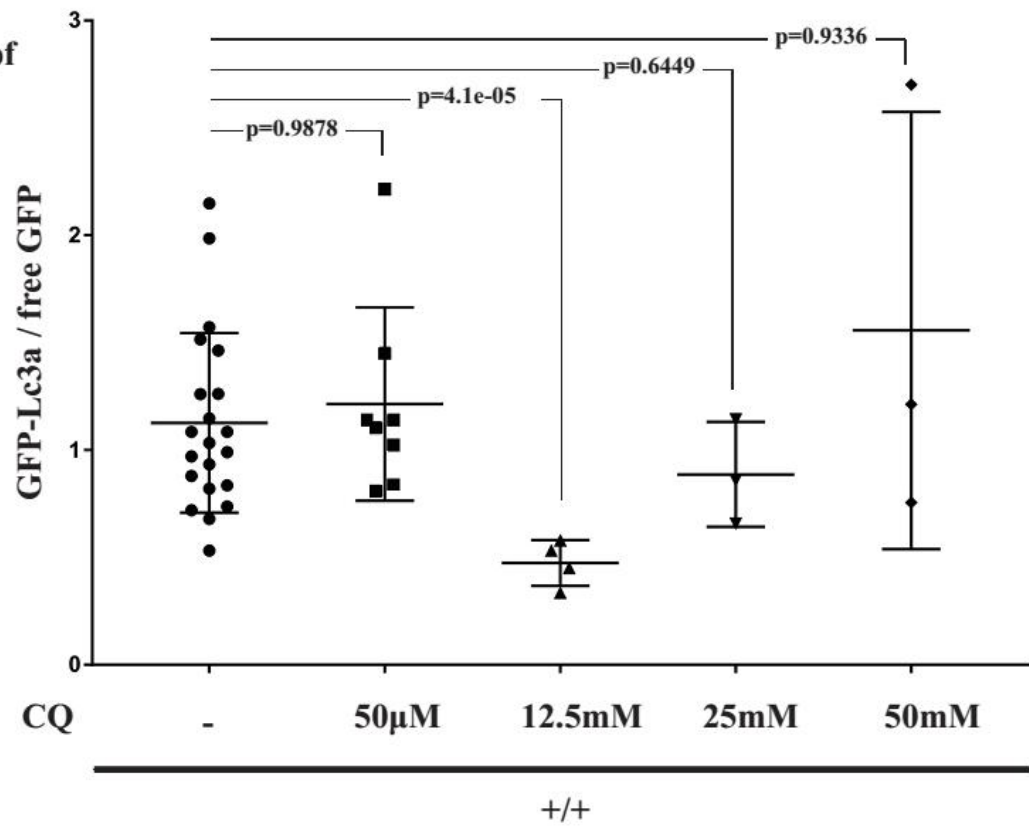
To test whether changes in the GFP-Lc3a / free GFP ratio reflect changes in autophagic flux, the GFP-Lc3a-GFP construct was expressed in embryos subjected to treatment with rapamycin or chloroquine. Treatment with rapamycin produced a significant decrease in the GFP-Lc3a / free GFP ratio ( $p=0.001$ , Figure 5A), reflecting the expected increase in autophagy. Unexpectedly, treatment with chloroquine, both at high (50mM) and low (50 $\mu$ M) concentrations resulted in significant decreases in the GFP-Lc3a / free GFP ratio (Figure 5A). This apparent increase in autophagy conflicted with chloroquine's activity as an autophagy inhibitor, which implied that an unanticipated factor could be distorting the observed ratio during the chloroquine treatments.





**B**

96 hpf



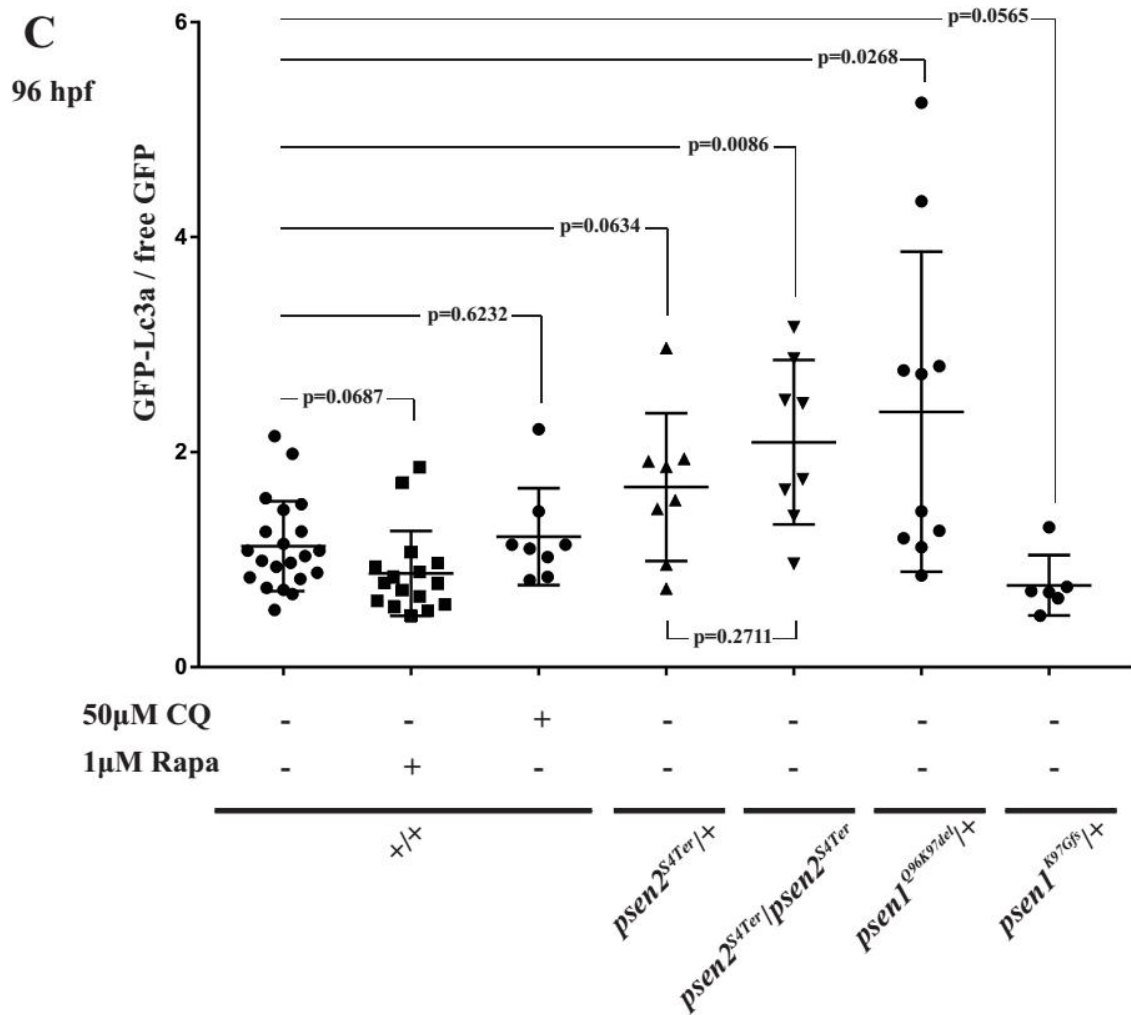


**Figure 5. Ratios (GFP-Lc3a / free GFP) from the GFP-Lc3a-GFP assay of autophagy.**

(A) Embryos at 48 hpf. +/+ embryos were treated with rapamycin, Rapa, or various concentrations of chloroquine, CQ. *psen2<sup>S4Ter</sup>* mutant embryos were not treated with these drugs. p-values are from two-tailed t-tests assuming either equal or unequal variances as appropriate.

(B) +/+ embryos at 96 hpf after treatment with various concentrations of chloroquine. The p value from Welch's ANOVA is  $0.04 < 0.05$ , showing that there was significant difference in autophagic flux over the concentrations of chloroquine treatment. p-

values from following Games-Howell tests are presented.

(C) Zebrafish embryos of various genotypes at 96 hpf. Only +/+ embryos were treated with rapamycin or chloroquine as indicated. p-values are from two-tailed t-tests assuming either equal or unequal variances as appropriate.

After investigating the scientific literature we discovered a report from Ni et al. in 2011 describing that both chloroquine and rapamycin treatments of HeLa cells can cause increased lysosomal pH and cleavage of GFP-LC3 to release free GFP (similar to the removal of polyQ from polyQ-GFP as observed by Schiffer et al (Schiffer, Broadley et al. 2007)). If this form of cleavage also existed in zebrafish it might provide an additional source of free GFP that would affect observed GFP-Lc3a / GFP ratios in embryos expressing the GFP-Lc3a-GFP assay transgene. To test this possibility we constructed a simple fusion of GFP to Lc3a by deleting the downstream GFP coding sequences from the GFP-Lc3a-GFP transgene to create GFP-Lc3a (Figure 2C). The GFP-Lc3a transgene was then expressed in zebrafish embryos in the same way as for GFP-Lc3a-GFP and the rapamycin and chloroquine treatments were then repeated. At 48 hpf, free GFP (i.e. not fused to Lc3a) can clearly be observed on western immunoblots (Figure 6A), confirming that a protease activity that separates GFP from Lc3a exists in zebrafish. Interestingly, the GFP-Lc3a protein from this transgene is apparently observable as both GFP-Lc3a-I and GFP-Lc3a-II forms whereas we have only observed a single form of GFP-Lc3a protein when this is produced from the GFP-

Lc3a-GFP transgene. A similar observation was made by Kaizuka et al. (Kaizuka, Morishita et al. 2016) for expression of GFP-LC3 from their GFP-LC3-RFP-LC3 $\Delta$ G construct when this was expressed from a transgene (as our protein fusions are) rather than from injected mRNA. The free-GFP derived from our GFP-Lc3a transgene is certainly non-negligible relative to the observed GFP-Lc3a-I (e.g. in untreated, wild type embryos, see Figure 6A) at 48 hpf. This implies that free GFP from cleavage of GFP-Lc3a may significantly affect GFP-Lc3a / GFP ratios from GFP-Lc3a-GFP-injected embryos at this developmental time point. When we observed cleavage of GFP-Lc3a in 96 hpf larvae, far less free GFP was seen relative to GFP-Lc3a-I. Therefore, the ratio of GFP-Lc3a to GFP may be less distorted by free GFP from cleavage of GFP-Lc3a at 96 hpf.

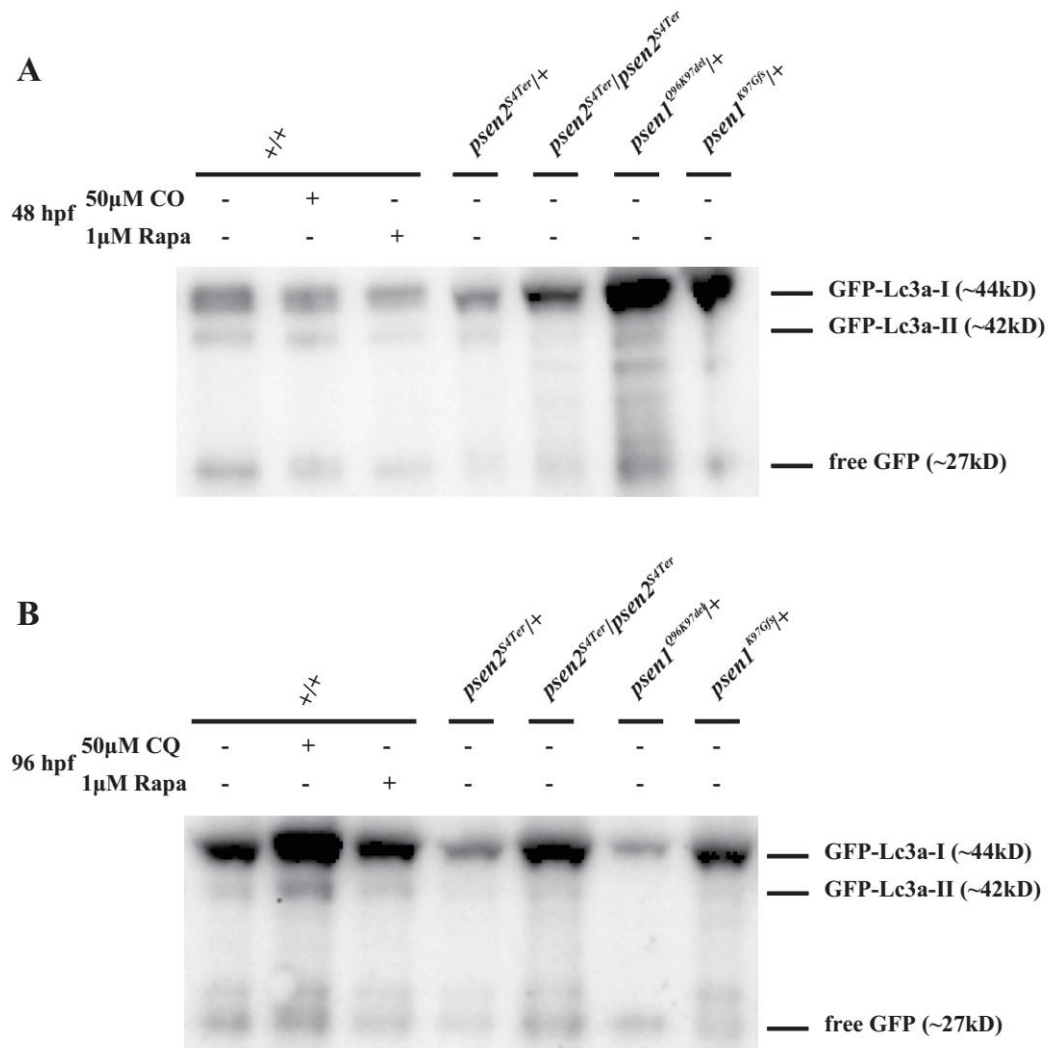


**Figure 6. Western immunoblots from GFP-Lc3a-injected embryos and larvae.**

(A) 48 hpf and (B) 96 hpf respectively. +/+ embryos and larvae were also treated with rapamycin (Rapa) or chloroquine (CQ) as indicated.

When we repeated the chloroquine treatments on GFP-Lc3a-GFP transgene-injected zebrafish embryos with lysis at 96hpf we then observed a slightly increased GFP-Lc3a / free GFP ratio at the lowest chloroquine dosage (50μM) although without apparent statistical significance ( $p=0.6232$ , Figure 5B). At higher concentrations of chloroquine

(12.5 mM and above) the GFP-Lc3a / free GFP ratio was decreased or was very variable (Figure 5B). Ni et al. reported that saturating doses of chloroquine in HeLa cells are able to block GFP-LC3 cleavage completely (Ni, Bockus et al. 2011) and this may also be occurring in some zebrafish embryos treated with 50 mM chloroquine. A large proportion of larvae (~80%) were dead at 96 hpf after the 50mM chloroquine treatment indicating high lethality of this chloroquine concentration.

We conclude that exploitation of the GFP-Lc3a-GFP assay is best performed at 96hpf or later to minimize the influence of generation of free GFP from cleavage of GFP-Lc3a. Generation of free GFP from cleavage of GFP-Lc3a reduces the sensitivity of the GFP-Lc3a-GFP construct for detecting decreases in autophagic flux.

### **Autophagic flux in zebrafish *psen* mutants expressing GFP-Lc3a-GFP**

Our tests of the GFP-Lc3a-GFP assay indicated that, when used at 96 hpf, it can reveal changes in autophagic flux without the toxicity and other problems encountered with the aggregation-based polyQ80-GFP-v2A-GFP assay. Therefore, we exploited the GFP-Lc3a-GFP assay to examine autophagic flux changes in a number of zebrafish *presenilin* mutants that we have generated in our laboratory (S3 File). These are: a typical fAD-like mutation in *psen1* lacking two codons but preserving the open reading frame, *psen1*<sup>Q96K97del</sup>; a putatively null mutation of the *psen2* gene, *psen2*<sup>S4Ter</sup>; and a zebrafish model of the unique, open reading frame-truncating PSEN fAD mutation *PSEN2*<sup>K115Efs</sup> (Jayadev, Leverenz et al. 2010). We have previously suggested that this

latter mutation causes fAD by inappropriate mimicry of expression of an hypoxia-induced, naturally-occurring truncated isoform of PSEN2 denoted PS2V (Moussavi Nik, Newman et al. 2015). In zebrafish, the PS2V-equivalent isoform is expressed from the *PSEN1*-orthologous gene, *psen1*. Therefore, we have modeled this mutation in zebrafish by generation of the *psen1* allele, *K97Gfs*.

The effects of the fAD-like mutations were tested in the heterozygous state corresponding to the dominant inheritance pattern shown by such mutations in humans. The effects of the putatively null mutation of *psen2* were tested in both homozygous and heterozygous embryos to examine, respectively, whether *psen2* activity has any effect on autophagy and whether this effect is haploinsufficient. Fertilized eggs bearing *presenilin* mutations were injected with the GFP-Lc3a-GFP transgene and then examined by western immunoblotting at 96 hpf (Figure 5C). Both heterozygosity for the fAD-like *psen1*<sup>*Q96K97del*</sup> mutation and loss of *psen2* activity were observed to decrease autophagic flux significantly ( $p=0.0268$  and  $p=0.0086$  respectively) as expected from previous analysis of fAD mutations in human *PSEN1* (Lee, Yu et al. 2010) and confirming that *psen2* also functions in autophagy. Heterozygosity for the putatively null mutation in *psen2* also appeared to reduce the GFP-Lc3a / free GFP ratio indicating decreased autophagic flux although this did not reach statistical significance ( $p=0.063$ ).

## Discussion

To monitor autophagic flux in zebrafish embryos, we first designed the polyQ80-GFP-v2A-GFP assay that is based on the assumption that polyQ80-GFP aggregates and is a target for autophagy while free GFP is primarily degraded via the proteasome. Since this assay provides 1:1 stoichiometric co-expression of polyQ80-GFP and free GFP protein within the same cells *in vivo* it should reflect changes in autophagic flux by changes in the ratio of polyQ80-GFP / free GFP as observed by western immunoblotting. Since both the polyQ80-GFP and the free GFP protein are detected simultaneously by the same primary antibody, polyQ80-GFP / free GFP ratios can be compared on separate immunoblots which greatly facilitates experimental replication and statistical analysis. Unfortunately, due to an error at the beginning of this project, the concentration of the chloroquine treatment used for manipulating the autophagic flux (50mM) was 1,000-fold higher than it should have been (50 $\mu$ M). However, the results (Figure 3) showed that the polyQ80-GFP-v2A-GFP assay was still revealed inhibition caused by treatment with chloroquine treatment at the extremely high concentration, possibly due to the internal control involved in this assay. While the rapamycin and chloroquine treatments of embryos injected with the polyQ80-GFP-v2A-GFP transgene produced ratio changes indicative of the expected changes in autophagic flux, the aggregation of polyQ80 may, itself, induce autophagy and this would limit the assay's sensitivity. This issue was overcome by replacing the polyQ80-GFP protein with a non-aggregating GFP-Lc3a fusion protein, based on the approach taken by Kaizuka et al. (Kaizuka, Morishita et al. 2016). Like the polyQ80-GFP-v2A-GFP construct, the GFP-Lc3a-GFP construct



produces 1:1 stoichiometric co-expression of two proteins in the same cells *in vivo* (GFP-Lc3a and free GFP proteins).

The GFP-Lc3a-GFP assay assumes that GFP-Lc3a protein is a target of autophagy while the free GFP protein remains in the cytosol as an internal control. However, the GFP-Lc3a-GFP transgene should not affect autophagic flux itself nor TORC1 activity as the related GFP-LC3-RFP-LC3 $\Delta$ G construct of Kaizuka et al. did not appear to do so (Kaizuka, Morishita et al. 2016). Nevertheless, the GFP-Lc3a-GFP assay has its own particular limitations. Cleavage of LC3 away from GFP was reported in HeLa cells when lysosomal pH was increased by chloroquine or rapamycin treatments (Ni, Bockus et al. 2011). Consistent with this, we also saw production of free GFP by cleavage of GFP-Lc3a in zebrafish embryos and larvae (Figure 6A and 5B). Since the free GFP produced by GFP-Lc3a cleavage provided an additional source of free GFP, this could affect the measured ratio of GFP-Lc3a / free GFP and reduce the sensitivity of the assay to detect decreases in autophagic flux. We found that this effect was minimized at 96 hpf compared to 48 hpf. (Note that the observations by Schiffer et al. imply that polyQ80-GFP will also form free GFP by removal of polyQ80 in zebrafish embryos (Schiffer, Broadley et al. 2007).)

It is possible that development of a GFP-Lc3a-RFP-GFP transgene-based autophagy assay might overcome the insensitivity caused by generation of free GFP from GFP-Lc3a since an RFP-GFP fusion would be easy to identify separately from any free GFP

in western immunoblotting. The accumulation of free GFP versus GFP-Lc3a in such an assay would be additionally informative regarding autophagic flux versus lysosomal accumulation.

Using the GFP-Lc3a-GFP assay, we were able to compare the levels of autophagic flux in zebrafish mutant and wild type larvae. In *psen2*<sup>S4Ter</sup>/*psen2*<sup>S4Ter</sup> larvae, and possibly *psen2*<sup>S4Ter</sup>/+ larvae, we detected decreased autophagic flux (Figure 5C), supporting that *psen2*, like *psen1*, plays a role in regulating cells' autophagic activity. This has not previously been tested. However, we should note that, in terms of Psen2 protein's role in  $\gamma$ -secretase activity, our previous work has shown that zebrafish Psen2 plays a greater role in Notch signaling than its corresponding mammalian orthologue (Selkoe and Kopan 2003) and we cannot exclude that zebrafish Psen2 is more similar to Psen1 in its role in autophagy than mammalian PSEN2 is similar to PSEN1. In heterozygous larvae of the "typical" (reading frame-preserving) fAD mutation model *psen1*<sup>Q96K97del</sup>, we also observed decreased autophagic flux (Figure 5C).

The *K115Efs* mutation of human *PSEN2* is unique among the human *PRESENILIN* fAD mutations in that it truncates the open reading frame of the gene. Nevertheless, our unpublished analyses of aged adult fish modelling this mutation show similar alterations in expression of the genes responding to hypoxia to those seen in aged fish carrying the more "typical" fAD-like mutation *Q96K97del* (Newman et al. *manuscript in preparation*). Therefore, it will be interesting to examine autophagic flux in such

aged fish to see whether it subsequently becomes inhibited (as is typical in Alzheimer's disease (Nixon, Wegiel et al. 2005)). To this end, we are currently determining whether the GFP-Lc3a-GFP transgene can be transmitted through the zebrafish germline for widespread expression in adult tissues.

In summary, we tested two GFP-based assays intended to detect changes in autophagic flux in zebrafish embryos and larvae by western immunoblotting: polyQ80-GFP-v2A-GFP and GFP-Lc3a-GFP. Both transgenes provide 1:1 stoichiometric co-expression of an autophagy target protein and of free GFP as an internal control. The two assays both appeared able to reflect changes in autophagic flux although each assay displayed particular limitations. Using the GFP-Lc3a-GFP assay, we found that lack of *psen2* activity in zebrafish reduces autophagic flux as does heterozygosity for a typically reading-frame-preserving fAD-like mutation of *psen1* (*Q96K97del*).

## References

- (2011). E3 medium (for zebrafish embryos). Cold Spring Harbor Protocols. **2011**: pdb.rec66449.
- Area-Gomez, E., A. J. de Groof, et al. (2009). "Presenilins are enriched in endoplasmic reticulum membranes associated with mitochondria." Am J Pathol **175**(5): 1810-1816.
- Boland, B., A. Kumar, et al. (2008). "Autophagy induction and autophagosome clearance in neurons: relationship to autophagic pathology in Alzheimer's disease." J Neurosci **28**(27): 6926-6937.
- Clark, K. J., M. D. Urban, et al. (2011). "Transgenic zebrafish using transposable elements." Methods Cell Biol **104**: 137-149.
- Cui, J., T. H.-F. Sim, et al. (2012). "Generation of transgenic zebrafish with liver-specific expression of EGFP-Lc3: A new in vivo model for investigation of liver autophagy." Biochemical and Biophysical Research Communications **422**(2): 268-273.
- Fleming, A. and D. C. Rubinsztein (2011). "Zebrafish as a model to understand autophagy and its role in neurological disease." Biochimica et Biophysica Acta (BBA) - Molecular Basis of Disease **1812**(4): 520-526.
- Ganesan, S., S. H. Moussavi Nik, et al. (2014). "Identification and expression analysis of the zebrafish

- orthologues of the mammalian MAP1LC3 gene family." *Exp Cell Res* **328**(1): 228-237.
- Grunwald, D. J. and J. S. Eisen (2002). "Headwaters of the zebrafish [mdash] emergence of a new model vertebrate." *Nat Rev Genet* **3**(9): 717-724.
- He, C., C. R. Bartholomew, et al. (2009). "Assaying autophagic activity in transgenic GFP-Lc3 and GFP-Gabarap zebrafish embryos." *Autophagy* **5**(4): 520-526.
- Jayadev, S., J. B. Leverenz, et al. (2010). "Alzheimer's disease phenotypes and genotypes associated with mutations in presenilin 2." *Brain* **133**(Pt 4): 1143-1154.
- Jayne, T., M. Newman, et al. (2016). "Evidence For and Against a Pathogenic Role of Reduced gamma-Secretase Activity in Familial Alzheimer's Disease." *J Alzheimers Dis* **52**(3): 781-799.
- Ju, J.-S., S. E. Miller, et al. (2009). "Quantitation of selective autophagic protein aggregate degradation in vitro and in vivo using luciferase reporters." *Autophagy* **5**(4): 511-519.
- Kaizuka, T., H. Morishita, et al. (2016). "An Autophagic Flux Probe that Releases an Internal Control." *Mol Cell* **64**(4): 835-849.
- Kawakami, K. (2007). "Tol2: a versatile gene transfer vector in vertebrates." *Genome Biol* **8**(1).
- Lee, J. H., W. H. Yu, et al. (2010). "Lysosomal proteolysis and autophagy require presenilin 1 and are disrupted by Alzheimer-related PS1 mutations." *Cell* **141**(7): 1146-1158.
- Moussavi Nik, S. H., M. Newman, et al. (2015). "Alzheimer's disease-related peptide PS2V plays ancient, conserved roles in suppression of the unfolded protein response under hypoxia and stimulation of gamma-secretase activity." *Hum Mol Genet* **26**.
- Ni, H. M., A. Bockus, et al. (2011). "Dissecting the dynamic turnover of GFP-LC3 in the autolysosome." *Autophagy* **7**(2): 188-204.
- Nixon, R. A., J. Wegiel, et al. (2005). "Extensive Involvement of Autophagy in Alzheimer Disease: An Immuno-Electron Microscopy Study." *Journal of Neuropathology & Experimental Neurology* **64**(2): 113-122.
- Orr, M. E. and S. Oddo (2013). "Autophagic/lysosomal dysfunction in Alzheimer's disease." *Alzheimers Res Ther* **5**(5).
- Pottier, C., D. Hannequin, et al. (2012). "High frequency of potentially pathogenic SORL1 mutations in autosomal dominant early-onset Alzheimer disease." *Mol Psychiatry* **17**(9): 875-879.
- Provost, E., J. Rhee, et al. (2007). "Viral 2A peptides allow expression of multiple proteins from a single ORF in transgenic zebrafish embryos." *Genesis* **45**(10): 625-629.
- Schiffer, N. W., S. A. Broadley, et al. (2007). "Identification of anti-prion compounds as efficient inhibitors of polyglutamine protein aggregation in a zebrafish model." *J Biol Chem* **282**(12): 9195-9203.
- Selkoe, D. and R. Kopan (2003). "Notch and Presenilin: regulated intramembrane proteolysis links development and degeneration." *Annu Rev Neurosci* **26**: 565-597.
- van Bebber, F., D. Paquet, et al. (2010). "Methylene blue fails to inhibit Tau and polyglutamine protein dependent toxicity in zebrafish." *Neurobiol Dis* **39**(3): 265-271.
- Yoon, Y. H., K. S. Cho, et al. (2010). "Induction of lysosomal dilatation, arrested autophagy, and cell death by chloroquine in cultured ARPE-19 cells." *Invest Ophthalmol Vis Sci* **51**(11): 6030-6037.
- Yu, W. H., A. M. Cuervo, et al. (2005). "Macroautophagy--a novel Beta-amyloid peptide-generating pathway activated in Alzheimer's disease." *J Cell Biol* **171**(1): 87-98.
- Zhang, X., K. Garbett, et al. (2012). "A role for presenilins in autophagy revisited: normal acidification of lysosomes in cells lacking PSEN1 and PSEN2." *J Neurosci* **32**(25): 8633-8648.

### 4.3 Supplementary Information

This section is included in the thesis as information supplementary to Section 4.2. It contains additional information not included in the main text of the manuscript.

#### Supporting Information File S1

##### (A) Sequence design for the polyQ80-GFP-v2A-GFP construct

Different regions of the sequence are labeled with different highlight colours corresponding to the legends below:

- EcoRV-BamHI-Kozak-Start-polyGlu80-GFP-v2A-GFP-Stop-ClaI-EcoRI-EcoRV
- G in polyGlu80 region refers to numerous silent mutations introduced in to the degenerate codon positions
- X in the downstream GFP region refers to numerous silent mutations introduced in to the degenerate codon positions

Sequence of polyQ80-GFP-v2A-GFP construct:

5'-

```
GATATC GGATCC GCCACC ATG CAACA G CAACA G CAACAACA G CA G CAACA  
G CAACAACAACA G CA G CA CA G CAACAACAACA G CAACA G CAACA G CA G CAA  
CAACAACA G CA G CAACA G CAACAACAACAACAACA G CAACA G CAACAAC  
ACAACA G CAACA G CA G CAACA G CA G CAACAACA G CA G CA G CAACA  
ACA G CAACAACA G CAACAACAACAACAACAACA G CAACAACAACA G CAA  
CAACA G CA G CAACAA ATGGTGAGCAAGGGCGAGGAGCTGTTACCGGGG  
TGGTGCCCATCCTGGTTCGAGCTGGACGGCGACGTAACGGCCACAAGTTC  
AGCGTGTCCGGCGAGGGCGAGGGCGATGCCACCTACGGCAAGCTGACCCT  
GAAGTTCATCTGCACCACCGGCAAGCTGCCCGTGCCCTGGCCACCCTCGT  
GACCACCCTGACCTACGGCGTGCAGTGCTTCAGCCGCTACCCCGACCAT  
GAAGCAGCAGACTTCTTCAAGTCCGCCATGCCCGAAGGCTACGTCCAGG  
AGCGCACCATCTTCTTCAAGGACGACGGCAACTACAAGACCCGCGCCGAG  
GTGAAGTTCGAGGGCGACACCCTGGTGAACCGCATCGAGCTGAAGGGCAT  
CGACTTCAAGGAGGACGGCAACATCCTGGGGCACAAGCTGGAGTACAAC  
ACAACAGCCACAACGTCTATATCATGGCCGACAAGCAGAAGAACGGCATC  
AAGGTGAACTTCAAGATCCGCCACAACATCGAGGACGGCAGCGTGCAGCT  
CGCCGACCACTACCAGCAGAACACCCCATCGGGCGACGGCCCCGTGCTGC  
TGCCCGACAACCACTACCTGAGCACCCAGTCCGCCCTGAGCAAAGACCC
```

AACGAGAAGCGCGATCACATGGTCCTGCTGGAGTTCGTGACCGCCGCCGG  
GATCACTCTCGGCATGGACGAGCTGTACAAGGGCTCCGGAGCTACAAATTT  
CTCTCTGTTGAAACAGGCTGGTGACGTCGAGGAGAATCCTGGCCCAATGG  
TGAGCAAGGGAAGAGGAGCTGTTACAGGAGTGGTGCCTATCCTGGTGGAG  
CTGGACGGAGACGTGAACGGACACAAGTTCAGCGTGAGCGGAGAGGGAG  
AGGGAGACGCTACATACGGAAAGCTGACACTGAAGTTCATCTGTACAACA  
GGAAAGCTGCCTGTGCCTTGGCCTACACTGGTGACAACACTGACATACGG  
AGTGCAGTGTTTCAGCAGATACCCTGACCACATGAAGCAGCACGACTTCTT  
CAAGAGCGCTATGCCTGAGGGATACGTGCAGGAGAGAACAATCTTCTTCA  
AGGACGACGGA AACTACAAGACAAGAGCTGAGGTGAAGTTCGAGGGAGA  
CACACTGGTGAACAGAATCGAGCTGAAGGGAATCGACTTCAAGGAGGACG  
GAAACATCCTGGGACACAAGCTGGAGTACA ACTACAACAGCCACAACGTG  
TACATCATGGCTGACAAGCAGAAGAACGGAATCAAGGTGA ACTTCAAGAT  
CAGACACAACATCGAGGACGGAAGCGTGCAGCTGGCTGACCACTACCAGC  
AGAACACACCTATCGGAGACGGACCTGTGTGCTGCTGCCGACAACCACTAC  
CTGAGCACACAGAGCGCTCTGAGCAAGGACCCTAACGAGAAGAGAGACC  
ACATGGTGCTGCTGGAGTTCGTGACAGCTGCTGGAATCACACTGGGAATC  
GACGAGCTGTACAAGTAGATCGATGAATTCGATATC-3'

## (B) Sequence design for the GFP-Lc3a-GFP construct

Different regions of the sequence are labeled with different highlight colours corresponding to the legends below:

- EcoRV-BamHI-Kozak-Start-GFP-LC3a-GFP-Stop-ClaI-EcoRI-EcoRV
- X in the downstream GFP region refers to numerous silent mutations introduced in to the degenerate codon positions

Sequence of GFP-Lc3a-GFP construct:

5'-

```
GATATC GGATCC GCCACC ATGGTGAGCAAGGGCGAGGAGCTGTTCACCGG
GGTGGTGCCCATCCTGGTCGAGCTGGACGGCGACGTAAACGGCCACAAGT
TCAGCGTGTCCGGCGAGGGCGAGGGCGATGCCACCTACGGCAAGCTGACC
CTGAAGTTCATCTGCACCACCGGCAAGCTGCCCGTGCCCTGGCCCACCCTC
GTGACCACCCTGACCTACGGCGTGCAGTGCTTCAGCCGCTACCCCGACCAC
ATGAAGCAGCAGACTTCTTCAAGTCCGCCATGCCCGAAGGCTACGTCCAG
GAGCGCACCATCTTCTTCAAGGACGACGGCAACTACAAGACCCGCGCCGA
GGTGAAGTTCGAGGGCGACACCCTGGTGAACCGCATCGAGCTGAAGGGCA
TCGACTTCAAGGAGGACGGCAACATCCTGGGGCACAAGCTGGAGTACAAC
TACAACAGCCACAACGTCTATATCATGGCCGACAAGCAGAAGAACGGCATC
AAGGTGAACTTCAAGATCCGCCACAACATCGAGGACGGCAGCGTGCAGCT
CGCCGACCACTACCAGCAGAACACCCCATCGGCGACGGCCCCGTGCTGC
TGCCCGACAACCACTACCTGAGCACCCAGTCCGCCCTGAGCAAAGACCC
AACGAGAAGCGCGATCACATGGTCCTGCTGGAGTTCGTGACCGCCGCCGG
GATCACTCTCGGCATGGACGAGCTGTACAAG ATGCCATCCGACAGACCCTT
CAAACAACGACGGAGCTTCGCTGATCGTTGCAAGGAAGTGCAGCAGATCC
GAGAGCAGCATCCTAATAAAATTCCGGTGATCATTGAGAGGTATAAGGGGG
AAAAGCAACTTCCAGTCTTGGACAAGACCAAGTTCCTTGTCCTGACCATG
TTAACATGAGTGAGCTGGTAAAGATTATCAGGCGTCGATTGCAGCTCAACC
CCACCCAGGCCTTTTTCCTTCTTGTCAATCAGCACAGCATGGTCAGCGTGT
CCACCCCATTTCTGAGATCTACGAACAAGAGCGGGACGAAGACGGCTTC
CTCTACATGGTTTACGCCTCCAGGAGACCTTCGGCTGC ATGGTGAGCAAG
GGAGAGGAGCTGTTCACAGGAGTGGTGCC TATCCTGGTGGAGCTGGACGG
AGACGTGAACGGA CACAAGTTCAGCGTGAGCGGAGAGGGAGAGGGAGAC
GCTACATACGGA AAGCTGACACTGAAGTTCATCTGTACAACAGGAAAGCT
GCCTGTGCCTTGGCCTACACTGGTGACAACA CTGACATACGGAGTGCAGTG
TTTCAGCAGATACCCTGACCACATGAAGCAGCACGACTTCTTCAAGAGCGC
TATGCC TGAGGGA TACGTGCAGGAGAGAACAATCTTCTTCAAGGACGACC
GAAACTACAAGACAAGAGCTGAGGTGAAGTTCGAGGGA GACACACTGGT
GAACAGA ATCGAGCTGAAGGGA ATCGACTTCAAGGAGGACGGAAACATCC
TGGGACACAAGCTGGAGTACAAC TACAACAGCCACAACGTGTACATCATG
GCTGACAAGCAGAAGAACGGAATCAAGGTGAACTTCAAGATCAGACACA
```

ACATCGAGGACGGAAGCGTGCAGCTGGCTGACCACTACCAGCAGAACACA  
CCTATCGGAGACGGACCTGTGCTGCTGCCTGACAACCACTACCTGAGCACA  
CAGAGCGCTCTGAGCAAGGACCCIAACGAGAAGAGAGACCACATGGTGT  
GCTGGAGTTCGTGACAGCTGCTGGAATCACACTGGGAATGGACGAGCTGT  
ACAAGTAGATCGATGAATTCGATATC-3'



### (C) Sequence design for the GFP-Lc3a construct

Different regions of the sequence are labeled with different highlight colours corresponding to the legend below:

- EcoRV-BamHI-Kozak-Start-GFP-LC3a-Stop-Clal-EcoRI-EcoRV

Sequence of the GFP-Lc3a construct:

5'-

```
GATATC GGATCC GCCACC ATGGTGAGCAAGGGCGAGGAGCTGTTCACCGG
GGTGGTGGCCATCCTGGTTCGAGCTGGACGGCGACGTAACGGCCACAAGT
TCAGCGTGTCCGGCGAGGGCGAGGGCGATGCCACCTACGGCAAGCTGACC
CTGAAGTTCATCTGCACCACGGCAAGCTGCCCGTGCCCTGGCCCACCCTC
GTGACCACCCTGACCTACGGCGTGCAGTGCTTCAGCCGCTACCCCGACCAC
ATGAAGCAGCAGCACTTCTTCAAGTCCGCCATGCCCGAAGGCTACGTCCAG
GAGCGCACCATCTTCTTCAAGGACGACGGCAACTACAAGACCCGCGCCGA
GGTGAAGTTCGAGGGCGACACCCTGGTGAACCGCATCGAGCTGAAGGGCA
TCGACTTCAAGGAGGACGGCAACATCCTGGGGCACAAGCTGGAGTACAAC
TACAACAGCCACAACGTCTATATCATGGCCGACAAGCAGAAGAACGGCATC
AAGGTGAACTTCAAGATCCGCCACAACATCGAGGACGGCAGCGTGCAGCT
CGCCGACCACTACCAGCAGAACACCCCATCGGCGACGGCCCCGTGCTGC
TGCCCGACAACCACTACCTGAGCACCCAGTCCGCCCTGAGCAAAGACCCC
AACGAGAAGCGCGATCACATGGTCCTGCTGGAGTTCGTGACCGCCGCCGG
GATCACTCTCGGCATGGACGAGCTGTACAAG ATGCCATCCGACAGACCCTT
CAAACAACGACGGAGCTTCGCTGATCGTTGCAAGGAAGTGCAGCAGATCC
GAGAGCAGCATCCTAATAAAAATTCCGGTGATCATTGAGAGGTATAAGGGGG
AAAAGCAACTTCCAGTCTTGGACAAGACCAAGTTCCTTGTCCTGACCATG
TTAACATGAGTGAGCTGGTAAAGATTATCAGGCGTCGATTGCAGCTCAACC
CCACCCAGGCCCTTTTCCTTCTTGTC AATCAGCACAGCATGGTCAGCGTGT
CCACCCCATTTCTGAGATCTACGAACAAGAGCGGGACGAAGACGGCTTC
CTCTACATGGTTTACGCCTCCAGGAGACCTTCGGCTGC TAG ATCGATGAAT
TCGATATC-3'
```

#### **(D) Sub-cloning of the GFP-based constructs into the Tol2 vector**

The pT2AL200R150G (Tol2) vector (~5.5 kbp) was provided by the Kawakami laboratory (Kawakami 2007). It contains a GFP expression cassette flanked by *Bam*HI and *Cla*I restriction sites. The GFP expression cassette (~700 bp) was removed through dual restriction enzyme cleavage using *Bam*HI-*HF*<sup>®</sup> and *Cla*I (NEB, R3136S and R0197S).

Both the polyQ80-GFP-v2A-GFP and the GFP-Lc3a-GFP coding sequences were synthesized by Biomatik. They were originally provided in the pBluescript II SK(+) vector. Both the polyQ80-GFP-v2A-GFP region (~1.8 kbp) and the GFP-Lc3a-GFP region (~1.8 kbp) were excised from their vectors using restriction enzyme cleavage with *Bam*HI-*HF*<sup>®</sup> and *Cla*I (NEB, R3136S and R0197S respectively), and then ligated into the Tol2 backbone (~4.7 kbp) using T4 DNA ligase (Sigma-Aldrich, KEM0020).

Kawakami, K. (2007). "Tol2: a versatile gene transfer vector in vertebrates." Genome Biol **8**(1).

## Supporting Information File S2

**Table 1.** Intensity ratios of western immunoblots for Figure 3B

TU polyQ80-GFP-v2A-GFP injected with nontreatment at 48 hpf		
polyQ80-GFP	free GFP	polyQ80-GFP / free GFP
14,498,847	7,759,620	1.868499617
21,474,160	11,707,000	1.834300846
7,731,342	4,183,250	1.848166378
3,826,060	1,909,124	2.004091929
TU polyQ80-GFP-v2A-GFP injected with 50mM Chloroquine at 48 hpf		
polyQ80-GFP	free GFP	polyQ80-GFP / free GFP
11,681,868	5,942,475	1.965825351
8,149,416	3,414,906	2.386424692
3,437,312	1,763,456	1.94919068
1,254,030	544,200	2.304355017
TU polyQ80-GFP-v2A-GFP injected with 1 $\mu$ M Rapamycin at 48 hpf		
polyQ80-GFP	free GFP	polyQ80-GFP / free GFP
9,733,899	8,463,586	1.150091581
11,274,655	7,505,820	1.502121687
8,219,406	5,247,346	1.566392992
5,336,812	3,293,472	1.620421245

**Table2.** Intensity ratios of western immunoblots for Figure 3D

TU polyQ80-GFP-v2A-GFP injected with nontreatment at 24 hpf		
polyQ80-GFP	free GFP	polyQ80-GFP / free GFP
8,653,702	4,962,268	1.74390057
5,754,224	2,276,400	2.527773678
5,565,504	2,795,436	1.990925208
TU polyQ80-GFP-v2A-GFP injected with nontreatment at 48 hpf		
polyQ80-GFP	free GFP	polyQ80-GFP / free GFP
10,040,730	5,601,680	1.79244977
8,491,950	5,235,390	1.622028158
2,155,167	1,046,925	2.058568665
TU polyQ80-GFP-v2A-GFP injected with nontreatment at 72 hpf		
polyQ80-GFP	free GFP	polyQ80-GFP / free GFP
2,893,472	1,839,744	1.57275795
4,548,273	3,152,068	1.442948883
2,000,684	1,056,104	1.894400551

TU polyQ80-GFP-v2A-GFP injected with nontreatment at 96 hpf		
polyQ80-GFP	free GFP	polyQ80-GFP / free GFP
2,893,472	1,839,744	1.84518448
7,826,031	10,280,358	0.761260551
1,209,186	727,078	1.663076039

**Table 3.** Intensity ratios of western immunoblots for Figure 5A

TU GFP-Lc3a-GFP injected with nontreatment at 48 hpf		
GFP-Lc3a	free GFP	GFP-Lc3a / free GFP
3,950,212	3,817,744	1.034698
3,145,700	2,042,920	1.539806
2,258,838	2,032,146	1.111553
1,990,170	1,769,940	1.124428
1,872,738	1,852,812	1.010754
1,870,272	1,643,058	1.138287
2,176,832	1,416,072	1.537233
1,259,356	1,205,064	1.045053
285,824	150,500	1.899163
3,577,644	3,187,072	1.122549
510,228	438,912	1.1624836
2,153,067	1,220,709	1.763784
2,583,780	2,129,060	1.21357782
495,615	434,188	1.14147558
1,319,140	984,260	1.3402353
1,621,326	1,431,948	1.132252
1,269,960	1,671,040	0.759982
1,737,144	1,988,946	0.87339928
1,640,484	1,659,114	0.98877112
1,687,770	1,345,734	1.25416316
2,796,020	2,066,900	1.35276017
TU GFP-Lc3a-GFP injected with 1 $\mu$ M Rapamycin at 48 hpf		
GFP-Lc3a	free GFP	GFP-Lc3a / free GFP
3,056,022	3,190,032	0.957991
3,069,846	3,277,116	0.936752
3,184,326	3,182,652	1.000526
2,986,326	2,895,606	1.03133
203,084	185,864	1.092648
1,223,712	1,233,512	0.992055
652,232	828,240	0.787492
1,032,108	849,772	1.21457
1,079,280	1,241,838	0.86909887

4,372,164	5,062,572	0.86362505
2,510,760	2,936,700	0.85495965
3,938,634	4,079,355	0.96550411
TU GFP-Lc3a-GFP injected with 50 $\mu$ M Chloroquine at 48 hpf		
GFP-Lc3a	free GFP	GFP-Lc3a / free GFP
2,660,580	3,439,260	0.77359083
4,291,002	4,516,974	0.9499727
2,539,680	2,421,820	1.04866588
5,487,020	6,388,080	0.85894666
TU GFP-Lc3a-GFP injected with 50mM Chloroquine at 48 hpf		
GFP-Lc3a	free GFP	GFP-Lc3a / free GFP
1,320,066	1,605,960	0.82197938
1,180,674	1,763,874	0.66936414
1,300,356	1,865,430	0.6970811
1,048,014	1,414,134	0.7410995
4,167,744	3,251,640	1.28173599
1,106,560	1,029,260	1.0751025
2,059,860	1,968,560	1.04637908
4,037,334	3,353,574	1.20388994
<i>psen2</i> <sup>S4Ter/+</sup> GFP-Lc3a-GFP injected with nontreatment at 48 hpf		
GFP-Lc3a	free GFP	GFP-Lc3a / free GFP
1,480,332	727,412	2.03506678
2,954,842	2,146,870	1.37634882
3,056,151	2,480,247	1.23219623
1,030,086	589,680	1.746855922
<i>psen2</i> <sup>S4Ter/psen2</sup> <sup>S4Ter</sup> GFP-Lc3a-GFP injected with nontreatment at 48 hpf		
GFP-Lc3a	free GFP	GFP-Lc3a / free GFP
927,675	709,737	1.3070687
3,620,232	2,372,526	1.525898
3,099,942	2,199,834	1.409171
1,388,289	963,543	1.44081686
1,790,558	1,295,206	1.38245036
2,729,748	1,561,875	1.74773782
2,639,472	1,454,112	1.81517792
1,605,076	1,205,336	1.331641965
853,360	489,720	1.742547
2,311,940	2,299,320	1.005489

**Table 4.** Intensity ratios of western immunoblots for Figure 5B

TU GFP-Lc3a-GFP injected with nontreatment at 96 hpf		
GFP-Lc3a	free GFP	GFP-Lc3a / free GFP

1,183,302	1,604,538	0.73747209
906,930	916,056	0.990038
814,536	537,282	1.516030688
720,846	820,116	0.878956
1,417,731	1,306,368	1.085246
782,800	620,380	1.26180728
286,300	397,800	0.719708
186,240	227,000	0.820441
128,840	154,120	0.835972
154,300	290,100	0.531886
851,634	912,345	0.933456
1,503,630	1,548,756	0.970863
1,448,503	921,025	1.572708
830,235	386,358	2.148875
913,857	842,646	1.084509
2,881,120	2,286,856	1.259861
2,525,309	3,718,528	0.679115
8,115,093	7,072,527	1.147411
4,307,205	4,169,592	1.033004
3,074,640	2,100,680	1.46364
7,226,899	3,639,635	1.985611
TU GFP-Lc3a-GFP injected with 50 $\mu$ M Chloroquine at 96 hpf		
GFP-Lc3a	free GFP	GFP-Lc3a / free GFP
413,010	362,484	1.13938822
655,082	780,596	0.839207
1,854,580	2,293,360	0.808673736
2,189,237	2,138,773	1.023595
481,257	332,052	1.449342
918,206	832,416	1.103061
732,424	642,774	1.139474
525,609	237,468	2.213389
TU GFP-Lc3a-GFP injected with 12.5mM Chloroquine at 96 hpf		
GFP-Lc3a	free GFP	GFP-Lc3a / free GFP
154,780	461,240	0.335574
204,360	384,580	0.531385
211,740	365,740	0.578936
129,306	286,534	0.451276
TU GFP-Lc3a-GFP injected with 25mM Chloroquine at 96 hpf		
GFP-Lc3a	free GFP	GFP-Lc3a / free GFP
327,810	286,755	1.143171
291,260	338,720	0.859884
293,664	446,754	0.657328
TU GFP-Lc3a-GFP injected with 50mM Chloroquine at 96 hpf		

GFP-Lc3a	free GFP	GFP-Lc3a / free GFP
880,380	725,814	1.21295539
248,382	328,680	0.755695509
175,518	64,962	2.701856

**Table 5.** Intensity ratios of western immunoblots for Figure 5C

TU GFP-Lc3a-GFP injected with nontreatment at 96 hpf		
GFP-Lc3a	free GFP	GFP-Lc3a / free GFP
1,183,302	1,604,538	0.73747209
906,930	916,056	0.990038
814,536	537,282	1.516030688
720,846	820,116	0.878956
1,417,731	1,306,368	1.085246
782,800	620,380	1.26180728
286,300	397,800	0.719708
186,240	227,000	0.820441
128,840	154,120	0.835972
154,300	290,100	0.531886
851,634	912,345	0.933456
1,503,630	1,548,756	0.970863
1,448,503	921,025	1.572708
830,235	386,358	2.148875
913,857	842,646	1.084509
2,881,120	2,286,856	1.259861
2,525,309	3,718,528	0.679115
8,115,093	7,072,527	1.147411
4,307,205	4,169,592	1.033004
3,074,640	2,100,680	1.46364
7,226,899	3,639,635	1.985611
TU GFP-Lc3a-GFP injected with 50 $\mu$ M Chloroquine at 96 hpf		
GFP-Lc3a	free GFP	GFP-Lc3a / free GFP
413,010	362,484	1.13938822
655,082	780,596	0.839207
1,854,580	2,293,360	0.808673736
2,189,237	2,138,773	1.023595
481,257	332,052	1.449342
918,206	832,416	1.103061
732,424	642,774	1.139474
525,609	237,468	2.213389
TU GFP-Lc3a-GFP injected with 1 $\mu$ M Rapamycin at 96 hpf		
GFP-Lc3a	free GFP	GFP-Lc3a / free GFP

802,548	906,804	0.88502918
824,562	1,422,612	0.579611
563,238	583,290	0.965622589
592,434	828,972	0.714661
402,174	651,654	0.617159
803,901	1,434,615	0.56036
825,740	1,256,160	0.657353
195,860	410,160	0.47752097
1,500,282	1,790,460	0.837931
1,335,810	2,551,395	0.523561
557,194	325,261	1.713067
972,660	1,243,780	0.782019
296,560	380,974	0.778425824
531,916	497,530	1.06911342
756,860	407,580	1.856960597
914,980	977,520	0.936021769
<i>psen2<sup>S4Ter/+</sup></i> GFP-Lc3a-GFP injected with nontreatment at 96 hpf		
GFP-Lc3a	free GFP	GFP-Lc3a / free GFP
273,903	374,997	0.73041384
488,103	331,527	1.472287
90,951	58,569	1.552886
212,760	222,660	0.955538
1,018,160	531,784	1.914612
1,400,720	471,960	2.967879
2,093,889	1,122,198	1.86588196
2,996,340	1,544,660	1.939806
<i>psen2<sup>S4Ter/psen2<sup>S4Ter</sup></sup></i> GFP-Lc3a-GFP injected with nontreatment at 96 hpf		
GFP-Lc3a	free GFP	GFP-Lc3a / free GFP
1,401,444	443,052	3.16315918
1,165,986	469,530	2.483305
341,316	195,426	1.746522981
206,400	125,120	1.649616
308,300	107,400	2.870577
463,840	330,120	1.405065
126,440	131,580	0.960936
1,986,270	809,666	2.45319675
<i>psen1<sup>Q96K97del/+</sup></i> GFP-Lc3a-GFP injected with nontreatment at 96 hpf		
GFP-Lc3a	free GFP	GFP-Lc3a / free GFP
565,824	663,705	0.852523335
300,090	236,460	1.269094
709,403	260,243	2.725925
3,511,318	3,143,709	1.11693481
2,228,380	795,900	2.799824



1,154,868	962,390	1.2
1,386,546	502,173	2.761092
2,239,568	1,545,061	1.449501
1,333,517	307,694	4.333906
1,370,622	260,986	5.251707
<i>psen1<sup>K97Gfs/+</sup></i> GFP-Lc3a-GFP injected with nontreatment at 96 hpf		
GFP-Lc3a	free GFP	GFP-Lc3a / free GFP
7,916,256	10,610,544	0.746074
4,420,980	6,906,720	0.640098339
2,937,921	4,154,871	0.707103
2,226,860	1,710,620	1.301785
4,459,158	9,294,142	0.47978157
6,757,366	9,708,578	0.69602

## Supporting Information File S3

### (A) Mutagenesis and breeding of the *psen2*<sup>S4Ter</sup>-carrying zebrafish

The putatively null mutation in zebrafish *psen2*, *psen2*<sup>S4Ter</sup>, was generated by CRISPR/Cas9 system (Hwang, Fu et al. 2013). A brief description of the mutagenesis of *psen2*<sup>S4Ter</sup> mutation were presented below. (The details of the mutagenesis process were published elsewhere, Jiang et al. *manuscripts in preparation*.)

A single guide RNA (sgRNA) with its protospacer adjacent motif (PAM) site targeting downstream close to the start codon of the *psen2* gene was designed and co-injected with the Cas9 protein into the Tübingen (TU) wildtype embryo at one-cell stage. Site-specific DNA double-stranded breaks (DSBs) induced by the CRISPR/Cas9 system were then supposed to be repaired through non-homologous end-joining (NHEJ) pathway (Hwang, Fu et al. 2013), which resulted in random mutations in zebrafish *psen2* gene. Thus, the F0 mutation-carrying fish (the CRISPR/Cas9-injected embryos) may carrying multiple genomes with different mutations. To separate these mutations, the F0 mutation-carrying fish were outbred with TU wildtype fish, so that their F1 progenies may be heterozygous mutants. Among all the mutations found in these F1 progenies, *psen2*<sup>S4Ter</sup> was selected as a putatively null mutation since its Ser-4 codon was substituted by a stop codon. However, this putatively null mutation has not been fully characterized, and we do not have an antibody against zebrafish Psen2 yet to demonstrate lack of Psen2 protein in homozygous mutants.

To generate embryos with certain genotype for our assays, the F1 heterozygous

(*psen2*<sup>S4Ter/+</sup>) parent was firstly outbred with another TU wildtype fish to generate more heterozygous (*psen2*<sup>S4Ter/+</sup>) fish. Those F2 heterozygous (*psen2*<sup>S4Ter/+</sup>) siblings were inbred with each other to generate homozygous (*psen2*<sup>S4Ter/psen2</sup><sup>S4Ter</sup>) fish (F3). The homozygous (*psen2*<sup>S4Ter/psen2</sup><sup>S4Ter</sup>) embryos were collected from pair-mating of homozygous (*psen2*<sup>S4Ter/psen2</sup><sup>S4Ter</sup>) parents, while the heterozygous (*psen2*<sup>S4Ter/+</sup>) embryos were collected from pair-mating of the homozygous (*psen2*<sup>S4Ter/psen2</sup><sup>S4Ter</sup>) parent and another TU wildtype fish.

### **(B) Mutagenesis and breeding of the *psen1*<sup>Q96K97del</sup> and *psen1*<sup>K97Gfs</sup> zebrafish**

The *psen1*<sup>Q96K97del</sup> and *psen1*<sup>K97Gfs</sup> mutations in zebrafish were also generated through CRISPR/Cas9 system, and the details of these mutagenesis were published elsewhere (Hin, Newman et al. 2018).

We pair-mated the homozygous (*psen1*<sup>Q96K97del/psen1</sup><sup>Q96K97del</sup>) with another TU wildtype fish to generate heterozygous (*psen1*<sup>Q96K97del/+</sup>) embryos for our assays. The heterozygous (*psen1*<sup>K97Gfs/+</sup>) embryos were collected through the same process.

Hin, N., M. Newman, et al. (2018). "Accelerated brain aging towards transcriptional inversion in a zebrafish model of familial Alzheimer's disease." [bioRxiv](#).

Hwang, W. Y., Y. Fu, et al. (2013). "Heritable and Precise Zebrafish Genome Editing Using a CRISPR-Cas System." PLoS ONE **8**(7): e68708.

Hwang, W. Y., Y. Fu, et al. (2013). "Efficient genome editing in zebrafish using a CRISPR-Cas system." Nat Biotech **31**(3): 227-229.

## Chapter 5 locomotion tests on *psen2* mutants

### 5.1 Abstract

Behavior has been considered a key component of phenotypes induced by genetic mutations affecting the development of the nervous system in zebrafish. This includes mutations that may impair the formation and function of mitochondria. Mutations affecting mitochondrial activity are implicated in Alzheimer's disease risk and since larval locomotion requires energy, we expect that mutations affecting mitochondrial function might also affect locomotion behavior. In the previous chapter we showed that mutation of *psen2* is predicted to have extensive effects on mitochondrial function and this raises the question of whether larvae bearing mutations in this gene show changes in locomotion behaviour. It is relatively easy to assess larval locomotion behavior using a DanioVision Observation Chamber. To identify whether the mutations described previously in this thesis (*psen2*<sup>S4Ter</sup>, *psen2*<sup>T141\_L142delinsMISLISV</sup> and *psen2*<sup>N140fs</sup>) affect the locomotion of zebrafish larvae, behavioral analysis on 6-day-old zebrafish larvae was performed and is described in this chapter. While we observed some trends of different mean velocities in larvae with different genotypes, these differences in velocity were not statistically significant. However, since too many unknown variables influenced the results of these locomotion tests, the experimental design must be improved for further research.

## 5.2 Introduction

Behavior, especially the behavioral development of sensory and motor functions, has been considered a key component of phenotypes induced by genetic mutations (Xi, Ryan et al. 2010; Mahmood, Fu et al. 2013) and drug treatments (Rihel, Prober et al. 2010) affecting the development of the nervous system in zebrafish (Elbaz, Yelin-Bekerman et al. 2012; Zhou, Cattley et al. 2014). Some drug treatments that impair mitochondrial bioenergetics affect the locomotion of zebrafish larvae (Zhang, Laurence Souders et al. 2017; Wang, Souders et al. 2018) Mutations that may impair the formation and function of mitochondria can also have this effect (Bretaud, Lee et al. 2004; Xi, Ryan et al. 2010). Since the function of mitochondria is thought to have important effects on the progression of AD (Hedskog, Pinho et al. 2013), mutations affecting mitochondrial activity are implicated in Alzheimer's disease risk (Moreira, Carvalho et al. 2010). Moreover, since larval locomotion requires energy that is provided by mitochondria (Voet, Voet et al. 2006), we expect that mutations affecting mitochondrial function might also affect locomotion behavior. Our previous studies on the putatively null *psen2* mutation (*psen2*<sup>S4Ter</sup>) indicated that *psen2* has important functions relating to mitochondria. (Jiang et al. manuscript in preparation). Therefore, we assumed the mutations generated previously in this thesis (*psen2*<sup>S4Ter</sup>, *psen2*<sup>T141\_L142delinsMISLISV</sup> and *psen2*<sup>N140fs</sup>) might affect the locomotion of zebrafish larvae as well.

In some studies, the behavior of zebrafish larvae in light has been monitored in small environments (such as in the wells of 96-well microtiter plates) with optical tracking devices (Lockwood, Bjerke et al. 2004; Orger, Gahtan et al. 2004). Some other studies have used infrared image analysis to monitor locomotion in both light and darkness (Prober, Rihel et al. 2006; Burgess and Granato 2007; Cahill 2007; MacPhail, Brooks et al. 2009). In our study, we performed behavioral analysis on 6-day-old zebrafish larvae using an infrared imaging system in 24-well plates. This allowed us to monitor 24 larvae simultaneously so that the behavior of multiple individuals of multiple genotypes from one family might be compared statistically. Using a 24-well plate rather than a 96-well plate gave each individual larva more space to permit more sophisticated behavior (e.g. greater ability to move longer distances). We presumed this might permit better resolution of any behavioural differences between genotypes.

### 5.3 Methods and materials

#### 5.3.1 Larvae and locomotion tests

For analysis of the *psen2<sup>S4Ter</sup>* mutation, a *psen2<sup>S4Ter/+</sup>* (heterozygous) fish was mated with a *+/+* (wild type) fish so that their progeny used for locomotion tests only included two genotypes, *psen2<sup>S4Ter/+</sup>* and *+/+* in close to a 1:1 ratio. Also, a *psen2<sup>S4Ter/+</sup>* (heterozygous) fish was mated with a *psen2<sup>S4Ter/psen2<sup>S4Ter</sup></sup>* (homozygous) fish so that the progeny would only include *psen2<sup>S4Ter/+</sup>* and *psen2<sup>S4Ter/psen2<sup>S4Ter</sup></sup>* fish in close to a

1:1 ratio. For the *psen2*<sup>T141\_L142delinsMISLISV</sup> and *psen2*<sup>N140fs</sup> mutations, a heterozygous mutant was mated with a wild type fish to generate embryos containing heterozygous mutants and wildtype siblings in a close to 1:1 ratio.

Embryos from each pair-mating were incubated in a 90mm diameter petri dish containing E3 embryo medium at 28.5°C. These embryos were light cycle-entrained by being placed in a light cycle incubator (lights on from 8:00 am until 10:00 pm, lights off from 10:00 pm until 8:00 am each day) from when they were zygotes until 5 days post fertilisation (dpf). At 5dpf, 24 larvae from each batch were selected randomly and each was placed in a separate well of a 24-well plate while maintaining the same light/dark cycle. 6 dpf larvae were then placed in the DanioVision Observation Chamber (Noldus Information Technology, Leesburg, VA, [www.noldus.com](http://www.noldus.com)), one hour before the tracking program started. The tracking program was set up using the EthoVision XT 11.5 software (Noldus Information Technology, Leesburg, VA, [www.noldus.com](http://www.noldus.com)), with the tracking time set for between 5:00 pm (at 6 dpf) until 1:00 pm on the next day (7 dpf) under the same light cycle to which the larvae were entrained.

After motion-tracking (including Velocity-Mean, Distance moved-Total and Movement-Cumulative Duration) and data collection of each larva during one hour intervals, the larvae were genotyped using the allele-specific PCR reactions designed in the previous chapters of this thesis (Methods and Materials sections in Chapter 2 and 3). The behaviour of each larva could then be associated with its genotype in the

EthoVision XT 11.5 software.

## 5.4 Results

### 5.4.1 Differences in locomotion between mutant and wild type larvae

Each type of pair-mating was conducted four times to provide four replicates of the locomotion tests. The mean velocities (mm/s) of larvae with different genotypes at each time point are presented in Figures 5.4.1 to 5.4.4. The mean velocities of replicates were highly variable. Although trends of different mean velocities were observed between larvae of different genotypes within families of siblings, these trends varied between different replicates from the same parents. For example, as shown in Figure 5.4.1 and the Appendix, when the data from all four replicates were pooled together, differences between the mean velocities of *psen2<sup>S4Ter/+</sup>* and *+/+* siblings could be observed, while differences between the mean velocities of *psen2<sup>S4Ter/+</sup>* and *+/+* siblings during light periods were seen for replicates C and D, but not for replicates A and B. When t-tests were applied to these data (performed for each hour time point between genotypes), no statistically significant differences in locomotion were found between different genotypes.

## 5.5 Discussion



### 5.5.1 Differences in locomotion between mutant and wildtype larvae

The mean velocities of locomotion of fish of the same genotype within replicates of pair-matings were variable such that no statistically significant differences could be observed between the mean velocities of mutants and their wild type siblings. This may have been due to uncontrolled variables affecting the behavior of the fish. For example, during their development the larvae were placed in an incubator which was subject to opening and closing several times per day by other people working in the laboratory and this may have caused fluctuation in light intensity (or in other stresses placed on different batches of larvae) between experimental replications. The light cycle entrainment of the larvae may have been affected by these uncontrolled factors.

Although trends of difference in mean velocity were observed for larvae with different genotypes, none of these differences reached statistical significance. We chose to use 6-day-old larvae for this locomotion test since these can still rely on their yolk as a food source and do not need to be fed. However, these 6-day-old larvae might be too young to present any significant differences in locomotion phenotype. The mean velocity of the larvae with the same genotype varied greatly in different families used in the locomotion tests (i.e. the velocity of wildtype larvae in light in Figure 5.4.1 varied from 1.5 mm/s to 3.5 mm/s between the four different families.). This may be due to the short entraining time (from day 0 to day 5) in the light system. However, if we had used older larvae and entrained them for longer, we may have needed to feed them during the

entraining process, which might have introduced additional variables into the experimental system. Thus, the locomotion test we designed for this work may not have been an appropriate method for analyzing behavioural differences between the mutant fish and their wild type siblings. It may be that *psen2* function does not affect the locomotion of zebrafish larvae despite its apparent effects on mitochondrial function. However, the RNA-seq data that revealed changes in the function of mitochondria caused by *S4Ter* were obtained from 6-month-old adult brains. 6-day-old larvae may be too young to present any similar changes. In human AD patients, PSEN2 mutation carriers show a wide variability of disease onset age, i.e. 39–83 years (Van Cauwenberghe, Van Broeckhoven et al. 2015). Thus, it seems that even for those mutations able to cause in AD, overt symptoms may not be observed at very young ages. Similar phenomena may occur in zebrafish, although a mutation (i.e. *S4Ter*) may impair the function of mitochondria, overt symptoms (such as behavioral differences) may not be detectable during the larval stage. Alternatively, the tests of behavior we performed may not have been discriminating for any specific changes in cognition caused by mutations in *psen2*. Thus, it will be interesting to perform behavioural tests (including locomotion tests) on adult fish carrying mutations in *psen2* (especially *S4Ter*) and their wild type siblings to verify whether those changes in the formation and function of mitochondria detected by RNA-seq are also detectable through behavioural tests.

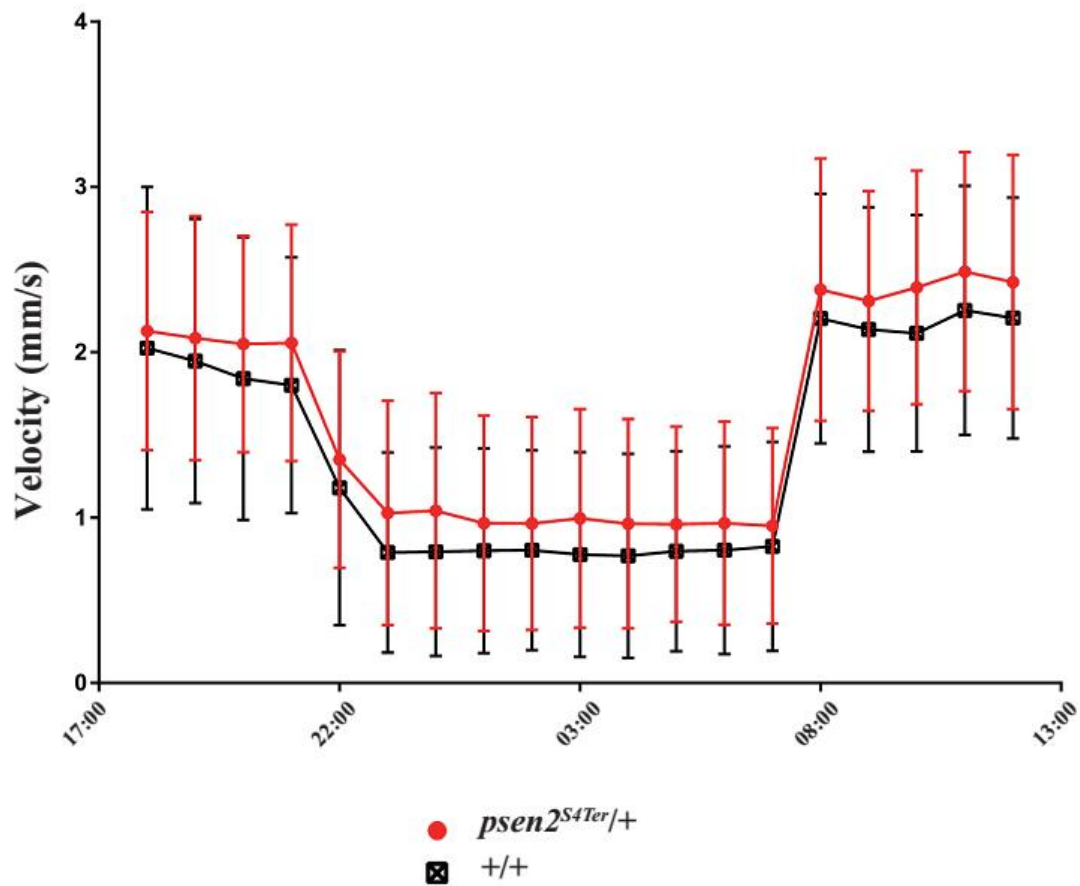


**Figure 5.4.1.** Locomotion tests on *psen2<sup>S4Ter</sup>* heterozygous vs wildtype larvae at 6 dpf. Red dots represent *psen2<sup>S4Ter/+</sup>* mean velocities; Black squares represent *+/+* mean velocities. Bars show SDs. Four replicates of locomotion tests were pooled together, including 41 *psen2<sup>S4Ter/+</sup>* vs 54 *+/+* larvae.

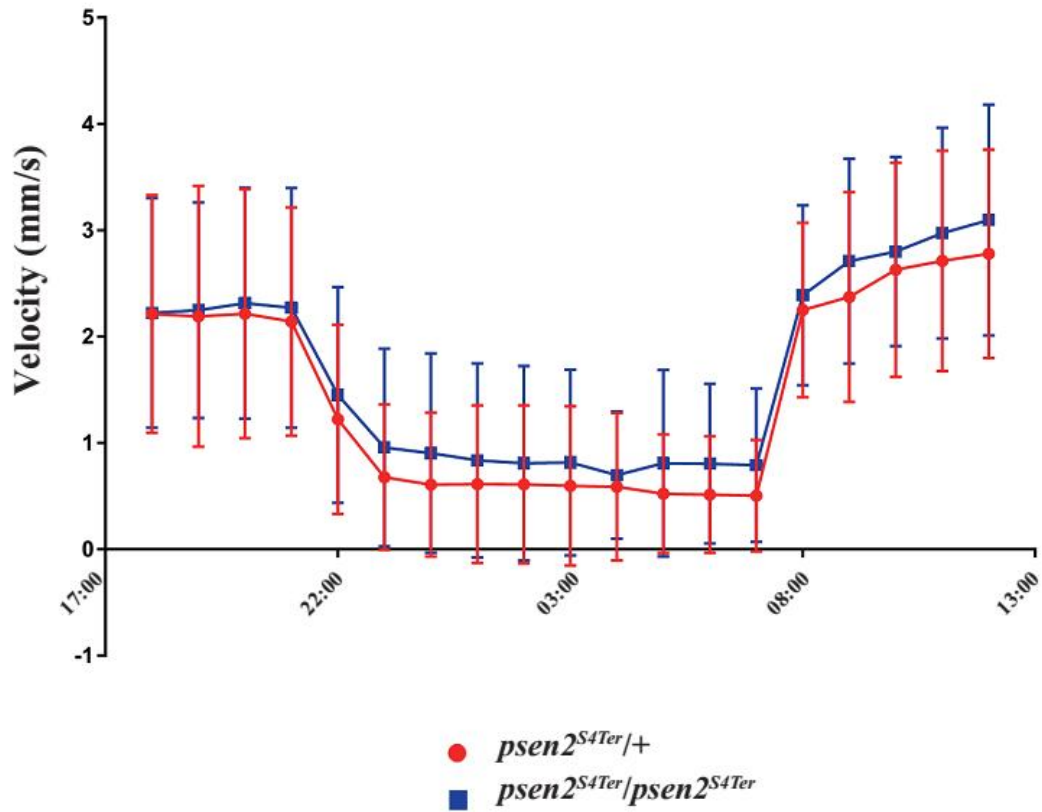


**Figure 5.4.2.** Locomotion tests on *psen2<sup>S4Ter</sup>* heterozygous vs homozygous larvae at 6 dpf.

Red dots represent *psen2<sup>S4Ter/+</sup>* mean velocities; the blue squares represent *psen2<sup>S4Ter/psen2<sup>S4Ter</sup></sup>* mean velocities. Bars show SDs. Four replicates of locomotion tests were pooled together, including 49 *psen2<sup>S4Ter/+</sup>* vs 42 *psen2<sup>S4Ter/psen2<sup>S4Ter</sup></sup>* larvae.

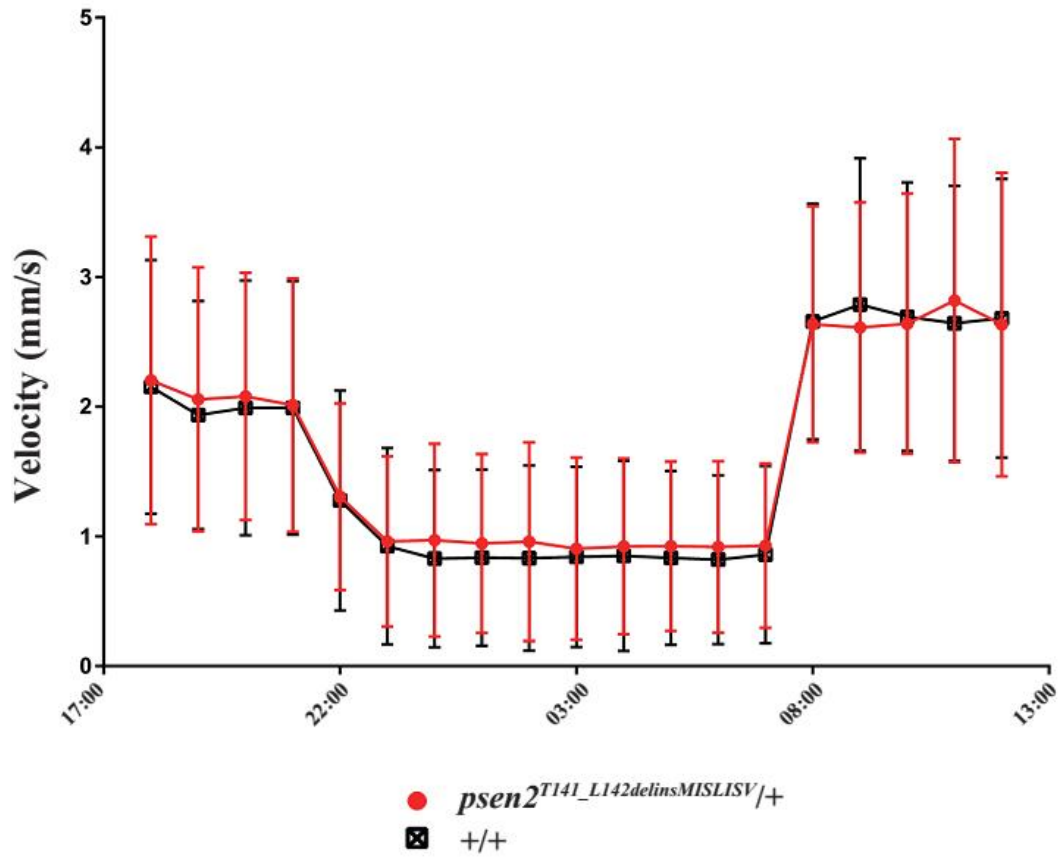


**Figure 5.4.3.** Locomotion tests on *psen2*<sup>T141\_L142delinsMISLISV</sup> heterozygous vs wildtype larvae at 6 dpf.

The red dots represent *psen2*<sup>T141\_L142delinsMISLISV/+</sup> mean velocities; the black squares represent +/+ mean velocities. Bars show SDs. Four replicates of locomotion tests were pooled together, including 53 *psen2*<sup>T141\_L142delinsMISLISV/+</sup> vs 43 +/+ larvae.

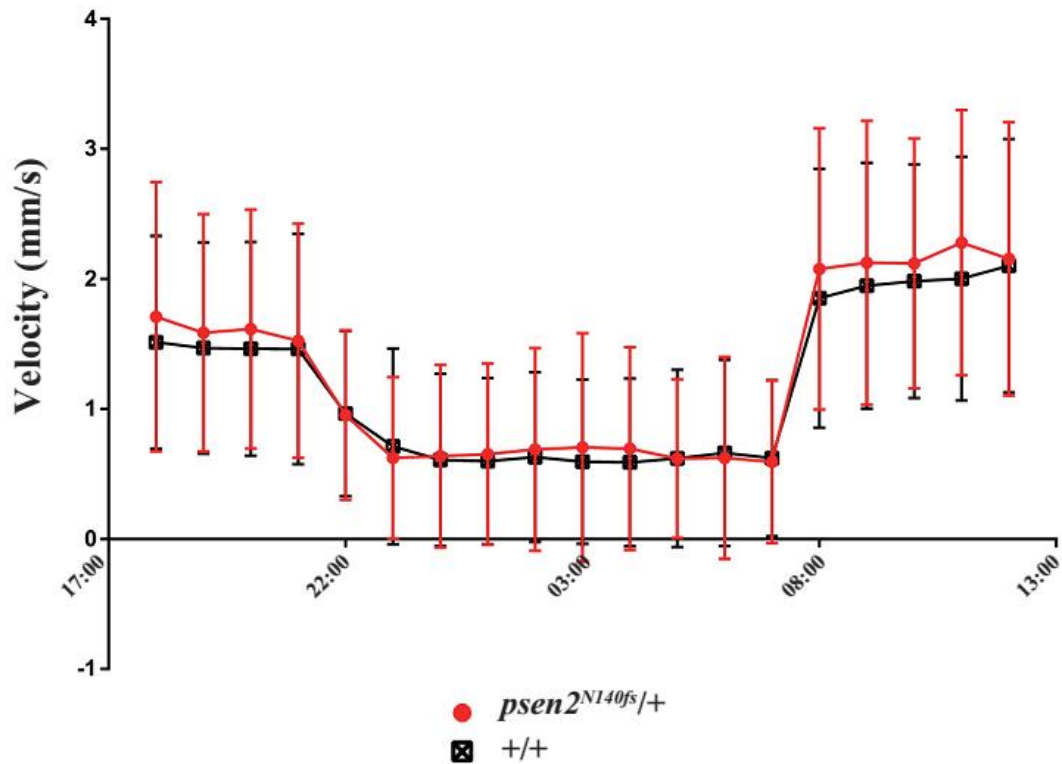


**Figure 5.4.4.** Locomotion tests on *psen2*<sup>N140fs</sup> heterozygous vs wildtype larvae at 6 dpf. The red dots represent *psen2*<sup>N140fs/+</sup> mean velocities; the black squares represent +/+ mean velocities. Bars show SDs. Four replicates of locomotion tests were pooled together, including 53 *psen2*<sup>N140fs/+</sup> vs 38 +/+ larvae.

\* Data of Locomotion tests from Figure 5.4.1 to 5.4.4 are presented in the Appendix with the file name “Mean velocities of Figure 5.4.1 to 5.4.4.xlsx”.

## 5.6 References

- Bretau, S., S. Lee, et al. (2004). "Sensitivity of zebrafish to environmental toxins implicated in Parkinson's disease." *Neurotoxicology and Teratology* **26**(6): 857-864.
- Burgess, H. A. and M. Granato (2007). "Modulation of locomotor activity in larval zebrafish during light adaptation." *J Exp Biol* **210**(Pt 14): 2526-2539.

- Cahill, G. M. (2007). "Automated video image analysis of larval zebrafish locomotor rhythms." Methods Mol Biol **362**: 83-94.
- Elbaz, I., L. Yelin-Bekerman, et al. (2012). "Genetic ablation of hypocretin neurons alters behavioral state transitions in zebrafish." J Neurosci **32**(37): 12961-12972.
- Hedskog, L., C. M. Pinho, et al. (2013). "Modulation of the endoplasmic reticulum-mitochondria interface in Alzheimer's disease and related models." Proc Natl Acad Sci U S A **110**(19): 7916-7921.
- Lockwood, B., S. Bjerke, et al. (2004). "Acute effects of alcohol on larval zebrafish: a genetic system for large-scale screening." Pharmacol Biochem Behav **77**(3): 647-654.
- MacPhail, R. C., J. Brooks, et al. (2009). "Locomotion in larval zebrafish: Influence of time of day, lighting and ethanol." Neurotoxicology **30**(1): 52-58.
- Mahmood, F., S. Fu, et al. (2013). "A zebrafish model of CLN2 disease is deficient in tripeptidyl peptidase 1 and displays progressive neurodegeneration accompanied by a reduction in proliferation." Brain **136**(Pt 5): 1488-1507.
- Moreira, P. I., C. Carvalho, et al. (2010). "Mitochondrial dysfunction is a trigger of Alzheimer's disease pathophysiology." Biochimica et Biophysica Acta (BBA) - Molecular Basis of Disease **1802**(1): 2-10.
- Orger, M. B., E. Gahtan, et al. (2004). Behavioral Screening Assays in Zebrafish. Methods in Cell Biology, Academic Press. **77**: 53-68.
- Prober, D. A., J. Rihel, et al. (2006). "Hypocretin/orexin overexpression induces an insomnia-like phenotype in zebrafish." J Neurosci **26**(51): 13400-13410.
- Rihel, J., D. A. Prober, et al. (2010). "Zebrafish behavioral profiling links drugs to biological targets and rest/wake regulation." Science **327**(5963): 348-351.
- Van Cauwenberghe, C., C. Van Broeckhoven, et al. (2015). "The genetic landscape of Alzheimer disease: clinical implications and perspectives." Genetics In Medicine **18**: 421.
- Voet, D., J. G. Voet, et al. (2006). Fundamentals of Biochemistry: Life at the Molecular Level, John Wiley and Sons: 547-556.
- Wang, X. H., C. L. Souders, et al. (2018). "Paraquat affects mitochondrial bioenergetics, dopamine system expression, and locomotor activity in zebrafish (*Danio rerio*)." Chemosphere **191**: 106-117.
- Xi, Y., J. Ryan, et al. (2010). "Impaired dopaminergic neuron development and locomotor function in zebrafish with loss of pink1 function." European Journal of Neuroscience **31**(4): 623-633.
- Zhang, J.-L., C. Laurence Souders, et al. (2017). "Quercetin, a natural product supplement, impairs mitochondrial bioenergetics and locomotor behavior in larval zebrafish (*Danio rerio*)." Toxicology and Applied Pharmacology **327**: 30-38.
- Zhou, Y., R. T. Cattley, et al. (2014). "Quantification of larval zebrafish motor function in multiwell plates using open-source MATLAB applications." Nat Protoc **9**(7): 1533-1548.

## Chapter 6 Conclusion and Perspective

### 6.1 Conclusion

The overall aim of this PhD project was to investigate the molecular changes caused by fAD-like mutations in the *psen2* gene in the zebrafish model. The conclusions drawn from this thesis are:

(1) Three mutations were generated in the zebrafish *psen2* gene, a putatively null mutation, *psen2*<sup>S4Ter</sup>, a fAD-like mutation, *psen2*<sup>T141\_L142delinsMISLISV</sup>, and the CDS-truncating mutation, *psen2*<sup>N140Wfs</sup>. These mutations provide potentially useful tools for identifying the specific cellular changes caused by fAD-like mutation of *psen2*, and may allow us to exclude the non-fAD-causative effects caused by simple loss of *psen2* function.

(2) RNA-seq and gene ontology analysis of the putatively null mutation *S4Ter* suggested changes in brain mitochondrial activity, glucocorticoid signalling activity and intracellular iron trafficking. These results are in agreement with, but also increase our knowledge regarding how human *PSEN2* is involved in AD pathology. We observed a severe haploinsufficiency effect of this mutation in relation to its effect in homozygous fish.



(3) The skin of *NI40fs* homozygous adult fish presented with gross loss of melanotic pigmentation while retaining pigmentation in the retinal pigmented epithelium. This likely indicates a loss of  $\gamma$ -secretase activity. The skin of *T141\_L142delinsMISLISV* homozygous adult fish presented with faint melanotic pigmentation, indicating that some  $\gamma$ -secretase activity still remains with this mutation. However, *S4Ter* homozygotes have normal adult pigmentation. Thus, the *NI40fs* mutation is most likely a true null (or severely hypomorphic) allele of zebrafish *psen2*, while the *S4Ter* mutation is not. On the other hand, the remaining of  $\gamma$ -secretase activity (revealed by the faint melanotic pigmentation in the skin of homozygous mutants) in *T141\_L142delinsMISLISV* homozygous indicates that this mutation is not like a null mutation (since this phenotype is different to those in *NI40fs* or *S4Ter* homozygotes mutants). This mutation is most likely a fAD-like mutation since it obeys the “fAD mutation reading frame preservation rule” as an in-frame mutation and also remains some  $\gamma$ -secretase activity.

(4) A GFP-based autophagic flux assay was designed and tested. The assay was designed in order to allow comparison of autophagic flux signals on different western immunoblots with the free GFP fragment functioning as an internal control. This new assay was employed to detect changes in autophagic flux caused by fAD-like mutations in *psen1* and *psen2*. The results revealed that the *presenilin* genes are important for autophagy with reduced autophagic flux evident in both heterozygous and homozygous *psen2*<sup>*S4Ter*</sup> mutants. This provided further evidence for the haploinsufficiency previously indicated by the transcriptomic analysis of this mutant.

In summary, three mutations were generated in zebrafish *psen2*, transcriptomic analysis was performed for the *S4Ter* mutation and a GFP-based assay for monitoring changes in autophagic flux was designed and tested on *psen1* and *psen2* mutants. Further analysis of these zebrafish mutation models may help dissect how fAD mutations cause Alzheimer's disease.

## 6.2 Perspective

The biological effects of the three mutations generated in this thesis have not been fully explored. Future work that could be performed includes the following:

(1) Since we did not have an antibody against zebrafish Psen2, we were unable to demonstrate loss of Psen2 at the protein level due to the *S4Ter* or *N140fs* mutations. Although transcriptomic analysis and assays of autophagic flux showed definite differences between *S4Ter* mutants and wildtype sibling zebrafish, additional protein-level evidence is required before we can be confident (or otherwise) that this mutation represents a loss of *psen2* function. An antibody against zebrafish Psen2 protein for western immunoblotting has been ordered and will be used by others to test for protein in *S4Ter* homozygous fish in future. While the *N140fs* mutation showed reduced levels of mutant transcripts presumably due to nonsense-mediated decay, it will also be useful to observe whether this allele allows production of a truncated protein since some

truncated Presenilin proteins have been observed previously to have dominant effects, even at low levels (Nornes, Newman et al. 2008; Newman, Wilson et al. 2014).

(2) In Chapter 2, we described transcriptomic analysis on *S4Ter*, which showed a severe haploinsufficiency effect of this mutation. Moreover, dqPCR results indicated that no NMD occurs in *S4Ter* mutants, and no gross loss of melanotic pigmentation was observed in the skin of *S4Ter* homozygous adults. All these results appear to indicate that *S4Ter* is likely not a true null mutation. However, to identify the specific cellular changes caused by fAD-like mutations, we need to exclude those changes caused by null mutations since none of the identified fAD mutations in human *PSEN1* and *PSEN2* appear to remove all gene function. Interestingly, the truncating mutation *NI40fs* (in Chapter 3) is most likely a true null mutation since NMD occurs (according to the dqPCR results) in heterozygous mutants and a gross loss of melanotic pigmentation (a loss of  $\gamma$ -secretase activity) was observed in the skin of homozygous mutants. The other mutation that we generated in Chapter 3, *T141\_L142delinsMISLISV*, is most likely a fAD-like mutation since it is in-frame mutation and retains some  $\gamma$ -secretase activity. With these two mutations (generated in Chapter 3), i.e. a null mutation and a fAD-like mutation, we may be able to achieve our original goals. In order to reduce genetic and environmental noise, a *T141\_L142delinsMISLISV* heterozygous (*psen2*<sup>*T141\_L142delinsMISLISV*/+</sup>) fish will be pair-mated with a *NI40fs* heterozygous (*psen2*<sup>*NI40fs*/+</sup>) fish to generate a large family of siblings with wild type (+/+), *psen2*<sup>*T141\_L142delinsMISLISV*/+</sup>, *psen2*<sup>*NI40fs*/+</sup>, or *psen2*<sup>*T141\_L142delinsMISLISV*/*psen2*<sup>*NI40fs*</sup></sup>

genotypes. Total RNA from brains of  $+/+$ ,  $psen2^{T141\_L142delinsMISLISV}/+$  and  $psen2^{N140fs}/+$  fish will be sent for RNA-seq analysis when they are 6-month-old, so that the following transcriptomic analysis will be able to identify the specific cellular changes caused by  $T141\_L142delinsMISLISV$ , excluding those changes caused by  $N140fs$  (Figure 6.2.1). Since null mutations in the *PRESENILIN* genes do not appear to cause fAD, the specific cellular changes caused exclusively by  $T141\_L142delinsMISLISV$ , as represented in the three-way comparison diagram below (Figure 6.2.1), may reveal the changes that (in humans) are critical for driving onset of Alzheimer's disease.

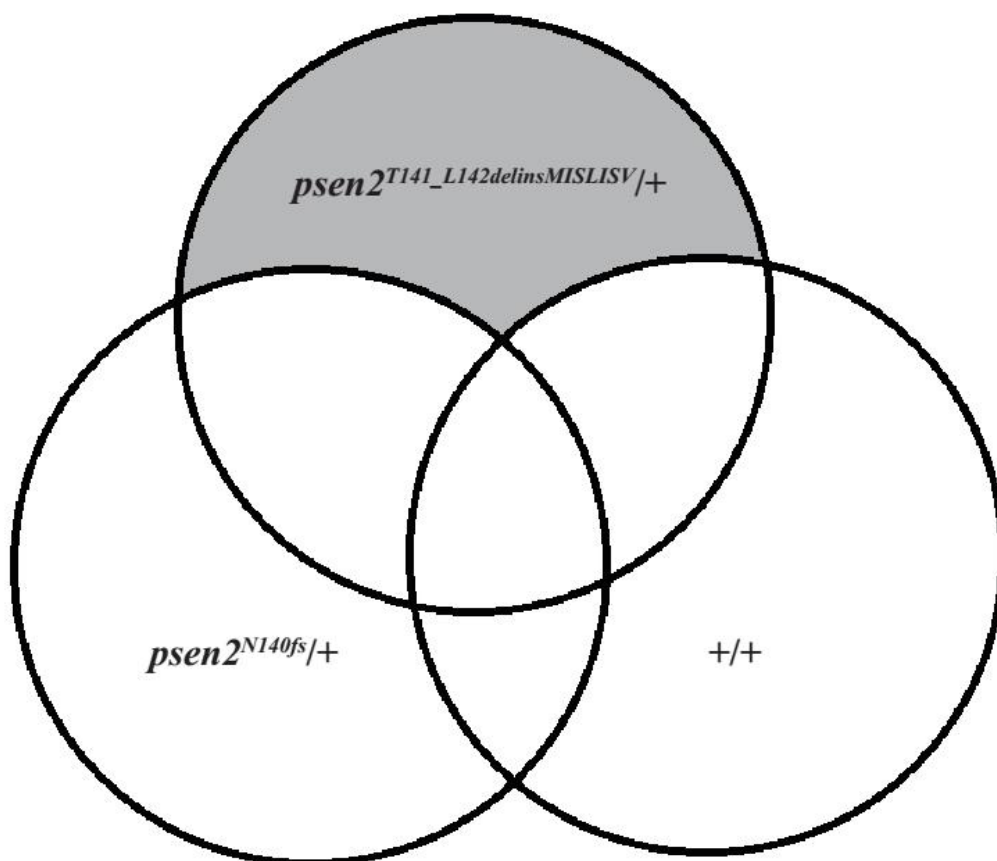


**Figure 6.2.1.** Schematic for the proposed transcriptomic analysis.

The gray part of this figure refers to the specific gene expression states caused by

*T141\_L142delinsMISLISV*, excluding those states seen in wild type fish (+/+) or caused by *NI40fs*.

(3) Beside molecular biological studies, other studies such as those in behavioristics may also be worthwhile to perform using the mutations generated in this thesis, since previous studies have shown that behavior can be considered a key component of phenotypes induced by genetic mutations (Xi, Ryan et al. 2010; Mahmood, Fu et al. 2013), especially those mutations affecting development of the nervous system in zebrafish (Elbaz, Yelin-Bekerman et al. 2012; Zhou, Cattley et al. 2014). Since the three mutations generated in this thesis are all located in *psen2*, a fAD-related gene, it will be interesting to identify whether the specific cellular changes caused by these mutations can affect the behavior of fish. Although locomotion tests (which may reflect the formation and function of mitochondria) on 6-day-old larvae did not show any statistically significant differences between any mutants (*S4Ter*, *T141\_L142delinsMISLISV* or *NI40fs*) and their wild type siblings, whether these mutations are able to affect the behavior of adult fish remains to be investigated.

(4) The melanotic pigmentation in the skin of adult mutants may be the subject of molecular biology analysis in the future since this phenotype is most likely related to  $\gamma$ -secretase activity (Kummer, Maruyama et al. 2009; Yang, Arslanova et al. 2010; Rochin, Hurbain et al. 2013). A gross loss of melanotic pigmentation in the skin of homozygous *T141\_L142delinsMISLISV* or *NI40fs* mutants that likely indicates a loss

of  $\gamma$ -secretase activity was observed, but strong melanotic pigmentation remained in their retinal pigmented epithelium. Additionally, abundant surface melanocytes in homozygous *N140fs* larvae indicated that the dependence of zebrafish adult skin melanotic pigmentation on *psen2* function is both cell type- and age-specific. Thus, it will be interesting to follow more closely the behaviour of surface melanocytes in aged homozygous fish (i.e. two years old or more) to identify whether the melanotic pigmentation can be restored by regeneration, or whether the loss of melanotic pigmentation becomes even more severe due to age. *In-situ* hybridisation against genes involved in the development of melanocytes in the skin of adult mutant fish may, in future, also help reveal how *psen2* is involved in melanotic pigmentation.

(5) In the GFP-based assay of autophagic flux, the stability of GFP-Lc3a and the free GFP fragments may affect its sensitivity. As Figure 6.2.2A shows, the GFP-Lc3a fragment may be cleaved in lysosomes, which provides additional free GFP and reduces its sensitivity in detection of decreased autophagic flux. Further improvement, such as redesigning the assay to avoid using GFP in both the autophagy-directed and non-directed arms of the assay construct, may be applied to solve this issue. As Figure 6.2.2B shows, a poly-FLAG fragment containing four copies of the FLAG tag could be added to both sides of the Lc3a-GFP construct, to make a FLAGs-LC3a-GFP-FLAGs construct. If this transgene was expressed in cells, the most C-terminal glycine residue of Lc3a would be cleaved by an endogenous ATG4 family protease, producing equimolar amounts of FLAGs-LC3a and GFP-FLAGs. The FLAGs-LC3a fragment

would then be taken into the autophagy pathway for degradation, while the GFP-FLAGs fragment should remain soluble in the cytosol as an internal control. Retaining GFP as part of the construct assists in selection of transiently transgenic embryos. Since this FLAG-based assay would use the anti-FLAG antibody for western immunoblotting, even if cleavage removing FLAGs from LC3a or GFP occurs in the lysosome, the free FLAGs (at ~4kDa in size) will not affect measurement of the ratio of FLAGs-LC3a (~20kDa) to GFP-FLAGs (~31kDa). Another issue that may need to be considered for such a FLAG-based assay is whether the stability of free GFP in the cytosol affects the final ratio of FLAGs-LC3a to GFP-FLAGs. To test this, a *odc1*PEST fragment can be added to the FLAG-based construct (Figure 6.2.2C), to form a FLAGs-LC3a-GFP-*odc1*PEST-FLAGs construct. The proline-glutamate-serine-threonine-rich (PEST) domain is responsible for the rapid proteasomal degradation of the protein ornithine decarboxylase (ODC) (Rechsteiner and Rogers 1996). It has already been reported in mice that the half-life of GFP fused to PEST-containing sequences from the mouse *Odc* gene was shortened to 5.5 h in stably transfected cells compared to about 26 h for wild type GFP (Corish and Tyler-Smith 1999; Kitsera, Khobta et al. 2007). For a new FLAG-based construct, a PEST-containing sequences from zebrafish *odc1* (the *odc1*PEST fragment) is added to the GFP-FLAGs fragment (Figure 6.2.2C) to destabilize the GFP domain. Although the half-life of *odc1*PESTfused GFP in zebrafish is still unclear, it will be interesting to investigate whether this FLAG-based construct with a destabilized GFP can increase the sensitivity of the autophagic flux assay. (The sequences of the two FLAG-based assays are presented in the Appendix.)

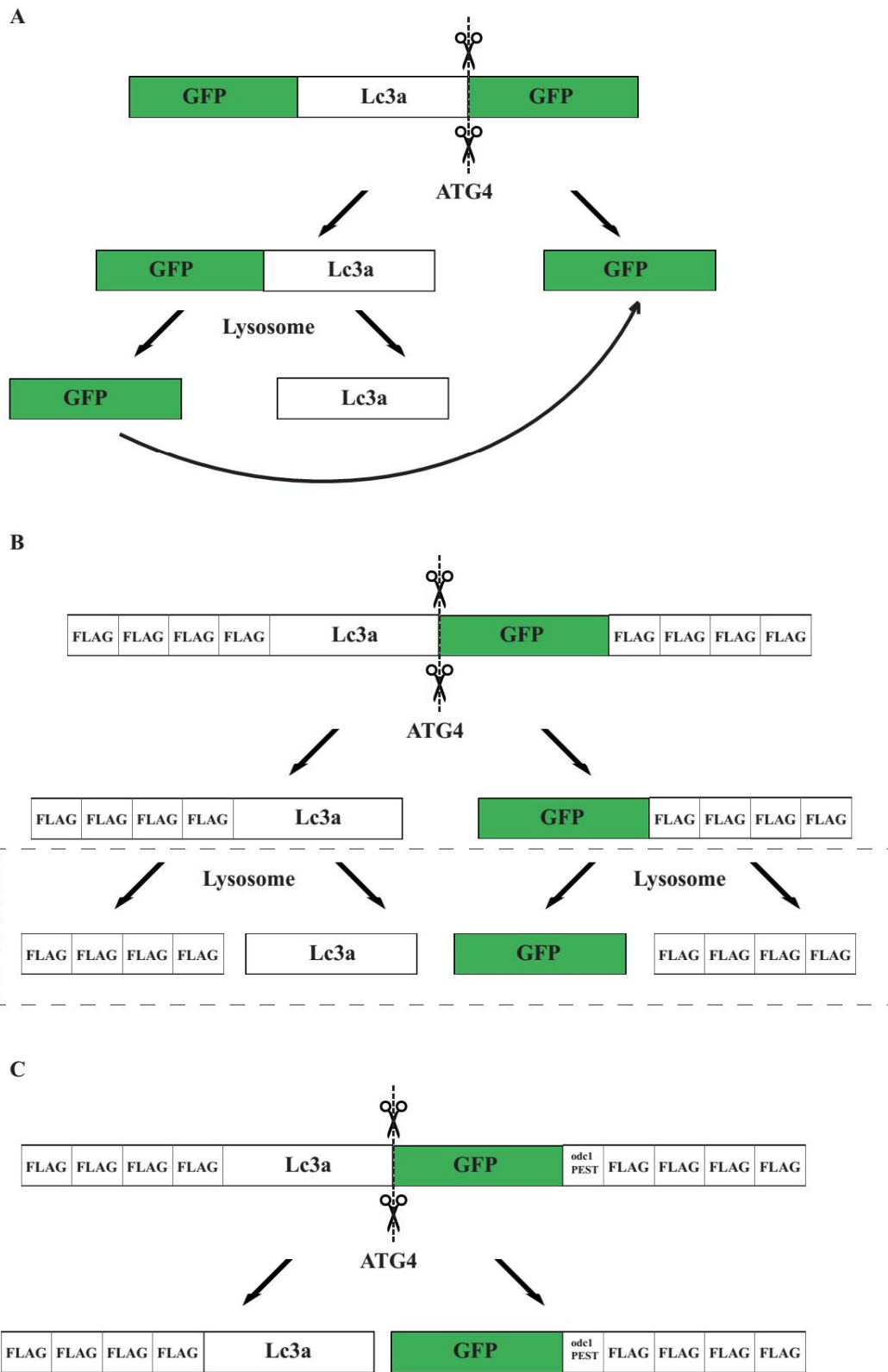


**Figure 6.2.2.** GFP- and FLAG-based assays.



- (A) GFP-Lc3a-GFP construct.
- (B) FLAGs-LC3a-GFP-FLAGs construct.
- (C) FLAGs-LC3a-GFP-odc1PEST-FLAGs construct.

### 6.3 References

- Corish, P. and C. Tyler-Smith (1999). "Attenuation of green fluorescent protein half-life in mammalian cells." Protein Eng **12**(12): 1035-1040.
- Elbaz, I., L. Yelin-Bekerman, et al. (2012). "Genetic ablation of hypocretin neurons alters behavioral state transitions in zebrafish." J Neurosci **32**(37): 12961-12972.
- Kitsera, N., A. Khobta, et al. (2007). "Destabilized green fluorescent protein detects rapid removal of transcription blocks after genotoxic exposure." Biotechniques **43**(2): 222-227.
- Kummer, M. P., H. Maruyama, et al. (2009). "Formation of Pmel17 amyloid is regulated by juxtamembrane metalloproteinase cleavage, and the resulting C-terminal fragment is a substrate for gamma-secretase." J Biol Chem **284**(4): 2296-2306.
- Mahmood, F., S. Fu, et al. (2013). "A zebrafish model of CLN2 disease is deficient in tripeptidyl peptidase 1 and displays progressive neurodegeneration accompanied by a reduction in proliferation." Brain **136**(Pt 5): 1488-1507.
- Newman, M., L. Wilson, et al. (2014). "Differential, dominant activation and inhibition of Notch signalling and APP cleavage by truncations of PSEN1 in human disease." Human molecular genetics **23**(3): 602-617.
- Nornes, S., M. Newman, et al. (2008). "Interference with splicing of Presenilin transcripts has potent dominant negative effects on Presenilin activity." Human molecular genetics **17**(3): 402-412.
- Rechsteiner, M. and S. W. Rogers (1996). "PEST sequences and regulation by proteolysis." Trends Biochem Sci **21**(7): 267-271.
- Rochin, L., I. Hurbain, et al. (2013). "BACE2 processes PMEL to form the melanosome amyloid matrix in pigment cells." Proc Natl Acad Sci U S A **110**(26): 10658-10663.
- Xi, Y., J. Ryan, et al. (2010). "Impaired dopaminergic neuron development and locomotor function in zebrafish with loss of pink1 function." European Journal of Neuroscience **31**(4): 623-633.
- Yang, T., D. Arslanova, et al. (2010). "In vivo manifestation of Notch related phenotypes in zebrafish treated with Alzheimer's amyloid reducing gamma-secretase inhibitors." J Neurochem **113**(5): 1200-1209.
- Zhou, Y., R. T. Cattley, et al. (2014). "Quantification of larval zebrafish motor function in multiwell plates using open-source MATLAB applications." Nat Protoc **9**(7): 1533-1548.

## Appendix

(1) Mean velocities of Figure 5.4.1 to 5.4.4.xlsx

(2) Sequences of constructs for FLAG-based assays

### Design of FLAGs-LC3a-GFP-FLAGs Construct

Different regions of the sequence are labeled with different highlight colours corresponding to the legend below:

- EcoRV-BamHI-Kozak-StartFLAGs-LC3a-GFP-FLAGsStop-Clal-EcoRI-EcoRV
- X in the downstream FLAGs region refers to numerous silent mutations introduced in to the degenerate codon positions

### Sequence of FLAGs-LC3a-GFP-FLAGs construct

5'-

GATATC GGATCC GCCACC ATGGACTACAAAGACGATGACGACAAGGAT TAC  
AAAGACGATGAT GACAA A GACTA TAA GACGATGACGAT AAGGACTACAA  
AGACGATGACGACAAGATG CCATCCGACAGACCCTTCAAACAACGACGGA  
GCTTCGCTGATCGTTGCAAGGAAGTGCAGCAGATCCGAGAGCAGCATCTA  
ATAAAATTCCGGTGATCATTGAGAGGTATAAGGGGGAAAAGCAACTTCCAG  
TCTTGGACAAGACCAAGTTCCTTGTCCCTGACCATGTTAACATGAGTGAGC  
TGGTAAAGATTATCAGGCGTCGATTGCAGCTCAACCCACCCAGGCCTTTT  
TCCTTCTTGTCAATCAGCACAGCATGGTCAGCGTGTCCACCCCATTTCTGA  
GATCTACGAACAAGAGCGGGACGAAGACGGCTTCTCTACATGGTTTACGC  
CTCCAGGAGACCTTCGGCTGC ATG GTGAGCAAGGGCGAGGAGCTGTTCA  
CCGGGGTGGTGCCATCCTGGTTCGAGCTGGACGGCGACGTAAACGGCCAC  
AAGTTCAGCGTGTCCGGCGAGGGCGAGGGCGATGCCACCTACGGCAAGCT  
GACCCTGAAGTTCATCTGCACCACCGGCAAGCTGCCCCTGCCCTGGCCCA  
CCCTCGTGACCACCTGACCTACGGCGTGCAGTGCTTCAGCCGCTACCCCG  
ACCACATGAAGCAGCACGACTTCTTCAAGTCCGCCATGCCCGAAGGCTAC  
GTCCAGGAGCGCACCATCTTCTTCAAGGACGACGGCAACTACAAGACCCG  
CGCCGAGGTGAAGTTCGAGGGGCGACACCCTGGTGAACCGCATCGAGCTGA  
AGGGCATCGACTTCAAGGAGGACGGCAACATCCTGGGGCACAAGCTGGAG  
TACA ACTACAACAGCCACAACGTCTATATCATGGCCGACAAGCAGAAGAAC  
GGCATCAAGGTGAACTTCAAGATCCGCCACAACATCGAGGACGGCAGCGT  
GCAGCTCGCCGACCACTACCAGCAGAACACCCCATCGGCGACGGCCCCG  
TGCTGCTGCCCGACAACCACTACCTGAGCACCCAGTCCGCCCTGAGCAA  
GACCCCAACGAGAAGCGCGATCACATGGTCCTGCTGGAGTTCGTGACCGC  
CGCCGGGATCACTCTCGGCATGGACGAGCTGTACAAG ATGGA TACAAG GA  
CGATGACGAT AAGGACTACAAAGAT GA GACGACAA A GACTACAA GACG  
A GACGACAAGGACTA AAAGA GATGA GACAAG TAG ATCGATGAATTCG  
ATATC -3'

## Design of FLAGs-LC3a-GFP-odc1PEST-FLAGs Construct

Different regions of the sequence are labeled with different highlight colours corresponding to the legend below:

- EcoRV-BamHI-Kozak-StartFLAGs-LC3a-GFP-odc1PEST-FLAGsStop-Clal-EcoRI-EcoRV
- X in the downstream FLAGs region refers to numerous silent mutations introduced in to the degenerate codon positions

## Sequence of FLAGs-LC3a-GFP-odc1PEST-FLAGs construct

5'-

```
GATATC GGATCC GCCACC ATGGACTACAAAGACGATGACGACAAGGAT TAC
AAAGACGATGAT GACAAAGACTATAAG GACGATGACGATAAGGACTACAA
AGACGATGACGACAAGATGCCATCCGACAGACCCTTCAAACAACGACGGA
GCTTCGCTGATCGTTGCAAGGAAGTGCAGCAGATCCGAGAGCAGCATCTA
ATAAAATTCGGGTGATCATTGAGAGGTATAAGGGGGAAAAGCAACTTCCAG
TCTTGACAAGACCAAGTTCCTTGTCCTGACCATGTTAACATGAGTGAGC
TGGTAAAGATTATCAGGCGTCGATTGCAGCTCAACCCACCCAGGCCTTTT
TCCTTCTGTCAATCAGCACAGCATGGTCAGCGTGTCCACCCCATTTCTGA
GATCTACGAACAAGAGCGGGACGAAGACGGCTTCTCTACATGGTTTACGC
CTCCAGGAGACCTTCGGCTGCATG GTGAGCAAGGGCGAGGAGCTGTTC
CCGGGGTGGTGCCATCCTGGTTCGAGCTGGACGGCGACGTAAACGGCCAC
AAGTTCAGCGTGTCCGGCGAGGGCGAGGGCGATGCCACCTACGGCAAGCT
GACCCTGAAGTTCATCTGCACCACCGGCAAGCTGCCCGTGCCCTGGCCCA
CCCTCGTGACCACCTGACCTACGGCGTGCAGTGCTTCAGCCGCTACCCCG
ACCACATGAAGCAGCACGACTTCTTCAAGTCCGCCATGCCCGAAGGCTAC
GTCCAGGAGCGCACCATCTTCTTCAAGGACGACGGCAACTACAAGACCCG
CGCCGAGGTGAAGTTCGAGGGCGACACCCTGGTGAACCGCATCGAGCTGA
AGGGCATCGACTTCAAGGAGGACGGCAACATCCTGGGGCACAAGCTGGAG
TACAACTACAACAGCCACAACGTCTATATCATGGCCGACAAGCAGAAGAAC
GGCATCAAGGTGAACTTCAAGATCCGCCACAACATCGAGGACGGCAGCGT
GCAGCTCGCCGACCACTACCAGCAGAACACCCCATCGGCGACGGCCCCG
TGCTGCTGCCCGACAACCACTACCTGAGCACCCAGTCCGCCCTGAGCAAA
GACCCCAACGAGAAGCGCGATCACATGGTCTGCTGGAGTTCGTGACCGC
CGCCGGGATCACTCTCGGCATGGACGAGCTGTACAAGATGCAGGGGATTCC
TGCACTTCCATTGGAGGAGCCGAGCGCTGGAAACGTGCCATCCCCTGCG
GGCGCGAGAGCAGTCTGGATGTTCCCGCCAAACCCTGCCCGACTCAAGTG
CTGATGGAAT TACAAAG GACGATGACGATAAGGACTACAAAGATGAC GACGA
CAAAGACTACAAAGACGACGACGACGACAAGGACTATAAAGAATGATGATGACA
AGTAGATCGATGAATTCGATATC-3'
```